Shale Gas Characterization and Production Forecasting: A Case Study on UK Bowland Shale and the US Barnett Shale

MICHAEL KENOMORE

The thesis is submitted in partial fulfilment of the requirements for the award of the degree

of

Doctor of Philosophy

of the

University of Portsmouth

June 2020

Declaration

Whilst registered as a candidate for the above degree, I have not been registered for any other research award. The results and conclusions embodied in this thesis are the work of the named candidate and have not been submitted for any other academic award.

Michael Kenomore
June 2020

Acknowledgment

I would first like to express my sincere gratitude to my advisor Dr. Mohamed Hassan for the continuous support of my Ph.D. study and research, for his patience, motivation, and immense knowledge. His guidance always helped me during the research and writing of this thesis. In addition, I would like to thank my Father for his wise counsel and sympathetic ear. You are always there for me. I would also like to thank my fellow doctoral students for their feedback, cooperation and of course friendship. I am also grateful to the members of my committee for their patience and support in overcoming numerous obstacles I have been facing through my research. The research project has been fully funded by the University of Portsmouth.

Abstract

Based on the recent reports from Oil and Gas Authority (OGA), a declining trend of hydrocarbon production capability is expected for UK, in upcoming years. In order to keep a relative self-sufficiency in terms of oil and gas supplies, access for new hydrocarbon resources seems necessary.

The giant unconventional reservoirs, such as Bowland shale gas, have been recently discovered in the Central Britain and there is a big potential for them to be the future gas sources in UK. However, the development of shale gas reservoirs is still challenging, there are several shale gas reservoirs around the world developed successfully, which provide us with valuable knowledge and experiences. Most of the efforts in discovery and development of these reservoirs, were performed in USA. A combination of advanced techniques, horizontal drilling and hydraulic fracturing, has enabled profitable extraction of shale gas trapped in low-permeability formations.

Development of shale gas reservoirs, besides of a comprehensive study on reservoir's properties, demands for a precise forecast of reservoir's production, in order to make the project economical.

In this study, the Bowland shale gas, as a high potential candidate for future developments in UK, have been analysed. We conducted a comprehensive study on every aspects of the reservoir, including geological, petrophysical, geochemical, and geomechanical properties. Meanwhile, Barnett shale gas, as a huge shale gas reservoir, which already developed in USA, has reviewed. The results used as a guidance and subsidiary information for appraising future development of Bowland shale gas.

Various methods of production forecasting, comprising numerical, analytical, and advanced machine learning techniques have been examined. Numerical and analytical methods provided favourable results in production forecasting of Barnet reservoir, compared with real production test data. Also, the use of time series methods, as a branch of machine learning techniques, provided us with even more precise forecasts. The numerical and time series methods, both considered to be reliable methods in production forecasting of Bowland shale gas.

The results of this study open up an executive workflow for any future development of Bowland reservoir. The workflow by accounting any available data from the reservoir and utilizing experiences from already developed similar reservoirs, will provide a clear projection of future behaviour of the reservoir. The high variety of available data, the use of advanced forecasting methods, and successful experience of hydraulic fracturing operation in Barnett, regarding the

similarities between the two reservoirs, give us the required feedback for any future development stage of Bowland.

Table of Contents

Publications by Candidate

➢ Peer Reviewed Publications

- M. Kenomore, M. Hassan, R. Malakooti, H. Dhakal, A. Shah **Shale gas production decline trend over time in the Barnett Shale.** J. Pet. Sci. Eng., 165 (2018), pp. 691-710, 10.1016/j.petrol.2018.02.032

- M. Kenomore, M. Hassan, H. Dhakal, A. ShahTotal organic carbon evaluation of the Bowland Shale Formation in the Upper Bowland of the Widmerpool Gulf. J Pet Sci Eng, 150 (2017), pp. 137-145

- Hassan Sayed, M, Fianu, JS, Malakooti, R, Salazar Misslin, PA, Kenomore, M & Gharavi, AH 2019, Petroleum engineering: a collaboration between academia and industry. in *Realising Ambitions: Proceedings of the 6th Annual Symposium of the United Kingdom & Ireland Engineering Education Research Network.* 1 edn, vol. 1, University of Portsmouth, Portsmouth, pp. 205-218, 6th Annual Symposium of the United Kingdom & Ireland Engineering Education Research Network, Portsmouth, United Kingdom, 1/11/18.

➢ Conference Publication

- Kenomore, M, Hassan Sayed, M, Dhakal, H & Shah, A 2018, Economic appraisal of shale gas reservoirs. in *SPE Europec featured at 80th EAGE Conference and Exhibition, 11-14 June, Copenhagen, Denmark.*, SPE-190824-MS, Society of Petroleum Engineers, 80th EAGE Conference & Exhibition, Copenhagen, Denmark, 11/06/18. https://doi.org/10.2118/190824-MS

➢ Other Publications

- Mohamed Hassan, Michael Kenomore, **John Fianu** , Amir Gharavi. Hydraulic Fracturing ,a UK prospective. Article published in London petrophysical society Newsletter.

- **Publications still under peer review**

  Analysis of Total Organic Carbon in the UK Upper Bowland Shale using Linear and Random Forest Regression in R.

Chapter 1 Introduction

1.1 Motivation

For many years, shale gas exploitation has been generating contradictory views in the UK and remains subject of rising debates throughout these years. Favourably backed by the government, looking upon it as potential mechanism for gas import independency and competitiveness in global gas industry whilst strongly opposed by stakeholders hence the notion of shale gas exploitation remains disputed with limited progress in past years and this challenge is worsened by obscurity of estimates for potential reserves and conflicting assessments on potential impact of shale gas. According to an Oil and Gas Authority (OGA), report in 2019, there is a gradual declining trend in UK hydrocarbon production predicted over the next years Figure 1-1. This implies the need for appraisal and development of new hydrocarbon resources in UK.

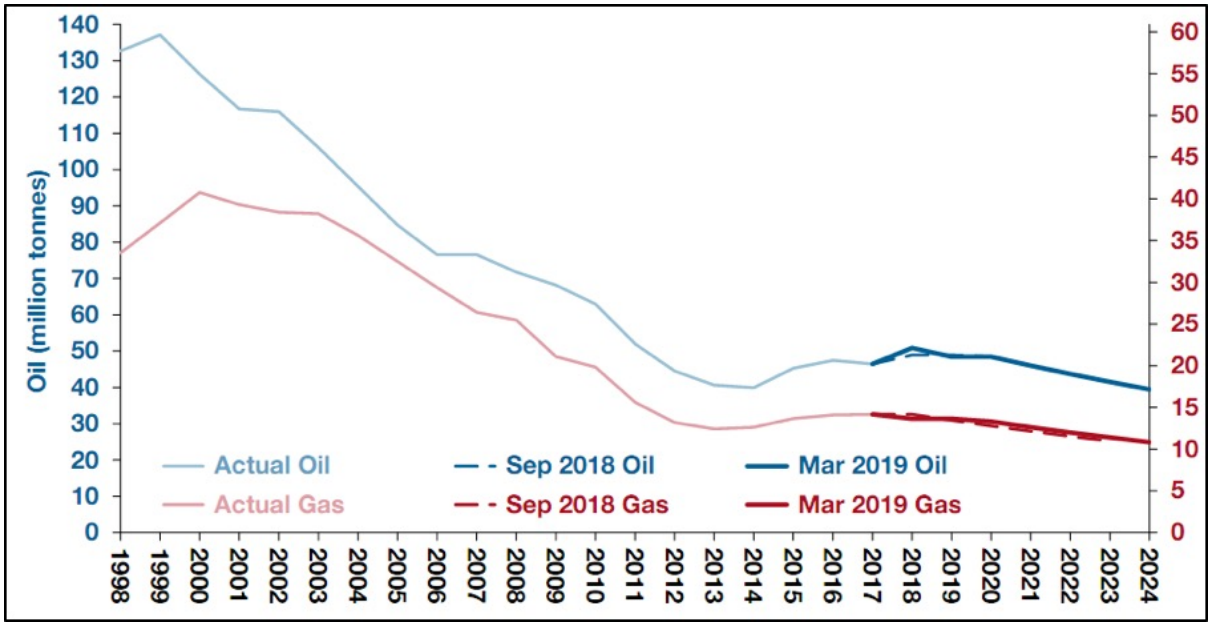

Figure 1-1: Oil and Gas Authority (OGA) Projections of UK Oil and Gas Production, 2019

The Bowland Basin, with 1900 m of Lower Carboniferous shale, is in the vanguard of UK shale gas development (Smythe, 2016). Though, to date, the US remains the only country to extract shale gas at a large commercial scale which led to a significant transformation of its natural gas industry. Production from shale gas plays is the largest contributor to natural gas production in the United States, accounting for almost two-thirds of total U.S. production by 2040 (EIA, 2017). Nations around the world including Argentina, Australia, China, India, South Africa, UK and other parts of the EU are currently attempting to replicate the shale gas success in North America from their domestic endowments (Hilaire, Nico, & Brecha, 2015).

A combination of economics, government support and hydraulic fracturing has enabled profitable extraction of shale gas trapped in low-permeability formations. This development has substantially altered US's energy portfolio leading to low gas prices, nearly self-sufficiency in terms of gas supply. Despite recent advances, there are still considerable challenges in shale gas resources; an issue is the variability of productivity from well to well, even within the same formation (Hammond, 2013). This poses a problem for stakeholders, production companies and financial traders (Hammond, 2013). It is therefore imperative to understand the economic and production feasibility of unconventional shale gas reservoirs.

The European environment has not experienced a similar boom compared to the US because of a variety of challenges, namely; infrastructural differences, complex geology, environmental regulations, land ownership and mineral rights, public contempt, and land area (Instituite for Directors, 2013). In addition, shale gas development in Europe is still at an infant stage and there has been no production in Europe (Instituite for Directors, 2013). The UK government is keen on tapping this energy resource to improve its energy security in the long term, create jobs (~ 64500 jobs are estimated) and reduce dependency on coal (Ernst and Young, 2014).

Exploration in shale gas reservoir relies in the identification of sweet spots i.e. areas of favourable reservoir properties where gas can be economically and easily produced at higher rates compared to unfavourable parts of the shale (Chopra *et al.*, 2013). A classic feature often experienced by shale gas reservoirs is the rapid decline in gas production – this decline is usually approximately 70% in the first year (King, 2010). The rapid decline rate, heterogeneity and extra low permeability of shale means that numerous amounts of wells are needed to drain the reservoir to obtain economic quantities of gas compared to conventional reservoirs. In the UK, 400 laterals are estimated to be needed for peak production (Ernst and Young, 2014). This thesis aims to reduce the research gap in terms of UK shale gas production and provide an opportunity to understand the production forecasting of shale gas in the UK.

1.2 Problem statement and Research Gaps

Since 1990, shale resource systems have become the most active target for the United States in its development of natural gas, which has led to the US becoming energy independent in natural gas reserves. Success in producing gas and oil from this ultra-low permeability and low porosity reservoirs has resulted in a worldwide exploration effort to find and produce such systems (Jarvie, 2012b). The US now has a well-established shale gas industry, and the Bowland-Hodder shale gas play in the UK is quickly becoming the next frontier for shale gas

exploration in Europe. Only seven shale gas exploration wells have been completed in the UK, of which one has been hydraulically fractured; as such, there is a lack of production data, and if available, there are strict contractual agreements preventing access for public or academic use. With only seven exploration wells drilled to date and only one vertical well fracture stimulation completed, the UK is still in the early stages of developing its shale gas plays and is very much at the frontier of exploration as such only a bottom-up resource assessment of gas in place, by (Andrews, 2013) has been published to date. The UK does not have any primary production data to use a more refined method, such as the USGS's Technically Recoverable Resource estimates. However, exploration and production programs have and can depend on analogous known successful plays (Bruner and Smosna, 2011; Jarvie, 2012a). The following research questions are discussed in section 1.3

1.3 Research questions

The following questions were answered in the course of this research and the methodology used and results obtained were guided by these questions:

- How we can effectively use the experience of previous shale gas developments around the world?
- What are the comparable relationships between the Barnett and Bowland shale?
- Can a numerical or analytical simulation model be developed to reflect the Bowland shale?
- What are the main factors that affects shale gas reservoir performance in relation to the aforementioned simulation models?
- Can these models be validated with appropriate production data from the Barnett shale?
- Can future shale gas production in the UK be predicted using the numerical simulation models?

1.4 Aim of study

The aim of this study was to understand the production potential of the UK Bowland shale gas, guided by experiences from the USA Barnett shale gas. The focal point is to characterize both reservoirs from Petrophysical, Geochemical, Geomechanical, and Geological perspective.

1.5 Objectives

- Characterize and compare the Bowland and Barnett shale gas reservoirs, from the petrophysical, geochemical, geological, and geo-mechanical and production analysis viewpoints – a bottoms-up approach.
- Compare the accuracy of the production forecasting methods for Barnett shale gas reservoir and determine the appropriate methodology. Use results as a validation for the Bowland Shale – a production extrapolation approach.
- Combine both methodologies to provide a better understand the production potential of the Upper Bowland Shale.

1.6 Methodology

The following steps were carried out in the study;

- Review of literature on previous work on shale gas reservoir characterisation, development and production forecasting workflows. In-depth analysis of reservoir properties, i.e. TOC, Porosity, Mineralogy and Water Saturation to support a bottoms-up approach in developing a reservoir simulation model capable of predicting UK shale gas production. Production forecasting methodologies with conventional and unconventional techniques to support a production extrapolation methodology and help validate the model considering the paucity of production data from the UK.

- Available data from the Bowland shale and Barnet Shale gas was used to understand the production behaviour, petrophysical, geochemical, and geo-mechanical properties of each reservoir. Data includes contour map data from the UK Oil and Gas Authority, Well log data from five UK wells and production data from 10000 horizontal shale gas wells from the Barnett Shale.

- Case Studies were carried out which uniquely answered unique research gaps that exists in the UK shale gas research environment. Case Study 3 allowed us to derive equations that can be used to widely predict Total Organic Carbon in the UK from well logs. Case Study 2 provided lessons learned from the Barnett Shale and how we can incorporate this into the UK shale gas development. TOC modelling can be added into future models to better investigate the gas content and thus provide a more accurate representation of gas production. Barnett Production forecasting was used in the simulation model to help validate the model.

- Inputs from the aforementioned step were used in the development of case studies that led to journal and conference publications as well as input into the reservoir simulation model for the Bowland shale to better understand both reservoirs.

1.7 Thesis Layout

Broadly, this work consists of a thorough examination of the Barnett shale production performance, petrophysical evaluation of the Bowland shale, development of numerical, analytical, and machine learning models for the Bowland shale and an understanding of the challenges that the UK faces in its shale gas development. Along with this workflow, the US Barnett shale reservoir was also analysed in as an analogous field. The thesis layout is;

Chapter 2: Provides an introduction and literature review to shale gas systems as an unconventional resource in comparison to other resources. The chapter also provides a full review of every possible workflow and scenario for characterization, forecast, and development of the shale gas reservoirs.

Chapter 3: Consists of Petrophysical, geological, geochemical, and geo-mechanical evaluation of the Bowland and Barnett shale to obtain the reservoir's properties e.g., Poisson's ratio, Young's modulus, porosity, permeability, and total organic carbon (TOC). These properties are implemented in the numerical and analytical models.

Chapter 4: Presents various empirical decline curve analysis methods and their application to production data obtained from the Barnett shale. Also, Time Series as an advanced machine learning technology have been utilized to forecast the production of Barnet shale gas. The performance of these methods is evaluated and used to generate Barnett shale type curves that will validate the numerical models and finding the optimum method for future Bowland development.

Chapter 5: Presents the numerical simulation of the Bowland Shale including sensitivities and how production compare to Barnett shale gas production.

Chapter 6: Concludes the thesis and provides the results from this for the future development of Bowland shale gas development and optimum workflow and scenarios that can be used for any future works and guiding any potential development strategies of Bowland shale gas.

Chapter 2 Literature Review

2.1. Introduction

The UK shale gas industry is in its infancy, and ahead of production testing there are no reliable indicators of potential productivity of its most prospective Jurassic, Carboniferous and Cambrian shale gas plays. For that reason, resource estimates can only be made by analogy with producing shale gas plays in America, although again ahead of drilling, hydraulic fracturing and flow testing these analogies may ultimately prove to be invalid. Hence the need to conduct this research to better understand how the Upper Bowland Shale would perform in the future.

Comprising a thermally mature source rock, the Barnett Shale is probably not a good analogue for the UK Jurassic plays of the Weald and Wessex basins, but it may provide an indicator of the possible productivity of the UK Carboniferous shale gas play. The Barnett Shale of the Forth-Worth Basin produces 268 mmcf/ km^2 shale gas (Faraj et al. 2004). However, it seems unlikely that all of the UK's Pennine Basin petroleum system could be similarly productive, but if so, its 17,500 $km^{2,}$ comprising a mosaic of separate sub-basins Figure 2-18 could potentially yield up to 4.7 TCF shale gas. There are "sweet spots" in the basing that have a higher production/ km^2. In this thesis, the Barnett was used as an analogy to validate the performance of the Upper Bowland Shale to address the research gap.

When it comes to shale gas, a complex workflow of reservoir analysis is required. However, exploration for shale gas is initially simpler than conventional hydrocarbon exploration, because problems of migration into non-source rock lithologies and the conventional reservoir characteristics are of no importance. Completion of wells in low permeability shales is likely to be a key hurdle in the UK, unless the US experience is directly transferable to the UK. Exploration needs to concentrate on identifying good hydrocarbon source rocks, their generative kitchens, areas of high total organic carbon (TOC), and areas of gas window maturity Hence an integrated reservoir analysis consisting of geological, petrophysical, geochemical, and geo-mechanical analysis needs to be performed along with a production forecast as needed. This chapter reviews existing work that has been carried out to address the research gap presented in this thesis.

2.2. Conventional and Unconventional Accumulations

Petroleum accumulations from the Earth's crust can be grouped into conventional (discontinuous) and unconventional (continuous) accumulations (Zhao et al., 2015). Schmoker (2002), classified shale gas, coalbed methane, and tight gas etc. as continuous unconventional accumulations i.e. extensive accumulations where hydrocarbons are present across the whole strata. Shale, in particular is not a rock type rather it is a term colloquially used to describe mudstones that contain extremely fine grains typically less than 4μm in diameter (Passey, Bohacs, Esch, Klimentidis, & Sinha, 2010). Some shales could also contain different amount of silt size particles which are up to 62.5μm while conventional sandstone rocks are composed of grains which can vary between 62.5μm and 2000μm in diameter (Passey, Bohacs, Esch, Klimentidis, & Sinha, 2010). A summary of the differences between conventional and unconventional accumulations is presented in Table 2-1.

Table 2-1: A comparisons between conventional and discontinuous accumulations (Zhao *et al.*, 2015)

Features	**Unconventional Accumulation**	**Conventional Accumulation**
Hydrocarbon distribution	Extensive and continuous with no defined boundaries.	The distribution is isolated, and its boundary is explicit.
Relationship between gas and water	No edge or bottom water	Edge or bottom water is common.
Trap types	No traps are necessary.	Structural, stratigraphic and combination traps.
Reservoir pressure	Abnormal pressure; overpressure is common.	Pressure can be abnormal and combination traps.
Distribution of resources	Resource is affluent but in low abundance	Resource is generally less, but abundance can be medium to high.
Filling and migration	Migration is insignificant.	Accumulation is usually the result of secondary migration and occurred either near or far away from the source kitchen.
Migration dynamics	Driving forces mainly come from overpressure and diffusion force. Buoyancy is weak.	The migration force is mainly buoyancy and hydrodynamic force.
Migration patterns	Non-Darcy surge flow and diffusion flow.	Darcy flow
Accumulation mechanism	Accumulation is controlled primarily by the quality of source rocks and sweet spots.	Accumulation is strictly controlled by conventional traps.
Distribution of source rock and reservoir	Source rocks also serve as reservoirs.	They are close to each other or separated.
Reservoir conditions	Inferior	Reservoirs are conventional
Location	Depressions and slopes.	Uplift and faulted fold zones.
Main controlling factors	Structure is not important, and trap is unnecessary.	Traps are necessary.

2.3. Key Factors of Shale Gas Plays

Key characteristics that affect shale gas production performance is dependent on the cost and technical requirement needed to overcome the challenge posed for gas production (King, 2010). Figure 2-1 shows a compilation of different criteria grouped by importance and manageability and ideal values for important parameters are presented in Table 2-2.

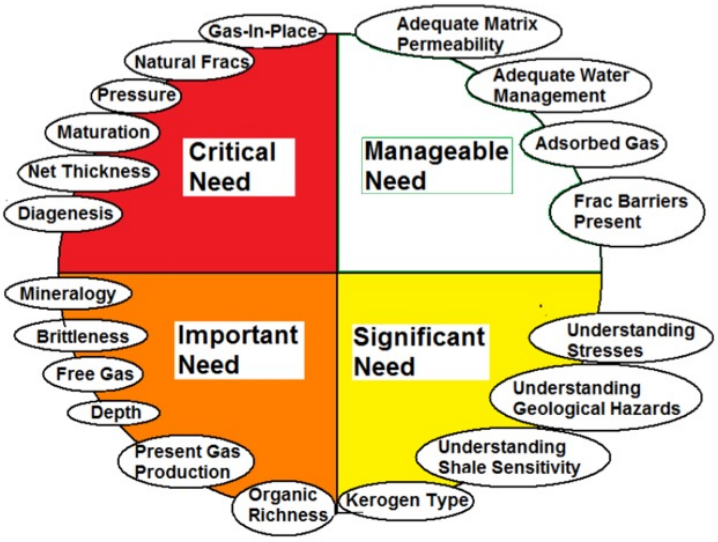

Figure 2-1: :Shale Candidate Criteria (King, 2010)

Table 2-2: Summary of the important geological and geochemical factors, which are common between high producing shale gas plays (Wright, 2016).

Factors	**Criteria for Success**
Total Organic Carbon (TOC)	≥ 2 wt%.
Kerogen Type	Type II, indicates a planktonic or marine origin.
Original Hydrogen Index (HI_o)	250-800 (mg/g/TOC).
Thermal Maturity	1.1%Ro, however, ideally ≥ 1.4%Ro.
Gas Saturation	Gas present in matrix, fractures and adsorbed gas, ideally > 100bcf/section.
Porosity	4-7%
Net Shale Thickness	> 15 meters
Mineralogy	< 40% clay by volume
Pre-existing Structure	Stable basins, simple structure

King, 2010 however, addressed that for every definition of a productive shale, there will be at least one example of a successful shale outside the limits described by the strict set of candidate criteria. The most critical factors mentioned in Figure 2-1 and Table 2-2 are discussed in the following sections.

2.3.1. Gas in Place

A profitable shale gas play must have sufficient gas in place (GIP) within the shale. Total gas in place in shale is a derived value that includes a combination of free gas, adsorbed gas, and absorbed gas (King, 2010). Shales with regional fractures and faults often have a more mobile free gas component; therefore, the first wells in such areas may have higher initial production rates than later wells. US productive shales have variable characteristics, for example including the high gas-content Barnett Shale, which contains mostly free gas and the average gas-content Antrim Shale, which contains mostly adsorbed gas. An obvious effect of this difference is a varying well production decline curve (Drake 2007). The result of gas in place is dependent on the accurate prediction of effective porosity, shale thickness, area and gas saturation at bottom-hole conditions (Jarvie *et al.*, 2004). The GIP generated is also a function of Total Organic Content (TOC) and thermal maturity (Wright, 2016).

The Upper Bowland Shale in the Bowland-Hodder unit is more prospective, primarily due to better well control which demonstrates its closer resemblance to the prolific North American shale gas plays, in which the productive zones are hundreds of feet thick compared to the lower unit which is largely undrilled. (Andrews, 2013). The total gas in place for the Upper Bowland unit shales across central Britain is 164-264-447Tcf (P90, P50, P10)(Andrews, 2013). This is not the amount that can be recoverable and has been carried out through a "bottom up" resource assessment of gas in place was carried out to accurately reflects the area's shale gas potential (Andrews, 2013). Over time, drilling and testing of new wells will provide an understanding of production rates.

Other non-geological factors such as gas prices, operating costs and the scale of development agreed by the local planning system, will allow estimates of the UK's shale gas reserves to be made (Andrews, 2013). The basin of interest in this thesis within the Bowland shale is the Bowland basin and is one of the largest basins in the assessment area conducted by Andrews, 2013 continuing westwards beneath the Irish Sea. The four key elements within the Bowland Basin in terms of shale gas resources are the Hodder Mudstone, the Lower Bowland Shale, Upper Bowland Shale and the Sabden Shale Group (Clarke, Bustin and Turner, 2014). The Upper Bowland Shale is of interest in this thesis.

2.3.2. Porosity

Gas storage in shale gas reservoirs occurs in the adsorbed state within the kerogen, in the free-state within kerogen porosity, in the free-state within the intergranular pore spacing (including micro-fractures) and in natural macro-scale fractures (Bust *et al.*, 2013). A

significant fraction of the free gas can be stored within kerogen porosity (Bust *et al.*, 2013). This is dependent on the size of the intrakerogen pores, which is a function of the nature of the kerogen and the degree of thermal maturity (Bust *et al.*, 2013). Small intra-kerogen pores may be occupied almost entirely by adsorbed gas, in which case the free gas will occur mostly in inorganic pores (Bust *et al.*, 2013). As more of the adsorbed gas is released into a free state, kerogen porosity will increase (Bust *et al.*, 2013). Larger kerogen pore sizes may be fill with free gas but adsorbed gas content will be small (Bust *et al.*, 2013). The effective porosity of the Upper Bowland shale samples through the section averages 2.8% and the water saturation averages 25%. The average matrix permeability is 1E-5 and there is a good correlation between gas filled porosity and unconfined matrix permeability (Clarke, Bustin and Turner, 2014). The porosity in the Upper Bowland Shale was calculated as the difference between the bulk and skeletal density thus is the porosity to gas and is used subsequently to calculate the total free gas in place (100% gas saturated porosity) (Clarke *et al.*, 2018). Following in-situ testing, the samples were then stage dried to determine water saturation (Sw). On the dried samples, the bulk density was measured using mercury immersion and the skeletal density was measured using helium pycnometry as performed on the as-received samples. The difference between the stage dried bulk and skeletal density provides the total porosity. The matrix permeability was determined by the GRI (Gas Research Institute) methods (CUI, BUSTIN and BUSTIN, 2009). The permeability in this method is widely used in the industry and has not been calibrated for in situ conditions so matrix permeability data should only be used for comparative purposes (Clarke *et al.*, 2018). The average porosity, water saturation and matrix permeability for three wells studied that pass through the Upper Bowland shale is shown in Table 2-3 and a cross plot of porosity vs permeability is shown in Figure 2-2.

Table 2-3: Results of porosity and water saturation analysis for three wells (Clarke *et al.*, 2018)

Well/Formation	*n*	Bulk Density (g cm^{-3})	Skeletal Density (g cm^{-3})	Effective Porosity (%)	Total Porosity (%)	Water Saturation (%)	Matrix Permeability (mD)
Grange Hill-1z							
Upper Bowland Shale	10	2.62	2.71	3.23	4.34	25.1	4.36E-05
Preese-Hall 1							
Upper Bowland Shale	31	2.60	2.70	2.82	3.70	25.5	1.50E-05
Becconsall-1z							
Upper Bowland Shale	8	2.59	2.66	2.49	3.92	37.07	1.07E-04

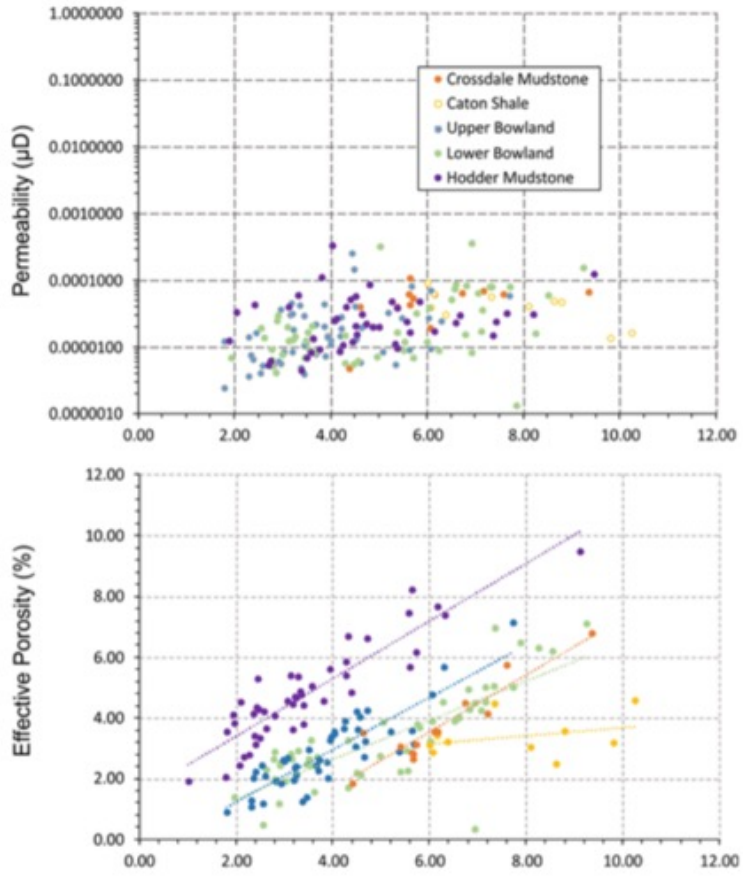

Figure 2-2: Plots of matrix permeability vs total porosity and effective porosity v porosity for combined data from Preese Hall 1, Grange Hill 1z and Becconsall 1z.

The summary data in Table 2-3 are consistent and compatible with the results from wireline logs where the wellbore in the gauge. Water saturation as determined from resistivity logs, is generally lower than laboratory values due to variable amounts of clay (Clarke *et al.*, 2018). The Barnett shale however, has an average total porosity of 6% (Bowker, 2003), which is within the acceptable range described in Table 2-2. Total porosity will put an upper limit on the free gas in place and may be composed of inter-clast and intraclast pores, as well as open natural fractures. Bowker, 2007 concludes that the Barnett is successful because of a combination of very high gas concentration within the Barnett and the rock's ability to fracture. When using the Barnett as an exploration model, it is important to find shales that can be hydraulically fractured, not shales that contain an open fracture network that we aim to connect through hydraulic fracturing (Wright, 2016). This is because natural fracture networks only make up approximately 1% of a shale's total porosity (Wright, 2016).

2.3.2.1. Porosity Challenges

A key challenge in petro physics is to distinguish qualitatively between the porosities associated with free and adsorbed gas (Bust *et al.*, 2013). Furthermore adsorbed, released(in kerogen pore space), and inorganic free gas may have different properties (Ambrose *et al.*, 2010). The amount of adsorbed gas as a percentage of the total gas volume vary approximately from 20-85% within target beds of major North American shale gas plays (Bust *et al.*, 2013). There are three components to total porosity. Firstly, there is the porosity within natural fractures, which provides flow conduits to the wellbore, perhaps via induced fractures (Bust *et al.*, 2013). Second, there is intergranular porosity, which contains electrochemically-bound water, capillary bound water and free fluids that are mostly presumed to comprise gas (Bust *et al.*, 2013). Intergranular porosity is non-zero in the effective porosity system only if the shale is not electrochemically and compositionally perfect: it is always non-zero in the total porosity system. Third, there is porosity due to the organic content (Bust *et al.*, 2013). This “organic porosity” sits much below the micro-porosity range (Bust *et al.*, 2013). A useful Petrophysical model has to consider the porosity created by gas desorption in the kerogen (Bust *et al.*, 2013). This is important because this created porosity can account for up to 50% of the kerogen volume (Elgmati *et al.*, 2011; Bust *et al.*, 2013). Kerogen porosity varies with thermal maturity so any model that takes into account kerogen porosity will have to define kerogen properties in relation to the degree of thermal maturity (Bust *et al.*, 2013). However, a model that differentiates between intrakerogen pore space and the kerogen itself will need to consider the organic porosity as possibly part of the total interconnected porosity (Bust *et*

al., 2013). The challenge is compounded by the observation that porosity could occur mostly within kerogen in some shales and mostly within intergranular pore space in others (Sondergeld *et al.*, 2010a; Bust *et al.*, 2013). The high clay mineral content in shale gas reservoirs means that conventional reservoir logging methods require large corrections to log responses (Bust *et al.*, 2013). The distribution of organic and inorganic porosity needs to be related to the natural fracture network. In the Barnett shale, for example, in situ porosity measurements derived from conventional logging methods such as neutron-density can be challenged because of the varying lithological and organic facies of the intervals. As a result of this, core analysis is heavily relied upon to obtain reservoir porosity and permeability porosity (Montgomery *et al.*, 2005).

2.3.3. Pressure

Higher pressure increases the amount of free gas stored in pores and fractures and increases the amount of gas adsorbed on organic materials. Different gases have different adsorption and desorption isotherms. Thus the produced gas composition may change over time during pressure drawdown (King, 2010). High-pressure shale wells may experience delays in recovery of adsorbed gas, but the higher pressure provides significant free gas and positive cash flow at the early stages (Myers, 2008).

2.3.4. Thermal Maturation

The maturity of the shales in terms of exploration criteria is more flexible, because recent biogenic shales can be expected to have lower vitrinite reflectance (%Ro <0.65). Older shales where recent groundwaters have introduced bacteria may have any level of maturity. However, the presence of oil in the shales lowers gas permeability significantly - Less mature shale tend to have a Ro value less than 1.4 and may reach gas energy values approximately between 1100 to 1300 BTU/Mcf, but hydrocarbon liquids will be present which can result in relative permeability problems, hence flow can be reduced except in cases where rock permeability is significantly higher (Jarvie *et al.*, 2004). Even the oil window shales are now being tested in America by some companies to produce shale oil rather than gas. Any cut-off by virtue of the thickness of shales is probably dependant on whether other stacked shale formations could be considered prospective, either above or below, and the poroperm characteristics of these shale formations.

For example, dry gas reservoirs with 1000 BTU/Mcf exists where vitrinite reflectance maturities are more significant than 1.4 to 2.0 while some reservoirs require Ro values of about 2.2 to

reach the 1000 BTU/Mcf level (King, 2010). Considering information from exploration of the Preese-Hall 1 well, the maturity of tested section as defined by Tmax and vitrinite reflectance ranged from the upper part of the oil window (Tmax~450c) in the Marsdenian Upper Shales (5000ft; 1524m) through to dry gas in the Brigantian Lower Bowland Shale (Tmax>470c) (Clarke, Bustin and Turner, 2014). In the Grange-Hill well, the maturity of the tested section ranges from the upper part of the oil window (Tmax c 450c) in the Crossdale Mudstone (5000ft; 1524m) through to dry gas in the upper part of the Brigantian well, Tmax ranges from ~ 450 to 460deg celsius through the same stratigraphic interval and lies mainly within the upper oil window (Clarke *et al.*, 2018). For Grange-Hill 1z and Preese-Hall 1, measured Ro values are compared with calculated vitrinite reflectance from the Tmax values (Clarke *et al.*, 2018). The Tmax values have been converted in Equation 1 to Ro (calc.) using the equation of (Jarvie *et al.*, 2001) which although not calibrated for the Bowland shale provides a semi-quantitative comparison between the Tmax data and measured vitrinite reflectance (Clarke *et al.*, 2018).

$$\%R_o(calc) = 0.0180T_{max} - 7.16$$

Equation 1

Where %Ro = Thermal Maturity
Tmax = temperature at which maximum rate of hydrocarbon generation occurs in a kerogen sample during pyrolysis

Mostly, the kerogen is too mature to type by Rock-Eval pyrolysis in the Bowland shale. The maturity of the Bowland-Hodder shales is a function of burial depth, heat flow and time, but subsequent uplift adds complication (Andrews, 2013). Where they have been buried to sufficient depth for the organic material to generate gas, the Bowland-Hodder shales have the potential to form a shale gas resource analogous to producing shale gas provinces of North America (e.g. Barnett and Marcellus Shale) (Andrews, 2013). In the Bowland shale study, shales are considered mature for gas generation (vitrinite reflectance > 1.1%Ro) at depths greater than 9500ft (2900m) (where there has been minimal uplift) (Andrews, 2013). Petrographically, there is significant humic material (Type III), however the wetness of the gas at the organically less mature top of the sampled section implies Type I/II kerogen which are less obvious microscopically (Clarke, Bustin and Turner, 2014). Potential unconventional reservoir rocks intersected in the Grange-Hill 1z, Preese Hall 1 and Becconsall 1z wells are for the most part, too mature to infer kerogen type from pyrolysis data. Organic petrology suggests that the organic matter is mainly type II/III (Clarke *et al.*, 2018). However, at such maturities, macerals that correspond to Type I and II kerogens are difficult to recognize, which

skews the observation data towards the macerals vitrinite, semifusinite and inertinite that corresponds to Type III and Type IV kerogen (Clarke *et al.*, 2018).

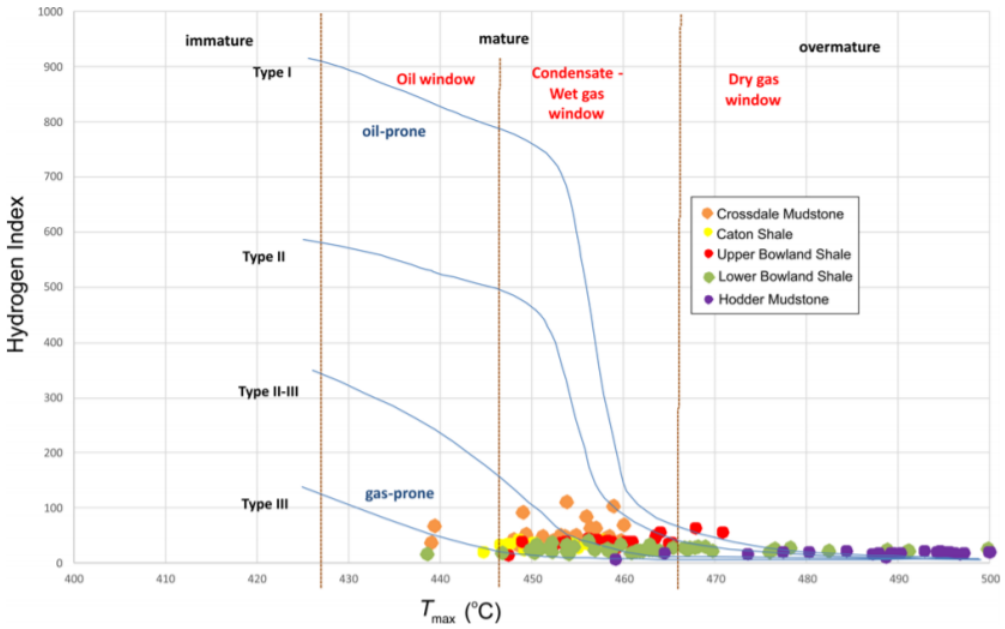

Figure 2-3: Cross plot of hydrogen index and Tmax from Rock Eval pyrolysis for strata in the Becconsall 1z well.

Over the maturity range of the shales (Ro = 1.0 to 2.0), the Tmax data at depths greater than 6500ft underestimated maturity relative to vitrinite reflectance. This discrepancy is due to wide scatter of the Tmax data at higher maturity values such that there is no correlation between Tmax and Ro (Clarke *et al.*, 2018). The data from Preese-Hall 1 and Grange-Hill 1z show higher levels of maturity (Ro > 2.0 in the Bowland Shale) when compared to Thistleton 1. This has been attributed to major variations in the thickness of Carboniferous sediments in these wells even though they are relatively close to each other (Clarke *et al.*, 2018). Variation in maturity is consistent with the variation in depth of burial and uplift in the basin and to a lesser extent the variation in heat flow. Jarvie *et al.*, 2004 outlined a Tmax based calculation of R_0 Table 2-4.

Table 2-4: Calculated Ro and corresponding Tmax values, after Jarvie et al.*, 2004).*

%R_o	**T_{max} (°C)**	**Maturity**
0.60	431	Early Mature
0.90	448	Peak Oil Generation
1.00 1.10 1.20 1.30	453 459 464 470	Earliest Condensate-Gas Window
1.40 1.70 2.00	476 492 509	Dry Gas Window

(Andrews, 2013) stated that R_0 = 1.0 to 3.5 represents the gas window, and the minimum values of R_0 range from 2.0 ((Wright, 2016). to 1.1 (Andrews, 2013). There is also a broad consensus that R_0 should be between 1.1-1.4, but ideally should be more significant than 1.4 (Jarvie *et al.*, 2004; Jarvie, 2012b; Rezaee, 2015; Waldo, 2015).

2.3.5. Thickness

Increasing total and net thickness of shale increases its total gas storage sites, and the likelihood of fracture treatment localizing within the shale. The top of the Bowland-Hodder unit lies at depths of up to 16000ft (4750m) across the assessment area Figure 2-4 with the greatest depth of burial occurring in the Bowland basin of Lancashire beneath the permo-triassic Cheshire basin and in eastern Humberside. The thickness of the Bowland-Hodder unit mirrors the regional Early Carboniferous structural configuration, with greatly expanded sections in the syn-rift basins.

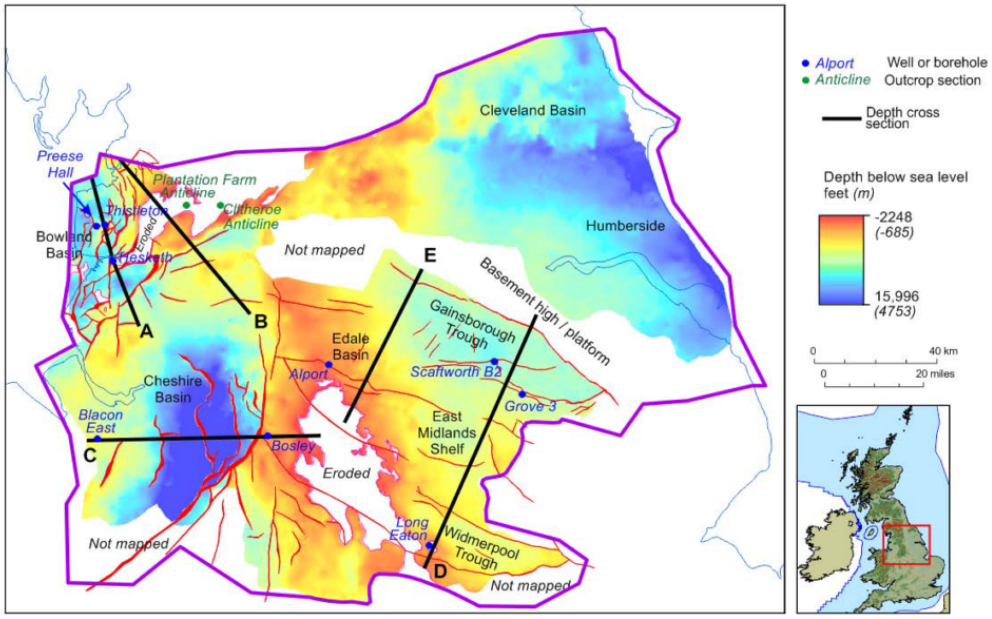

Figure 2-4: Depth (ft.) to the top of the Bowland-Hodder unit, Central Britain (Andrews, 2013)

From outcrop data, the Bowland basin is estimated to contain up to 880ft (268m) of Bowland shale and 3000ft (900m) of Hodder Mudstone (Andrews, 2013). In the subsurface, seismic interpretation suggests the complete Bowland-Hodder unit reaches a thickness of up to 6300ft (1900m) in the same basin (Andrews, 2013). This may be a conservative approximation, as the Tournaisan-Visean thicknesses has thickness of 13000ft (4000m) and 8200ft (2500m) respectively (although both apparently include the Courceyan-Chatburn Limestone Group and are thus not directly comparable to the Bowland-Hodder unit) (Andrews, 2013). The Thistleton 1 well drilled 2911ft. (887m) of the Bowland-Hodder unit, but terminated in Brigantian-aged shales and sandstones and the lower part of the unit was not reached (Andrews, 2013). (Bowker, 2007) suggested that 30m is minimum net thickness needed for the Barnett to be economic. However, more recent production data from Zou, 2013 suggests that the minimum net accumulation is 15m. Plays with > 15m net thickness should be sought and the conventional wisdom of "the thicker the better" still applies (Jarvie, 2012b; Andrews, 2013). Some of the important factors that makes Barnett a good exploration model is shown in Table 2-5.

Table 2-5: Summary of the factors that makes the Barnett a good exploration model (Wright, 2016).

Factors	**Barnett**
TOC	4wt%
Kerogen Type	Type II
HI_o	392-475
Thermal Maturity (%Ro)	1.45
Porosity	6%
Net Shale Thickness	> 15m economic
Mineralogy	35% Clay
Structure	Stable foreland basin, few major structures

In the Bowland shale study, shales are considered mature for gas generation (vitrinite reflectance > 1.1%) at depths greater than 9500 ft (2900 m) (where there has been minimal uplift) (Andrews, 2013). However, Central Britain has experienced a complex tectonic history and rocks here have been uplifted and partially eroded at least once since Carboniferous times (Andrews, 2013). Because of this, the present day depth to the top of the gas window is dependent on the amount of uplift, and can occur significantly shallower than 9500 ft (Andrews, 2013). In addition, the total volume of potentially productive shale in central Britain was estimated using a 3D geological model generated using seismic mapping, integrated with outcrop and deep borehole information (Andrews, 2013). The volume was truncated upwards at a depth of 5000 ft (1500 m) below land surface (a suggested US upper limit for thermogenic shale gas production) or the depth at which the shale is mature for gas generation (Andrews, 2013).

2.3.6. In-situ Stresses and Anisotropy

Accurate geomechanical information about the rock and its variation through the shale are important because stresses along the wellbore can control fracture initiation and fracture development ((Britt and Schoeffler, 2009). Tectonic forces drive stresses along the wellbore, depth of burial, formation thickness, uplifts, changes in rock fabric, and stresses generated by fracturing or during production. The fracture size and the path direction of large volumes of water may be the biggest causes of stress changes in the reservoir (George E King, 2010) Micro seismic measurements can help suggest real-time stress changes along the wellbore during fracturing, often enough to change fracture direction and greatly influence production (George E King, 2010). (Clarke *et al.*, 2018) also found that lithological composition is an important control on TOC and the highest TOC lithologies plot consistently near the clastic

line. The pervasive occurrence of TOC contents of up to 3% throughout the shale stratigraphy in suggests a background sapropelic input from the water column. Consequently, the relationship between higher TOC and lithologies with higher clastic contents may indicate an additional input of terrestrially derived type III kerogen. Such influxes may be from adjacent emergent sediment source areas during periods of low stands.

This alternating pattern was also suggested by Gross *et al.*, 2015 where they identified alternations of dominantly sapropelic and dominantly terrestrial source rocks in their Bowland shale study in the Widmerpool basin. Dominance of organic material of marine origin is associated with maximum flooding surfaces, while terrestrial material is more abundant in parts of the succession deposited at times of marine low stand and is dominant in turbiditic sediments.

2.3.7. Mineralogy and Brittleness

The mineralogy of a shale directly impacts the mechanical properties of the shale and the effectiveness of artificial fracture hence the improvement of the permeability of the shale (Wright, 2016). Shales with high Young's Modulus and low Poisson's ratio are brittle (usually because increased silica and sometimes detrital calcite) and are easily fractured, opening flow paths that may remain stable (even when mostly un-propped) after relieving fracturing pressure and gas starts to flow (Rickman *et al.*, 2008). Clay content should be low (<40% by volume), as a high clay content results in a more ductile response to fracturing with the shale deforming in a flexible manner instead of fracturing (Waldo, 2015). Shales that are ductile may, therefore, require more proppant and deeper high-temperature shales that may withstand loads outside the norm (LaFollette and Carman, 2010). Mineralogy is also related to depositional environments - for example, marine deposited shales tend to have a lower clay content and hence a higher brittle mineral content (Rezaee, 2015). The ease of fracture of shale also relates to the degree of overpressure in the formation. (Wright, 2016).

Britt and Schoeffler, 2009 conducted a test to observe the relationship between dynamic (log derived) and static (core derived) Young's Modulus, and this showed a strong correlation between prospective gas shales and tight gas sandstone reservoirs (Figure 2-5) corroborating with the geological description of gas "shales" as very fine-grained sandstones or siltstones with the description of "shale" only as a particle size indicator (King, 2010). The non-prospective shales did not fit the model and are mostly high clay formations with a low static modulus and scattered dynamic modulus.

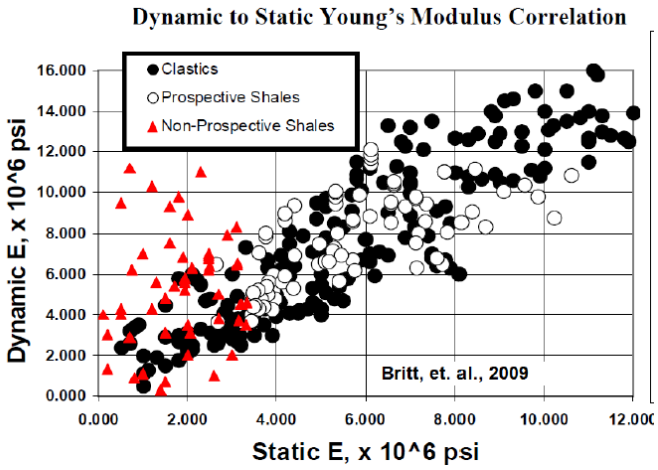

Figure 2-5: Dynamic to Static Young's Modulus Correlation (Britt and Schoeffler, 2009; King, 2010)

Within the leading shale gas producing areas of the US, brittle mineral content is usually higher than 50%, and clay content is less than 50% (Wright, 2016) Figure 2-6. A study of one well by Bruner and Smosna, 2011 concluded that the Barnett has a low clay fraction, with no sample greater than 40% clay. This agrees with the averaged data presented in Bowker, 2003; Waldo, 2015 that the primary producing facies of the Barnett is volumetrically composed of 35-50% quartz and less than 35% clay. Bowker, 2003 concluded that there is only minor calcite and dolomite content. In addition, a study by Jarvie et al., 2007 found that it contains 40-60% quartz, 40-60% clay and highly variable calcite content. Spears and Jackson, 2009 also provided the average mineralogical composition for a typical Barnett shale Table 2-6.

Table 2-6: Average Mineralogical Composition in the Barnett Shale (Spears and Jackson, 2009)

Mineral	Average Composition (wt. %)
Quartz	45
Illite	27
Calcite and Dolomite	8
Feldspar	7
Organic Minerals	5
Pyrite	5
Siderite	3

Using the Barnett as an exploration model, a successful shale gas play should have a relative brittleness greater than 40%. The Barnett shale is generally characterised as an organic rich, siliceous shale with variable amounts of limestone, minor dolomite, and a scattering of minerals like pyrite and apatite (Montgomery *et al.*, 2005).

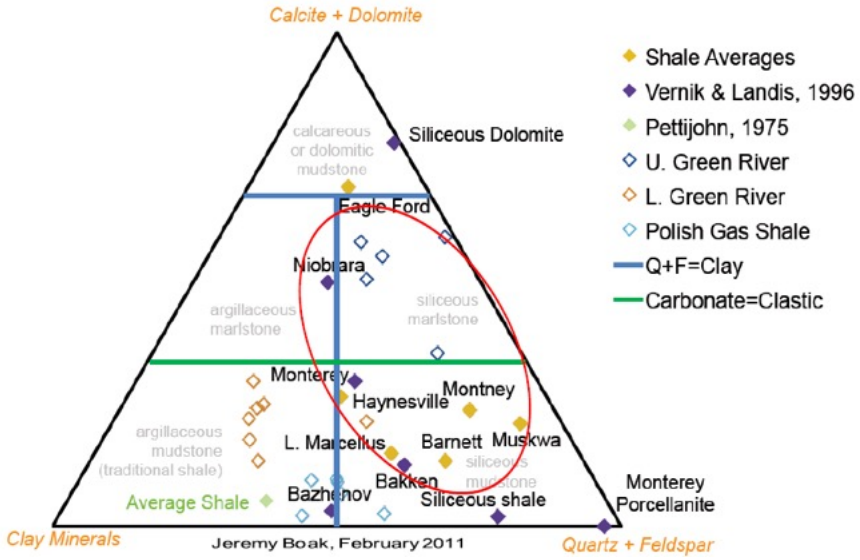

Figure 2-6: Ternary diagram of selected shales. Note how US shales generally have >50% brittle mineral content, averages of US shales fall in the red circle (Waldo, 2015).

The clay mineralogy in the Bowland shale is dominated by illite, kaolinite and chlorite in decreasing order. and the illite contains only minor amounts of expandable water-sensitive clays (<5%) (Clarke *et al.*, 2018). The vertical distributions are shown in Figure 2-7.

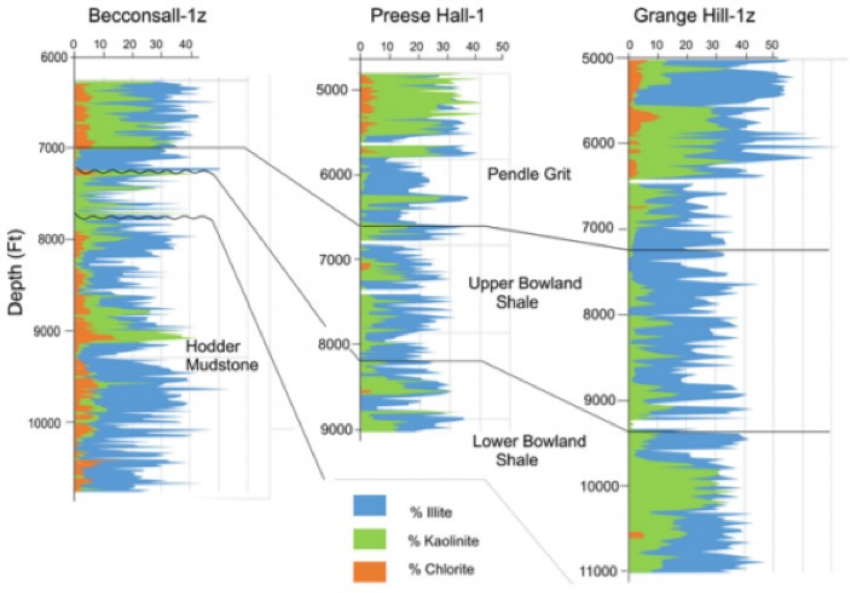

Figure 2-7: The vertical distribution of the three main clay mineral species in the exploration wells studied (Clarke *et al.*, 2018).

In Figure 2-7, kaolinite shows a marked increase from the Upper Bowland Shale into the Pendle Grit sequence in Grange Hill and Preese Hall (Clarke *et al.*, 2018). The close link with a major change in facies and increased non-marine influence suggests that much of the kaolinite is detrital in origin and derived from the weathered northerly hinterland (Clarke *et al.*, 2018). The clay mineral variations also show spatial variations, for e.g. the total abundance of clay minerals increases from Grange Hill 1z in the north to Becconsall 1z in the south Figure 2-8, this also reflects the facies variations across the basin (Clarke *et al.*, 2018).

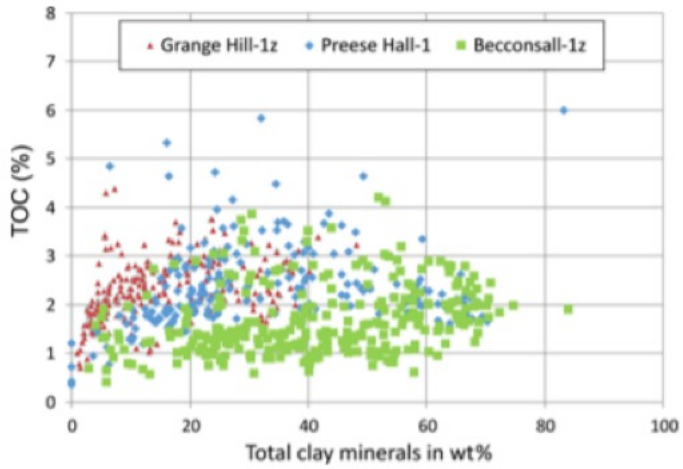

Figure 2-8: TOC vs total clay minerals (wt. %). The general trend indicates an increase in clay content southwards along the depositional slope (Clarke *et al.*, 2018).

The higher illite content at Becconsall-1z results from the greater abundance of hemipelagic facies in the Hodder Mudstone interval (Clarke *et al.*, 2018). The reason for the greater abundance of kaolinite in the north and stratigraphically higher sections to indicate its coarser grain size relative to illite, which is more widely dispersed in the basin (Clarke *et al.*, 2018).

A major challenge for petro-physical evaluation regarding mineralogy is how to evaluate standard log responses such as density, neutron porosity, sonic transit time in the presence of heterogeneous inorganic solids and organic matter (Bust *et al.*, 2013). A clay mineral volume fraction is important and many shale indicators over estimate this fraction (Bust *et al.*, 2013). The problems can be compounded when there are disparities between core analyses from different laboratories and log delivered from different logging companies (Ramirez *et al.*, 2011; Bust *et al.*, 2013). Multi-mineral petro-physical models is often viewed as a possible solution to this challenge as it can provide non-unique results that require tuning of the input parameters to core data (Bust *et al.*, 2013). This problem highlights the importance of X-ray diffraction (XRD) and X-ray fluorescence (XRF) in support of log analysis (Bust *et al.*, 2013).

These data are especially important given the presence of heavy minerals such as pyrite (Bust *et al.*, 2013). The classical porosity-evaluation concept of a matrix and clay-mineral system breaks down in shale gas formations, where grains have to be considered collectively and kerogen is present (Bust *et al.*, 2013). This makes it difficult to identify rock types, which are needed for prioritizing candidate intervals for hydraulic fracturing (Bust *et al.*, 2013). A pertinent aspect of mineralogical characterization is the recognition of geologically-driven mineralogical trends across a shale system (e.g. (Mullen, 2010); this can provide an overprint for the occurrence of different electro lithofacies (Bust *et al.*, 2013).Full mineralogy modelling and characterization of shale gas reservoirs can be achieved through the integration of standard nuclear, electrical and acoustic logs with geochemical measurements to solve for all the significant minerals present in the shale gas formation (Bust *et al.*, 2013). The fraction of organic matter can be estimated either independently using simple correlations with other logging curves (inputted into the mineral model) (Bust *et al.*, 2013). Validation of the mineral model is achieved through the direct comparison of the resulting elemental composition with core XRD and XRF. Achieving a match to core may involve adjusting mineral end points and other input parameters, as well as refining the model specifications (Bust *et al.*, 2013). The model complexity is based not only on the mineralogy of the shale gas reservoir but also on the number of log curves available, taking account of the projected optimization of the data acquisition program during the drilling of non-key wells (Bust *et al.*, 2013). The output from the analysis of key well data will be the input parameters and assumptions for the mineralogical evaluation of non-key wells (Bust *et al.*, 2013). The output has to be useful in rock typing – for example, (Kale, Rai and Sondergeld, 2010) used a threefold core derived rock typing scheme for the Barnett shale with calcite content, porosity and total organic carbon as discriminators (Bust *et al.*, 2013). When rock typing is not possible, another way is to construct a variable grain-density curve from a geochemical log calibrated to XRD and XRF (Querein, 2010). An option to circumnavigate the problem is to use NMR as it exhibits reduced dependence on grain properties (Jacobi *et al.*, 2008). However, NMR primarily benefits porosity but the need for a mineralogical characterization remains paramount (Bust *et al.*, 2013).

2.3.8. Permeability

Shale permeability is dependent on matrix and fracture permeability. Natural fractures dominate early flow and are the predominant flow path in production. Matrix permeability influences the rate of produced gas decline and ultimate recovery. The lower the matrix permeability, the more hydraulic fracture contact area is required (Bello, Wattenbarger and Texas, 2008). However, fracture permeability, when present, dominates the effective gas

delivery permeability of the formation (King, 2010). Natural fractures, even when closed or partially/nearly fully mineralized, are typically one to three orders of magnitude higher permeability than shale matrix permeability (King, 2010). The importance of matrix permeability has been previously ignored, citing that the pore throats in most shales are too small to act as active flow paths for methane within economic time (Wang and Reed, 2009; George E King, 2010).

2.3.9. Total Organic Carbon

Total Organic Carbon is a measure of the organic carbon present in a sediment sample and is split into Kerogen and Bitumen however it is not a sole measure of its generation potential (Ruble, Drozd and Heck, 2012)(Jarvie, 2012b). In a nutshell, if there is no kerogen, there is no source rock within the shale system (Bust *et al.*, 2013). This simple conclusion makes TOC the most important parameter in shale gas evaluation (Bust *et al.*, 2013).
(Andrews, 2013) stated that organic content of the Bowland-Hodder shales is typically in the range 1-3% but can reach 8%. Kerogen forms part of the matrix (Figure *2-9*) and in terms of petro-physical analysis, the main features include its low density (close to the density of water), long travel time, high neutron porosity, and high resistivity (Glorioso and Rattia, 2012). Hence it is essential to establish kerogen content in weight and volume (Glorioso and Rattia, 2012).

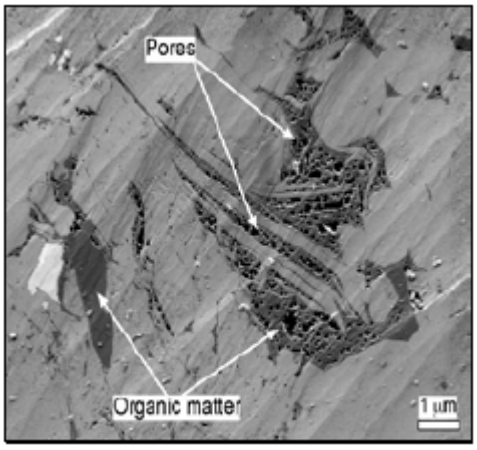

Figure 2-9: SEM showing pores in organic matter. This can be considered secondary porosity as it results after maturity and subsequent expulsion of hydrocarbons (Glorioso and Rattia, 2012).

From the volume of kerogen, it is possible to derive the TOC (Glorioso and Rattia, 2012). To establish the source potential of shales, it is not only important to know the original kerogen content; the present volume of kerogen through petro-physical assessment of shale gas

reservoirs is also as important to enable the estimation of adsorbed gas content and porosity with sufficient accuracy (Glorioso and Rattia, 2012). Initially, shale gas exploration will target high TOC shales and Accordingly (King, 2010), described organic richness as an "important" need (Figure 2-1). TOC values are highly variable throughout a source rock, primarily due to facies differences and thermal maturity (Wright, 2016).

There is a broad consensus that TOC values higher than equal to 2wt% are regarded as the minimum to make a shale viable exploration target (Waldo, 2015) (Table 2-2). In the Bowland Shale, the total organic carbon content varies through the stratigraphy (Clarke, Bustin and Turner, 2014). The average total organic carbon content of the cored intervals ranges from 1 to 7% and averages 2.65% and in the cutting samples average 2.2% (Clarke, Bustin and Turner, 2014). The TOC content of the Bowland shale varies mainly between 2 and 2.5wt% (Clarke *et al.*, 2018). The highest values (up about 5wt% TOC) occur in marine bands associated with the Caton Shale and Crossdale mudstone (Clarke *et al.*, 2018). Overall, the variation in TOC in the Bowland Shale is similar to that found in other Mississippian Shale in the Pennine Province (Andrews, 2013, Gross 2015). Variations in TOC in the cuttings and core samples in the downhole profiles of the Preese-Hall 1, Becconsall -1z and Grange Hill 1z are plotted in Figure 2-10.

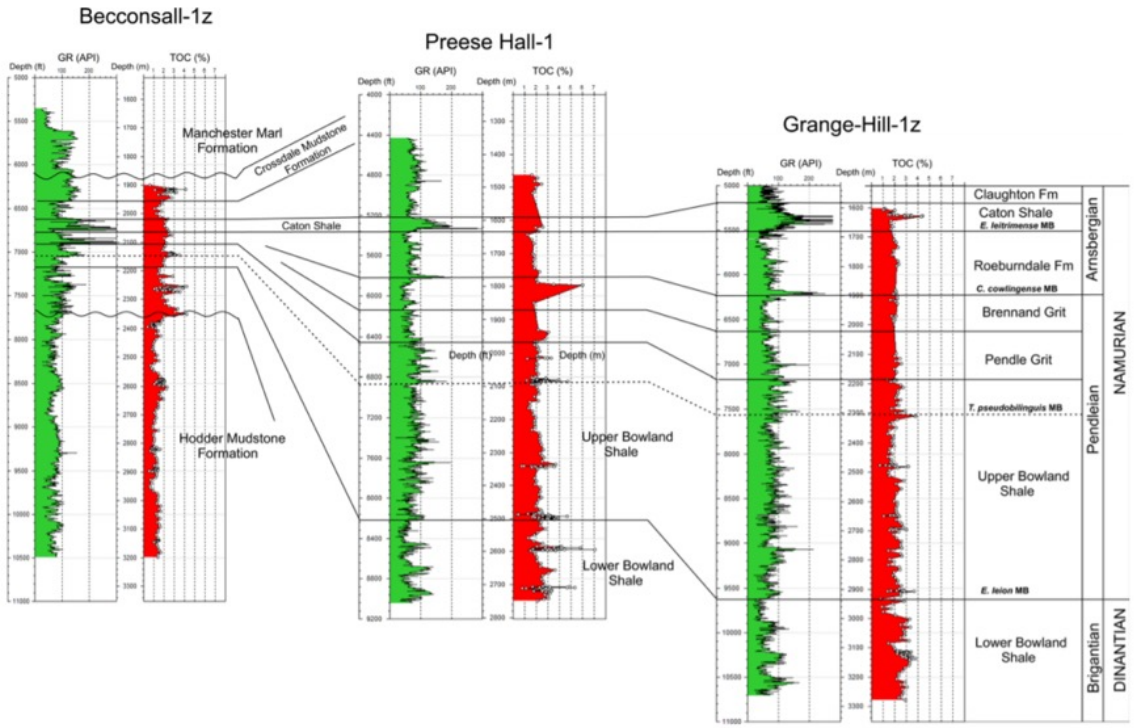

Figure 2-10: Stratigraphic plots of TOC (%) and gamma log profiles for Becconsall 1z, Preese Hall 1 and Grange Hill 1z. The datum is the base of Caton Shale.

Jarvie, 2012b) presented a minimum of greater than equal to 1wt% by accounting for varying degrees of maturity and facies differences. Table 2-7 shows average values reported in some shale gas reservoirs.

The average total organic carbon (TOC) in the Barnett shale is 3.1–5.1%. As the value of TOC depends on the thermal maturity of the shale it can be as high as 11–13% in some locations. The porosity of the shale ranges from 3.8 to 6.0%.

Table 2-7: TOC weight percentage of some shale gas reservoirs (Glorioso and Rattia, 2012)

Marcellus	**Barnett**	**Haynesville**	**Fayetteville**	**Vaca-Muerta**
Argillaceous mudstone	Siliceous mudstone	Argillaceous calcareous mudstone	Siliceous mudstone	Argillaceous siliceous and calcareous mudstone
Average TOC: 6	Average TOC: 5	Average TOC: 4	Average TOC: 4	Average TOC: 2.5 - 3.5

A number of core and log-based models have been developed for TOC estimation (Bust *et al.*, 2013). Empirical relationships between core-derived TOC and log curves (e.g. density, resistivity, and uranium content) have proved to be robust in creating a continuous estimate of TOC along the logged interval of the wellbore (Bust *et al.*, 2013). For example, (Schmoker, 1981) computed organic content from density logs based on (I). Correlation between organic content and pyrite content (II). The kerogen porosity being grouped with the kerogen. It was assumed that there was no free gas and that all the gas was in the kerogen (Schmoker, 1981). TOC was expressed as function of the difference between a reference density log response in the absence of kerogen and the density log response (Bust *et al.*, 2013). The problems is in the assumed constancy of total porosity over the interval and sensitivity of the density too to borehole rugosity (Bust *et al.*, 2013). Other drawback is the assumption that no large variations in other parameters exists to affect the log readings (Bust *et al.*, 2013). For example, the presence of pyrite in sufficient volumes may mask the effect of organic matter on the density and resistivity logs (Passey *et al.*, 2010; Bust *et al.*, 2013). The presence of apatite in marine source rocks, may also create an erroneous relationship between TOC and uranium content (Jacobi *et al.*, 2008; Bust *et al.*, 2013). An example of how litho-facies can affect empirical methods discussed is seen in *Figure 2-11*.

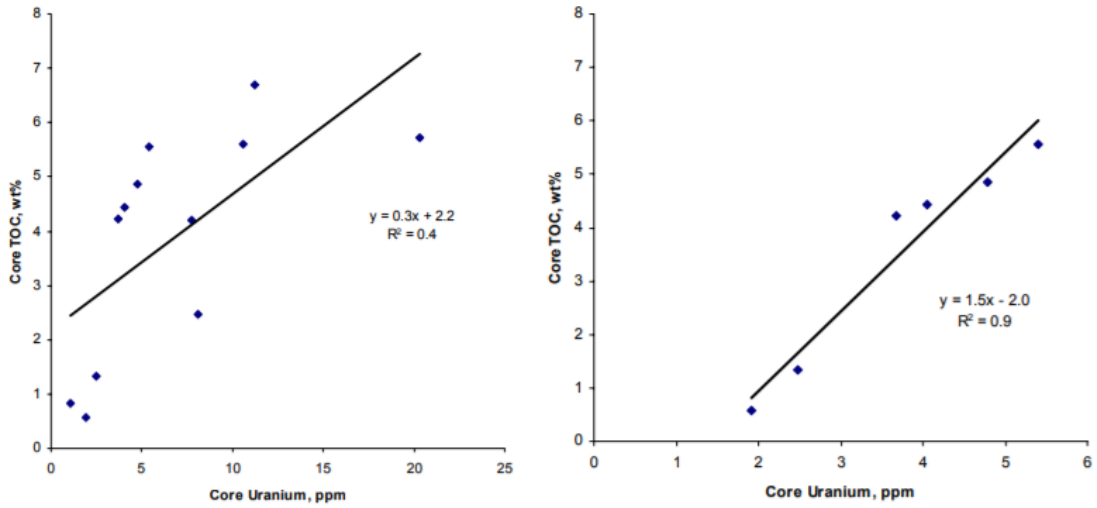

Figure 2-11: Correlation between weight percent of TOC and ppm uranium content for core data from a Barnett well with all cores (left) and excluding cores with significant amounts of apatite (right) (Rezaee, 2015).

Uranium has been proposed to exhibit a positive linear relationship with the total organic carbon for some marine source rocks (Fertl and Rieke III, 1980)*. However, the uranium concentrated in organogenic and authigenic calcium phosphate, such as apatite, which is a common mineral that contributes to the phosphatic content of organic marine sections such as the Barnett, must be compensated for before the empirical relationship yields a favourable results* (Kochenov and Baturin, 2002)*.* Recent advances in pulsed-neutron mineralogy offer a possible solution to this problem (Jacobi *et al.*, 2008; Bust *et al.*, 2013). *In addition to the mineral apatite, both pyrite and siderite found in many litho-facies can elevate rock, grain densities that could also present a challenge when using bulk density as a method for determining the TOC of shale gas intervals.* (Schmoker, 1981)*, observed large density contrasts between organic and inorganic formations and suggested the use of bulk density logs for TOC evaluation. However, it was realised that density logs can only be used if porosity, fluid, TOC density and matrix density do not significantly vary over the interval of interest and empirical corrections are made to remove density anomalies caused by pyrite.* To infer the TOC empirically, without accounting for facies and mineralogical factors causes great uncertainty with estimates of the total gas value using the (Montgomery *et al.*, 2005). Because of the potential effect of these mineralogy and litho-facies variances, measuring in situ carbon from the formation using a geochemical logging sonde should be preferred for deriving a TOC estimate (Jacobi *et al.*, 2008). The inability to make a direct measurement of TOC from the wellbore and thus the reliance on empirical approaches is one of the reasons why core analysis is used more readily for determining TOC and estimating the maturation of source rocks (Montgomery *et al.*, 2005). TOC is calculated from geochemical data in key wells,

having first allocated part of the measured carbon content to the inorganic carbon components within the shale gas formation. The results of the geochemical log analysis can be verified through the use of acoustic and resistivity image logs and also through NMR-derived TOC (Jacobi *et al.*, 2008; Bust *et al.*, 2013). Irrespective of the technique used, calibration to laboratory measured TOC is most important (Jacobi *et al.*, 2008; Bust *et al.*, 2013). Different calibration baselines may also be required to zone the reservoirs because of variable mineralogy and water salinity (Jacobi *et al.*, 2008; Bust *et al.*, 2013). The fact that discrete baselines can be established over extended intervals supports the concept of a scenario approach to shale gas evaluation (Jacobi *et al.*, 2008; Bust *et al.*, 2013). For example, (Passey *et al.*, 1990) used an overlay method involving sonic and resistivity logs to obtain TOC calibrated to core sample data. Both the standard-log approaches and the pulsed-neutron methods should be investigated in key wells. The target deliverable is a methodology that can be used in conjunction with standard logs in other wells. An important requirement is to identify the relationship between TOC and solid kerogen volume so that an appropriate porosity model can be developed (Guidry and Walsh, 1993). There are two main methodologies for the in-situ TOC determination in the shale gas layers: the pulsed neutron mineralogy tool and the Passey DeltaLogR methodology (Rezaee, 2015);

2.3.9.1. Pulsed Neutron Mineralogy Tool

The pulsed neutron mineralogy tool can determine the amount of carbon in the formation (Rezaee, 2015). The most important matrix minerals containing carbon are calcite, dolomite, and siderite (Rezaee, 2015). Therefore the excess carbon can then be interpreted as organic carbon, hydrocarbon, coal, or organic matter using the following relationship (Jacobi *et al.*, 2009) (Equation 2);

$$C_{TOC} = C_{Measured} - C_{Calcite} - C_{Dolomite} - C_{Siderite}$$

Equation 2 (Jacobi *et al.*, 2009)

Where

Cmeasured = measured amount of carbon

Ccalcite = amount of carbon in calcite matrix

Ccalcite = amount of carbon in dolomite matrix

Csiderite = amount of carbon in siderite matrix

The elemental ratio of silicon to carbon determines whether the excess carbon is coal or not (Rezaee, 2015). To determine whether the excess carbon is oil or organic matter, a cut-off value for uranium is used (Rezaee, 2015). If the uranium is above the minimum value, the

excess carbon is assumed to be organic matter; otherwise it should be hydrocarbon (Rezaee, 2015). The minimum uranium cut-off is from 4 to 7 ppm for most shale gas layers (Pemper *et al.*, 2009). Measuring in situ carbon for TOC estimation using pulsed neutron mineralogy tool is preferable compared to other techniques where TOC is determined from well log data (Rezaee, 2015).

2.3.9.2. Passey DeltaLogR Methodology

This is a practical methodology first developed by (Passey *et al.*, 1990) for identifying and calculating TOC in organic rich rocks using well logs. This method employs overlaying of a properly scaled porosity log (generally the sonic transit time curve) on a resistivity curve (preferably from a deep reading resistivity tool) and then calculating the separation between these two curves by defining a baseline (Rezaee, 2015) Equation 3:

$$\Delta \log R = \log_{10}\left(\frac{R}{R_{baseline}}\right) + 0.02 * (\Delta t - \Delta t_{baseline})$$

Equation 3 (Rezaee, 2015)

Where

Δ *logR = Separation between resistivity and sonic, log scale*

Δt = Sonic transit time, microseconds/ft

$\Delta t_{baseline}$ = Baseline sonic transit time, microseconds/ft

R = Resistivity, ohm-meter

$R_{baseline}$ = Baseline resistivity, ohm-meter

Baseline is determined when sonic and resistivity directly overlay each other or just track each other (Rezaee, 2015). According to Passey's method, this condition will exist at the organic-lean interval (Rezaee, 2015). The amount of TOC can then be determined from the following relationship by knowing the level of maturity (LOM) (Passey *et al.*, 1990) Equation 4;

$$TOC = \Delta logR * 10^{(2.297 - 0.1688 * LOM)}$$

Equation 4 (Passey *et al.*, 1990)

Although this methodology is used extensively for TOC determination in the shale layers, there are many uncertainties in its evaluation (Rezaee, 2015). This method requires similar clay minerals or similar conductive minerals (e.g., pyrite) in both organic-lean shale (baseline) and the organic-rich interval (Rezaee, 2015). Extensive vertical heterogeneity of the shale layers may result in very high uncertainty for the calculated TOC (Rezaee, 2015). Moreover, this method requires knowledge of the LOM for converting the apparent ΔlogR to a quantitative TOC (Rezaee, 2015). In exploration wells the LOM may not be known or may also change with depth (Pemper *et al.*, 2009; Rezaee, 2015). According to the ΔlogR technique, an increase in the resistivity and sonic transit time is also a function of hydrocarbon saturation

(Rezaee, 2015). (Passey *et al.*, 1990) concluded that an increase in the amount of hydrocarbon at the higher thermal maturity level could be correlated to the present TOC content of the rock (Rezaee, 2015). However, this assumption seems not to be correct all of the time (Rezaee, 2015).

A summary of other methods is shown in Table *2-8* and Table *2-9*. In particular the LECO method of estimating total organic carbon measures TOC values by combusting the organic carbon and measuring the resulting carbon dioxide produced in a LECO carbon analyser. Samples are treated prior to analysis to remove the inorganic carbon (carbonate) from the rock. The sample is then combusted in the presence of excess oxygen, allowing carbon dioxide to form from the free (organic) carbon in the rock. The amount of carbon dioxide is directly proportional to the amount of organic carbon or the TOC of the rock. The TOC measured by the LECO method does not include a measurement of the free hydrocarbons present in the sample. The free hydrocarbons would be volatized when samples are dried after acid treatment is performed to remove the inorganic carbonate minerals. Thus, if a sample has a high free hydrocarbon content, the LECO TOC value will be smaller than a Rock-Eval TOC value, which includes free hydrocarbons (S1) in the TOC calculation. However, with the ROCK EVAL pyrolysis method, Pyrolysis is the decomposition of organic matter by heating in the absence of oxygen. This method can be used to measure organic richness and maturity of source rocks. Rock Eval Pyrolysis has completely replaced the LECO method

S1: free hydrocarbons present in the sample before analysis
S2: the volume of hydrocarbons that formed during thermal pyrolysis
S3: the carbon dioxide yield during thermal breakdown of kerogen
S4: the residual carbon content of the sample

Table 2-8: TOC measurement methods limitation (using rock sample)(Ma, Zee Y; Holditch, 2016)

Methods	Limitation
Filter Acidification	Some organic carbon can be lost by hydrolysis (Ma, Zee Y; Holditch, 2016).
Nonfilter Acidification	Oven corrosion
Total minus coulometric	Slow, large (split) sample (Ma, Zee Y; Holditch, 2016)
Rock-Eval	Incomplete combustion for models prior to v.6 (Ma, Zee Y; Holditch, 2016)
LECO Method	Requires lab core analysis; no response for inert carbon (Ma, Zee Y; Holditch, 2016)
Drifts	Oil-based mud must be removed; kerogen type and maturity affect absorption (Ma, Zee Y; Holditch, 2016).

Table 2-9: TOC measurement method limitations (wireline)(Ma, Zee Y; Holditch, 2016)

Methods	Limitation
Gamma Ray Log	Responds mainly to U, not kerogen; depends on many factors, e.g. Eh(redox potential)/pH (Schmoker, 1981).
Spectral Gamma Ray	Local calibration; uranium minerals interfere, e.g. phosphates (Fertl and Chilingar, 1988).
Bulk density	Assumes inorganic density = 2.69 g/cm3, underestimates TOC in clay and carbonate-rich rocks (Schmoker and Hester, 1983).
Delta Log R	Maturity sensitive; assumes similar properties for baseline and organic-rich units; clay interfere (Qu, Yoon and Mudawar, 2004).
Pulsed Neutron Spectral Gamma Ray, Litho-Scanner	Requires separate capture and inelastic spectroscopy measurements; borehole and formation corrections for inorganic carbon (Pemper *et al.*, 2009).

2.3.9.3. Linear Regression

Typically regression analysis is used to model the relationship between a dependent variable and one or more independent variables (Casella, Fienberg and Olkin, 2017). The true relationship between X (dependent variable) and Y (independent variable) can be described as (Casella, Fienberg and Olkin, 2017) Equation 5 ;

$$Y = \beta_0 + \beta_1 X_1 \ldots\ldots \beta_K X_K \ + \epsilon$$

Equation 5 (Casella, Fienberg and Olkin, 2017)

This is the population regression line and it describes the true relationship between the dependent and independent variable and is generally not known (Casella, Fienberg and Olkin, 2017). Regression analysis determines the sample regression line Equation *6* that minimizes the sum of the squared errors (SSE) or residual sum of squares (RSS) thus providing an estimate of the population regression line.

$$Y = \beta_0 + \beta_1 X_1 \ldots\ldots \beta_K X_K$$

Equation 6 (Casella, Fienberg and Olkin, 2017)

When fitting a linear regression model to a particular data set, several assumptions needs to be honoured (Casella, Fienberg and Olkin, 2017);

i. Linearity of the response-predictor relationships (Casella, Fienberg and Olkin, 2017)
ii. Correlation of error terms (Casella, Fienberg and Olkin, 2017)
iii. Non-constant variance of error terms (Casella, Fienberg and Olkin, 2017)
iv. Outliers (Casella, Fienberg and Olkin, 2017)
v. High-leverage points (Casella, Fienberg and Olkin, 2017)
vi. Collinearity (Casella, Fienberg and Olkin, 2017)

2.3.9.3.1. Linearity

When the relationship is far from linear, the prediction accuracy of the model can be significantly reduced (Casella, Fienberg and Olkin, 2017). Residual plots are a useful to identify non-linearity in regression models (Casella, Fienberg and Olkin, 2017). As seen in Figure *2-12* there should be little pattern in the residuals. The presence of a pattern may indicate some non-linearity in the data (Casella, Fienberg and Olkin, 2017).

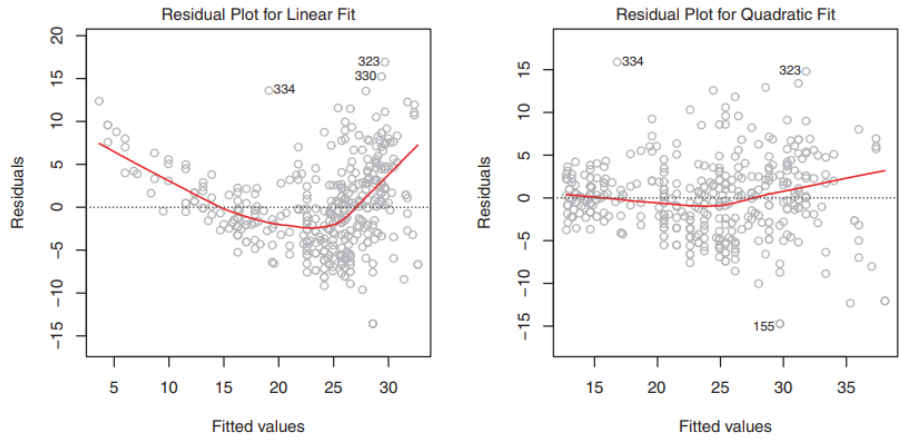

Figure 2-12: Plot of residuals versus predicted (or fitted values)(Casella, Fienberg and Olkin, 2017)

If the residual plot indicates non-linear associations in the data, a simple solution is to use non-linear transformations of the independent variable such as log X, $\sqrt{X}$ and X^2 in the regression model (Casella, Fienberg and Olkin, 2017).

2.3.9.3.2. Autocorrelation / Correlation of Error Terms

An assumption of the linear regression model is that there is no correlation of error terms i.e. $\epsilon_1, \epsilon_2, \epsilon_3, \ldots\ldots, \epsilon_n$ are uncorrelated. If ϵ_i is positive, it should not give an indicator of the sign of ϵ_{i+1} (Casella, Fienberg and Olkin, 2017). If there is correlation among the error terms, the estimated standard errors will tend to underestimate the true standard errors (Casella, Fienberg and Olkin, 2017) so confidence and prediction intervals will be narrower than normal. In addition, p-values associated with the model will be lower than they should be; this could cause us to erroneously conclude a parameter is statistically significant (Casella, Fienberg and Olkin, 2017).

2.3.9.3.3. Non-Constant Variance of Error Terms

The error terms in the linear regression model should have a constant variance as the standard errors, confidence intervals and hypothesis tests associated with the linear model rely on this assumption (Casella, Fienberg and Olkin, 2017). Another name for non-constant variance is heteroscedasticity – the funnel shape on Figure *2-13* shows the magnitude of the residuals increasing with the fitted values (Casella, Fienberg and Olkin, 2017).

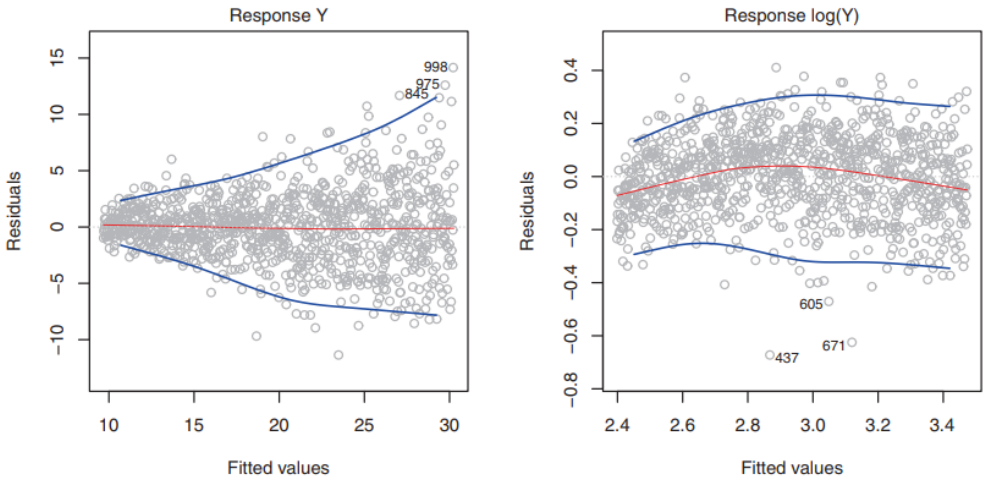

Figure 2-13: Left: The funnel shape indicates heteroscedasticity. Right: The response on the right has been log transformed and there is now no evidence of heteroscedasticity (Casella, Fienberg and Olkin, 2017)

A simple analogy for Heteroscedascity is when an individual's income increases, the variability of food consumption will increase so a poorer individual will spend a constant amount eating inexpensive food whereas a wealthier person has the choice to occasionally eat inexpensive food. One way to solve this challenge is to transform the dependent variable using a concave function such as log Y or $\sqrt{X}$ (Casella, Fienberg and Olkin, 2017). These transformation shrinks the large responses leading to a reduction in heteroscedasticity (Casella, Fienberg and Olkin, 2017) Figure *2-13*

2.3.9.3.4. Collinearity

Collinearity refers to the situation in which two or more predictor variables are closely related to one another (Casella, Fienberg and Olkin, 2017). The presence of collinearity can pose problems in the regression because it can be difficult to separate the individual effects of collinear variables on the response (Casella, Fienberg and Olkin, 2017). Simply if two variables increase or decrease together, it can be difficult to determine how each variable is associated with the response (i.e. dependent variable) (Casella, Fienberg and Olkin, 2017). Collinearity reduces the accuracy of the estimates of the regression coefficients as it increases the standard error and p-value and therefore reduces the t-statistic (Casella, Fienberg and Olkin, 2017). Therefore, in the presence of collinearity, it is possible to fail to reject the null hypothesis i.e. the probability of correctly detecting a non-zero coefficient is reduced by collinearity (Casella, Fienberg and Olkin, 2017). A simple way to detect collinearity is to use a correlation matrix for all the predictors (Casella, Fienberg and Olkin, 2017). However, not all collinearity problems can be detected by visualising a correlation matrix because it is possible for collinearity to exist between three

or more variables even if no pair of variables has a high correlation (Casella, Fienberg and Olkin, 2017). This is termed Multicollinearity (Casella, Fienberg and Olkin, 2017). A better way to assess Multicollinearity is to compute the variance inflation factor (Casella, Fienberg and Olkin, 2017) Equation 7. The smallest possible value for VIF is 1 which indicates the complete absence of collinearity though there would be a small amount in practise(Casella, Fienberg and Olkin, 2017). Typically, a VIF value that exceeds 5 or 10 indicates a large amount of collinearity (Casella, Fienberg and Olkin, 2017).

$$VIF(\hat{\beta}_J) = \frac{1}{1 - R^2_{X_{j|X_{-j}}}}$$

Equation 7 (Casella, Fienberg and Olkin, 2017)

Where $R^2_{X_{j|X_{-j}}}$ is, the R^2 from a regression of Xj onto all of the other predictors. If $R^2_{X_{j|X_{-j}}}$ is close to one, then collinearity is present and therefore VIF will be large (Casella, Fienberg and Olkin, 2017). Two simple solutions is to drop one of the problematic variables because the presence of this variable is redundant in the presence of the other variables (Casella, Fienberg and Olkin, 2017). The second solution is to combine the collinear variables together into a single predictor i.e. perhaps take the average of the two or three variables that are highly correlated to create a new variable (Casella, Fienberg and Olkin, 2017).

2.3.9.3.5. Evaluating Model Accuracy

The quality of a linear regression model can be assessed using the residual standard error and the R^2 statistic (Casella, Fienberg and Olkin, 2017). There is always an error term associated with each observation so even if the true coefficient were known, it would not be perfectly possible to still predict Y from X (Casella, Fienberg and Olkin, 2017). The *Residual Standard Error (RSE)* is an estimate of the standard deviation of the population error term (Casella, Fienberg and Olkin, 2017). In simple terms, it is the average amount that the response will deviate from the true regression line and is computed using Equation 8 (Casella, Fienberg and Olkin, 2017);

$$RSE = \sqrt{\frac{1}{n-p-1} RSS}$$

Equation 8

Where
n = number of observations
p = number of variables

RSS = Residual sum of squares

RSE = Residual square errors

The RSE provides an absolute measure of lack of fit of the model to the dataset but it is measured in units of the dependent variable so it can be unclear what contributes to a good RSE (Casella, Fienberg and Olkin, 2017). R^2 is independent of the dependent variable and simply describes the proportion of variance explained therefore it is always between 0 and 1 (Casella, Fienberg and Olkin, 2017).

R^2 can be determined using Equation *9* ;

$$R^2 = \frac{TSS - RSS}{TSS} = 1 - \frac{RSS}{TSS}$$

Equation 9 (Casella, Fienberg and Olkin, 2017)

Where $TSS = \sum(y_i - \bar{y})^2$ is the total sum of squares which is the total variance in the response Y i.e. it is the amount of variability already existing in the response variable before the regression was performed (Casella, Fienberg and Olkin, 2017). RSS measures the amount of variability that is left unexplained after the regression has been performed therefore TSS – RSS measures the amount of variability in the response that is explained by performing the regression (Casella, Fienberg and Olkin, 2017). R^2 measures the proportion of variability in Y that can be explained by using X (Casella, Fienberg and Olkin, 2017). R^2 is the proportion of the SST or (TSS) been explained (Machine Learning Plus, 2019).

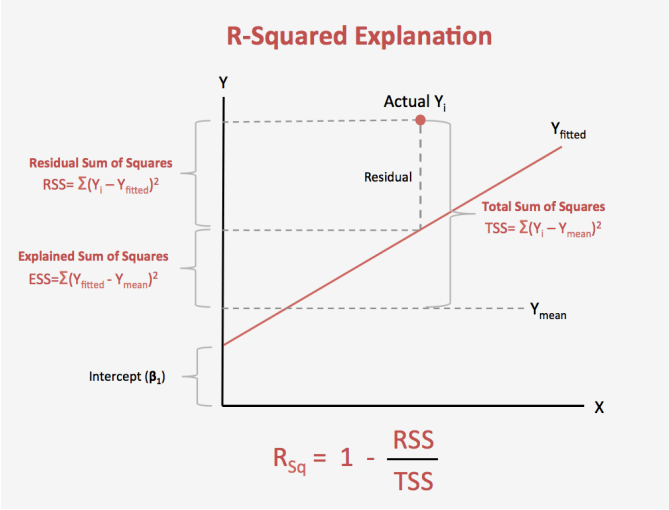

Figure 2-14: R^2 Intuition (Machine Learning Plus, 2019)

With Adjusted R^2, as more variables are added to the model, the RSS always decreases therefore the R^2 always increases as more variables are added (Casella, Fienberg and Olkin, 2017). The adjusted R^2 is calculated using Equation *10*;

$$Adjusted\ R^2 = 1 - \frac{RSS/(n-d-1)}{TSS/(n-1)}$$

Equation 10 (Casella, Fienberg and Olkin, 2017)

A large value of adjusted R^2 indicates a model with a small test error (Casella, Fienberg and Olkin, 2017). Unlike the R^2 statistic, the adjusted R^2 penalises the inclusion of unnecessary variables in the model R^2 (Casella, Fienberg and Olkin, 2017).

2.3.9.3.6. Five - Fold Cross Validation

One way to assess the predictive power of a model especially when the dataset is limited is to use cross-validation (Brinberg, 2019). Typically after splitting the test set, there is a potential to lose some crucial data from the training set or losing patterns, which may go unnoticed by the model (Srinidihi, 2019). This can lead to overfitting or under-fitting (Srinidihi, 2019). To avoid this issue, enough data need to appear in both the training and test set hence K-fold cross validation can be used (Srinidihi, 2019). Cross-Validation iteratively splits the dataset into two sections - a test and training set (Brinberg, 2019). The average prediction error from each of the test set for the whole model is then determined (Brinberg, 2019) . Figure *2-15*, illustrates the concept of cross-validation.

Figure 2-15: Cross-Validation Intuition (Brinberg, 2019)

The model is fit to the test/training data based on a chosen number of K times i.e. number of folds. The prediction error from each model fitting is then averaged to determine the prediction statistics for the model (Brinberg, 2019) . The choice of the number of splits (or "folds") to the data is up to the research (hence why this is sometimes called *K-fold cross-validation*), but five and ten splits are used frequently (Brinberg, 2019). The choice of the

number of splits does impact bias (the difference between the average/expected value and the correct value - i.e., error) and variance. Generally, the fewer the number of splits, the lower the variance and the higher the bias/error (and vice versa) (Brinberg, 2019). Based on 5-fold cross-validation on the dataset in this study, the optimum R^2 that can be obtained is approximately 39% (Table *4-24*).

2.3.9.4. Random Forest Regression

Random Forest Regression is based on ensemble learning[1] and is simply a way of combining multiple algorithms to result in a more powerful and stable predictive model (Eremenko, 2019). The intuition is that producing a single complicated and complex mode that may have a high variance from overfitting or might be too simple and have a high bias from under-fitting, random forest generates plenty models and then averaging their outputs (Eremenko, 2019).

Random forest regression works in the following ways (Eremenko, 2019);

i. Pick random K data observations from the Training Set
ii. Build a decision tree associated to the selected K data points
iii. Choose the number of trees to be built and repeat the two previous steps.
iv. For every new data observation, each one of the trees should predict the value of the dependent variable for each observation and assign the average across all of the predicted Y values.

This ensures that multiple predictions (> 500 trees) can be obtained for each observation thus improving the predictive accuracy of the model based on a forest of trees (Eremenko, 2019). Averaging the trees helps to reduce variance and also improve the performance of decision trees on the dataset (Eremenko, 2019). Another popular ensemble algorithm is called Bagging or Bootstrap Aggregation. The term “bootstrap” refers to a statistical method for estimating a quantity (e.g. mean, standard deviation, regression coefficient, confidence intervals etc.) from a data sample (Brownlee, 2016). It works by creating many random sub-samples of the dataset and then calculate the required statistic (e.g. mean for each subsample) (Brownlee, 2016). The average of all the means is then used as the estimated mean for the dataset (Brownlee, 2016). The bootstrap can be used to improve statistical learning methods such as decision trees. Decision trees tend to have a high

[1] Ensemble learning is a type of supervised learning where the basic intuition is to generate multiple models on a dataset and simply average their output to create a model with strong performs and does not over-fit whilst balancing the bias-variance trade-off (Eremenko, 2019).

variance i.e. if the training data is split into two parts at random, and fit a decision tree to both halves, the results would be quite different (Casella, Fienberg and Olkin, 2017). Whereas, a low variance will yield similar results if applied repeatedly to distinct datasets (Casella, Fienberg and Olkin, 2017). Random Forest is an improvement on bagged decision trees – the problem with bagged decision trees is that the algorithm chooses which variable to split on that results in a high bias (Brownlee, 2016). Therefore, bagged decision trees can have many structural similarities and therefore a high correlation in their predictions (Brownlee, 2016). Ensemble methods works best when sub-models are uncorrelated or at best weakly correlated (Brownlee, 2016). Random forests provide an improvement over bagged trees by way of a random small tweak that de-correlates the trees (Casella, Fienberg and Olkin, 2017). Just like bagging, a number of decision tress are built on the basis of bootstrapped training samples (Casella, Fienberg and Olkin, 2017). But when building these decision trees, each time a split in a tree is considered, a random sample of m predictors is chosen as split candidates from the full set of p predictors (Casella, Fienberg and Olkin, 2017). When selecting a split point in random forest, the algorithm is limited to a random sample of features of which to search (Brownlee, 2016). The number of features that can be searched at each split point (m) must be specified to the algorithm (Brownlee, 2016). (m) is the number of randomly selected features that can be searched at a split point and p is the number of input variables. The split is allowed to use only one of those m predictors. A fresh sample of m predictors is taken at each split, and typically we choose m ≈ $\sqrt{p}$ – i.e. the number of predictors considered at each split is approximately equal to the square root of the total number of predictors (Casella, Fienberg and Olkin, 2017). In other words, in building a random forest, at each split in the tree, the algorithm is not allowed to consider a majority of the available predictors (Casella, Fienberg and Olkin, 2017). The rationale is that, if there is a very strong predictor in the dataset, along with a number of other moderately strong predictors (Casella, Fienberg and Olkin, 2017). Then in the collection of bagged trees, most or all of the trees will use this strong predictor in the top split (Casella, Fienberg and Olkin, 2017). So all the bagged trees will look similar and predictions from these bagged trees will be highly correlated (Casella, Fienberg and Olkin, 2017). Averaging highly correlated quantities does not lead to a large enough reduction in variance as averaging many uncorrelated quantities (Casella, Fienberg and Olkin, 2017). In particular, this means that bagging will not lead to a substantial reduction in variance over a single tree (Casella, Fienberg and Olkin, 2017). Random forest overcomes this problem by forcing each split to consider only a subset of the predictors (Casella, Fienberg and Olkin, 2017). Therefore, on average $(p - m)/p$ of the splits will not even consider the

strong predictor so other predictors have a chance of been used (Casella, Fienberg and Olkin, 2017). This is a process of de-correlating the trees thereby making the average of the resulting trees less variable and more reliable (Casella, Fienberg and Olkin, 2017). The main difference between bagging and random forest is the choice of predictor subset size m (Casella et al., 2017). For instance, if a random forest is built using $m = p$, then this is simply bagging (Casella, Fienberg and Olkin, 2017). Using a small value of m in building a random forest will typically be helpful when we have a large number of correlated predictors (Casella, Fienberg and Olkin, 2017). As with bagging, random forest will not over fit if we increase B, so in practise we use a value of B sufficiently large for the error rate to have settled down (Casella, Fienberg and Olkin, 2017).

2.3.9.4.1. Estimating Decision Tree Performance

For each bootstrap sample taken from the training data, there will be samples left behind that were not included (Brownlee, 2016). These samples are called the Out-Of-Bag samples or OOB (Brownlee, 2016). The OOB sample is the set of observations which are not used for building the current tree, but it is used to estimate the prediction error and then to evaluate variable importance (Genuer, Robin; Poggi, Jean-Michel; Tuleau, 2008). The estimated performance is often call the OOB estimate of performance (Brownlee, 2016) . The performance of each model on its left out samples when averaged can provide an estimated accuracy of the decision tree model (Brownlee, 2016). The OOB samples is a very straightforward way to estimate the test error of a bagged model, without the need to perform cross-validation or the validation set approach (Casella, Fienberg and Olkin, 2017). The resulting OOB error is a valid estimate of the test error for the bagged model since the response for each observation is predicted using only the trees that were not fit using the in-bag observations (Casella, Fienberg and Olkin, 2017). When B is very large, OOB error is equivalent to leave-one-out cross validation (Casella, Fienberg and Olkin, 2017). The OOB method for estimating the test error is convenient when performing bagging on large datasets for which cross validation would be computationally challenging (Casella, Fienberg and Olkin, 2017).

2.3.10. Kerogen Type

The Kerogen type is described by (George E King, 2010) as a “significant need” for a prospective shale. Shale kerogen type is a function of the depositional environment; hence, marine shales relate to Type II kerogens, lacustrine shales are associated with Type I kerogen, and finally, terrestrial shales are associated with Type III kerogen (Wright, 2016).

Approximately 97% of gas shales are in a marine environment, and marine shales also contain the highest average TOC (Rezaee, 2015). Typically Type I kerogen tend to generate liquid hydrocarbons, type III generates gas, coal (often coalbed methane) and in extreme conditions, oil. It is generally considered that Type IV kerogen is incapable of generating hydrocarbons (Glorioso and Rattia, 2012). Gas shales' should ideally contain Type II or be a mix of Type II-III (Jarvie, 2012a).

2.3.11. Original Hydrogen Index

The Hydrogen Index is a Rock evaluation parameter used to characterise the kerogen type of organic matter and is a measure of the hydrogen richness of kerogen (Wright, 2016). It is calculated from the S2 and TOC using the expression Equation 11.

Equation 11

$$\boldsymbol{HI = \frac{S_2}{TOC} * 100}$$

Equation 12

Where

HI = Hydrogen Index
S_2 =

For success, the original hydrogen index should fall in the range of 250-800mg/g/TOC, indicating a type II or type II-III mix of kerogen (Jarvie, 2012a; Andrews, 2013). The hydrogen index is in units of mg hydrocarbon/g of total organic carbon. For immature kerogen, a hydrogen index of 600-950 suggests "Type I kerogen," 400-600 for Type II kerogen, and 0-300 for Type III and IV kerogen (Wright, 2016). If the kerogen type is known, the hydrogen index may also be used to calculate the maturity of the kerogen (Wright, 2016).

Original Hydrogen Index values from (Jarvie *et al.*, 2007), for the Barnett fall in the range of 392-475 (mg/g/TOC) which is within the bounds of the Original Hydrogen Index range in section 2.3.11. This Original Hydrogen Index range indicates that Type II kerogen is present which is a function of the depositional environment (Wright, 2016). Palaeo-geographic reconstructions from (Bruner and Smosna, 2011) (Figure 2-16) depict the Forth-Worth basin as a narrow, restricted inland seaway - this marine depositional environment is associated with Type II kerogen, supporting the Original Hydrogen Index and kerogen interpretations of (Jarvie *et al.*, 2007).

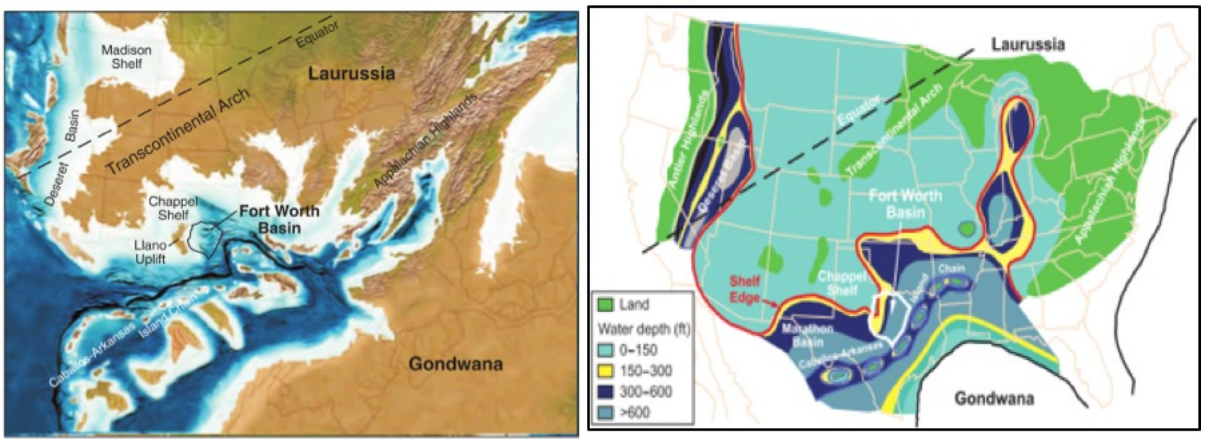

Figure 2-16: Paleogeographic reconstructions of the southern mid-content region during the Late Mississippian showing position and water depth of the Fort Worth Basin (Bruner and Smosna, 2011)

2.3.12. Pre-existing Structure and Burial History

Shale gas plays should typically be within large stable basins without a complex tectonic history (Wright, 2016). Monoclines with less than 5-degree dip and simple structural architecture are permissible (Waldo, 2015). In America, the higher production in the Late Jurassic Haynesville Shale compared to the Barnett Shale is attributed to a better seal and an absence of overlying reservoirs. However, the structure within a shale gas play should be minimal, with the shale defining a continuous mappable system (Andrews, 2013) which allows the drilling of horizontal production wells with little chance of intersecting significant faults, which minimizes risk of stimulating earthquakes during fracking, or the need to revise the trajectory of the well after crossing a fault (Wright, 2016). In the UK we have not reached this level of exploration sophistication, and the presence of overlying or nearby (small) conventional reservoirs is considered to be an initially important consideration. The age of the shale, affecting permeability, might also be a factor. Jurassic shales in the UK have not been so adversely affected by the Alpine Orogeny as Carboniferous and Lower Palaeozoic rocks affected by the Variscan and/or Caledonian orogenies. These deformation fronts form a triangle (Midland Microcraton) in south and central England and Wales that is comparatively unaffected by folding and intrusion of igneous rocks (Smith 1987). There is no evidence of overpressure in UK basins, so it is unlikely that well production rates will be as high in the UK as in America. The interval of interest in the UK is informally termed the Bowland-Hodder unit since this is the key interval within the Bowland basin that was targeted by the Preese-Hall 1 well in Western Lancashire the UK's first shale gas exploration well Figure 2-17 and Figure 2-18.

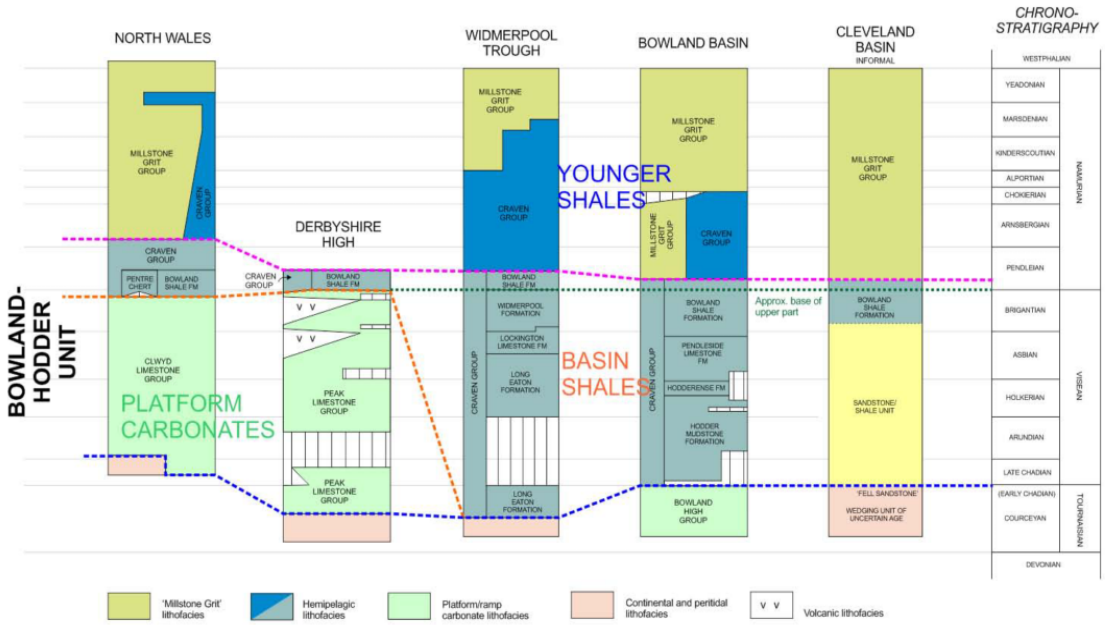

Figure 2-17: Litho-Stratigraphical framework of the Carboniferous Bowland-Hodder Unit in Central Britain (Dean *et al.*, 2011)

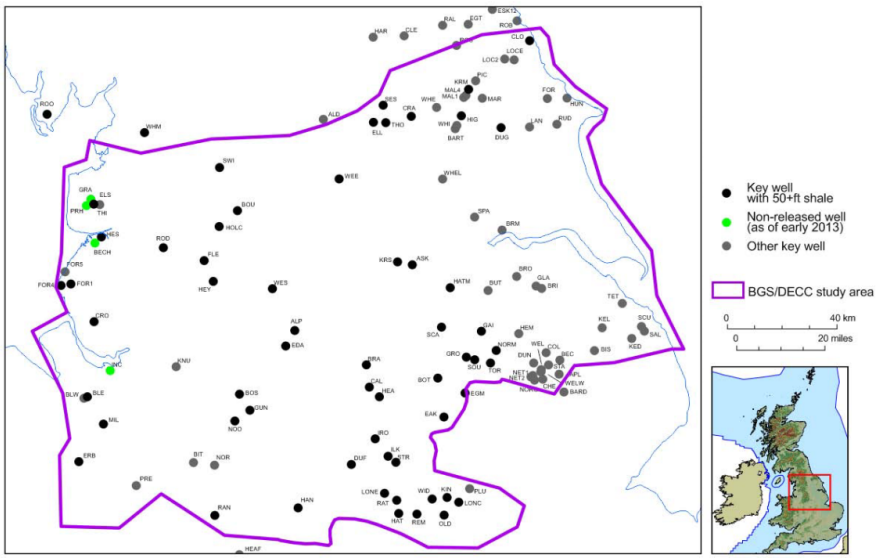

Figure 2-18: Location of key wells, non-released wells and other wells providing important stratigraphic information used to assess the shale gas potential of Central Britain (Andrews 2013)

These marine shales in the Bowland Shale were deposited in a complex series of tectonically active basins across central Britain during the Visean and Namurian epochs of the Carboniferous (c347-318) (Andrews, 2013) (Figure 2-19). Paleo-magnetic evidence also suggests that Britain was situated near equatorial latitudes during Visean times, and the

Carboniferous was a period of glacial Eustasy, with sea-level fluctuations likely to have had a significant impact on deposition. A phase of late Devonian to early Carboniferous rifting produced significant paleo-relief with numerous basins occupying subsiding grabens and half-grabens and emergent highs associated with horsts and tilt-block high (Leeder, 1982). The Bowland basin was formed by active rifting during the late Devonian-Dinantian times (Leeder, 1982). The Upper Bowland shale is Pendleian (serpukhovian) in age and corresponds to a major marine flooding event which deposited organic rich shales over much of the UK, western and central Europe (Clarke, Bustin and Turner, 2014).

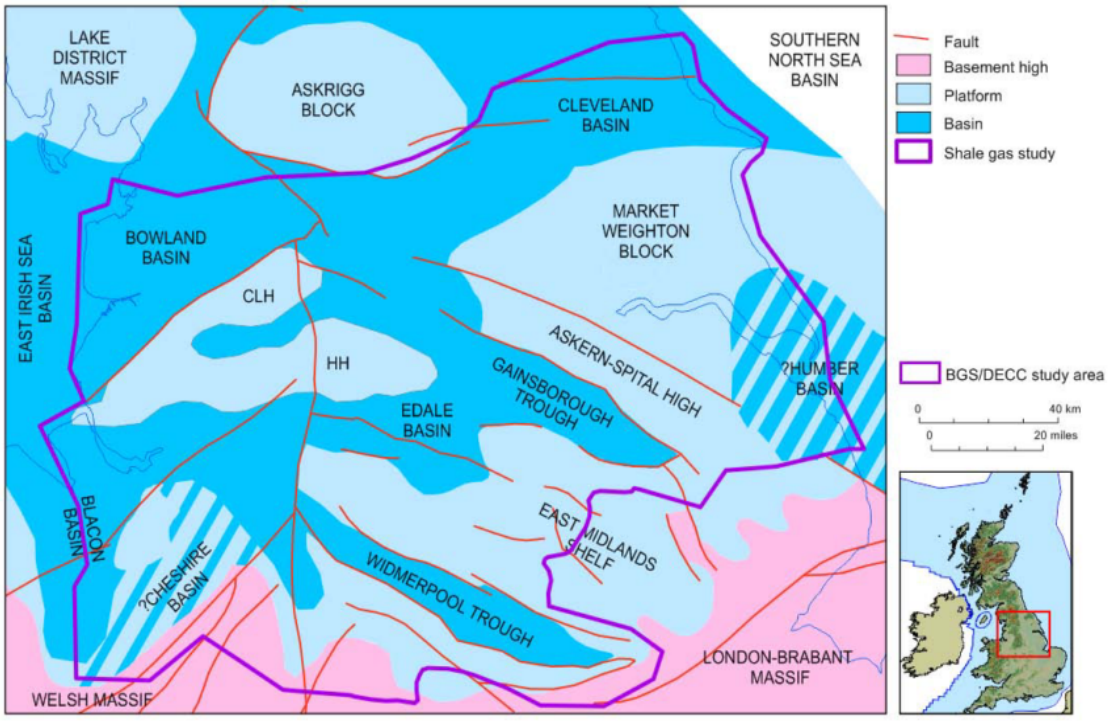

Figure 2-19: The Early Carboniferous basins and platforms of Central Britain (Andrews, 2013)

The Barnett shale is also of carboniferous age and resides within the Fort Worth Basin in Texas (Pollastro *et al.*, 2007; Bruner and Smosna, 2011). The lithology is split into two sections; the Upper and Lower Barnett, separated by the Forestburg limestone. The Lower Barnett is considerably thicker and contributes “about 70 to 80%” of the gas production in most wells (Kennedy, Luo, & Vello, 2016). The Barnett shale encompasses 24 counties (Figure 2-20) with most of the gas production being from the core counties. A Limestone barrier (Viola Limestone) separates the core of the Barnett Shale from the underlying water-bearing Ellenberger Formation making it possible for companies to pump large fracture treatments (Almadani, 2010). Above the Barnett is the Marble Falls Limestone, a low porosity thick limestone interval (Spears and Jackson, 2009).

Core Counties	Non-Core Counties	
Denton	Archer	Hood
Johnson	Bosque	Jack
Tarrant	Clay	Montague
Wise	Comanche	Palo Pinto
	Cooke	Parker
	Coryell	Shakleford
	Dallas	Somervell
	Eastland	Stephens
	Ellis	
	Erath	
	Hamilton	
	Hill	

Figure 2-20: Core and Non-Core Counties in the Barnett Shale

In the non-core area (in the north, south and west of the core area) where the Viola Limestone is absent, vertical wells with large hydraulic fracture treatments are at risk of communicating with the underlying water-bearing Ellenberger formation (Almadani, 2010). To avoid the problem, companies have effectively used horizontal drilling and multiples of smaller hydraulic fracture treatments along the horizontal well section. Overlying the Barnett is the Marble Falls, which is a barrier to hydraulic fractures' growth.

Most sediments in the Barnett shale have been deposited in a deep marine environment (Spears and Jackson, 2009), with gas production been highest in the northern part of the basin where the shale is relatively thick. The Barnett shale is colloquially interpreted as having been deposited within the "Fort Worth Basin" or to be more specific as a foreland basin surrounded by the Muenster arch, Red River arch, Bend arch and Llano uplift (Spears and Jackson, 2009) Figure 2-21. The "Ouachita Structural Belt" provides the eastern limit of the Barnett; this belt is a very large thrust fault system that was created during a period of crustal plate convergence in the late Mississippian to early Pennsylvanian period (Hill *et al.*, 2007; Spears and Jackson, 2009). (Pollastro *et al.*, 2007), identified structures within the Forth-Worth Basin, they include minor faults, local folds, fractures, karst-related collapse features and thrust-fold structures. (Bowker, 2007), noted that wells in the Barnett that are located on or near structural flexures, karst, fault zones, and natural fracture networks and tend to be poorer producers than wells not associated with such structures. The structures may deflect the

energy from hydraulic fracture stimulation away from the target Barnett shale and toward adjacent, unproductive formations. Bowker's conclusion aligns with those of (Jarvie, 2012a) and (Andrews, 2013) that wells should be drilled away from such structures.

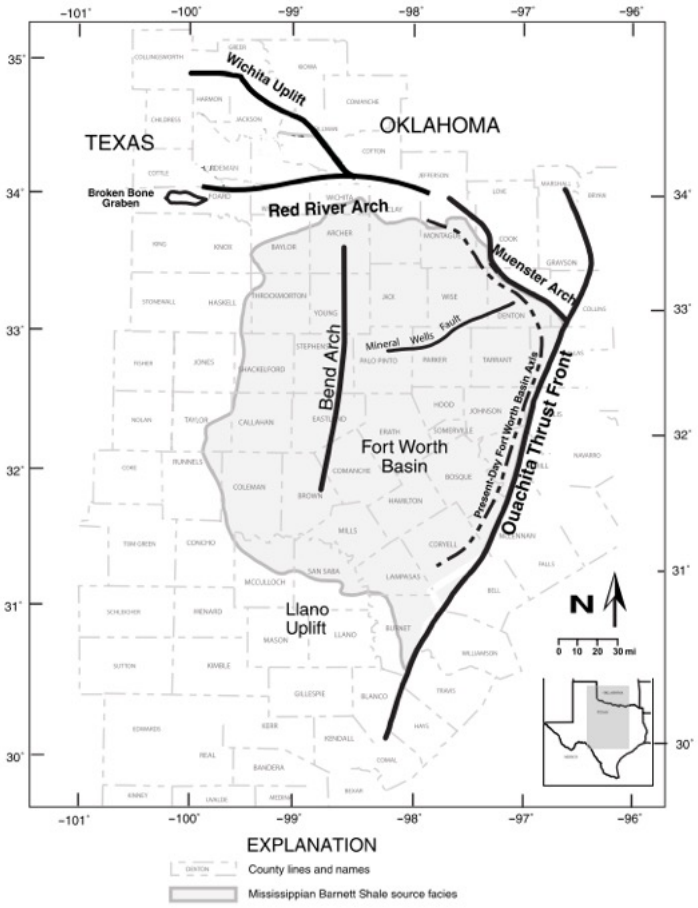

Figure 2-21: Generalised structural map of the Forth-Worth Basin of North-Central Texas, modified after (Pollastro *et al.*, 2007)

A brief comparison of Barnett and Bowland shale gas reservoirs presented in Table 2-10.

Table 2-10: Geological comparison of Bowland with Barnett shale play (Spears and Jackson, 2009).

Shale Play	**Barnett**	**Bowland**
Age	Early Carboniferous	Late Carboniferous
Mineralogy	35% clay, relative brittleness > 40%	50% clay, relative brittleness ~ 30%
Depth (ft)	7500	10,000
Thickness (ft)	300	Over 6000 in basin center
TOC_{pd} High (wt. %)	9.94	8
TOC_{pd} Average (wt. %)	3.74	1–3
Kerogen Type	Type II	Type II-III
Original Hydrogen Index (mgHC/gTOC)	392 - 475	150 - 400
Thermal Maturity	1.45	0.8 – 2.5
Gas Content	300-500 scf/ton	10-40scf/ton

2.4. Well Log Signatures of Gas Shale Formations

2.4.1. Resistivity and Induction Logs

The key property of the clay that affects the resistivity of the rock is the cation exchange capacity (CEC) which varies on the type of clay and mixed layers; the higher the CEC, the lower the resistivity of the rock (Glorioso & Rattia, 2012). Smectite has a far greater specific surface area than the other clays making it more conductive (Passey *et al.*, 2010; Rezaee, 2015). The effect of CEC on the shale conductivity depends on the formation water salinity – if the formation water salinity is greater that sea water salinity, the effect of excess conductivity due to clay minerals is minimal (Passey *et al.*, 2010; Rezaee, 2015). In situations of over-matured kerogen and when graphite has been produced, a drastic reduction in resistivity is observed since graphite is conductive (Glorioso and Rattia, 2012).

Anisotropy in shale gas is a factor that controls the interpretation of resistivity log and water saturation estimation in shale layers and results in a disparity between laterologs and induction resistivity measurement in shales (Rezaee, 2015). Induction devices are sensitive only to the horizontal resistivity of the formation while laterologs measures a combination of both horizontal and vertical resistivity (Chemali, Gianzero and Su, 1987; Rezaee, 2015). Due to the vertical transverse isotropy (VTI), Rv (vertical resistivity) is expected to be higher than Rh. The uncertainty is whether the true resistivity of the shale gas is closer to Rh (horizontal resistivity) or Rv (Rezaee, 2015). Figure 2-22 shows the typical response of an electrical tool in a sand/shale sequence - the lower resistivity shales is due to the presence of bound water in clays that undergo surface conduction.

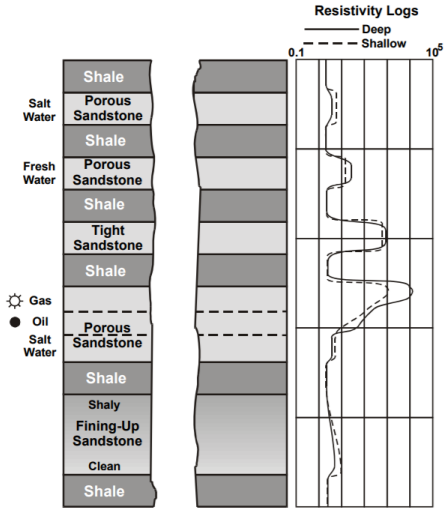

Figure 2-22: Resistivity log response in a sand shale sequence

In *Figure 2-23*,

- If all three curves are low resistivity, and overlie each other, the formation is an impermeable shale, or rarely, the formation is permeable and water bearing but the mud filtrate has the same resistivity as the formation water.
- If all three curves are higher resistivity than the surrounding shales, and overlie each other, the formation is an impermeable cleaner formation (sandstone, limestone).
- If the shallow curve has low resistivity but the medium and deep penetrating tools have a higher resistivity that is the same (they overlie each other), the formation is permeable and contains only formation water.
- If the shallow curve has low resistivity, the medium has a higher resistivity, and the deep one has an even higher resistivity (i.e. there is a separation of the medium and deep tool responses), the formation is permeable and contains hydrocarbons.

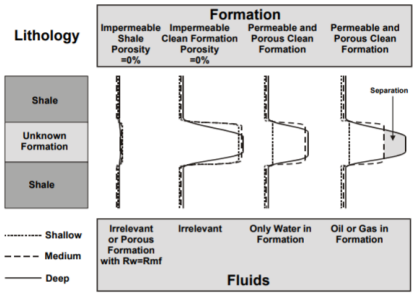

Figure 2-23: Resistivity logs response in various lithology with various fluids

Typically, anomalous elevated resistivity and gamma ray measurements are signature responses for some organic rich black shales, but these responses can be heavily influenced by the complicated mineralogical modifications that happen suddenly across the shale gas interval.

2.4.1.1. Determination of Water Saturation

Estimation of water saturation from resistivity logs require a number of empirical relationships that were established in a series of experiments published in 1942 (Archie, 1942). Archie used clean, clay-free, sandstone samples saturated with a brine of known resistivity (Rw) to estimate the in-situ resistivity of the rock (Ro), this led to the formation resistivity factor (F).

$$F=Ro/Rw$$

Equation 13

Archie demonstrated that there is a strong relationship between the logarithmic transform of the formation resistivity factor and the porosity of the sandstones;

$$F=1/\varnothing\text{^}m$$

Equation 14

Where m, the slope of the line, which had different values depending on the consolidation of the sandstone: the numerator was later generalized to the term “a” to accommodate different classes of sandstone. The terms a and m are known as the tortuosity factor and cementation factor respectively. In a fully saturated sample, the Archie equation becomes;

$$S_w = \sqrt[n]{\frac{aR_w}{\emptyset^m R_t}}$$

Equation 15

Where

Ro is the resistivity of a fully brine saturated sample,
Rw is the resistivity of the saturating brine
Rt is the resistivity of the sample at different values of saturation
n is saturation exponent

Through a log-log plot of F against porosity for a number of similar rock types, it is possible to obtain the slope of the line, m, or the cementation factor The value of m varies for different rock types as a function of the degree of cementation, ranging from <1.6 for poorly cemented rocks to >3.5 for well cemented rocks; the default value form is usually 1.8-2.2. The tortuosity factor, a, reflects the complexity of the connected pores and is usually set to 1.

The resistivity index is determined by measuring the resistivity of a sample at a number of different saturations, as the sample is slowly desaturated. At each saturation point, the sample is removed from the apparatus and weighed to determine the remaining saturation; this relates to Rt. The default range of values for n is 1.8-2.2.

The saturation exponent (n) was considered to be 1.7 based on (Luffel, Guidry and Curtis, 1992) who report that a saturation exponent of 1.7 for shales provides a good match to core-derived water saturation (Rezaee, 2015). In a nutshell, the resistivity log values for deep tools Rt in reservoir intervals can be used with a reliable porosity from the formation water resistivity Rw, and m and n values that are derived from laboratory measurement on core, to calculate the water saturation in the zone.

The Archie relationship were developed from clean brine-bearing sands; in a real reservoir, the sands are likely to contain clays and hydrocarbons to complicate the electrical system. The complexities of shales would suggest that using the Archie equation may seem too simple for estimating the water saturation (Rezaee, 2015). However, the Archie equation (Equation 15) has been accepted as an industrial standard for water saturation determination of shale gas layers based on porosity and resistivity logs.

Determining some parameters of the Archie equation in shale gas is challenging in shale gas reservoirs as compared to conventional reservoirs;

- Salinity of the formation water and thus pore water resistivity.
- Archie parameters of the shale gas layers (a, m, and n).

The formation water salinity of the shale formations cannot be obtained directly since these layers do not normally produce formation water (Rezaee, 2015). There are large variations in salinity over short vertical distances therefore it is difficult to determine a fixed value for Rw and a result the validity of estimating water saturation using Archie's formula is questionable (Sondergeld, Newsham, *et al.*, 2010; Rezaee, 2015).

Archie model also does not differentiate the electrical contribution of different types of water saturating the shale matrix and uses a single value for water resistivity (Rezaee, 2015). This simplification can turn out to be erroneous when different electrical contributions exist from clay-bound water and free water (Rezaee, 2015). With conventional reservoirs, water resistivity can be obtained in both porous and permeable reservoirs that have a bottom water leg (Rezaee, 2015). (Glorioso and Rattia, 2012; Rezaee, 2015) proposed that for shale gas reservoirs, water resistivity could be calculated over intervals with no kerogen content. Within these intervals, the assumption is that water saturation is high because there is no organic matter generating hydrocarbon therefore the lean shale intervals could be similar to the water saturated intervals in conventional reservoirs (Glorioso and Rattia, 2012; Rezaee, 2015). In conventional reservoirs, formation water provides path for electric currents while in shale formations, due to the presence of large amount of interconnected clays accompanied by formation water, there are more paths for electric currents (Rezaee, 2015). These extra paths increase the ease of electric current flow in shale (Yu and Aguilera, 2011; Rezaee, 2015). This phenomenon would be reflected by a reduction in formation factor and as a result, in cementation factor exponent to a value smaller than 2 (Zhao, Givens and Curtis, 2007; Ramirez *et al.*, 2011; Rezaee, 2015).

In cases where within a shale formation, there are both lean shale intervals and organic rich shales, the simplified Archie equation $S_w = \left(\frac{R_O}{R_t}\right)^{\frac{1}{n}}$, can be used to quantify the gas saturation (Rezaee, 2015). Within lean shale intervals where water saturation is very high, rock resistivity is low (similar to the wet zone in a conventional reservoir rock), whereas with TOC-rich, gas mature shale intervals, water saturation is low and thus rock resistivity (Rt) is high in comparison with the lean shale (Rezaee, 2015).

In this thesis, Archie saturation was not capable of determining the water saturation accurately and in some cases results from Archie's method was extremely noisy to be iterated to fit core saturation data. To overcome the inherent challenges of using Archie's method in shale formations, the Simandoux method was used as it gave the best match to core data. The simandoux equation considers the volume of shale in the matrix to properly account for the

excess of conductivity. Below is the expression for the Simandoux equation – when n = 2, this gives the standard Simandoux equation and when n is not equal to 2, this gives the modified Simandoux equation. Where Rsh = shale resisitivity, SW = Water Saturation, n = saturation exponent and Rt = Rock Resistivity.

$$\left(\frac{\phi^m}{a.Rw}\right) SW^n + \left(\frac{Vsh}{Rsh}\right) SW - \frac{1}{Rt} = 0$$

Figure 2-24: Simandoux Equation

2.4.2. Gamma Ray Log

The presence of shale increases the level of natural radioactivity of the formation (Glorioso and Rattia, 2012). Amongst sediments, shales have the strongest GR radiation hence GR log is mainly used to derive shale volume quantitatively (Rezaee, 2015). Abnormally high natural radioactivity in shale gas is mainly caused by the presence of concentrated uranium, or uranium ions, e.g. as a result of reductive conditions in the marine environment (Glorioso and Rattia, 2012). Therefore, a spectral gamma ray tool would be a better choice in evaluating such formations. The ability to separate levels of thorium, potassium, and uranium radiation is highly advantageous in relation to the total gamma ray count (Glorioso and Rattia, 2012). Illite, mica and feldspar are the main contributors of potassium; detrital (adsorbed) clay minerals and mica are the main contributors of thorium and uranyl ions are the main contributors of uranium. The effect of montmorillonite, chlorite and kaolinite on radiation levels is less significant (Glorioso and Rattia, 2012). The potassium content of the clay mineral varies markedly (Rezaee, 2015). Illite contains the greatest amount of potassium while kaolinite has very little or none (Rezaee, 2015). This means that clay mixtures with a high kaolinite or high smectite content will have lower potassium radioactivity that clays made up of predominantly illite (Rezaee, 2015). However, since most clays consist of a mixture of several clay minerals, this differences are minimal (Rezaee, 2015). The average shale has a potassium content of about 2-3.5% (Rider, 1986; Rezaee, 2015). Uranium forms unstable soluble salts that are present in sea water and rivers. Uranium content has a positive relation with the TOC deposited under marine conditions (Fertl and Rieke III, 1980; Rezaee, 2015). In lacustrine settings, due to paucity of uranium, there is no relationship between uranium and TOC (Rezaee, 2015); therefore in these cases, GR could be used as a clay volume indicator but not TOC content. It should be noted that the use of uranium is suitable for shale gas reservoirs that do not have uranium-enriched minerals like apatite (Kochenov and Baturin, 2002; Rezaee, 2015). In these reservoirs, elevated uranium could not be used to predict TOC (Rezaee, 2015). Unlike Uranium, Thorium is extremely stable and will rarely pass into solution; thus its

concentration can be attributed to the provenance (source area) of the accumulated sediment (Rezaee, 2015). The relative immobility of thorium, as a stable, conserved, trace element in the marine environment, compared to the transient mobility of uranium due to fluctuations in oxidation-reduction potential is a relationship used to delineate the possible sequence stratigraphy in the target gas shale layer (Jacobi *et al.*, 2008). Consequently, including GR data into TOC models can enhance the performance of these models (Mahmoud *et al.*, 2017). Furthermore, if there is no gas present in the formation, the neutron porosity to density porosity difference tends to have a linear response with rock's clay content. This is because the neutron porosity tool is very sensible to the high hydrogen index of clays, while the bulk density tool does not. Even better, the difference does not depend upon Gamma Ray, so it provides a GR independent estimator. Clay minerals like kaolinite, chlorite, illite, and montmorillonite, have a high hydrogen index. However, the minerals quartz & feldspar, calcite, and dolomite, present in clean sandstones, limestones, and dolostone matrices, don't (Pemper et al. 2006).

2.4.3. Neutron Log

Like other conventional well log data, neutron log interpretation in the gas shale layers is complex and need to consider a variety of parameters (Rezaee, 2015). Neutron logs are affected by the hydrogen in organic matter, the hydrogen in clays OH+, and furthermore by the hydrogen in water and hydrocarbons present also affects neutron porosity measurements (Rezaee, 2015). The neutron porosity of kerogen is high but it has limited use in estimating TOC (Glorioso and Rattia, 2012). This is one of the conventional logs seldom used in detecting and evaluating the organic content and productive potential of shale gas (Glorioso and Rattia, 2012). The hydrogen index of kerogen is lower than that of water, therefore neutron porosity tend to reduce according to the amount of kerogen present although the reduced porosity due to lack of hydrogen in gas and kerogen is complex in shale (Glorioso and Rattia, 2012). In a nutshell, the neutron-density logs are of limited use in locating gas and kerogen due to the strong impact of clays that increase neutron porosity or due to the presence of calcite and dolomite that result in complex and contrasting neutron log responses - for example, Calcite tends to reduce the neutron porosity of a shale gas formation and this can easily be confused with gas effects (Glorioso and Rattia, 2012). The neutron log is less affected by the condition of the wellbore walls although any other factor that may alter the formation in areas close to the borehole walls can impact on the quality of the measurement (Glorioso and Rattia, 2012). As can be seen in *Figure 2-25* due to the clay effect, the NPHI log response shows a higher value in the Lower and Upper Carynginia shale while the middle section, a sandy shale member, and NPHI values decrease (Rezaee, 2015).

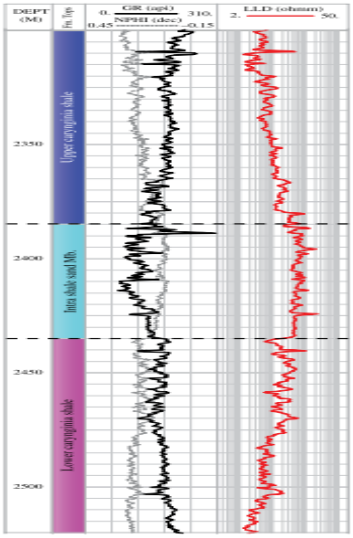

Figure 2-25: Typical well log response from a well in the Carynginia Shale, Perth Basin, WA (Rezaee, 2015).

It is also expected that NPHI log response will be reduced in the gas shale layers due to the lower hydrogen index (HI) of gas and organic matter compared to water, although quantifying the effects of reducing porosity due to lack of hydrogen in gas and organic matter is complex (Glorioso and Rattia, 2012). To some extent, the effect can be observed on the lower Carynginia shale in *Figure 2-25*. Between 2435m and 2475m, the resistivity is higher and NPHI is lower compared to the lower part of the section (i.e. between 2475m and 2520m), possibly due to the presence of gas (Rezaee, 2015). (Zhao, Givens and Curtis, 2007) and (Labani and Rezaee, 2012) observed that neutron porosity decreases with increasing thermal maturity in the shale gas layers. The following points can justify this behaviour (Rezaee, 2015);

- HI of generated hydrocarbons in the final stages of thermal maturity (i.e. gas window) is lower than the oil window; for example, HI of dry gas is less than that of wet gas.
- By increasing thermal maturity, smectite converts to Illite, and HI of transformed Illite is lower than that of Smectite.
- Reduction of the water saturation at a high thermal maturity level causes a relatively lower HI values for the shale layers.

2.4.4. Density Log

The bulk density log can be used in modelling the porosity of shale gas layers if the mineral composition (or matrix density) is properly determined using mineralogical tools (Vernik and Milovac, 2011). The density of the organic matter is typically low (1.1-1.4g/cm3) compared to the matrix density (2.6g/cm3) of the shale layers (Rezaee, 2015). Due to this low density value,

the presence of organic matter can decrease the measured bulk density of the formation along with high levels of gas content (Rezaee, 2015). The presence of pyrite and siderite found in organic rich shale can elevate formation density (Rezaee, 2015). The most favourable environment for siderite formation are reducing freshwater systems (potential environment for kerogen type I), while pyrite commonly occurs in marine sediments (potential environment for kerogen type II)(Passey *et al.*, 2010). The density log can give a qualitative indication for estimating the thermal maturity of the shale gas layers (Labani and Rezaee, 2012), for example, in some wells in the Perth Basin, there is a decreasing trend for density log responses with increasing thermal maturity in potential shale gas layers (Rezaee, 2015). This relationship is not so strong but it seems compatible with what occurs in the shale gas layers during thermal maturity evolution (Rezaee, 2015). By increasing thermal maturity in the organic rich shale layers, the following changes may happen;

- Changes in the type of saturated fluid from brine to gas.
- Changing of the heavier components of hydrocarbon into lighter ones and finally dry gas.
- Generation of porosity in the organic matter due to its thermal transformation (Loucks *et al.*, 2009; Rezaee, 2015).
- Increase in pore pressure due to mineral transformation (smectite to Illite) and hydrocarbon generation.

All of these transformations can result in decreasing the density of the formation with increasing thermal maturity (Rezaee, 2015). It is worth nothing that sometimes the use of the density log and NPHI log as a thermal maturity indicator is not possible (Rezaee, 2015). For example, the presence of heavy minerals could increase the density and hide the decreasing effect of thermal maturity (Rezaee, 2015). Therefore, we can conclude that conventional logs can only be used for thermal maturity estimation if the lithology of the formation does not vary significantly over the interval of interest (Rezaee, 2015).

2.5. Hydraulic Fracturing

2.5.1. Fracture Complexity

Cipolla et al., (2009), observed that fracture complexity or network fracturing is a combination of establishing main fractures with high conductivity and more contact areas created by opening and stabilizing natural fractures in the rock. They proposed schematics of several fracture styles and described an orderly complex or network fracture system Figure 2-26.

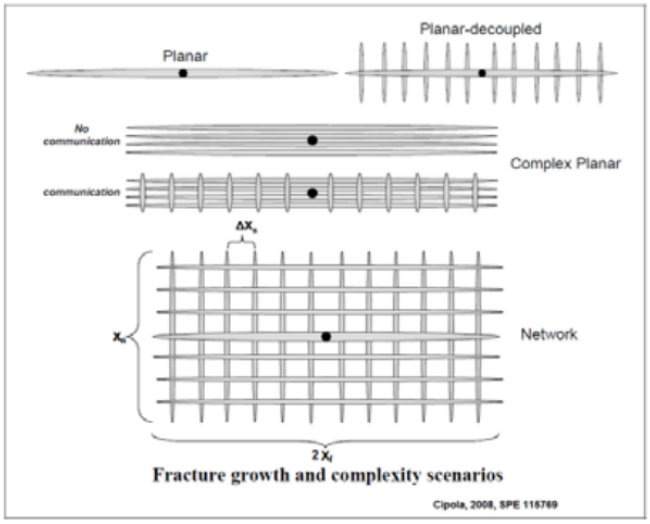

Figure 2-26: Theoretical concepts of complex fracture systems with formations with primary and secondary fractures (Cipolla *et al.*, 2009).

The orderliness of the network is strongly influenced by local and regional stresses and post depositional modifications as they affect the way fractures open and the order of how they open.

(Warpinski *et al.*, 2009), observed that the entire reason for the success of water fractures in the Barnett shale is the ability of the low viscosity fluid of a water fracture to activate, dilate and shear offset natural fractures. Complexity, therefore, is related to use of slick water fractures and influenced by injection rate and injection pressure.

As an example, (Olsen, Bratton, and Thiercelin, 2009), listed four conditions that made fracture complexity in the Barnett a desired and possible outcome:

1. Orthogonal regional tensile fractures,
2. Low horizontal stress and stress anisotropy,
3. Low Poisson's ratio and extremely low matrix permeability.

Irrespective of these conditions, proppant transfer through the complex fracture network is one of the most challenging elements to predict or investigate in any shale. Small scale pumping simulators have helped to understand only basic concepts, but the most challenging variables is the anisotropic nature of the formation itself and the changing stress states during fracturing.

(Cipolla *et al.*, 2010), defined the fracture complexity index as the total width of the micro-seismic cloud with its length. Figure 2-27 shows various complexities of shales and sands with respect to the ability to form a fracture complexity index.

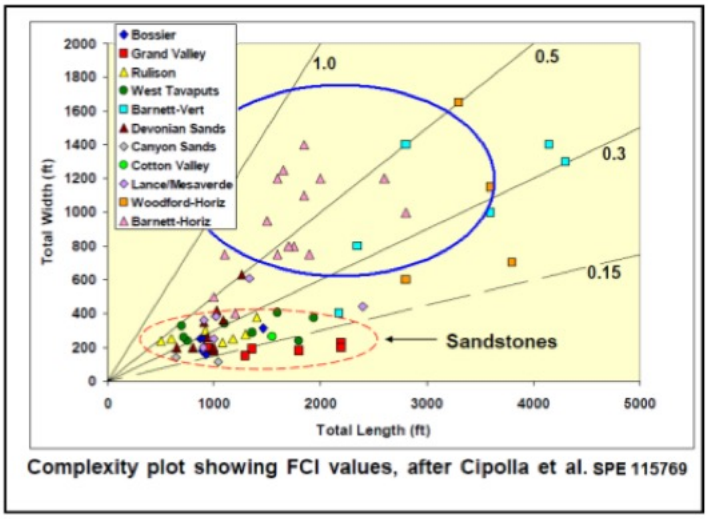

Figure 2-27: Fracture complexity includes comparisons of several formations. The total width is the enhanced fracture flow path width not the actual planar fracture width. The oval contains many of the Barnett wells (Cipolla *et al.*, 2010)

Most of the Barnett shale is a relative brittle, fine grained siltstone with a high Young's modulus and a moderately low Poisson's ratio (King, 2010). These formations are more easily fractured with slick water than the more ductile shales.

The Barnett horizontal well data reflect completions that are cased and cemented with multiple short perforation clusters spaced to assist in developing complexity in the fracture. The silica-rich parts of the shale have a high Young's modulus and a Low Poisson's ratio. Fractures opened in these zones tend to remain open, at least initially after simulation, increasing the effective permeability of the shale and the potential for gas recovery.

Brittleness may have a linkage to factors contributing to production (Jarvie *et al.*, 2007). Whether the more brittle rock is a hydrocarbon generator comparable to its production capacity is not stated, but the storage capacity for free gas in a highly brittle rock is likely higher than a more ductile rock with considerably more clays and organics and less interconnected matrix and frac porosity (Jarvie *et al.*, 2007).

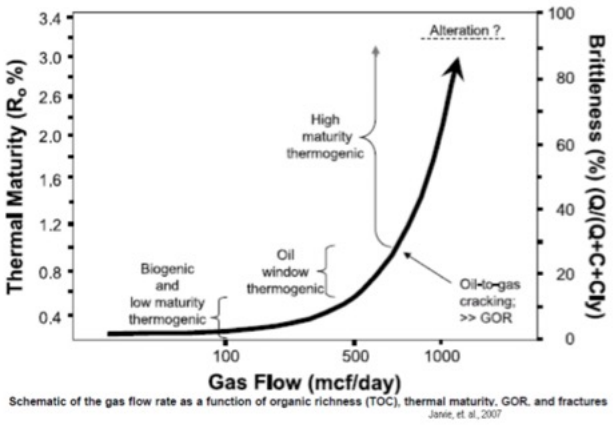

Figure 2-28: The graph shows a linkage of thermal maturity to gas flow projections from several shales and cross-plots a measure of rock brittleness linked to those wells (Jarvie *et al.*, 2007)

The goal of increasing fracture complexity is increasing recovery of the gas in place in the shale. Optimizing the recovery, especially in ultra-low permeability shales, requires generating both extensive reservoirs contact to access the natural fractures and keeping the fracture pathway open after fracturing stresses have been released.

If the fractures are unpropped, the matrix permeability's of 100 to 200nD (0.0001 to 0.0002 md) and the permeability of the healed natural fractures (variable perms) are simply too low to feed much gas into the main fractures. As has been found in lower permeability reservoirs, large areas of the reservoir are often largely undrained with wells on conventional spacing. In shales with the possibility of fracture complexity, opening and increasing linkage of natural fractures can achieve the same result with a smaller surface footprint of fewer wells.

Net pressure rise during fracturing has been linked with increasing fracture complexity in some shales (Palmer, Moschovidis and Cameron, 2007) and pressure changes during the job are used by some as an indicator of frac quality (King *et al.*, 2008). For example, a net pressure rises of about 700 to 1000 psi net (corrected for fluid slurry column density and friction) is an indicator of a frac that is building complexity in zone.

In the Barnett shale, it was observed that a modest net pressure rise of 1 to 5 psi per minute has been correlated with an increase in complex fracture development (a width over length complexity development ratio), fracs staying in zone without a lower frac barrier and solid production increases compared to offset wells of high tech operators (King *et al.*, 2008). A more rapid net pressure rise of 8 to 15 psi per minute has been linked to what appear to be potential screen-outs and some cases of breaking out of zone following the sharp pressure

rise (King *et al.*, 2008). (Palmer, Moschovidis and Cameron, 2007) describes complexity events as shear failures on planes of weakness outside the path of the main fracture plane (the events are marked by micro-seism's). The complexity is created by shear and/or tensile fractures and describes a failed reservoir volume (FRV) that implies a higher potential gas rate. In low matrix permeability formations such as shale, the developing shear (and tensile) failures typically produce a pore pressure increase in and transmitted by the natural fracture system. This pressure transmission along with increasing difficulty of generating more fracture volume in these complex fractures leads to increasing net pressure during the frac.

2.5.2. Rate

The fracture injection rate described as the key factor that produces the pressure required to drive the type of fractures needed in a completion but to drive fractures from multiple initiation points is complex and is not only dependent on rate rather a carefully spaced cluster perforation is also important. In some situations, 20bpm per perforation cluster can be used as a minimum but as fracture grows and leak-off increases, any injection rate will reach an optimum point where the injected fluid is completely lost in leak off and the fracture no longer grows (King, 2010).

2.5.3. Flow back and Fracture Load Recovery

The amount of fracture fluid recovery in gas shales is variable depending on shale characteristics, fracture design and the type of fluid (Crafton, 2008). Low complexity fractures often flow back quickly and a high percentage of frac fluid is recovered while in shale with extensive and complex fracture network, the amount of fluid recovered may be around 10 to 50% of the total pumped and the time for fluid recovery may extend over several weeks. Smaller natural fractures adding complexity to the fracture network may be the cause of delays in water recovery. Relative permeability effects in the narrow fractures, wettability issues, and the tortuous pathway in the fractures are the main causes of delays. This means that the stimulated reservoir volume (SRV) (Mayerhofer *et al.*, 2010) is not the same as the failed reservoir volume (FRV) (Palmer et al., 2007) or the outer extent of fracture fluid penetration. The difference between the two volumes could simply be that most of the load water that is not recovered from a frac is probably still in the smaller natural fracs and is blocking part of the flow path (Penny et al., 2006). As reservoir pressure in the shale fractures declines over time, there is less possibility that water in these small fractures will be displaced (George E King, 2010). For slick water fluids, capillary pressure is important as permeability's decline because this increases capillary pressure which makes it challenging to remove liquids from the smallest pores and smallest fractures (George E King, 2010). Fluid saturation also has an impact on liquid removal – most shale gas pores often have a water saturation between 25 to

45%, but the after-frac water saturation on the smaller natural fractures is higher initially until gas saturation increases which increases the capillary pressure (George E King, 2010). This explains the rapid decline rates of shale gas wells after fracturing because the total pressure to initiate flow is significant (George E King, 2010). The amount of pressure needed to flow is the capillary end effects which is the capillary pressure plus the additional pressure for fluids to exit the pore or the fracture (George E King, 2010).

2.6. Reservoir Simulation

(Medeiros *et al.*, 2010), presented a semi analytical solution for modelling fluid flow in hydraulic fractured horizontal reservoirs. Analytical solutions for fluid flow in naturally fractured reservoirs were also presented by Warren and Root (1963) and Kazemi (1969). However analytical solutions to fluid flow in naturally fractured reservoirs cannot accurately describe or capture the long transient flow behaviour in the matrix of shale gas reservoirs as a result of the ultralow permeability of the shale matrix. These solutions have been integrated into numerical reservoir simulation to improve run-time, but they still lack the ability to model transient flow in the matrix blocks.

A detailed method to model shale gas reservoirs is to refine the entire reservoir to include the fracture networks, hydraulic fracture, matrix blocks and unstimulated regions however this increases the simulation time (Cipolla *et al.*, 2010). The more practical method proposed by (Cipolla *et al.*, 2010) is to;

- Use the dual permeability method to represent all fracture networks in the stimulated and unstimulated volumes.
- Locally refine the grid in the stimulated volumes using a logarithmically spaced grid design.

This method was defined as the “DK-LS-LGR method” (i.e. dual permeability, logarithmically spaced, locally refined grid) for modelling hydraulically fractured shale gas reservoirs (Cipolla *et al.*, 2010). The logarithmic spaced grid design along with the local grid refinement helps to capture the typical long transient flow that exists to and within the fracture network. The dual permeability design helps in modelling flow in the matrix and fractures inside and outside the stimulated volumes. In the CMG Model, specifying a matrix property implies the matrix and hydraulic fracture while the fracture property consists of the natural fractures and secondary fractures Figure 2-29.

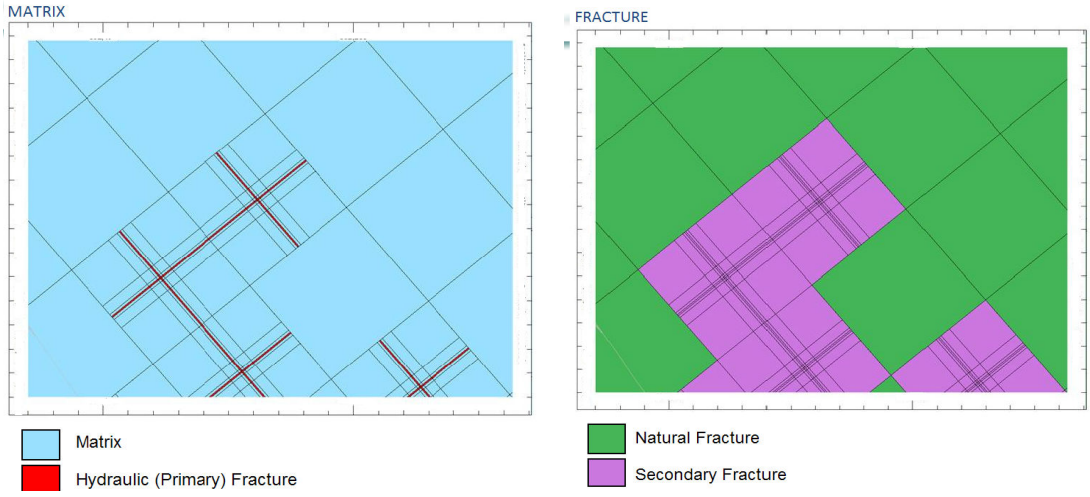

Figure 2-29: CMG's Interpretation of Matrix, Hydraulic Fracture and Secondary Fracture

Modelling of shale reservoirs is certainly different from coal bed methane because there is both Darcy flow and diffusion in the matrix whereas only diffusion in coal matrix (CMG, 2015). In addition to reservoir flow modelling, micro seismic fracture mapping provides the total volume of reservoir rock that has been stimulated i.e. the stimulated reservoir volume (SRV) whilst special core analysis can provide measurements of matrix permeability (Cipolla *et al.*, 2010).

Understanding of these two key parameters, enables the use of reservoir simulation models to estimate the fracture spacing or the level of complexity, as well as the fracture conductivity (Cipolla *et al.*, 2010). According to (Cipolla *et al.*, 2010), the complexity and conductivity of the fracture network are important components that impact well productivity in shale gas reservoirs. Production profiles from the model can then be compared with historical production data to evaluate the stimulation efficiency and fracture conductivity.

2.7. Forecast Methods of Shale Gas Recoverable Resource

(McGlade, Speirs and Sorrell, 2013) stated that understanding and providing resource estimates in undeveloped shale regions like the Upper Bowland Shale require a bottom-up analysis of geological parameters. The bottoms up approach relies upon geological appraisals of the extent and characteristics of the shale rock to estimate the volume of shale gas and apply a percentage recovery factor to produce the recoverable resource. Using this method require a large number of parameters to be calculated as shown in (Figure 2-30). The recovery factor tends to be established based on the mineralogy and geological complexity. This methodology is used in this thesis to understand the production potential of the Upper Bowland shale.

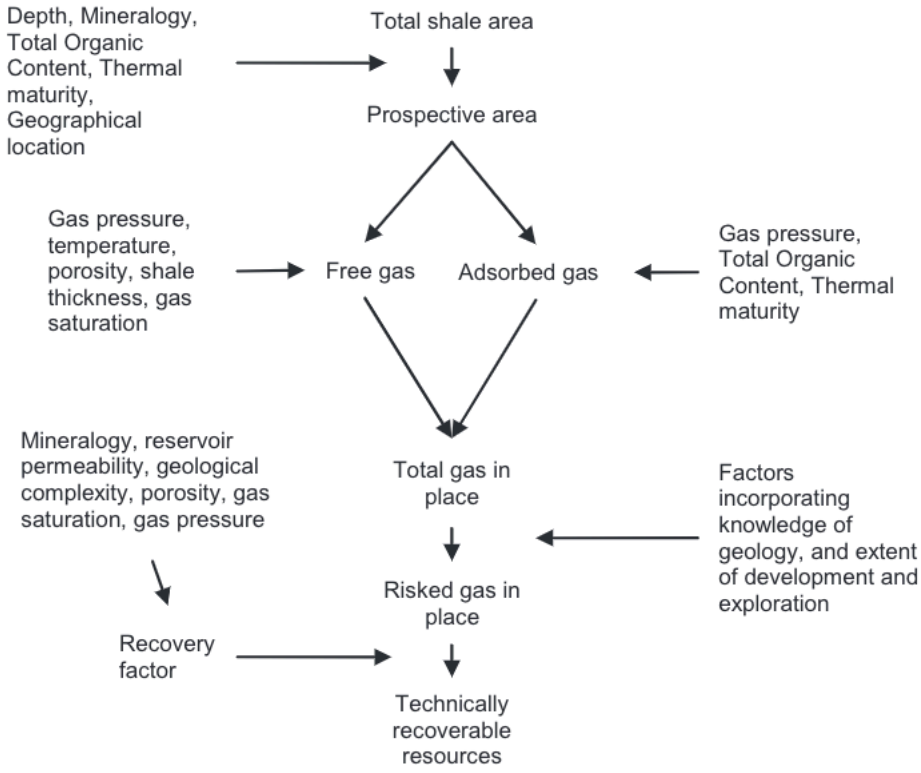

Figure 2-30: Schematic representation of the steps used in the geological based approach (McGlade, Speirs and Sorrell, 2013)

With the bottoms up approach, data may only be available for a subset of these and for unexplored shale plays, such estimates may have large confidence bounds as compared to applying the same methodology in conventional systems (McGlade, Speirs and Sorrell, 2013). (McGlade, Speirs and Sorrell, 2013) remarked that for conventional petroleum resource estimates: 'it is easy to show that no geological information exists other than that provided by drilling that has a range of uncertainty of less than several orders of magnitude'. Even when exploratory drilling has taken place, the range of uncertainty may still be wide. For example, it is often difficult to estimate the gas saturation from well-log data, a key parameter in the estimation of the gas in place (Lee and Sidle, 2010). A key problem with this methodology can be in the choice of analogue, for e.g. the choice of analogue used by the UK DECC varied by a factor of ten. The USGS also suggested using a probabilistic approach with more than one analogue to reduce this problem which appeared to be more sensible (McGlade, Speirs and Sorrell, 2013).

Advanced Resources International (ARI) employed this approach to estimate the volumes of gas that exists in shale plays around the world for which there is little or no drilling data, for e.g. the Cambay, Krishna-Godavari, and Cauvery shale basins in India (McGlade, Speirs and

Sorrell, 2013). (Andrews, 2013) also employed this approach to understand recoverable resource in the Bowland Shale. There have been two detailed investigations of three shale basins in India – the Cambay, Krishna-Godavari and Cauvery (Andrews, 2013). One by ARI used the bottom up geological approach (EIA, 2013), to estimate a total of 1.59Tcm and the second by the USGS used the extrapolation approach to estimate 0.17Tcm – an order of magnitude difference. Since no production history exists for these shale plays, the USGS employed analogues based on US shale plays for the well spacing, the EUR/well, and success factor (McGlade, Speirs and Sorrell, 2013). The choice of an appropriate analogue was based on many of the same factors used in geological approach including: shale thickness, total organic content, shale mineralogy, thermal maturity, gas pressure, and geological complexity (Charpentier and Cook, 2013).

(Weijermars, 2013) made a first attempt to evaluate the economics of undeveloped European shale plays (Poland, Austria, Germany, Sweden and Turkey) applying a type curve analysis assuming an exponential decline function and applying an estimated ultimate recovery/well from Kuhn and Umbach's 2011 study based on various reports and unspecified analysis.

(Taylor, Lewis and Byles, 2013) paper focussing on the United Kingdom shale gas production potential production assumes an average EUR/well from developed US shale plays and an initial production rate. The validity of results based on average EUR/well is highly unlikely.

(McGlade, Speirs and Sorrell, 2013) also suggested an approach to produce resource estimates by extrapolation of production experience but advised that this method should only be used in developed regions where production is relatively advanced. It relies upon analysing the production experience in the region and then extrapolating these results to either undeveloped areas of the same shale or to new shales (Anandarajah and Nwaobi, 2015). Extrapolation of production experience require the investigated area to be split into more and less productive sectors to determine the EUR and average well spacing per area (Anandarajah and Nwaobi, 2015). Estimate of EUR per well can be derived by statistically fitting a declining curve to the historical production from a well or group of wells and extrapolating forward into the future using decline curve analysis. (McGlade, Speirs and Sorrell, 2013) urged that this method is only applicable in regions where production is well established and requires a significant amount of data on historic production from multiple wells. This approach was used in this thesis to better understand the Barnett Shale and apply the results to undeveloped shales like the Bowland Shale to better answer the research gap as outlined in section 1.3. The main challenge with this extrapolation method is that production from shale gas wells declines continuously and rapidly within a month or two of initial production, with the rate of

production frequently declining by as much as 50% within one year (McGlade, Speirs and Sorrell, 2013). Higher rates of production decline lead to a shorter production life and a lower ultimate recovery (McGlade, Speirs and Sorrell, 2013). But with only 2–3 years of production experience, it is difficult to know whether production will continue to decline at the same rate, or whether the rate of decline will slow in the future (McGlade, Speirs and Sorrell, 2013). Different choices are available for the 'shape' and rate of future production decline and these different choices can lead to significantly different estimates of the EUR/well (McGlade, Speirs and Sorrell, 2013).

Some decline curve methods are discussed in the following sections:

2.7.1. Arp's Hyperbolic and Modified Hyperbolic Method

Production decline is commonly modelled by either a negative exponential 'decline curve', which has a constant rate of decline, or a hyperbolic decline curve which has a rate of decline that reduces over time (McGlade, Speirs and Sorrell, 2013). The parameters for these curves are usually derived by statistically fitting such curves to historical production data, with the key parameter being termed the 'b constant' (Ilk *et al.*, 2008). Larger values of b imply slower rates of production decline and larger ultimate recovery. it is important to note showed that b values equal to or greater than one can cause physically unreasonable results at time tends to infinity. If there is sufficient data to reach boundary dominated or stabilized flow regime, the value of b that would fit the data would be less than one (Lee and Sidle, 2010). Without stabilized data, forecasting future production with the Arp's hyperbolic can result in an overestimation of reserves. Data on shale gas decline rates is sparse given their commercial sensitivity, but b constants between 1.4 and 1.6 have been used by shale gas companies currently active in the US (McGlade, Speirs and Sorrell, 2013). There is some support in the current literature for b constants in this range: for example, data from 8700 horizontal wells in the US Barnett Shale were best fit to hyperbolic decline curves with b values ranging from 1.3 to 1.6, and a mean of 1.5 (Fan *et al.*, 2011). Additionally, analysis of 1957 horizontal wells in the Barnett, Fayetteville, Woodford, Haynesville and Eagle Ford shale plays suggests that while the data does not always support b constants as high as 1.4, values exceeding unity are realistic in shale gas plays (Baihly *et al.*, 2011). The Arp's decline equation is conveniently used because it can have a best fit for the long transient linear-flow regime observed in shale gas wells with b-values greater than one despite exceeding the limit of the Arp's equation (Duong, 2011).

An analysis by Chesapeake Energy of a group of 44 wells with over 12 months production experience in the Haynesville shale - Chesapeake fitted a hyperbolic curve to this data with a

b constant of 1.1 (McGlade, Speirs and Sorrell, 2013). However, this estimate is optimistic and shows that curves with a range of different b constants fit the data comparably well (McGlade, Speirs and Sorrell, 2013). (McGlade, Speirs and Sorrell, 2013) suggested that a b constant of 0.5 would more accurately reflect the uncertainty to investors. This difference significantly affects the EUR/well: a b constant of 1.1 results in an estimate of 185 mcm/well, while a value of 0.5 results in only 85 mcm/well.

Fundamentally the general Arp's hyperbolic decline is described as:

$$q = q_i \frac{1}{(1 + bD_i t)^{(1/b)}}$$

Equation 16

Where 0<b<1. When b=0, the equation becomes an exponential equation;

$$q = q_i e^{-at}$$

Equation 17

A special case when b=1, the Arp's equation becomes harmonic;

$$q = q_i \frac{1}{(1 + D_i t)}$$

Equation 18

Attempting to use the Arp's hyperbolic equation for shale gas wells requires a b value greater than 1 which is beyond the limit specified by Arp's. Using b values greater than 1 result in physically unreasonable outcomes as illustrated in the following equations (Lee and Sidle, 2010);

$$Q = \int_0^t q(t)dt$$

Equation 19

Then, for exponential decline,

$$Q = \frac{q_i - q}{a}$$

Equation 20

As $t \to \infty, Q \to \frac{q_i}{a}$ – this is a realistic and finite limit

For hyperbolic decline,

$$Q = \frac{{q_i}^b}{D_i(b-1)}\left(q(t)^{(1-b)} - {q_i}^{(1-b)}\right)$$

Equation 21

For 0 < b < 1, as t→ ∞, $Q \rightarrow \frac{q_i}{D_i(1-b)}$ – another finite limit. However for hyperbolic decline but with b > 1, as $t \rightarrow \infty$, $\lim_{t\to\infty} Q = \frac{{q_i}^b}{D_i\ (b-1)}\left[\frac{1}{q\ (t)^{(b-1)}} - \frac{1}{{q_i}^{(b-1)}}\right] \rightarrow \infty$.

The reason the data fits well with the observed data when b>1 is because the data is still in the transient flow regime (Fetkovich, Vienot, Bradley, & Kiesow, 1987). Though as more data becomes available the best fit b value to the data decreases (Blasingame & Rushing, 2005); (Rushing, Perego, Sullivan, & Blasingame, 2007), (Lee and Sidle, 2010). On a physical basis, if there was enough data at very late time, the b value that will fit those data in the boundary dominated flow regime will be less than 1(Lee and Sidle, 2010). Using the Arp's general equation, without stabilized flow data, will not forecast production with confidence. Typically, the hyperbolic decline is typically an excessive predictor of reserves particularly in shale gas reservoirs as the decline rate decreases over time and shale gas reservoirs show a long period of linear transient flow which is not governed by Arp's (Ilk *et al.*, 2008). The modified hyperbolic method attempts to resolve Arp's hyperbolic long-term decline behaviours (Cauter, 2013). It was proposed in 1988 and works by switching the initial hyperbolic decline to an exponential tail at a predetermined fixed decline rate when the decline rate is achieved (Cauter, 2013) - typically, a 5% terminal decline rate is often used in shales (Joshi and Lee, 2013). The exponential tail mathematically represents systems of low compressibility, boundary dominated flow and stable operating conditions (Cauter, 2013).

2.7.2. Doung's Method

Doung's method was developed on the basis that production-rate and time would have a power law relation when plotted on a log-log scale (Kanfar and Wattenbarger, 2012a) Equation 22. The Doung's power law relation contains the time exponent, "m" to help match field data(Joshi, 2012)

$$\frac{q}{G_p} = at^{-m}$$

Equation 22

This model is mostly accurate for transient linear flow and production trends will curve from a log-log straight line when boundary dominated flow is reached (Kanfar and Wattenbarger, 2012a) Equation for production rate is;

$$q = q_1 t(a, m) + q_\infty$$

Equation 23

Where,

$$t(a, m) = t^{-m} exp^{\left(\frac{a}{1-m}\left(t^{1-m}-1\right)\right)}$$

Equation 24

The q_∞ term was added by (Doung, Rate-Decline Analysis for Fracture-Dominated Shale Reservoirs, 2011) to provide a better fit to some field data that showed an intercept instead of a straight line to the origin when plotting $q\ vs\ t(a, m)$ (Kanfar and Wattenbarger, 2012a). The term can be positive or negative. Results from this method matched historical rates accurately provided that they are used during linear flow. Linear flow can be observed as a half slope on a log-log plot of gas rate against time (Kanfar and Wattenbarger, 2012b). Doung's diagnostic plot i.e. q/Gp against time also yields a straight line on a log-log plot – data on the straight line suggest the presence of linear flow (Duong, 2011). Prior to linear flow, bilinear flow can occur for a short time and is represented with a quarter slope on a log-log plot of gas rate against time (Kanfar and Wattenbarger, 2012b). For cases where bilinear flow is also observed in the historical data, (Kanfar and Wattenbarger, 2012b) observed that Doung's method typically fits the data accurately compared to Arp's hyperbolic, Ilk's method, and Valko's method.

(Joshi and Lee, 2013) proposed a model referred to as the modified Doung's to address the limitations of the original Doung's model. The modified Doung's method, consists of the original Doung's model followed by an Arp's hyperbolic model to account better for late time boundary dominated flow. This method is applicable when forecasting is carried out since it is unlikely that the well will remain in linear transient flow for the rest of its production. To account for fracture interference and structural boundaries which result in boundary dominated flow, modified Doung's was developed. In this model, two modifications are made;

1) the initial Doung's model switches to a hyperbolic tail at a point when the effective decline rate reaches an arbitrary value (typically 5%). (Joshi and Lee, 2013), used a b value of 0.4 as proposed by (Fetkovich, Fetkovich, & Fetkovich, 1996) for a gas well with the flowing bottom hole pressure that is 10% of the reservoir pressure. (Joshi and Lee, 2013), showed that the

Modified Doung's outperforms the Modified Hyperbolic and Stretched Exponential in terms of accuracy and precision for production histories greater than 18 months.

2) (Joshi and Lee, 2013) observed that using a non-zero value for q at infinity lead to unrealistic results when only 6-12 months of historical production data are available. The flow rate at infinity term introduced by (Duong, 2011) was an attempt to fit production data under different operating conditions.

2.7.3. Ilk Method – Power Law Exponential Decline

Ilk used an attenuation power function to characterize the decline rate D, defined as:

$$D = D_{\infty} + D_1 t^{-(1-n)}$$

Equation 25

Equation 25 indicates that the attenuation power function can be used to describe the decline rate at the transient, transition and boundary dominated flow period. On a log-log case study, the D function Equation 25 is a straight line with slope n-1 at the early stage and tends to a constant (D $_{\text{infinity}}$) at a late stage (Hedong, 2015). At early times, the impact of D_{∞} on D is negligible whereas at late times the time dependent terms attenuate therefore D_{∞} becomes a controlling factor (Moghadam & Mattar, 2009). Substituting the decline rate Equation 17 into Ilk's exponential rate-time equation leads to:

$$q = \hat{q}_i e^{-D_{\infty} t - \hat{D}_i t^n}$$

Equation 26

The power function is similar to an exponential function as it solves the problem of b-value attenuating with time in the Arp's method. This method can satisfactorily match historical production data during the transient stage prior to reaching boundary dominated flow – hence this method is better applicable to shale gas reservoirs since transient flow regime is often the dominant flow regime in shale reservoirs (Hedong, 2015).

2.7.4. Mattar Method – Modified Power Law Exponential Decline

The Ilk Power Law function has four unknowns namely $\hat{q}_i, \hat{D}_i, D_{\infty}, and\ n$. Owing to this, there can be many acceptable matches to the same to historical data which will yield different future forecasts (Moghadam & Mattar, 2009). Mattar's method attempts to constrain the degrees of freedom to make the production forecast more unique. (Moghadam & Mattar, 2009), modified

the power law exponential decline to make it compatible with linear and radial flow analytical reservoir models each followed by boundary dominated flow (BDF). The Ilk's equation can be modified for the radial flow stage by reducing the equation to

$$q = \hat{q}_i e^{-\hat{D}_i t^n}$$

Equation 27

Where (0<n<0.13)
Equation 27) is only valid for transient flow stage.
During transient radial flow, n is 0.13. The exponent n, is related to the slope of the log-log plot of D versus time and can be described as; N exponent = slope +1

For linear flow, the n-exponent becomes the slope on the log-log plot and for linear flow is -1 but substituting an exponent of zero in Equation 27 does not result in a power law exponential decline therefore Equation 28 should be used for linear flow where n=0.

$$q = \frac{q_i}{\sqrt{t}}$$

Equation 28

Once BDF regime is reached, the transient flow equation is no longer valid and the value of D at that instance is the limit decline rate and exponential decline equation is used for forecasting Equation 25
The time when BDF occurs or starts can be evaluated from:

$$t_{BDF} = \frac{40}{\pi} \frac{\phi \mu A}{\bar{p} k}$$

Equation 29

All of the aforementioned mathematical discussion in this section have been based on liquid flow considerations. The reservoir models are based on constant compressibility-viscosity liquid properties which are not valid for gas as there are big changes in compressibility due to declining reservoir pressure (Moghadam & Mattar, 2009). For the transient part of the data, the same procedure can be applied but with time as pseudo-time however practically the effect is relatively small. For BDF, assuming a constant decline rate (i.e. exponential decline), is not valid but can be easily approximated by assuming a hyperbolic decline with a b exponent of 0.5 therefore at the start of BDF where $D=D_{limit}$, hyperbolic decline is assumed as follows Equation 30) (Moghadam & Mattar, 2009);

$$q = \frac{q_i}{(+0.5 D_i t)^2}$$

Equation 30

The initial flow rate and decline rate are the values at the start of BDF.

2.7.5. Mattar Method – Modified Power Law Exponential Decline

- From the historical production data, estimate the instantaneous decline rate using the appropriate equation and plot on a log-log plot of D vs t.

- Conduct linear regression on through the points ensuring that the slope of the line is confined to the range of -1 to -1.13 with more weight been applied to the later time data.

- The intercept of the line at t=1, equals n$\widehat{D}_i$, hence $\widehat{D}_i$ can be estimated.

- On a semi log plot of log q vs t, plot equation x and adjust initial rate to match the measured historical production data.

- Based on Equation 29), showing the time when BDF starts, hyperbolic decline can then be used from that point in time to complete the production forecast.

2.7.6. Stretched Exponential Production Decline (SEPD) (Valko's Method)

The SEPD method was proposed by (Valko, 2009), and is simply a sum of exponential decays at different times controlled by two parameters which are regarded as the shape and scale factors. The SEPD model works on the basis that group production from a large number of wells follow a stretch exponential decline pattern. The SEPD method tend to be more accurate with wells that have long production histories greater than 36 months (Valko, 2009). The two advantages of the SEPD over Arp's are that the EUR is bounded, and it is designed to model transient flow.

2.7.7. General Behaviour of the Decline Exponent in Shale Gas Wells - The Decline Exponent

The following are a summary of reasons why b values greater than 1 can be expected (Kupchenko, Gault and Mattar, 2008);

- Wrong interpretation of historical production data.

- The historical production data is still under transient flow regime and has not reached boundary dominated flow regime.
- Reservoir layering can cause b values > 1.
- Some fractured gas wells have shown b values up to 3.5.

Theoretically, a hydraulically fractured well should experience the following flow regimes: Linear Flow, Transient Flow, flow transition between transient to BDF, and BDF (Kupchenko, Gault and Mattar, 2008). The decline exponent, b, from the production data can give an indication of which flow regime the shale well is currently experiencing (Kupchenko, Gault and Mattar, 2008). Summary of the decline exponent behaviour are shown on Table 2-11.

Table 2-11: Determination of Flow Regime based on the Decline Exponent (Kupchenko, Gault and Mattar, 2008)

Decline Exponent	**Flow Regime**
$b = 4$	Bilinear Flow
$b = 2$	Linear Flow
$b \leq 0.5$	Boundary Dominated Flow
Decline Exponent Increases (b from 2-20)	Transient Flow
Decline Exponent Decreases	Boundary Influenced Flow

As shown on Table 2-11, the decline exponent is not constant during the shale well producing life except during linear flow. Boundary dominated flow may not be reached until after several years (Kupchenko, Gault and Mattar, 2008). A lower decline exponent is commonly observed with increasing fracture efficiency (Kupchenko, Gault and Mattar, 2008). Better effective fractures can be obtained by (Kupchenko, Gault and Mattar, 2008);

- Increasing the length and conductivity of the fracture
- Fracture orientation perpendicular to the maximum permeability direction

During the boundary dominated flow, the decline exponent is expected to decrease with drawdown (Kupchenko, Gault and Mattar, 2008). Since tight gas wells are generally operated at high drawdown hence decline exponent of 0.5 can be expected for a single layer reservoir (Kupchenko, Gault and Mattar, 2008). For wells with larger hydraulic fractures operating at a higher drawdown, decline exponent can decrease up to 0.25 during BDF (Kupchenko, Gault and Mattar, 2008).

Chapter 3 Production Analysis and Economics

3.1. Case Study 1 – Application of Arp's Hyperbolic Decline to the Barnett Shale

Despite the limitations of the Arp's method in shale gas reservoirs, Arp's method can be easily applied to shale reservoirs to get a first estimate of decline performance. In this case study, publicly available production data from 59 wells in the Barnett Shale, were used to carry out decline analysis. Since shale reservoirs are ultra-low permeability reservoirs and highly heterogeneous, more wells, typically a minimum of 100 wells are needed to obtain a sufficient representation of the shale play. Before carrying out the Arp's decline analysis, the type of decline model shown by the historical production data was first investigated. The flow chart on Figure 3-1 shows the procedure used to determine whether the data was exponential, harmonic or hyperbolic decline.

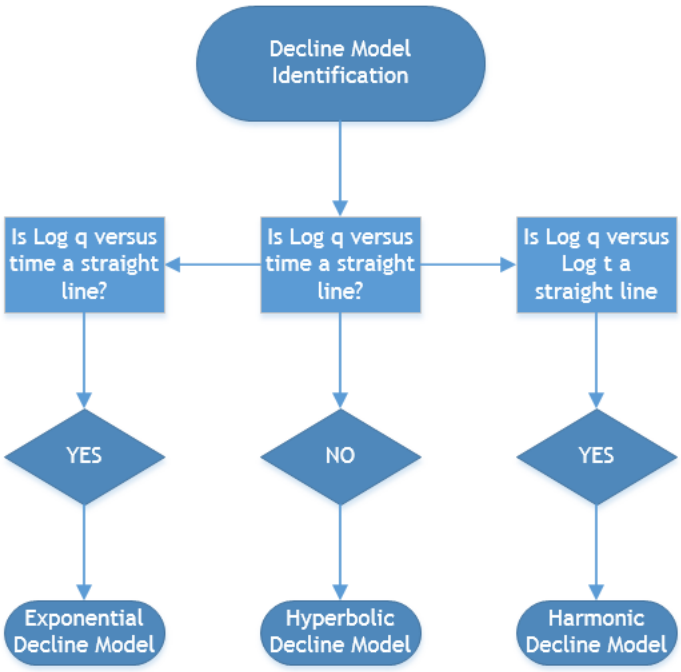

Figure 3-1: Flow Chart for Model Identification

Graph of Log q versus log t was not a straight line which meant the data was not representing harmonic decline Figure 3-2.

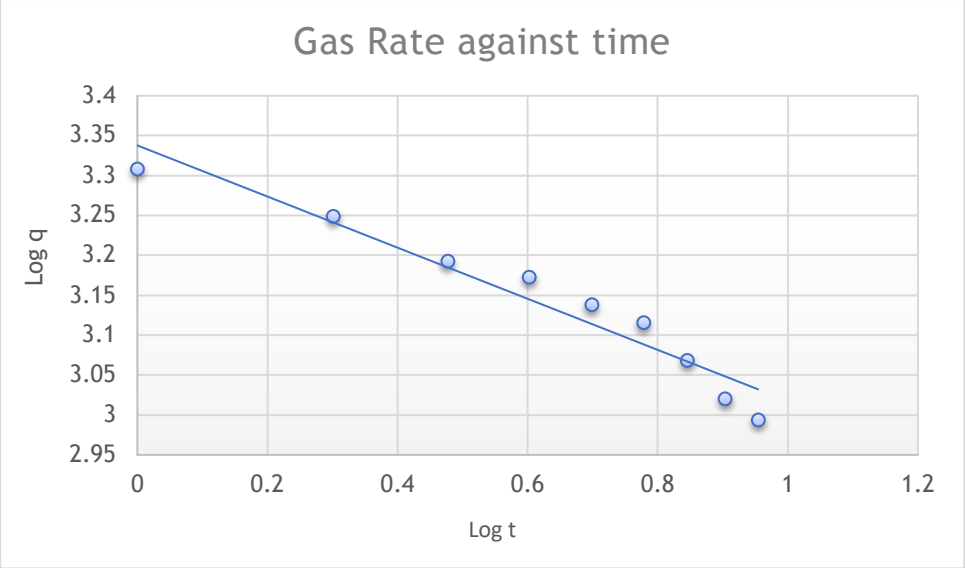

Figure 3-2: Graph of Log q vs Log t

Graph of log q versus t was also not a straight line, which meant the data was not representative of exponential decline Figure 3-3.

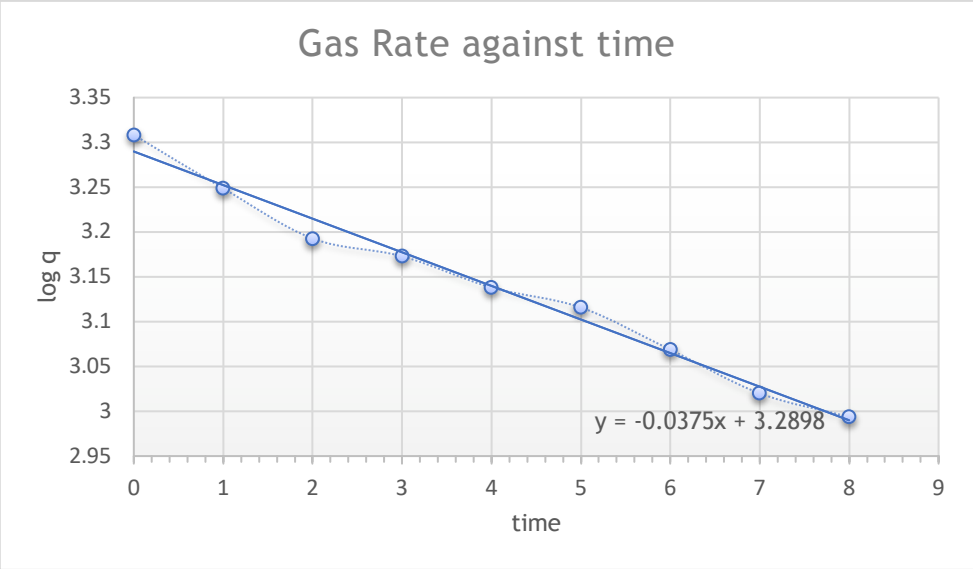

Figure 3-3: Graph of Log q versus t

To confirm that Figure 3-3, is truly not a straight line, residuals of data were plotted i.e. residuals of the y axis (Figure 3-4). The residual is the difference between the data and the line of best fit data.

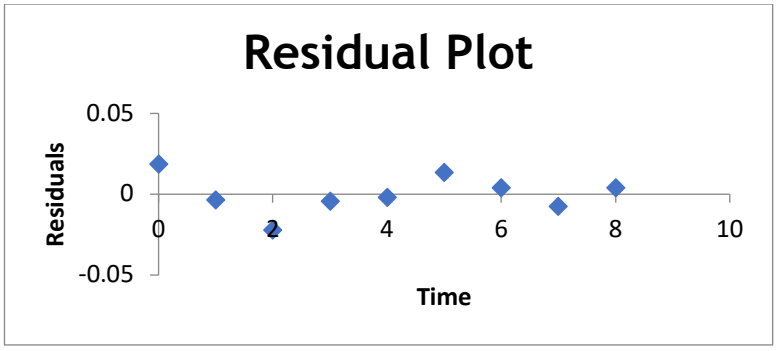

Figure 3-4: Residual Plot

If the data fits poorly to the line of best fit, the residual plot will have a pattern but if the data fits well with the line of best fit, the residual plot will be random (Figure 3-4). In this case study, the residual had a pattern suggesting that the data is not a straight line as shown on Figure 3-3. This means the decline model is hyperbolic as we have eliminated the other two models. Since the b value for hyperbolic typically ranges between 0 and 1, it was estimated for the data using Newton Raphson iteration and 0.53 was obtained. This conclusion agrees with report published by (King, 2010). Gas production rates was calculated using the hyperbolic decline equation. The results of the decline analysis are shown on (Figure 3-5). The blue data points show the results of the hyperbolic decline equation while the red data points showed the historical production data from the 59 wells.

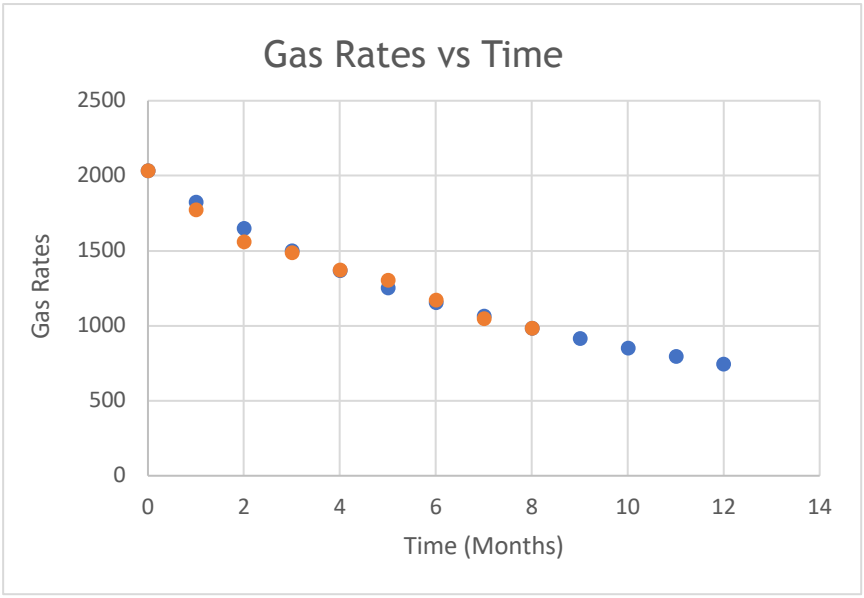

Figure 3-5: Gas Rate Plot (History versus Observed)

The decline model bares a close resemblance to the historical data for the eight months that was investigated. The aim of decline analysis is to then allow us to predict future production and ultimately measure the estimated ultimate recovery (EUR).

3.2. Case Study 2 – Shale Gas Production Decline Trend over Time in the Barnett Shale

3.2.1. Summary

This case study attempts to provide an update on two previously published work (by the same authors) on assessing production decline trends and forecasting estimated ultimate recovery on US shale gas basins but with focus on the Barnett shale. The first case study was presented in 2010 at the SPE Technical Conference (SPE-135555) and the second case study was presented in 2015 at the Unconventional Resources Technology Conference (SPE-178674). These case studies both highlighted the scepticism from consultants and investment firms commonly placed on forecasting EUR accurately in shale gas wells. Production in the Barnett shale have declined by 69% from 2015 hence this case study seeks to provide an additional perspective on the EUR estimate obtained for the Barnett shale from the two previous publications to assist in making sound strategic decisions and regulatory reserves reporting. In this case study, we used horizontal wells from core and non-core counties within the Barnett shale compared to only horizontal wells from core counties as used in the aforementioned publications. Aside from the general Arp's hyperbolic used in previous publications, other decline curve methods like the Doung's method and Modified Arp's hyperbolic were employed to assess EUR in addition to the general Arp's hyperbolic. This study showed that reliable and conservative estimates of EUR can be obtained. This case study allowed the research gap to be better understood by examining the extrapolation method of analysing production as described in section 2.7.

3.2.2. Introduction

With the surge in exploiting unconventional shale gas, the need to forecast production and EUR to improve investment decisions have grown (Cauter, 2013). A quick widely used method is decline curve analysis and is employed in this study. DCA is not the only method to estimate EUR - other methods include; type curves, volumetric, material balance, analogies, numerical or analytical models (Cauter, 2013). However, because unconventional shale reservoirs are poorly understood, applying any of these methods brings complexity, increased cost and significant uncertainty (Lee and Sidle, 2010). (Baihly *et al.*, 2010), carried out an assessment of EUR on various shale plays, including the Barnett shale using horizontal wells with a date of first production (DOFP) from 2003 to wells with a DOFP from 2009 Figure 3-6. In this case study, horizontal Barnett shale wells with a DOFP from 2008 to 2015 were used to understand

decline trend and forecast EUR Figure 3-6. The EUR for DOFP 2008 and 2009 was calculated in the (Baihly *et al.*, 2010) study and these were compared to results from this case study in later sections.

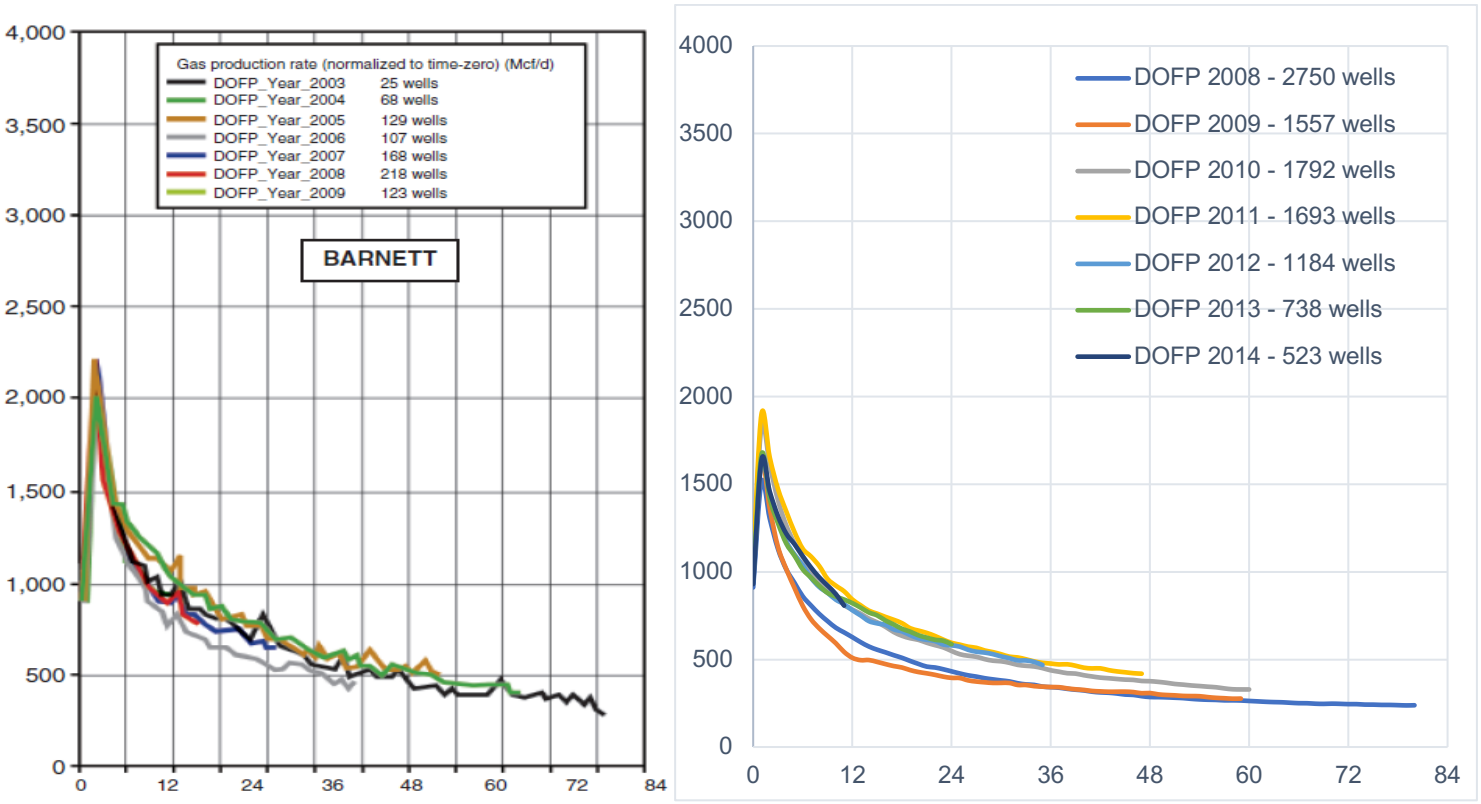

Figure 3-6: **Barnett shale average daily production rate per well in MSCF/day (y-axis) against time (months) grouped by DOFP. Left plot shows result from** (Baihly *et al.*, 2010) **and right plot shows results from this case study.**

The area of interest in the (Baihly *et al.*, 2010) was located in the Tarrant, Wise, Denton, and Parker counties; which are the Barnett shale core counties. However, the non-core counties were also included in this study except Archer, Comanche, and Cooke, Coryell, Hamilton, Shakleford and Stephens counties (Figure 3-7).

Core Counties	Non-Core Counties	
Denton	Archer	Hood
Johnson	Bosque	Jack
Tarrant	Clay	Montague
Wise	Comanche	Palo Pinto
	Cooke	Parker
	Coryell	Shakleford
	Dallas	Somervell
	Eastland	Stephens
	Ellis	
	Erath	
	Hamilton	
	Hill	

Figure 3-7: Core and Non-Core Counties in the Barnett Shale (Railroad Commisson of Texas, 2017)

The areas of study for Barnett shale wells in (Baihly, Malpani, Altman, Lindsay, & Clayton, 2015) was also located in the Tarrant, Wise, Denton and Parker counties. A total of 1,138 horizontal wells from 2003 to 2013 were considered compared to 10237 wells in this case study (Figure 3-8), representing an 800% increase in well count compared to (Baihly, Malpani, Altman, Lindsay, & Clayton, 2015).

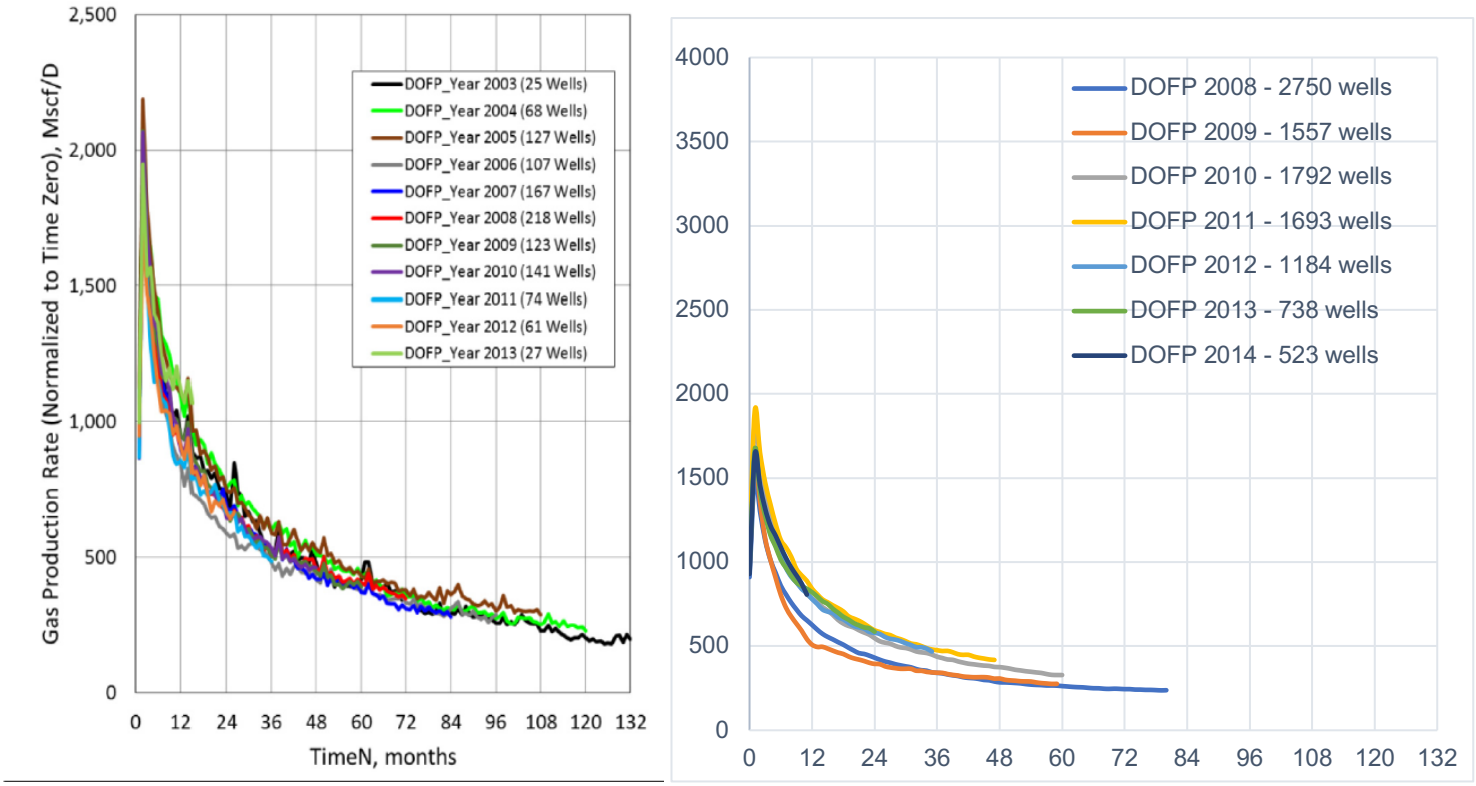

Figure 3-8: Barnett shale average daily production rate per well in MSCF/day (y-axis) against time (months) grouped by DOFP. Left plot shows result from *(Baihly, Malpani, Altman, Lindsay, & Clayton, 2015)* **and right plot shows results from this case study.**

There were no production improvement over time in the Barnett shale because the initial production rate are in a tight range – the Barnett typically have the lowest initial production of all the shale gas plays in the US (Baihly *et al.*, 2010) (Baihly, Malpani, Altman, Lindsay, & Clayton, 2015) (Figure 3-8) Figure 3-6. Similar to the (Baihly, Malpani, Altman, Lindsay, & Clayton, 2015) and (Baihly, Altman, Malpani, & Luo, 2010) case study, the production trends were parallel with similar slopes over the years (Figure 3-8) Figure 3-6. Though (Baihly, Malpani, Altman, Lindsay, & Clayton, 2015), stated that from 2003 to 2013, lateral length increased by 50% and proppant per lateral increased by 33%. The implication is that wells are becoming tightly spaced and interfering with older offset wells. Despite improved fracturing treatments, the production trends in the Barnett are consistent which asserts that the impact of reservoir quality is significantly greater than that of completion quality on the productivity of the play (Baihly, Malpani, Altman, Lindsay, & Clayton, 2015) (Baihly *et al.*, 2010). The results obtained in (Baihly *et al.*, 2010) and (Baihly, Malpani, Altman, Lindsay, & Clayton, 2015) only employed the use of Arp's hyperbolic decline in determining the EUR. In this case study, Doung's method and Modified hyperbolic was used in determining EUR in addition to Arp's hyperbolic. Doung's method is more suited to unconventional shale gas reservoirs compared to Arp's models as it is based on long term transient linear flow regime commonly observed in shales (Kanfar and Wattenbarger, 2012b). The use of Doung's method was justified using the log-log diagnostic plot of gas rate vs time (Kanfar and Wattenbarger, 2012b). The objective of this case study is to provide a reliable update on the EUR estimates obtained from (Baihly, Malpani, Altman, Lindsay, & Clayton, 2015) and (Baihly *et al.*, 2010) (Appendix A).

3.2.3. Methodology

The methodology applied in this study was similar to that used in (Baihly, Malpani, Altman, Lindsay, & Clayton, 2015) and (Baihly *et al.*, 2010). The steps are outlined below:

1. Horizontal monthly gas production data (in MScf/day) from wells in the Barnett shale producing from 2008 to 2015 was sorted and arranged in order of DOFP. Wells with a 2015 DOFP were excluded from the analysis as the group had only four months production which was insufficient for appropriate conclusions to be made.

2. The production data was quality checked on a well by well basis by removing abrupt changes in production data from each well. Possible reasons can be associated with pipeline constraints and re-stimulation (Baihly, Malpani, Altman, Lindsay, & Clayton,

2015). The rate data (in MScf/day) were shifted with respect to time such that all wells were normalized to start at “time zero”.

3. A final production type curve was generated by applying a cut-off to the initial production type curve at a point in time when the well count in each data group began decreasing drastically. This is because at this point, the calculated rate no longer represents the original group of wells; decreased number of wells in a group can cause erroneous decisions to be made about the production decline. Figure 3-9, shows how the well count varies over time for each year group.

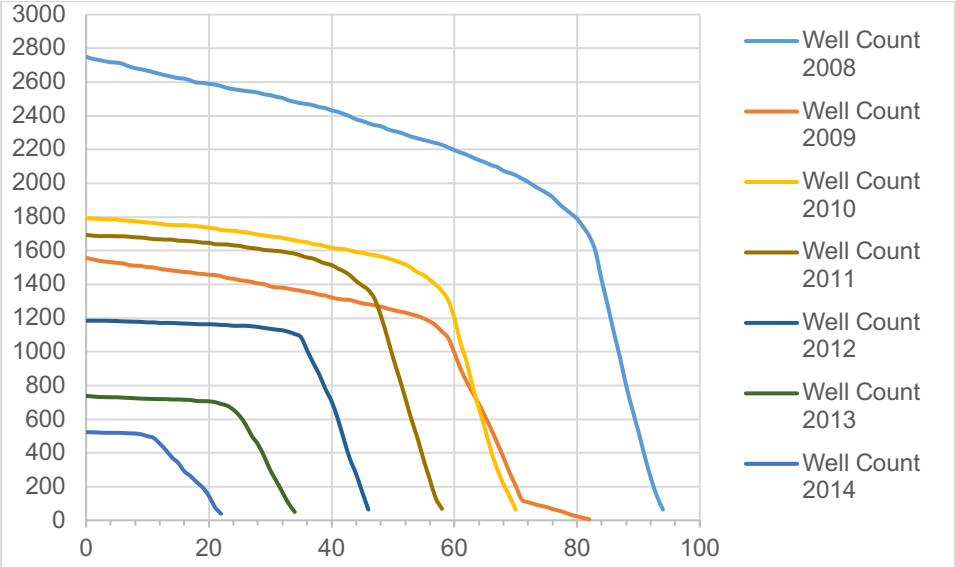

Figure 3-9: Well Count for Barnett Shale Wells over Time (months, x-axis)

4. The cut-off time for each year group were at the following months; 78 months for DOFP2008, 59 months for DOFP2009, 60 months for DOFP2010, 46 months for DOFP 2011, 35 months for DOFP 2012, 24 months for DOFP 2013, and 11 months for DOFP 2014. Excluding the data beyond the cut-off times ensured that that the resultant average production type curve better represent the original group of wells since the number of producing wells remain nearly constant.

5. Decline curve analysis (DCA) was performed on each type curve for each year group The DCA was performed using the Arp’s hyperbolic method, modified hyperbolic method and the Doung’s method.

6. After obtaining a match with the production data, the EUR at 30 years was then computed for the three methods to validate results to work carried out by (Baihly,

Altman, Malpani, & Luo, 2010) and (Baihly, Malpani, Altman, Lindsay, & Clayton, 2015). Detailed historical match using the Doung's method is presented in Appendix A. Finally all production data for each DOFP group were combined to obtain a single type curve and EUR; the results were compared to work from (Baihly, Malpani, Altman, Lindsay, & Clayton, 2015) and (Baihly *et al.*, 2010).

3.2.4. Results

The variation in EUR at 30 years over all the year groups are presented on (Table 3-1). The production rates for wells with a DOFP of 2008 and 2009 are presented on (Figure 3-10) showing all the DCA methods used. The combined average type curve for all the time groups in this case study are shown on (Table 3-2) along with results from (Baihly *et al.*, 2010) and (Baihly, Malpani, Altman, Lindsay, & Clayton, 2015).

Table 3-1: EUR Variation over all Time Groups

	EUR at 30 years – Barnett Shale				
	Arp's Hyperbolic (BCF)	**Doung (BCF)**	**Modified Hyperbolic @5% switch (BCF)**	(Baihly, Altman, Malpani, & Luo, 2010) **– Arp's Hyperbolic (BCF)**	(Baihly, Malpani, Altman, Lindsay, & Clayton, 2015) **– Arp's Hyperbolic (BCF)**
DOFP 2008	2.218 (b=1.3008;Di=0.0996)	2.184	2.208	2.895	n/a
DOFP 2009	2.280 (b=1.7550;Di=0.2138)	2.489	2.180	2.867	n/a
DOFP 2010	2.697 (b=1.6479;Di=0.1638)	2.582	2.595	n/a	n/a
DOFP 2011 (1693 wells)	2.980 (b=1.6188;Di=0.1419)	2.960	2.873	n/a	n/a
DOFP 2012	2.929 (b=1.9254;Di=0.1633)	2.842	2.761	n/a	n/a
DOFP 2013	2.984 (b=1.7374;Di=0.1287)	2.766	2.850	n/a	n/a
DOFP 2014	2.024 (b=1.1458;Di=0.1091)	2.694	2.005	n/a	n/a

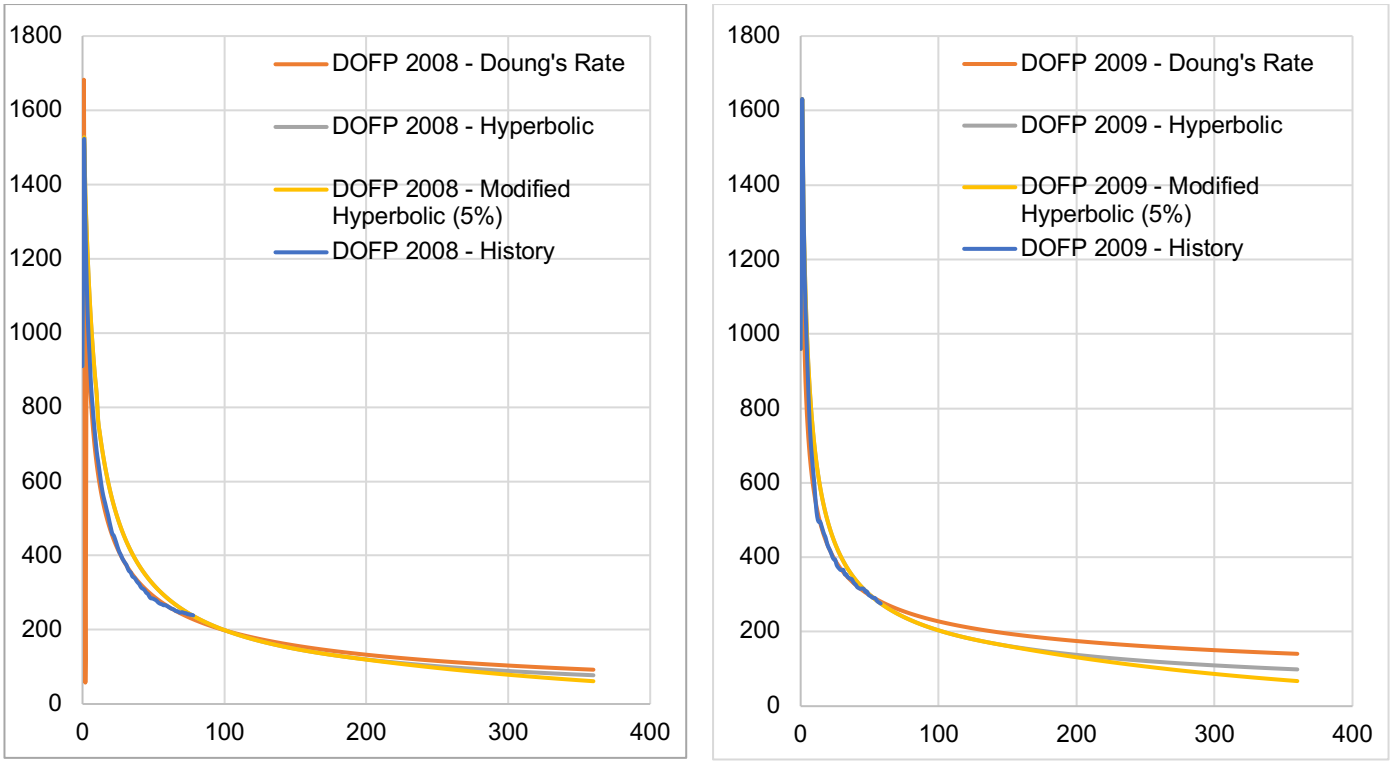

Figure 3-10: Gas Production Rate (MScf/day) against Time (months) for DOFP 2008 (left) and DOFP 2009 (right)

Table 3-2: Comparison of EUR for the combined time groups

EUR at 30 years – Barnett Shale				
Current Update Arp's Hyperbolic (BCF) b=1.6871;Di=0.1966	**Current Case study Doung (BCF)**	**Current Case study Modified Hyperbolic @5% switch (BCF)**	(Baihly, Altman, Malpani, & Luo, 2010) **– Arp's Hyperbolic (BCF)** Di=0.0766;b=1.5933	(Baihly, Malpani, Altman, Lindsay, & Clayton, 2015) **– Arp's Hyperbolic (BCF)** Di=0.1061;b=1.5181
2.323 (60 months, 10237 wells)	**2.328** (60 months, 10237 wells)	**2.230** (60 months, 10237 wells)	**2.989** (64 months, 731 wells)	**3.121** (108 months, 1,138 wells)

3.2.5. Discussion

Comparing the EUR results between this case study and (Baihly *et al.*, 2010) for wells with a 2008 DOFP and also with wells with a 2009 DOFP respectively (Table 3-1), a 31% increase was observed for wells with a 2008 DOFP in (Baihly *et al.*, 2010) compared to this case study while a 26% increase was observed for wells with a 2009 DOFP in (Baihly *et al.*, 2010) compared to this case study (Table 3-1). Results were not available for other time groups and in (Baihly, Malpani, Altman, Lindsay, & Clayton, 2015), no results were provided (Table 3-1). These differences can be attributed to more wells been used in this study across both years (1160% and 1165% more wells for 2008 and 2009 respectively) compared to the well counts in (Baihly *et al.*, 2010) thus providing a better representation of the Barnett shale. EUR results from (Baihly *et al.*, 2010) were obtained from wells in the core area of the Barnett shale i.e. the most productive parts of the Barnett shale gas production, therefore there is a stronger potential of obtaining higher EUR values compared to those in this study. This further highlights the importance of this study as wells from both core and non-core counties were included in the analysis resulting in conservative estimates of EUR. Other DCA methods used in this study showed lower results compared the Arp's hyperbolic reflecting the need to use multiple empirical methods in defining EUR to obtain a range of results (Table 3-1) (Figure 3-10). Finally, a combined average type curve was generated in this study across all time groups to obtain the EUR and these were compared results from (Baihly, Malpani, Altman, Lindsay, & Clayton, 2015) and (Baihly *et al.*, 2010) (Table 3-2). This study showed a 71% and 66% decrease in EUR from (Baihly *et al.*, 2010) and (Baihly, Malpani, Altman, Lindsay, & Clayton, 2015) despite having a 93% decrease in well count (Table 3-2).

3.2.6. Conclusion

The following conclusions were evident in this study;

1. Results from (Baihly, Malpani, Altman, Lindsay, & Clayton, 2015) and (Baihly *et al.*, 2010) overestimated EUR for the Barnett shale in comparison to all the DCA methods used in this study.

2. This study showed a more reliable and conservative estimate of EUR as more wells were used in the analysis covering a wider acreage.

3. The general decline trend of the Barnett shale wells in this case study was similar to the decline trend in (Baihly, Malpani, Altman, Lindsay, & Clayton, 2015) and (Baihly *et al.*, 2010).

4. Marginal changes in initial production suggests that rock properties are relatively consistent in the Barnett shale.

5. Doung's method provided the most conservative EUR estimate and the modified hyperbolic method provided the most optimistic EUR estimate in this study.

3.3. Case Study 3 – Economic Appraisal of Barnett Shale Reservoirs

3.3.1. Summary

Natural gas produced from shale formations has increased rapidly in the past decade altering the oil and gas industry markets remarkably. Shale gas development is more expensive compared to conventional developments and as such, understanding the economic feasibility are of greater importance in successfully developing the resource. Using the estimated ultimate recoverable (expressed in terms of P10, P50 and P90) from 2751 horizontal well production data (all starting production from 2008) from the Barnett shale, a discounted cash flow economic model (MS- Excel based) was used to quantify the effect of finding and development costs (F&DC) and gas prices on the economic viability of horizontal wells within four out of five basins (Strawn Basin, Ouachita Folded Belt, Forth-worth Syncline and Bend-arch Basin) in the Barnett shale. The investment hurdle in the economic model was a rate of return of 20% and a payback period of 60 months or less. This case study is first to help determine the percentage of wells within basins in the Barnett shale that would be economically viable at various F&DC and gas prices subject to satisfying the prescribed investment hurdle. This case study allows us to understand the economic environments and lessons learned from the Barnett shale reservoir to examine the parameters that may be transferable to the development of the Upper Bowland Shale.

Based on information from (Figure 2-20), the basins considered in this case study fall under the following counties;

Strawn Basin: *Bosque, Erath, Hood, Johnson, Somervell and Tarrant counties*
Forth-Worth Syncline: *Clay, Denton, Jack, Montague, Parker and Wise counties*

Ouachita Folded Belt: *Hill, Ellis and Dallas counties*
Bend-Arch Basin: *Eastland and Palo Pinto counties*

Horizontal wells that started production in 2008 and were analysed and interpreted from four out of five basins within the Barnett shale. This covers the core and non-core counties resulting in a total of 2751 horizontal wells being examined. The fifth basin was neglected due to insufficient data in that area (operations are sparse in those areas).

This case study aims to improve the work carried out by (Almadani, 2010) where 14000 wells, some of which have been drilled in 1980, in unspecified areas in the Barnett, consisting predominantly of vertical wells, were examined to understand the impact of changes in F&DC and gas prices on the economic performance. This was carried out by determining the estimated ultimate recoverable[2] (EUR) in terms of P10, P50, and P90 before implementing these figures in the economic model. The investment hurdle in the economic model is a rate of return of 20% and a payback period of 5 years or less. The discounted cash flow period was for 26 years, an average well life. Contrast to (Almadani, 2010), this case study is first to economically appraise the Barnett shale in terms of its basins using recent and up-to-date (all starting in 2008) well production data from horizontal wells that are more representative of the Barnett shale production outlook.

(Almadani, 2010), used the method adopted by the United States Geological Survey (USGS) for continuous-type resources to calculate the EUR for wells in a resource area of interest. The EUR for a producing well is calculated by analysing its production rate for a specific time frame. During the analysis, a hyperbolic curve is fitted through the data to obtain EUR. The USGS method simply involves defining a distribution (typically log-normal distribution for the Barnett shale) for all the calculated EUR's, e.g. by using the @RISK software, then a cumulative distribution function is generated from monte-carlo simulation using @RISK to estimate the EUR for all wells in the unconventional resource area. The results obtained by Almadani from Monte-carlo simulation (100,000 iterations) from 14000 wells, generated the following probabilistic distribution for EUR;

1. 90% of the Barnett shale wells have a EUR of 0.25 BCF or more (P10 or 10th percentile) compared to 0.74BCF in this case study.

[2] The amount of oil and gas expected to be economically recovered from a reservoir or field by the end of its producing and it can be referenced to a well, a field or a basin (Schlumberger, 2017).

2. 50% of the Barnett shale wells have a EUR of 1.5 BCF (P50 or 50th percentile) compared to 2.59 BCF in this case study.

3. 10% of the Barnett shale wells have a EUR of 4 BCF or more (P90 or 90th percentile) compared to 6 BCF in this case study.

The economic model used in (Almadani, 2010), was the same employed in this case study albeit under different economic scenarios. Two major economic scenarios (Scenario 1 and 2) were implemented in (Almadani, 2010) to investigate the impact of F&DC and gas prices on the economic performance (i.e. can these wells exceed the investment hurdle?) of the Barnett shale at each EUR i.e. 10th percentile, 50th percentile and 90th percentile. However, Almadani also varied several F&DC e.g. from $250,000 to $4,000,000.

The assumptions for each scenario include;

Scenario 1

- F&DC - $2 million
- 0% Royalty burden
- 100% probability of success
- 0% escalation of gas prices and costs
- 0% fuel and shrinkage
- LOE of $1.0/MCF
- 10% annual discount rates
- No floor and ceilings for gas prices

Scenario 2

- F&DC – $2 million
- F&DC – 25% royalty burden
- 90% probability of success
- 0% escalation of gas prices and costs
- 6% fuel and shrinkage
- 0% fuel and shrinkage
- LOE of $1.0/MCF
- 10% annual discount rates
- No floor and ceilings for gas prices

The economic parameters used in this case study to investigate the impact of F&DC and gas prices on economic feasibility of wells includes;

- F&DC - $1 million, $2 million and $4 million
- 20% Royalty burden
- 100% probability of success
- 0% escalation of gas prices and costs
- 6% fuel and shrinkage
- LOE of $1.0/MCF
- 10% annual discount rates
- Gas prices varied between $2/MCF, $4/MCF, $6/MCF, $8/MCF, $10/MCF, $12/MCF and $13/MCF based on Henry Hub prices from 2008.

In this section, the gas prices and F&DC that satisfy the investment hurdle for each basin with the Barnett shale is presented. The comparison between the results from this case study and (Almadani, 2010) is also presented.

3.3.2. Results from Almadani compared to current work

To compare the results from (Almadani, 2010) to results from this case study, the following economic scenario was implemented in the economic model across both case studies;

- F&DC - $3 million
- 25% royalty burden
- 90% probability of success
- 0% escalation of gas prices and costs
- 6% fuel and shrinkage
- LOE[3] of $1.0/MCF
- 10% annual discount rate

The results of the comparison are shown on Table 3-3

[3] Lease Operating Expenses

Table 3-3: Comparison of gas prices between current case study and Almadani (2010)

Percentiles	Gas Price ($/MCF) – Almadani (2010)	Gas Price ($/MCF) - Current work
P10 (90% of Barnett Shale wells)	45.60 @ 0.23 BCF	16 @ 0.74 BCF
P50 (50% of Barnett Shale wells)	9.20 @ 1.35 BCF	5.29 @ 2.59 BCF
P90 (10% of Barnett Shale wells)	4.60 @ 3.6 BCF	2.85 @ 6 BCF

3.3.3. Methodology

1. The dataset consisted of only horizontal wells that started production from 2008 with 1835 wells from the Strawn Basin, 137 wells from the Ouachita Folded Belt, 55 wells from the Bend-Arch Basin and 724 wells from the Forth-Worth Syncline.

2. Data from each well in each basin was analysed initially on Microsoft Excel (macro-enabled) to determine the EUR. The range of EUR from each basin were loaded in the @Risk software and a log normal distribution typical of Barnett shale wells was fitted to the dataset.

3. Monte Carlo simulation was then carried out using @RISK over 1000 iterations to obtain cumulative distribution plots (Appendix C) showing the probabilistic distribution (P10, P50, and P90) of EUR for each basin (Figure 3-11). The P10, P50 and P90 EUR values for each basin were used in the economic model.

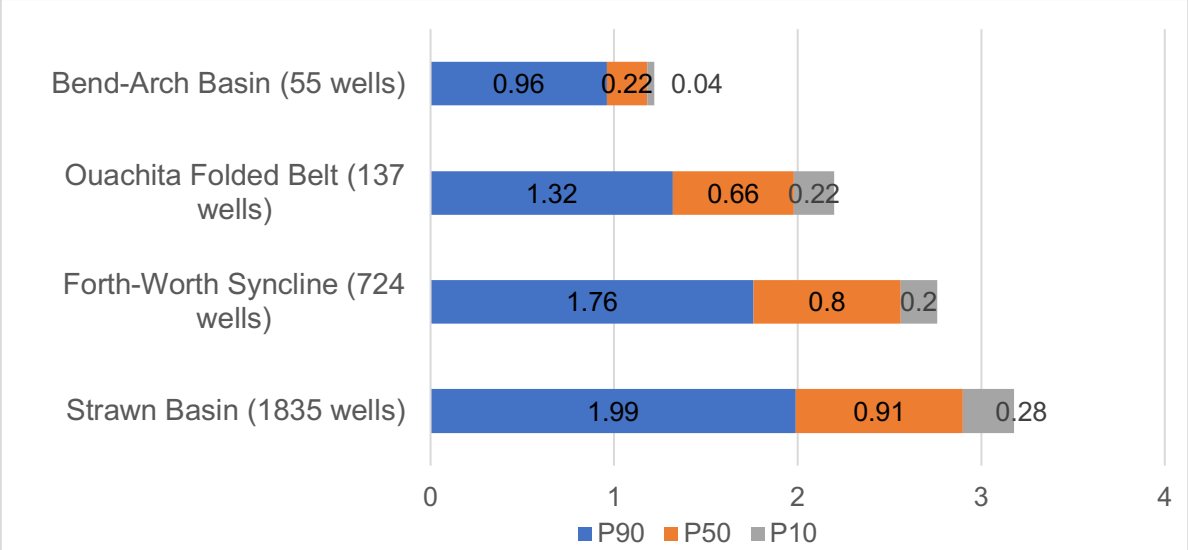

Figure 3-11: Probabilistic distribution of EUR (in BCF) obtained from @RISK software across basins in the Barnett shale.

4. Gas production from an individual well with a EUR similar to the calculated EUR was chosen and rescaled over a 26-year period to fit the calculated EUR values for each basin at the respective percentiles i.e. P10 (10^{th} percentile), P50 (50^{th} percentile) and P90 (90^{th} percentile).

5. The rescaled production was entered into the economic model to determine the effect of the finding and development costs and gas price on satisfying the proposed investment hurdle. The investment hurdle was a rate of return of 20% and a payback period of 5 years or less. The discounted cash flow period was for 26 years, an average well life.

6. The finding and development costs used in this case study (assumed to consist only of the drilling and completion costs) were £1 million, £2 million and £4 million while the gas price was varied from $2/MCF-$13/MCF based on Henry Hub spot prices from 2008.

3.9.5. Results

The economic model used in (Almadani, 2010), was the same employed in this case study albeit under different economic scenarios. Two major economic scenarios (Scenario 1 and 2) were implemented in (Almadani, 2010) to investigate the impact of F&DC and gas prices on the economic performance (i.e. can these wells exceed the investment hurdle?) of the Barnett shale at each EUR i.e. 10th percentile, 50th percentile and 90th percentile. However, Almadani also varied several F&DC e.g. from $250,000 to $4,000,000. The assumptions for each scenario include;

Scenario 1

- F&DC - $2 million
- 0% Royalty burden
- 100% probability of success
- 0% escalation of gas prices and costs
- 0% fuel and shrinkage
- LOE of $1.0/MCF
- 10% annual discount rates
- No floor and ceilings for gas prices

Scenario 2

- F&DC – $2 million
- F&DC – 25% royalty burden
- 90% probability of success
- 0% escalation of gas prices and costs
- 6% fuel and shrinkage
- 0% fuel and shrinkage
- LOE of $1.0/MCF
- 10% annual discount rates
- No floor and ceilings for gas prices

The economic parameters used in this case study to investigate the impact of F&DC and gas prices on economic feasibility of wells includes;

- F&DC - $1 million, $2 million and $4 million
- 20% Royalty burden
- 100% probability of success
- 0% escalation of gas prices and costs
- 6% fuel and shrinkage
- LOE of $1.0/MCF
- 10% annual discount rates
- Gas prices varied between $2/MCF, $4/MCF, $6/MCF, $8/MCF, $10/MCF, $12/MCF and $13/MCF based on Henry Hub prices from 2008.

In this section, the gas prices and F&DC that satisfy the investment hurdle for each basin with the Barnett shale is presented. The comparison between the results from this case study and (Almadani, 2010) is also presented.

3.9.6. Results from Almadani compared to current work

To compare the results from (Almadani, 2010) to results from this case study, the following economic scenario was implemented in the economic model across both case studies;

- F&DC - $3 million
- 25% royalty burden
- 90% probability of success
- 0% escalation of gas prices and costs
- 6% fuel and shrinkage
- LOE[4] of $1.0/MCF
- 10% annual discount rate

The results of the comparison are shown on Table 3-4

Table 3-4: Comparison of gas prices between current case study and Almadani (2010)

Percentiles	Gas Price ($/MCF) – Almadani (2010)	Gas Price ($/MCF) - Current work
P10 (90% of Barnett Shale wells)	45.60 @ 0.23 BCF	16 @ 0.74 BCF
P50 (50% of Barnett Shale wells)	9.20 @ 1.35 BCF	5.29 @ 2.59 BCF
P90 (10% of Barnett Shale wells)	4.60 @ 3.6 BCF	2.85 @ 6 BCF

3.9.5. Discussion and Conclusion

Appendix B shows the gas prices and costs required for wells within various basins (Strawn basin, forth-worth syncline, bend-arch basin, and Ouachita folded belt in the Barnett shale to be economic i.e. to meet or exceed the investment hurdle. In the Strawn basin, the minimum gas price and F&DC required for 10% of wells in the Strawn basin, Forth-Worth Syncline and Ouachita Folded Belt to meet the investment hurdle is $4/MCF and $1,000,000 respectively. Whereas in the bend-arch basin, the minimum gas price and F&DC required for 10% of wells in the bend-arch basin to meet the investment hurdle is $6/MCF and $1,000,000 respectively.

[4] Lease Operating Expenses

The bend-arch basin is the least economic area within the Barnett shale with only 10% of the wells satisfying the investment hurdle. This was then followed by the Ouachita Folded belt. The bend arch basin consists of the Eastland and Palo Pinto counties which are both non-core counties and are less thick and contribute less to gas production in the Barnett shale. The basins consisting of the core counties are the best areas to drill wells to easily satisfy the investment hurdle considering that 90% of all the wells in all the basins did not satisfy the investment hurdle at the gas prices and costs (F&DC) considered. Comparing the results from this case study to (Almadani, 2010), the gas prices required to be economic based on the scenario considered was lower and more realistic (Table 3-4). Results from (Almadani, 2010) were overestimated compared to this case study – hence the use of only recent horizontal wells from 2008 in this case study resulted in a more representative and realistic outcomes on the economic appraisal of the Barnett shale.

Chapter 4 Petrophysical Characterisation of the Upper Bowland Shale

4.1. Introduction

Shale gas reservoirs have historically been difficult to characterize accurately due to extremely low porosity and permeability, variable clay content, and complexities in relation to water saturation. The complex nature of the porous structure coupled with large bound fluid volumes generated by high clay volumes often causes challenges in conventional evaluation tools (Spears and Jackson, 2009) - for example, resistivity devices tends to be overwhelmed by conductive effects originating from the shale matrix (Spears and Jackson, 2009). Some of the effects are extremely high gamma ray radiation due to the presence of kerogen, low bulk density and high thermal neutron porosity due to kerogen (i.e. crossover), slowing effects on the sonic travel time data due to the presence of kerogen and very clear patterns on photoelectric logs due to lithological effects (Spears and Jackson, 2009). High uranium concentrations are also a diagnostic feature when identifying the presence of kerogen in both hydrocarbon source formations and shale gas reservoirs and often can be found in natural fractures found in gas shales (Luffel, Guidry and Curtis, 1992). In reduced environments, the presence of uranium raises the gamma ray log reading above normal levels as restricts the ability to accurately estimate clay volume with a total GR curve (Glorioso and Rattia, 2012). More detailed log responses are discussed in section 2.4 and the methodology required to estimate some key properties like toc, porosity is discussed in section 2.3.

4.2. Results and Discussions

4.2.1. Log Editing and Environmental Corrections

Before analysis, the logs were depth shifted against the gamma ray log to ensure consistency across all the depths for the different logging tools. Environmental corrections were also carried out on the logs prior to analysis.

4.2.2. Preese Hall 1

4.2.2.1. Volume of Shale

The volume of shale was calculated using both the gamma ray method and the neutron-density method to determine the volume of shale. The gamma ray log, neutron log and density log were all corrected for TOC. The results are shown in the log plot in Figure 4-1 – the interval of interest i.e. the upper Bowland shale was calibrated in 35 zones to enable accurate determination of the sands and shale zones.

Figure 4-1: Log View of Vshale Calculations for Preese-Hall 1

The results of both methodologies were highly variable across the interval of interest with the Vshale from Gamma ray log been more variable and less consistent compared to the Vshale from Neutron-Density. This is because of the complex tectonics that exist in the Upper Bowland shale and mineralogical sequences/ lithological heterogeneity present in the Upper Bowland shale (see section 2.3.12). The neutron density method for measure the volume of shale is also more stable and less affected by complex mineralogical and lithological changes hence using the gamma ray method for this interval would create larger uncertainties and an unwanted confidence in the results – see section 2.4.2

Descriptive summary of the results is shown in Table 4-1.

Table 4-1: Descriptive summary of results

	Vshale Gamma Ray	Vshale Neutron Density
Mean	0.520	0.235
Standard Deviation	0.304	0.097
Max	2.0248	0.6533
Min	-0.2499	0.0117

4.2.2.2. Porosity and Water Saturation

Water saturation was calculated using the Simandoux equation as Archie's method was unable to match with core saturation data. a, m and n values used is shown in Table 4-2 and the log plot in Figure 4-2. The challenges of using the Archie's method is predominantly due to the complicated clay minerals existing in most shales which adds an extensive conductive system which fails when Archie's method is applied to determining water saturation. Hence Simandoux equation was more appropriate in matching with the core data for water saturation – see section 2.4.1.1

Table 4-2: Tuning Parameters for the Simandoux Equation

Depth	a	m	n
	1	0.65	2
	1	1.2	1.5

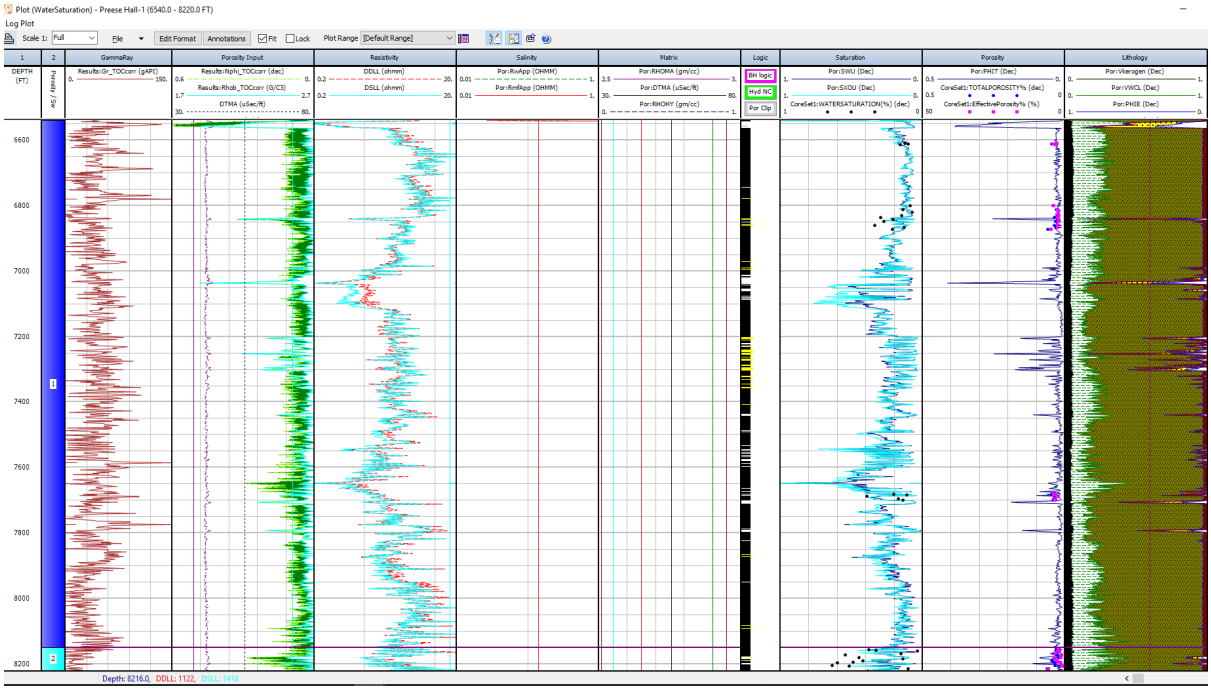

Figure 4-2: Log View of Porosity and Water Saturation Calculation for Preese-Hall 1 Well

The porosity was calculated using the density log this is shown in Figure 4-2. The density log is typically used to determine porosity in shale gas reservoirs despite the complicated porosity systems in shale and the high clay mineral content in shale gas reservoirs means that conventional reservoir logging methods require large corrections to log responses. Hence it is imperative to validate logging data with core derived data. See section 2.4.4.

The resistivity track suggests a formation with low permeability as the shallow and deep resistivity log perfectly align across most of the interval. The match with the data was evaluated

to determine the RMSE between the predicted (from log) and the actual observed value from the core analysis data used to validate the model for water saturation (Table 4-3) and porosity Table 4-4.

Table 4-3: Descriptive summary of results for water saturation

	Actual Results
Mean	0.206
Min	0.014
Max	0.988
std	0.116

Table 4-4: Descriptive summary of porosity results

	Actual Results
Mean	0.031
Min	0.001
Max	0.413
std	0.039

4.2.2.3. TOC

The TOC results using Passey's method is shown in Figure 4-3. A level of maturity (LOM) of 10.6 and a Passey modifier of 0.8 was used to obtain a match to core data obtained from RockEval Analysis. Some descriptive statistics are shown in Table 4-5. See section 2.3.9.2

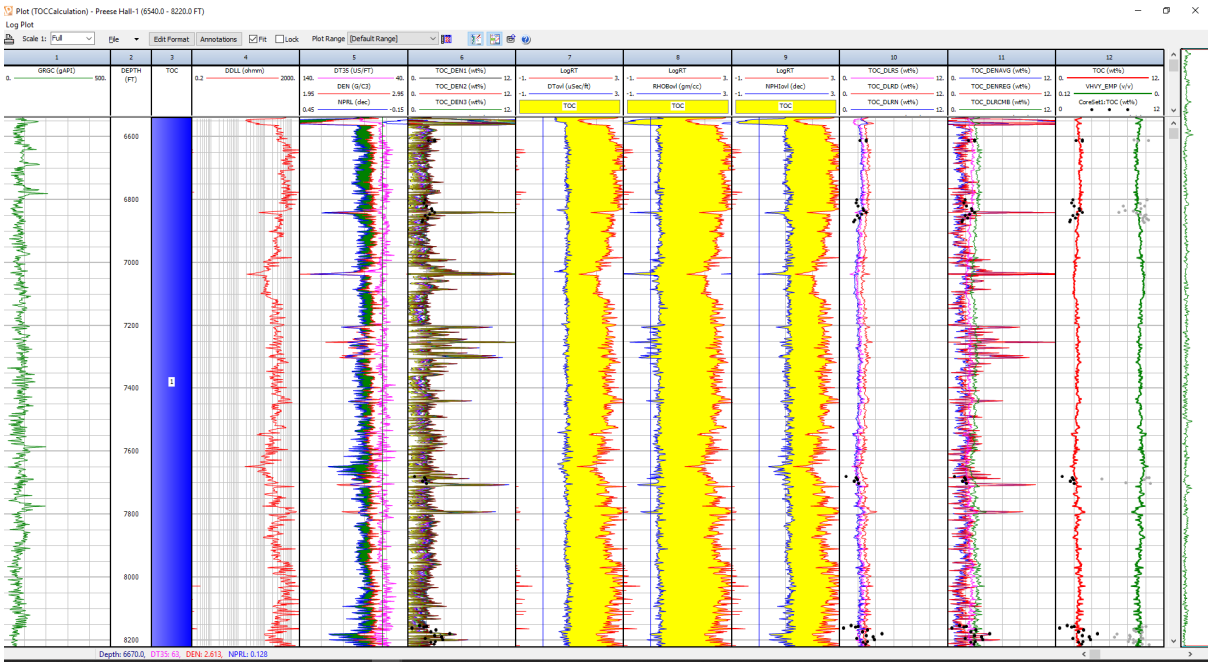

Figure 4-3: Log View of TOC Calculation

Table 4-5: Descriptive Statistics for TOC

	Core TOC	Passey's TOC
Mean	2.33	2.27
Max	4.65	3.38
Min	0.43	1.13
Standard Deviation	0.93	0.28
RMSE	1.0173	

The Passey Modifier acts as an offset to the TOC computed from Passey's method. Passey's initial method (Qu, Yoon and Mudawar, 2004) used to develop the DeltaLogR response only covered low LOM and was designed to compute 0 TOC when the curves overlaid, but this was later modified with an offset of 0.8 as that was sometimes found to give a better fit. Passey Mod can be adjusted, in combination with Level of Maturity to achieve a fit to the core TOC data. A Passey modifier of 0.8 was sufficient for the Upper Bowland Shale in Preese-Hall 1. The volume of pyrite from core XRD data was also introduced into the model to fine tune the match. The pyrite multiplier was 0.357 and is applied to the Final TOC to compute the volume of Pyrite which is then validated using core pyrite data in (v/v). The basis of this is the very strong geo-chemical relationship between TOC and the precipitation of pyrite. The default value is 0.357 which usually provides a reasonable match to volumes of pyrite from core XRD data.

4.2.2.4. Mineralogy

A mineralogical model was developed for Preese-Hall 1 that is capable of predicting the volume fractions of minerals within the well. The model was validated using core data from XRD.

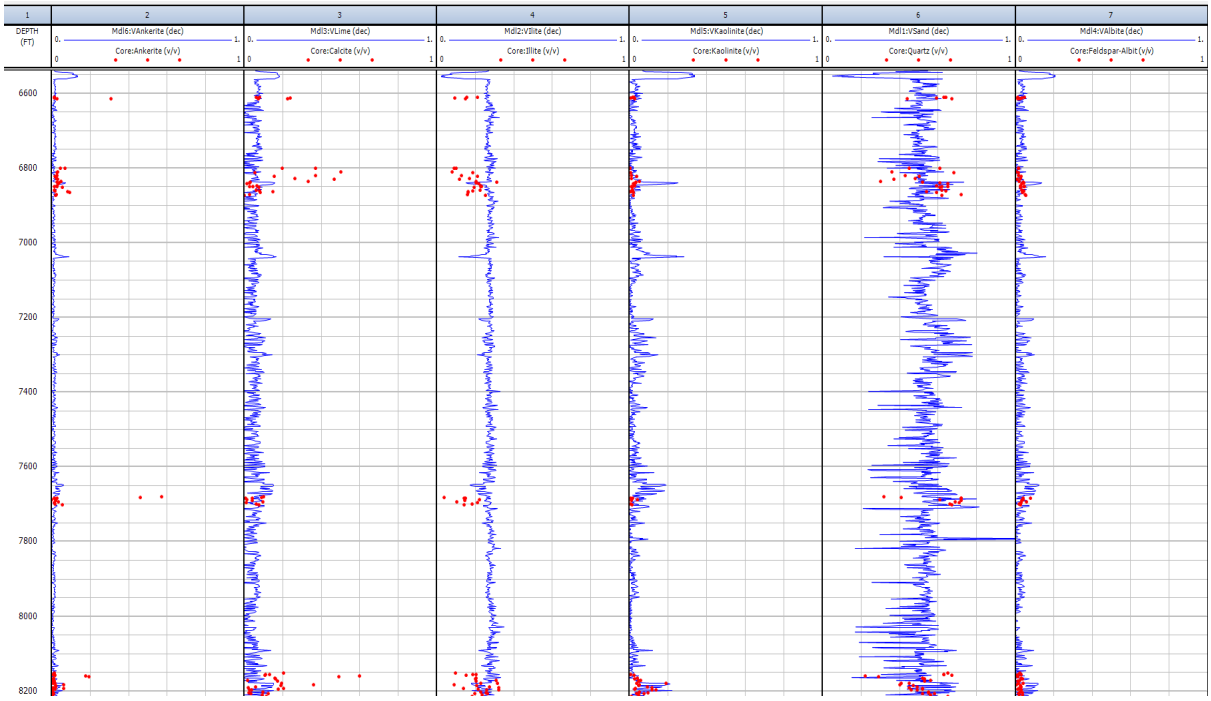

The average composition of the minerals model is shown in Table 4-6. Here we can observe a high quartz content and illite content suggesting a degree of brittleness in some depths and ductility in some depths. This will inform fracking decisions.

Table 4-6: Average mineral composition of Preese - Hall 1

Mineralogy	Average composition (v/v)
Albite	4%
Ankerite	2%
Calcite	7%
Illite	26%
Kaolinite	5%
Quartz	55%

The accuracy of the model was evaluated using the RMSE metric with the model most capable of predicting Albite (Figure 4-4). Generally, the model had an accuracy ranging from ~ 85% to 96% (Figure 4-4).

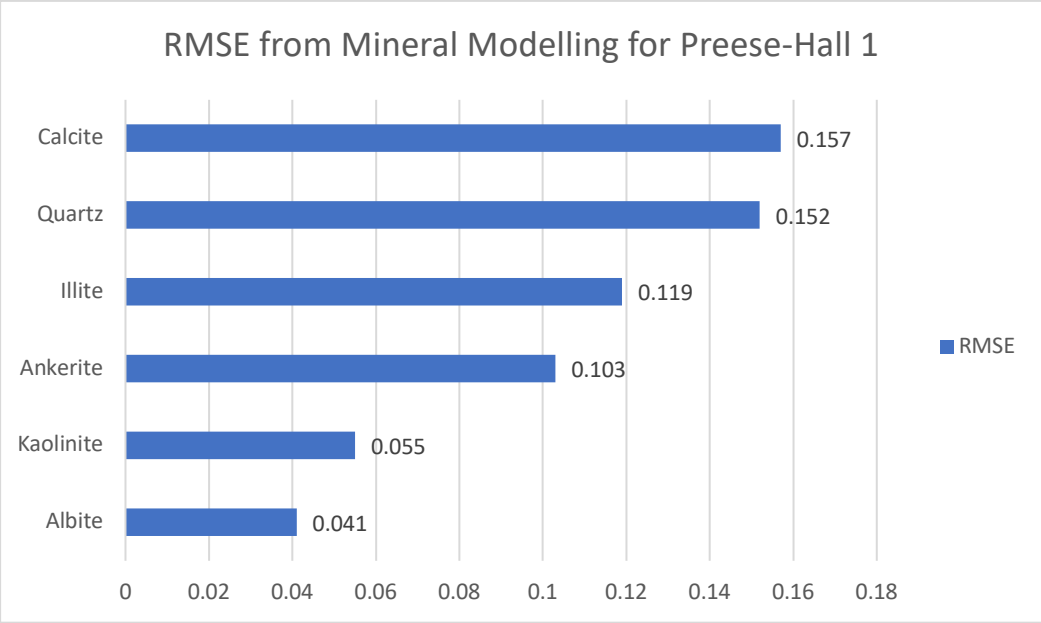

Figure 4-4: RMSE for Preese - Hall 1 well

4.2.3. Grange Hill 1z

4.2.3.1. Volume of Shale

In the Grange-Hill 1z well, the gamma ray method for calculating Vshale was not suitable due to high presence of various sources of radioactivity in a complex stratigraphy distorting the evaluation. See section 4.2.2.1

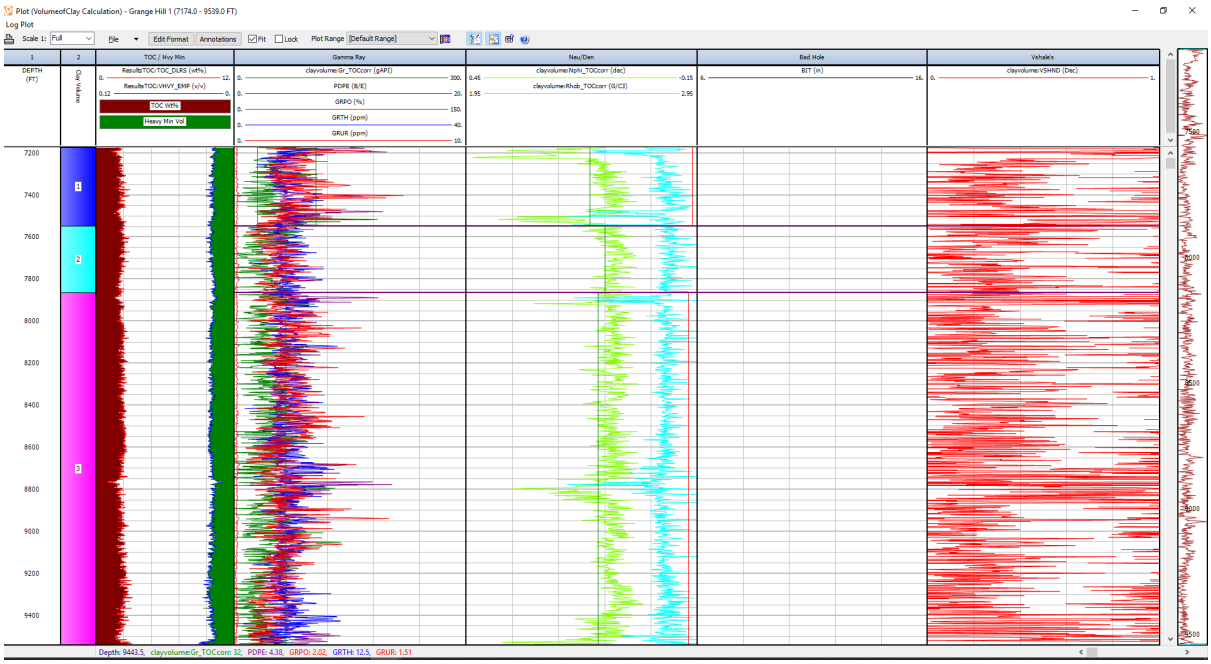

Figure 4-5: Volume of Shale for Grange-Hill

Table 4-7: Descriptive Statistics for Vshale for Grange-Hill 1z

	Vshale Neutron Density
Mean	0.257
Standard Deviation	0.40
Max	2.8
Min	0

4.2.3.2. Porosity and Water Saturation

Water saturation was calculated using the Simandoux equation as Archie's method was unable to match with core saturation data. a, m and n values used is shown in x and the log plot in Figure 4-6.

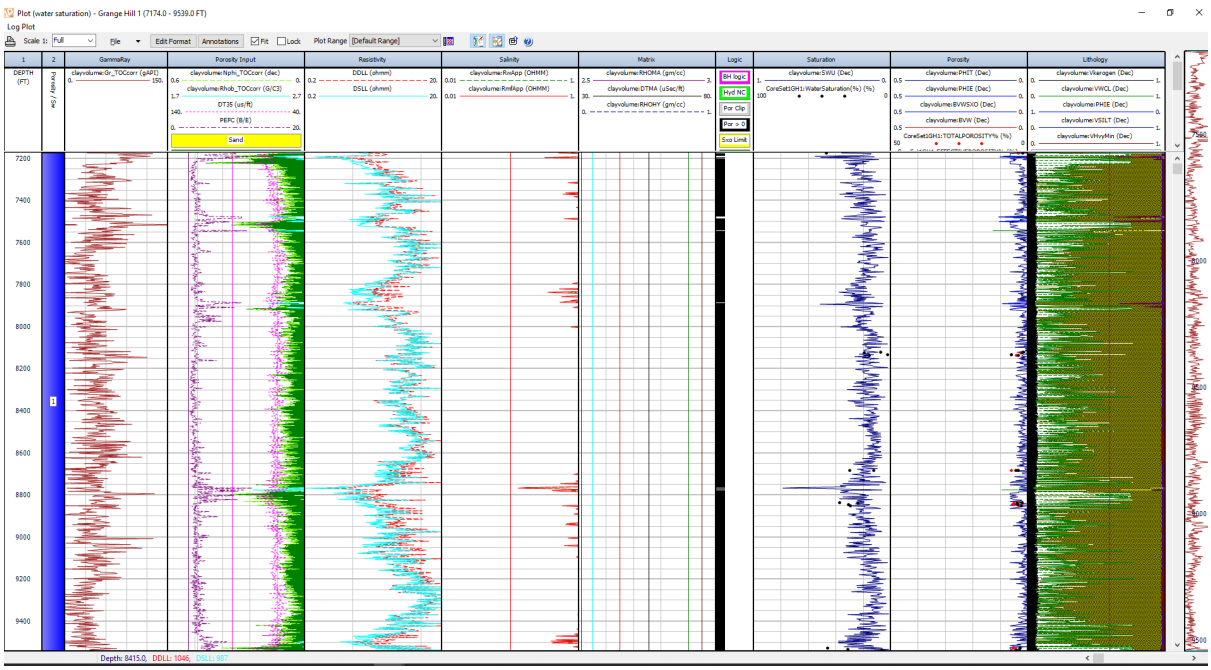

Figure 4-6: Log View of Porosity and Water Saturation Calculation

The porosity was calculated using the density log (see section 4.2.2.2), this is shown in Figure 4-6. The resistivity track suggests a formation with low permeability as the shallow and deep resistivity log perfectly align across most of the interval.

An overview of the results is shown in Table 4-8 and Table 4-9

Table 4-8: Saturation Results for Grange-Hill 1z

Measure	Actual Results
Mean	0.181
Min	0.008
Max	0.789

Table 4-9: Porosity results for Grange-Hill 1

	Actual Results
Mean	0.019
Min	0
Max	0.142

4.2.3.3. TOC

The TOC results using Passey's method is shown in Figure 4-7. A level of maturity (LOM) of 14 and a Passey modifier of 0.7 was used to obtain a match to core data obtained from RockEval Analysis Table 4-10. A RMSE of ~ 0.75 was obtained between the predicted TOC from Passey's method and the actual TOC from core XRD analysis Table 4-11. See section 4.2.2.3

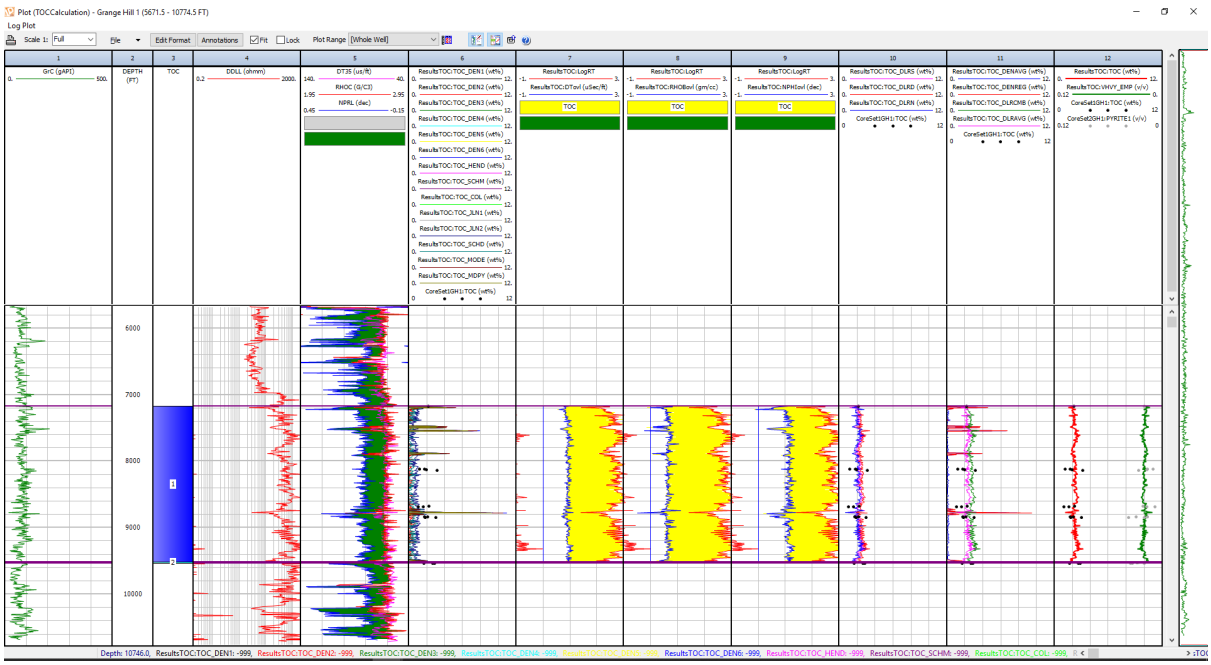

Figure 4-7: Log View of TOC Calculation

Table 4-10: TOC fine tuning parameters to match core TOC

Depth	LOM	Passey Modifier	Pyrite Multiplier
	14	0.7	0.857
	14	0.7	1

Table 4-11: Descriptive Statistics for TOC

	Core TOC	Passey's TOC
Mean	2.14	2.25
Max	3.15	3.51
Min	1.07	0.95
Standard Deviation	0.64	0.25
RMSE		0.7458

4.2.3.4. Mineralogy

A mineralogical model was developed for Grange Hill 1 that is capable of predicting the volume fractions of minerals within the well. The model was validated using core data from XRD.

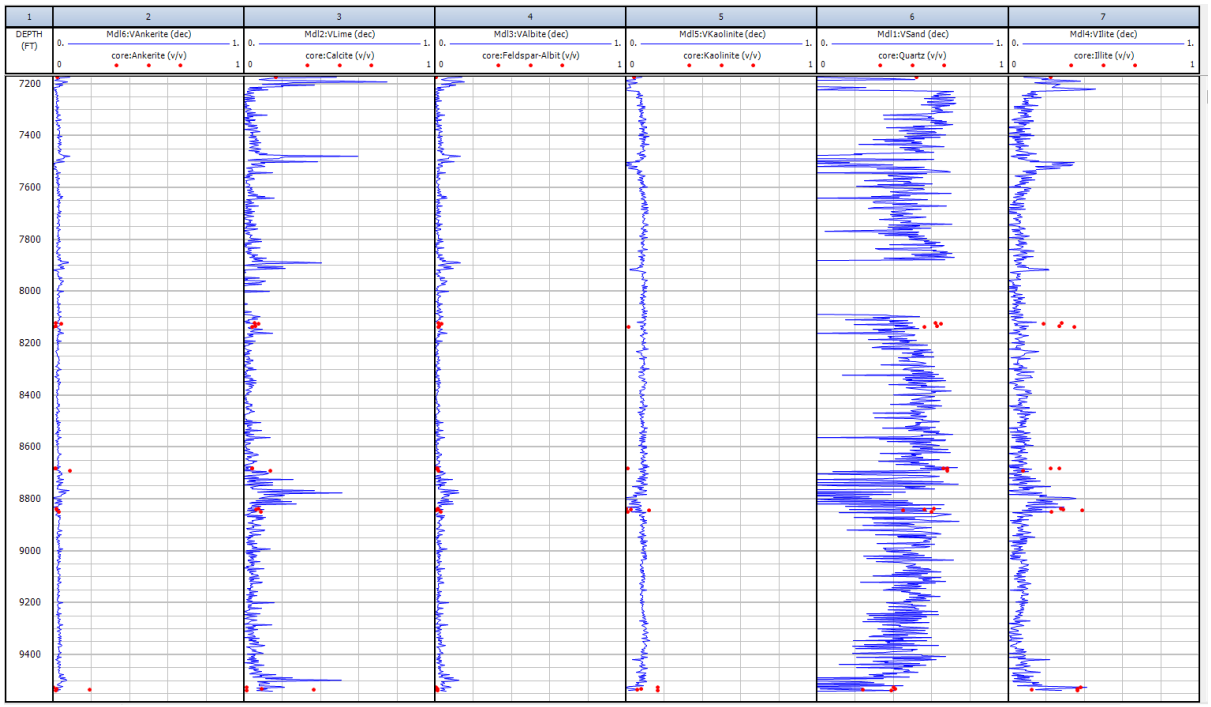

Figure 4-8: Mineralogy Model

The average composition of the minerals model is shown in Table 4-12. In Grange-Hill 1 we still observe a comparable quartz content compared to Preese-Hall 1 but an illite content half of Preese-Hall 1. Quartz and Illite are the top two minerals present in the Upper Bowland Shale. Variability in Illite or clay contents would bring challenges in drilling and fracturing the shale matrix. Compared to the Barnett Shale, the Grange-Hill and Preese-Hall 1 wells have similar mineralogies See section 2.3.7.

Table 4-12: Average Mineralogy

Mineralogy	Average Composition (v/v)
Albite	3%
Ankerite	3%
Calcite	6%
Illite	12%
Kaolinite	7%
Quartz	41%

The accuracy of the model was evaluated using the RMSE metric with the model most capable of predicting Albite Figure 4-9. Generally, the model had an accuracy ranging from ~ 80% to 98%.

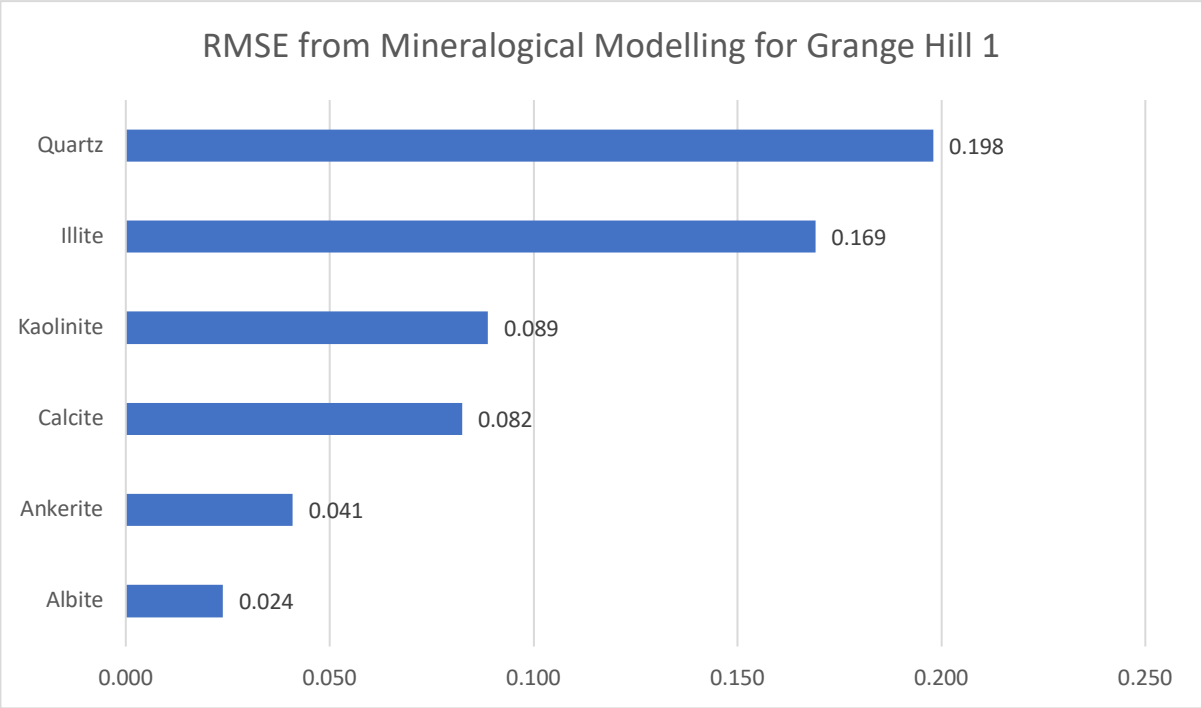

Figure 4-9: RMSE for Grange-Hill 1

4.2.4. Thistleton 1

4.2.4.1. Volume of Shale

The neutron density method provides a more conservative estimate of Vshale but due to the bad hole conditions, the Vshale from the gamma ray was a better choice (Figure 4-10) for this particular well. The depth of the Upper Bowland Section in the Thistleton 1 well has not experienced complex tectonics compared to the depth reached by the core shale gas wells. Hence the Vshale from gamma ray was sufficient in this well. Lack of mineralogy data means that it is challenging to further validate the results.

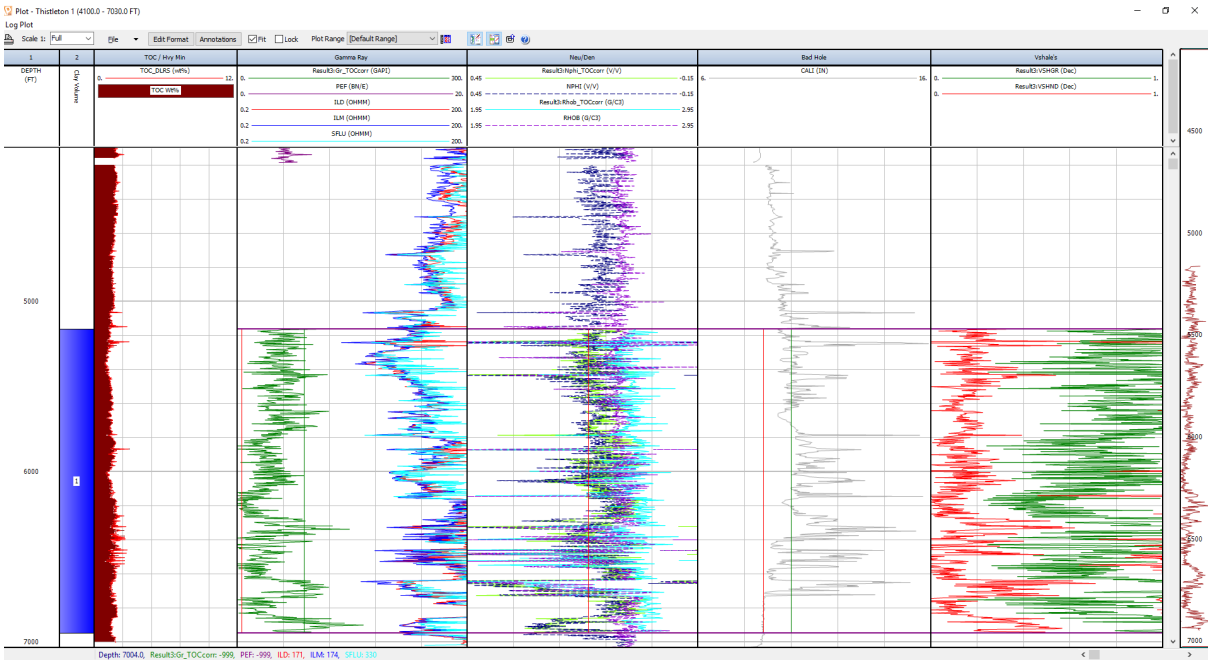

Figure 4-10: Vshale Log View

4.2.4.2. TOC

The TOC results using Passey's method is shown in Figure 4-11. A level of maturity (LOM) of 10.6 and a Passey modifier of 0.7 was used to obtain a match to core data obtained from Rock-Eval Analysis Table 4-13. A RMSE of ~ 0.294 was obtained between the predicted TOC from Passey's method and the actual TOC from core XRD analysis Table 4-14. In this well, Passey's method was accurately predicted TOC compared to the other wells, this has been attributed to the LECO method been used to determine core TOC compared to the Pyrolysis method used in Preese-Hall 1 and Grange-Hill 1 hence TOC was not as variable. It further confirms that the lithology was not complicated at the depths considered in Thistleton 1. See section 2.3.9.2

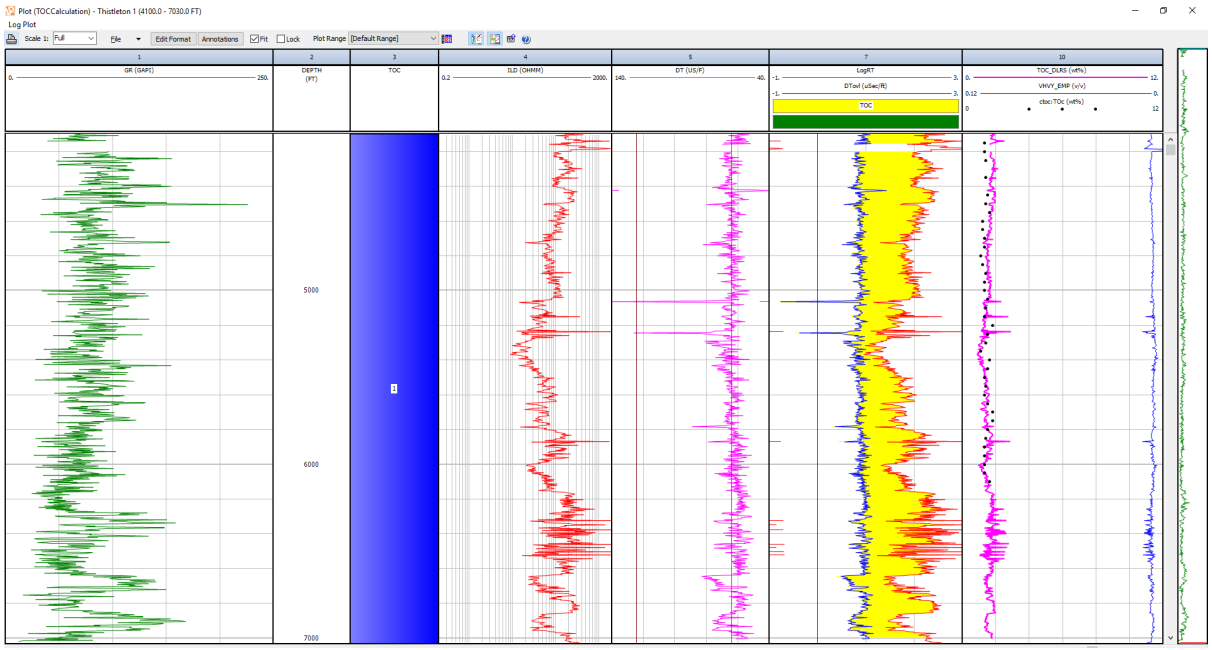

Figure 4-11: TOC Calculation

Table 4-13: Fine tuning parameters for TOC

LOM	Passey Modifier	Pyrite Multiplier
14.1	0.7	0.357

Table 4-14: Descriptive Statistics for TOC

	Core	Passey
mean	1.4	1.9284
max	1.8	1.9475
min	1.1	1.0806
RMSE	0.294	

4.2.5. Hesketh

4.2.5.1. Volume of Shale

The log view of the Vshale calculation is shown in Figure 4-12. Here the Vshale was determined using the neutron density method – see section 4.2.3.1

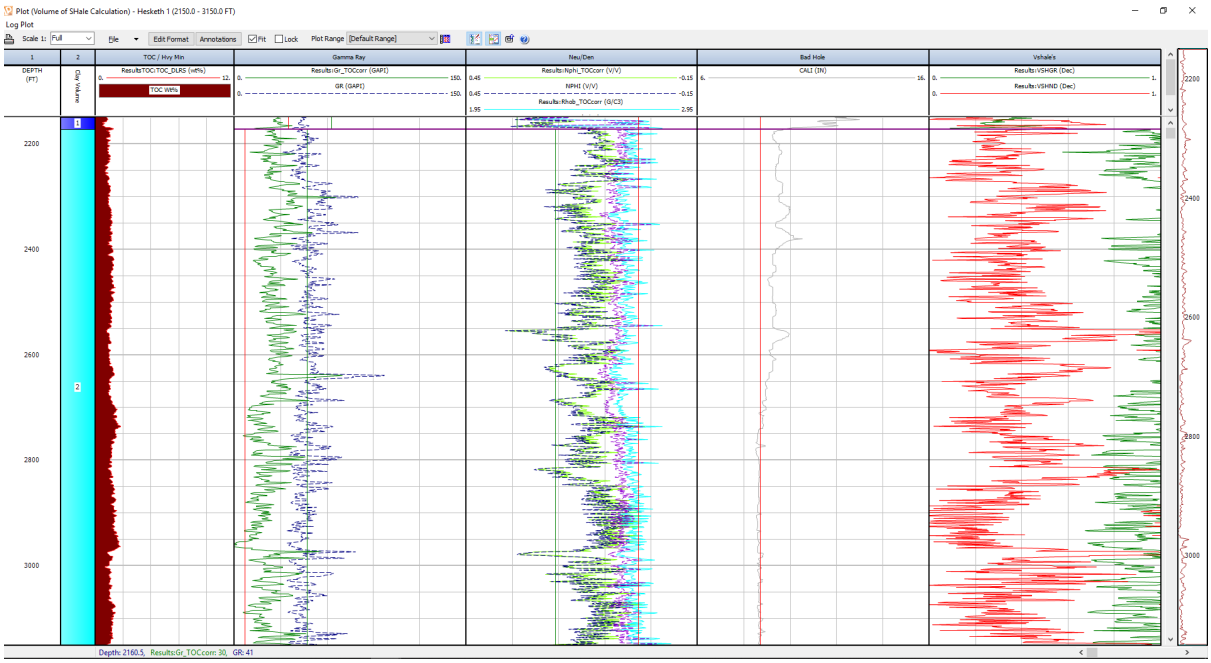

Figure 4-12: Vshale Calculation

4.2.5.2. TOC

The TOC results using Passey's method is shown in Figure 4-13. A level of maturity (LOM) of 14.1. and a Passey modifier of 0 was used to obtain a match to core data obtained from Rock-Eval Analysis Table 4-15. A RMSE of ~ 0.23 was obtained between the predicted TOC from Passey's method and the actual TOC from core XRD analysis Table 4-16. See section 4.2.3.1

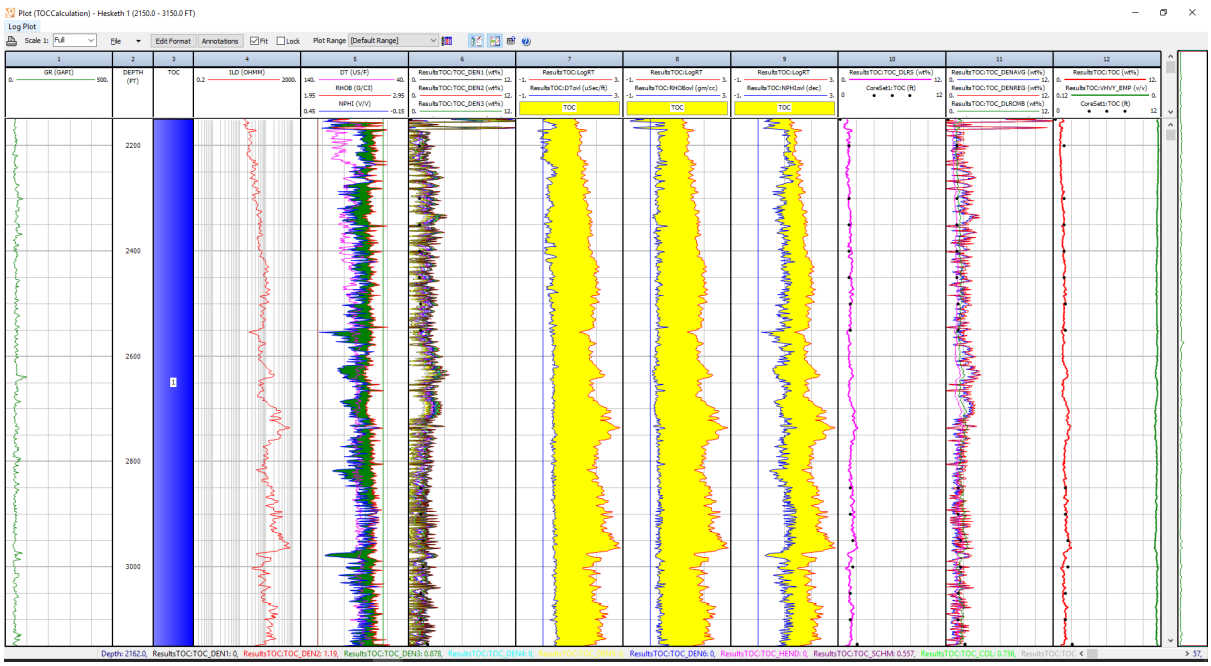

Figure 4-13: TOC Calculation

Table 4-15: Fine tuning parameters

LOM	Passey Modifier	Pyrite Multiplier
14.1	0	0.357

Table 4-16: Descriptive Statistics for TOC

	Core TOC	Passey's TOC
Mean	1.29	1.37
Min	0.22	0.60
Max	2.10	2.18
RMSE		0.22572

4.2.6. Becconssall 1z

4.2.6.1. Volume of Shale

The volume of shale calculation is shown in Figure 4-14 with some descriptive statistics in Table 4-17. it is easy to observe that the gamma ray method provided more realistic result compared to the neutron density method highlighting the complex lithological variations in the Upper Bowland Shale but particularly very high quartz and less variations in clay content.

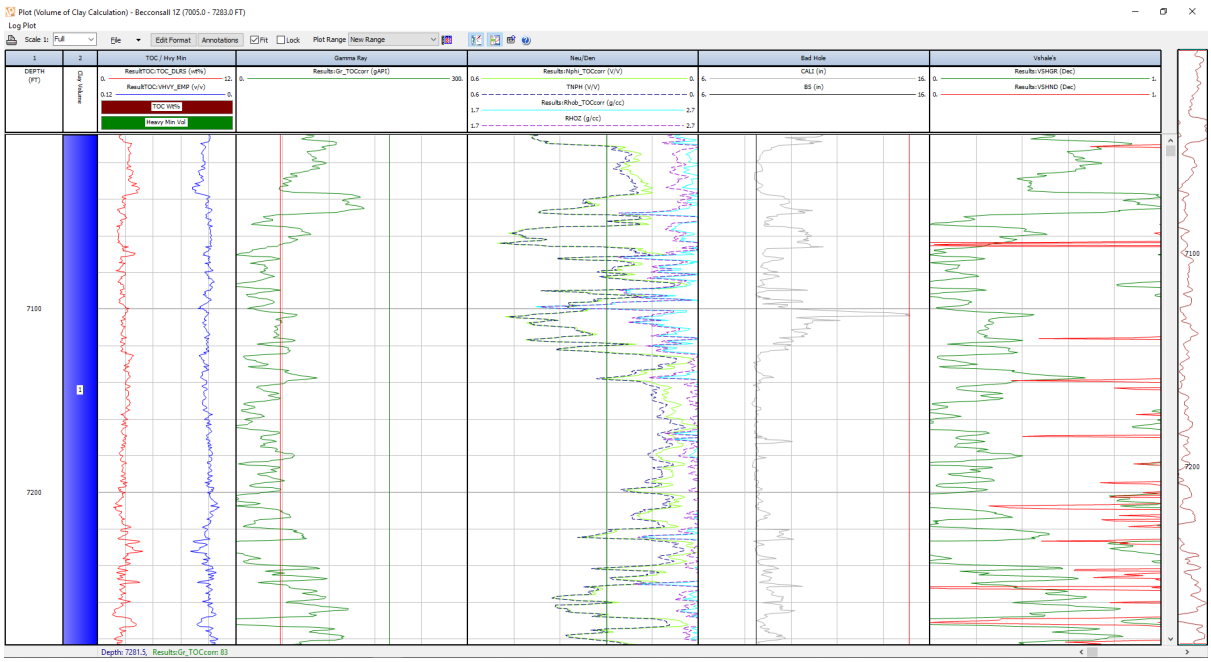

Figure 4-14: Log View of Shale Volume

Table 4-17: Vshale Statistics

Standard Deviation	0.269
Mean	0.284
Min	0
Max	1.048

4.2.6.2. Porosity and Water Saturation

Water saturation was calculated using the Simandoux equation as Archie's method was unable to match with core saturation data. a, m and n values used is shown in x and the log plot in Figure 4-15. See section 2.4.1.1

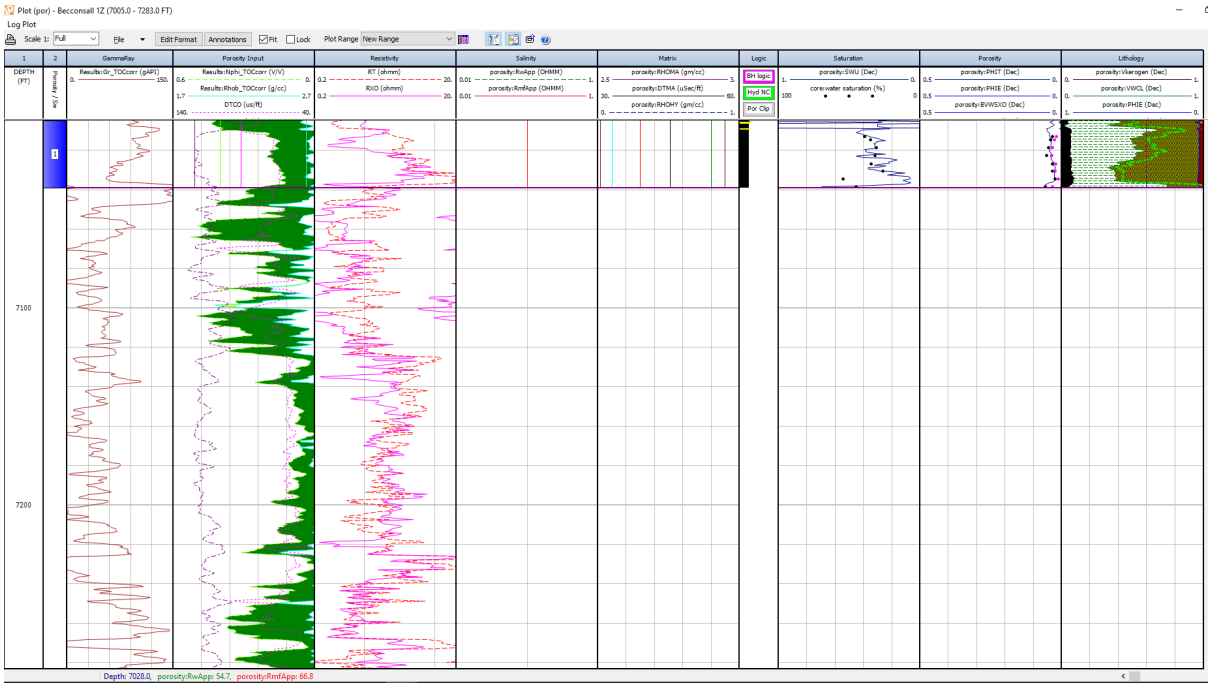

Figure 4-15: Log View of Porosity and Water Saturation

The porosity was calculated using the density log this is shown in Figure 4-15. The resistivity track suggests a formation with low permeability as the shallow and deep resistivity log perfectly align across most of the interval. Model statistics is shown in saturation Table 4-19 and porosity Table 4-18. See section 2.4.4

Table 4-18: Porosity Statistics

Min	0.022
Max	0.057
Mean	0.036
Standard Deviation	0.009

Table 4-19: Saturation

Min	0.063
Max	1.3
Mean	0.376
Standard Deviation	0.009

4.2.6.3. TOC

The TOC results using Passey's method is shown in Figure 4-16. A level of maturity (LOM) of 13.5 and a Passey modifier of 0.85 was used to obtain a match to core data obtained from Rock-Eval Analysis Table 4-20. A RMSE of ~ 0.24 was obtained between the predicted TOC from Passey's method and the actual TOC from core XRD analysis Table 4-21. See section 4.2.2.3. The TOC variations was also stable which corroborates with the high quartz content of 54% - eight percent higher than Grange-Hill 1 and Preese-Hall 1 and even the Barnett Shale. We observed an average TOC of about 2 wt% in all the wells considered also confirming similar marine environment between Barnett and UK shale wells. See section 2.3.9

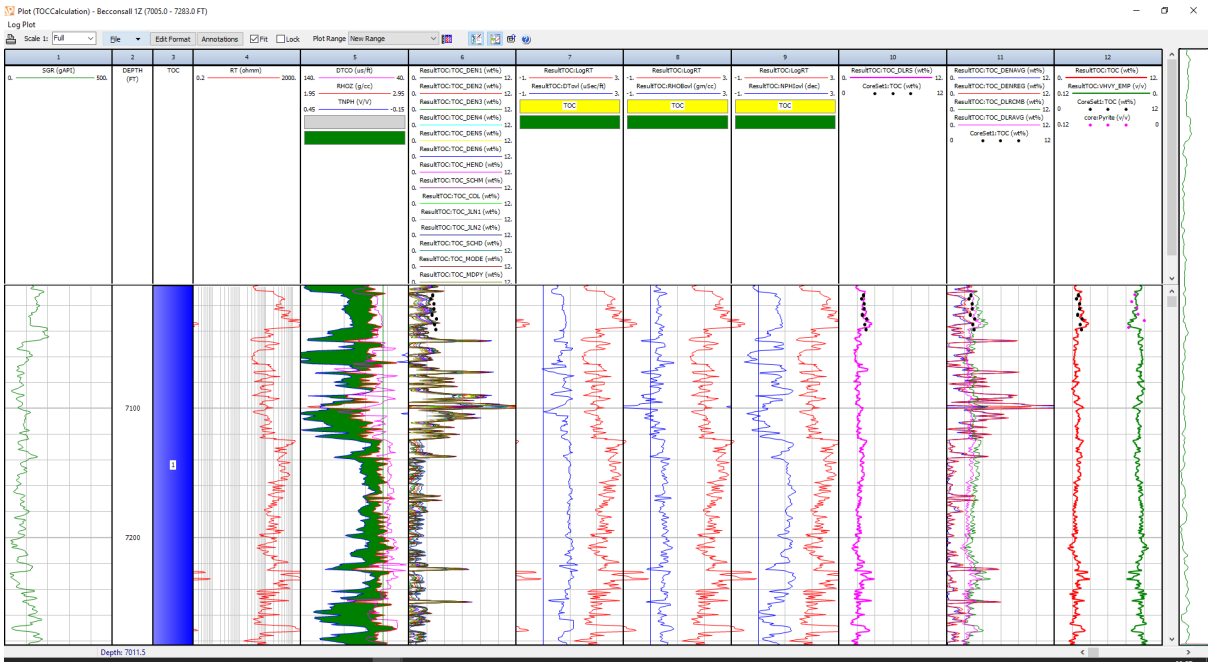

Figure 4-16: Log View of TOC

Table 4-20: Fine tuning of TOC Calculation

LOM	Passey Modifier	Pyrite Multiplier
13.5	0.85	1

Table 4-21: Descriptive Statistics for TOC

	Core TOC	**Passey's TOC**
mean	2.80	2.86
max	3.06	3.62
min	2.49	2.10
std	0.20	0.34
RMSE		0.244

4.2.6.4. Mineralogy

A mineralogical model was developed for Becconssall 1 that is capable of predicting the volume fractions of minerals within the well. The model was validated using core data from XRD Figure 4-17. Some of the results are shown in Table 4-22. Our validated mineralogical model can now be incorporated into the reservoir simulation model such that appropriate completion decisions can be made per well.

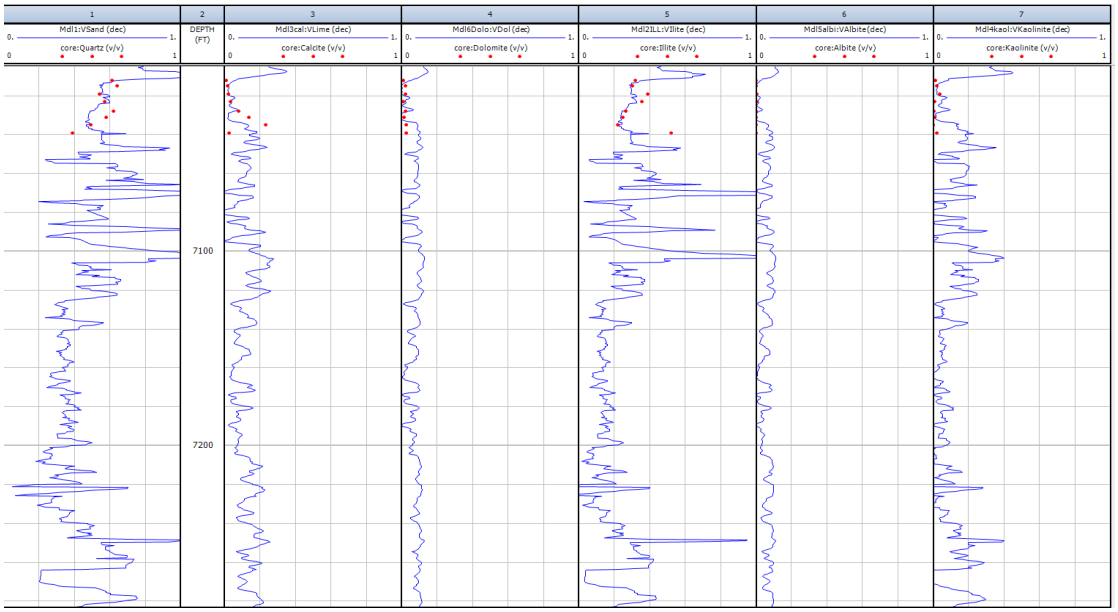

Figure 4-17: Mineralogical Model

Table 4-22: Average mineral composition

Quartz	54%
Kaolinite	7%
Illite	28%
Calcite	7%
Dolomite	4%
Albite	3%

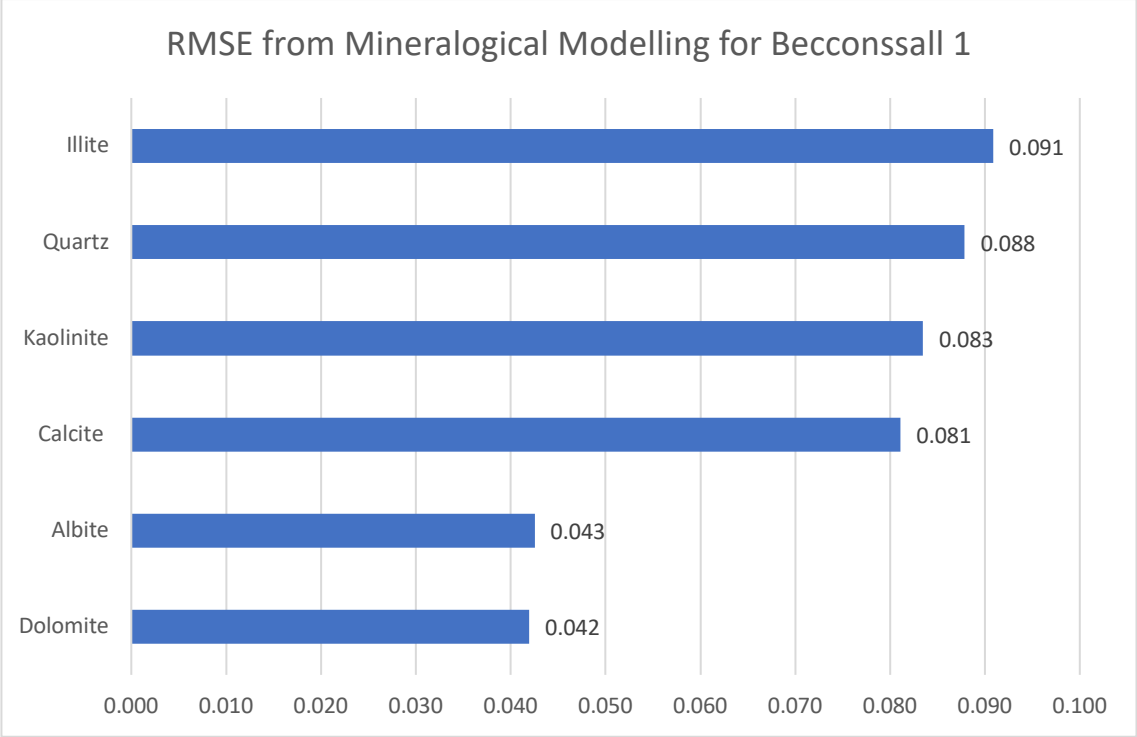

Figure 4-18: RMSE for Becconssall

The accuracy of the model was evaluated using the RMSE metric with the model most capable of predicting Albite. Generally, the model had an accuracy ranging from ~ 90% to 96% Figure 4-18. Though mineralogy appears similar to an average Barnett shale well, results from our mineralogical model suggest great variations in different minerals and more clay content suggesting that a “one paint brush” cannot be applied from the Barnett to the Upper Bowland Shale

4.3. Case Study – Analysis of TOC using Regression

4.3.1. Summary

The objective of this study is to develop an empirical equation from linear regression to determine TOC from the UK Upper Bowland Shale. The wells of interest within the Bowland-Hodder shale in this study are the Preese-Hall 1, Hesketh 1, Thistleton 1 and Grange-Hill 1 wells. Within the Bowland-Hodder unit, the interval of interest is the Bowland basin which was targeted by the Preese-Hall 1 well in Western Lancashire and this was the UK’s first shale gas exploration well (Andrews, 2013). The TOC core points from the Upper Bowland Shale for Preese-Hall 1 well, Thistleton 1 well, Hesketh 1 well, and Grange-Hill 1 were from 6611 to 8211 ft., 4250 to 6100 ft., 2300ft to 3100ft., and 7174ft to 9538ft respectively. In this study, organic richness in the Upper Bowland shale was determined using Multiple Linear Regression and Random Forest Regression analysis based on core data (core canister) from Preese Hall 1. The core TOC dataset consisted of 48 observations from Preese-Hall 1 in the

Upper Bowland Shale. Furthermore, random forest and linear regression models was also developed to predict TOC in other wells like the Hesketh 1, Thistleton 1 and Grange-Hill 1 well all of which have passed through the Upper Bowland Shale. The regression models were trained using 28 data points from Preese-Hall 1 well logs - Gamma Ray (GR), Deep Resistivity (DDLL), Sonic (DT), and Bulk Density (DEN) and tested on 20 data points from Preese-Hall 1. The trained model was also tested on other wells, namely, at specific intervals to assess the accuracy of the regression model. The linear regression model resulted in a R^2 of 41% on the test data and a R^2 of 33% on Hesketh 1 well. The random forest model was able to explain 80% of the variation on the training data set but resulted in a R^2 value of 43% on the test set based on 900 trees. Consequently, the random forest model was poor on predicting the TOC from the other wells i.e. Thistleton 1 (37 test data points), Grange-Hill 1 (15 test data points) and Hesketh 1 (12 data points).

4.3.2. Methodology

- The dataset was pre-processed i.e. scaling, removing outliers and high leverage points, log transformation of variables that were not normally distributed i.e. deep resistivity.
- Models were trained on the Preese-Hall 1 well and then used to predict the TOC on other wells that passed through the Upper Bowland Shale.
- Models were also cross validated to understand the test performance before building the model. For e.g. 5-fold cross validation was carried out in R for the linear model and the OOB results were used for the random forest model for cross validation.
- The final linear model was checked for autocorrelation, Heteroscedascity, collinearity using statistical tests to ensure that the model honours the assumptions of multiple linear regression.

4.3.3. Results and Discussions

4.3.3.1. Preese-Hall 1 (Random Forest Regression Results)

In Table 4-23, we can infer that 900 trees provided the best %Var explained based on the OOB samples. These results inform of the predictive performance of the random forest model.

Table 4-23: Fitting the Random Forest Regression Tree to the Whole Dataset

Number of Trees	% Var Explained	Mean of Squared Residuals
500	38.3	0.5210193
600	39.13	0.5140174
700	39	0.5151377
800	39.29	0.5127153
900	39.85	0.507998
1000	39.35	0.5121519

From this result, the variable importance was determined in terms of the %IncMSE and IncNode Purity.

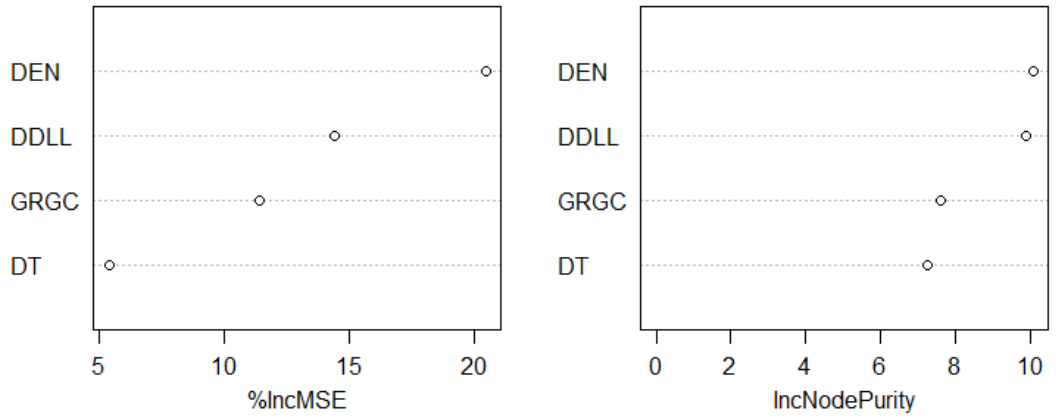

Figure 4-19: Variable Importance Data

Fitting the Random Forest Regression Tree to the Training Set

Based on 900 trees, the random forest regression model was trained on the dataset to obtain a R^2 value of 80.3% and a MSE of 0.174 (Figure 4-20).

Number of Trees	% Var Explained	Mean of Squared Residuals
900	13.58	0.7644341

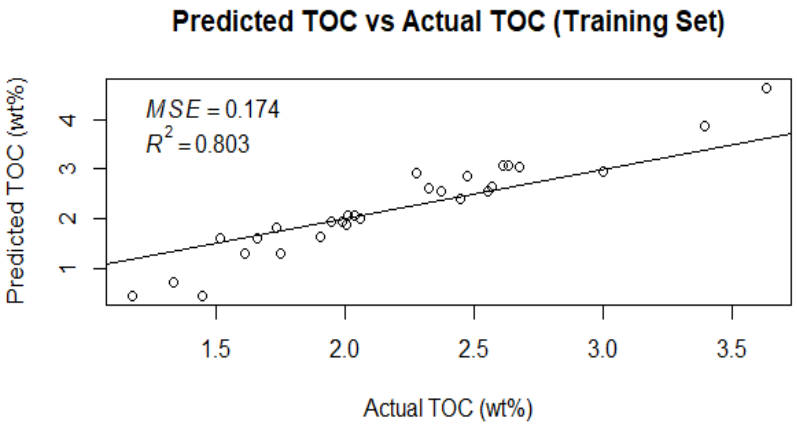

Figure 4-20

Fitting the Random Forest Regression Tree to the Test Set

The random forest model was then used to predict unseen test data to assess the predictive capability. This resulted in a R^2 value of 42.9% (Figure 4-21) which was greater and close to the estimate obtained from when the model was trained on the whole dataset and tested on the OOB samples (*Table 4-23*).

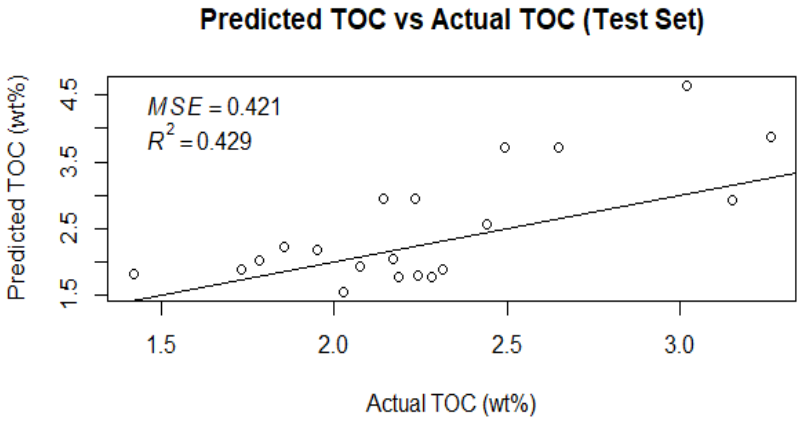

Figure 4-21

4.3.3.2. Random Forest Performance on Grange-Hill 1

Using the random forest model trained on the training dataset for Preese-Hall 1, we attempt to predict the TOC of Grange-Hill 1 but R^2 was negative which means the regression line is worse than using the mean value.

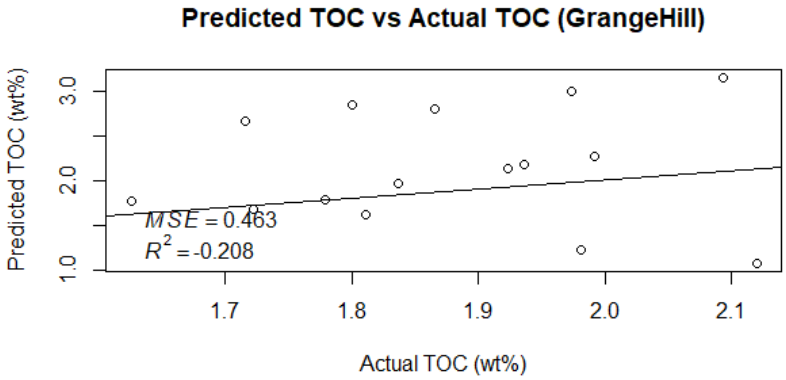

Figure 4-22

4.3.3.3. Random Forest Performance on Hesketh 1

Using the random forest model trained on the training dataset for Preese-Hall 1, we attempt to predict the TOC of Hesketh 1 but R^2 was negative which means the regression line is worse than using the mean value.

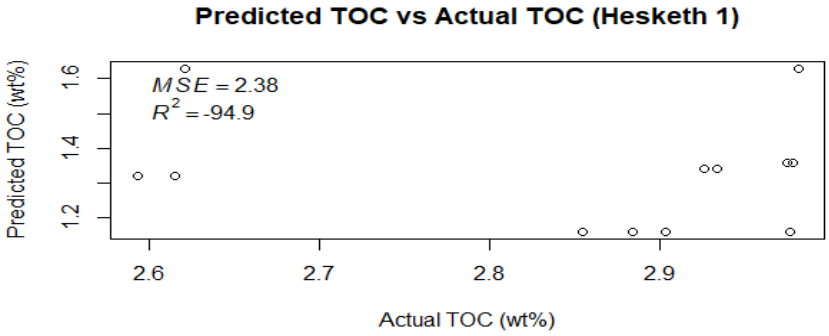

Figure 4-23

4.3.3.4. Random Forest Performance on Thistleton 1

Using the random forest model trained on the training dataset for Preese-Hall 1, we attempt to predict the TOC of Thistleton 1 but R^2 was negative which means the regression line is worse than using the mean value.

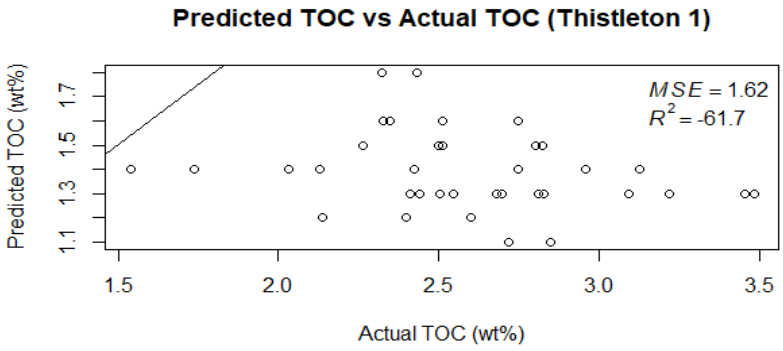

Figure 4-24

4.3.3.5. Linear Regression Results

4.3.3.5.1. Five - Fold Cross Validation

Based on 5-fold cross-validation on the dataset in this study, the optimum R^2 that can be obtained is approximately 39% (Table *4-24*). The average for RMSE, R^2, and MAE is ~ 0.22, 0.23 and 0.16 respectively. Figure *2-15*, illustrates the concept of cross-validation.

Table 4-24: Cross-Validation Results

	RMSE	R^2	MAE
1	1.5142945	0.20458528	0.8895658
2	0.8048858	0.17819749	0.6559766
3	0.7118428	0.02786657	0.5942032
4	0.9447385	0.39320616	0.6382171
5	1.0170472	0.12103606	0.8509521

Standard deviation around R^2: 0.1346866

4.3.3.5.2. Range of Parameters used to Train the Model (before feature scaling)

Scaling ensures that the data is standardized such that all the variables are on a comparable scale as well as having a mean of zero and a standard deviation of one. The **scale** function in R performs this process (Kumar, 2014). The **scale** function uses the Z-score standardisation method which performs better than the min-max normalization technique especially if there is a need for outliers to get weighted more than the other values (Kumar, 2014). The range of parameters used before feature scaling is shown in Table *4-25*

$$Z = \frac{X - \mu}{\sigma}$$

Equation 31 (Kumar, 2014)

Table 4-25: Descriptive stastics of the portion of the dataset used to train the linear regression model.

	GR (API)	DDLL (ohmm)	DT (µsec/ft.)	DEN (g/cm^3)	Core TOC (wt%)
Maximum	130.02	844.52	75.954	2.699	4.65
Minimum	25.19	64.14	51.933	2.143	0.43
Mean	69.47	342.87	64.991	2.588	2.35
Standard Deviation	23.99	214.17	5.645	0.101	0.96
Median	66.27	286.03	65.791	2.606	2.04
Range	104.83	780.37	24.021	0.556	4.22
CoV	0.35	0.62	0.087	0.039	0.41

4.3.3.5.3. Test for Normality

A series of QQ plots was used to visually check that the dataset is normally distributed. From *Figure 4-25*, it was apparent that the deep resistivity and density were significantly not normally distributed. In addition, a correlation matrix diagram *Figure 4-26* was also plotted to further investigate normality in the dataset.

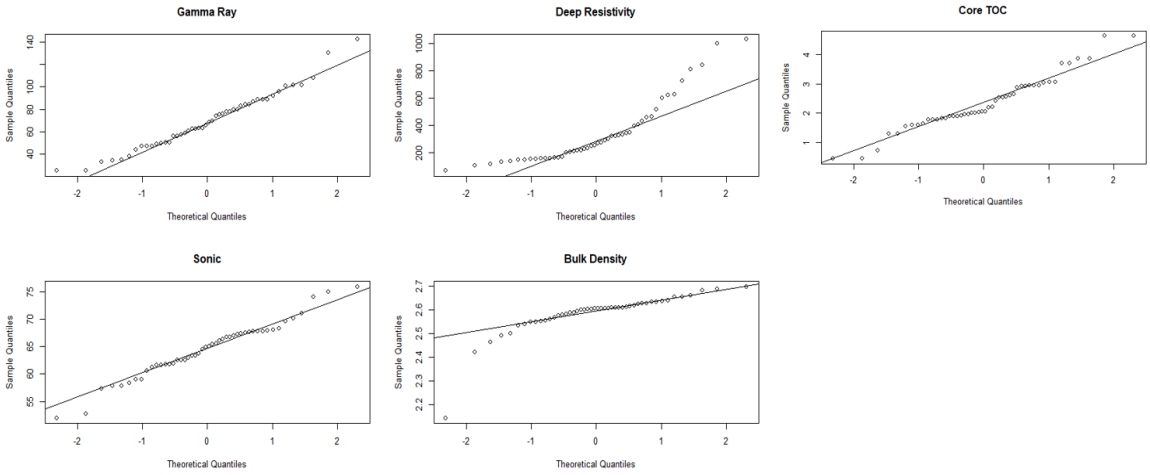

Figure 4-25: Test for Normality in the Dataset

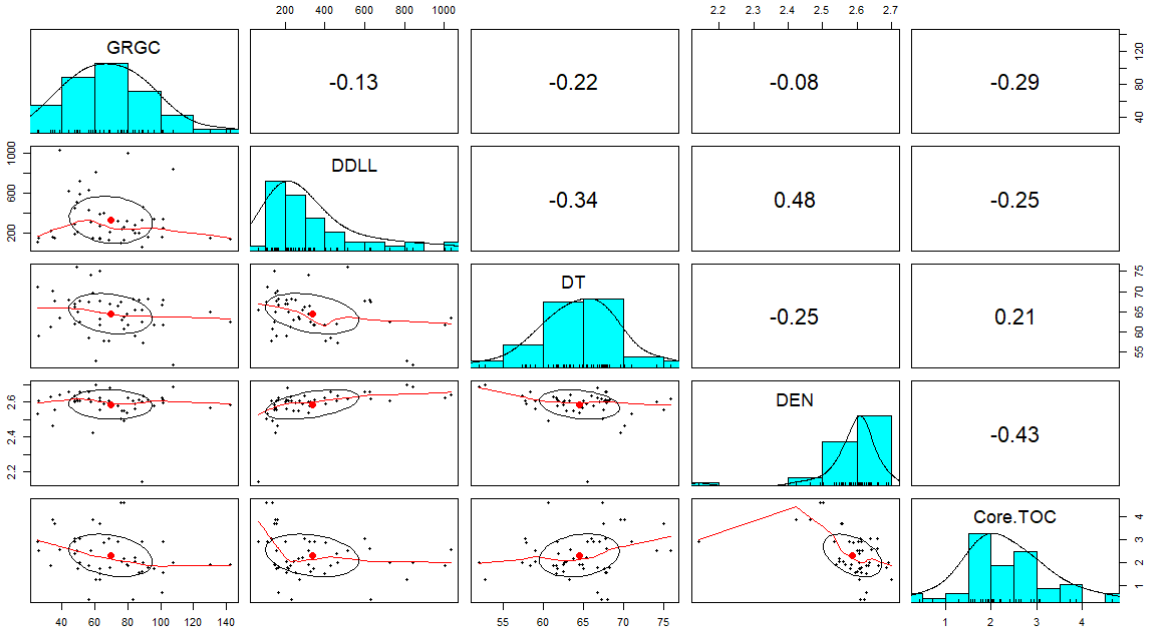

Figure 4-26: Investigation of Normality (Before Transformation)

Using *Figure 4-26*, the resistivity data, density and the dependent variable were log transformed as shown in *Figure 4-27*;

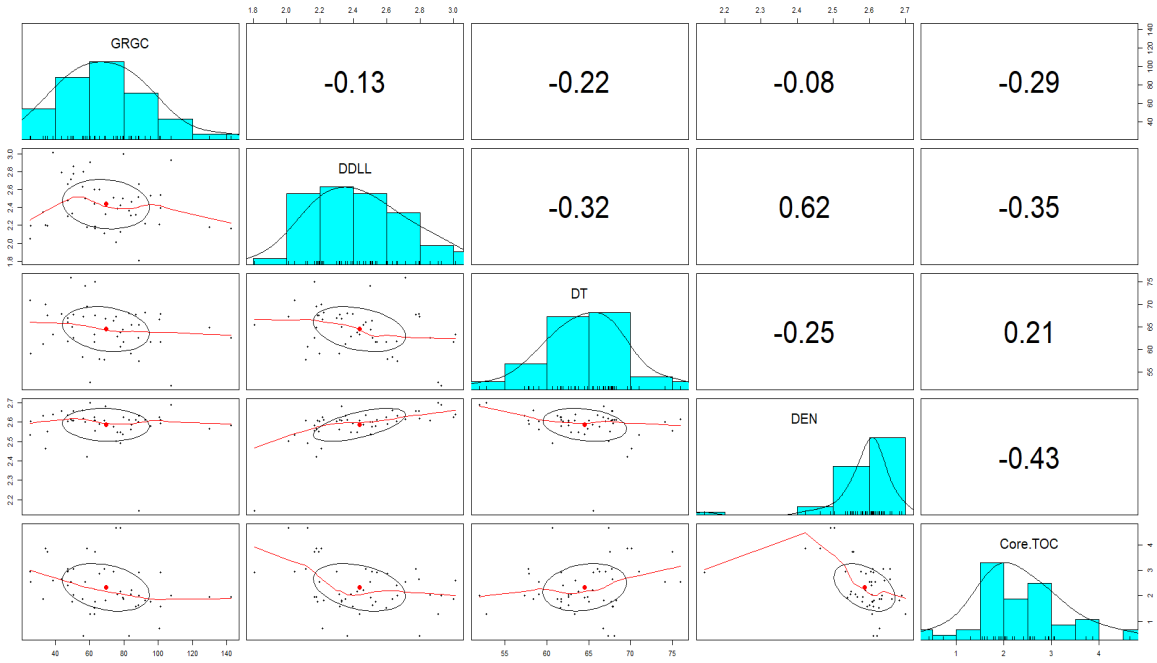

Figure 4-27: Investigation of Normality (After Transformation)

After log transformation, we can visually observe that the DDLL is now more normally distributed. Removing the outlier (Observation 9) in DEN makes the dataset normally distributed.

4.3.3.5.4. Visual Inspection of Linearity

As described in section 2.3.9.3.1, a linear relationship can exist between TOC and the independent variables so a plot of the dependent variable against the independent variables were plotted and shown in *Figure 4-28*.

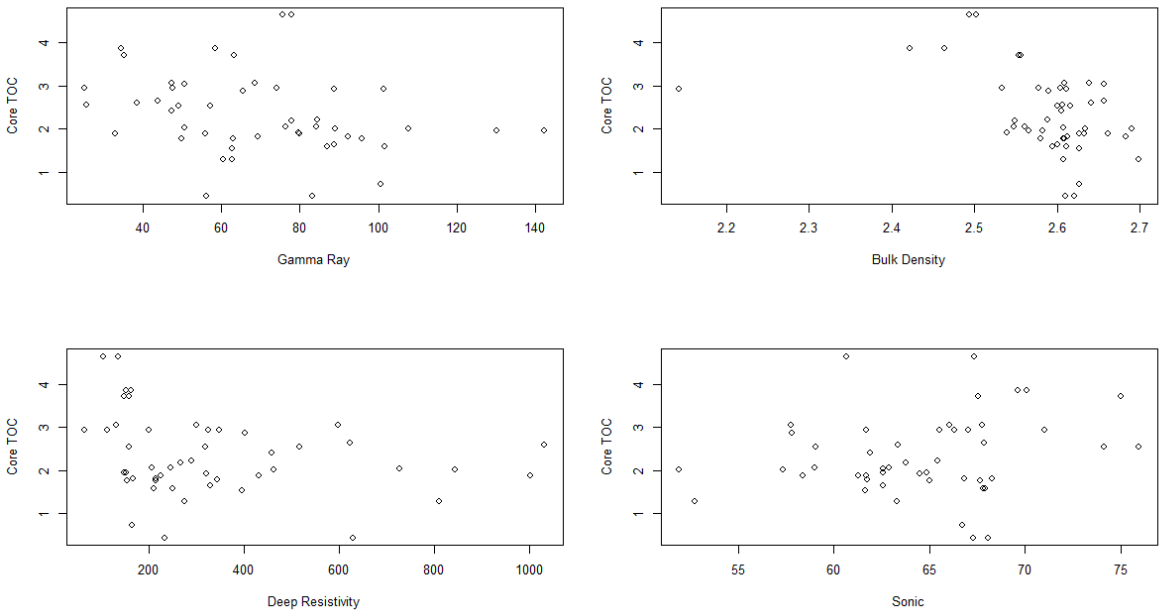

Figure 4-28: TOC against all the independent variables

Despite the scattering present, it would be possible to fit a straight line in each independent variable albeit a weak relationship.

4.3.3.5.5. Multiple Linear Regression Fit to the Dataset

Using a process of backward elimination, the regression model was fit to the training set over a series of steps. In Figure *4-29*, none of the well log input data was statistically significant at the 5% significant level. The p value of 0.11 suggest a conclusion to fail to reject the null hypothesis that none of the well logs can be used to predict TOC along with a residual error of 0.8846.

Regression Output (all Variables)

```
Coefficients:
            Estimate Std. Error t value Pr(>|t|)
(Intercept)  2.36504    0.16897  13.996 9.67e-13 ***
GRGC        -0.28506    0.19797  -1.440    0.163
DDLL        -0.22014    0.26486  -0.831    0.414
DT           0.05834    0.17914   0.326    0.748
DEN         -0.19940    0.20983  -0.950    0.352
---
Signif. codes:  0 ‘***’ 0.001 ‘**’ 0.01 ‘*’ 0.05 ‘.’ 0.1 ‘ ’ 1

Residual standard error: 0.8846 on 23 degrees of freedom
Multiple R-squared:  0.2696,    Adjusted R-squared:  0.1426
F-statistic: 2.122 on 4 and 23 DF,  p-value: 0.1106
```

Figure 4-29

Regression Diagnostics

From *Figure 4-30*, the cook's distance plot (allows us to determine influential points) (observation 9) shows an outlier in the training set while the residuals vs fitted shows that Heteroscedascity is present in the training data.

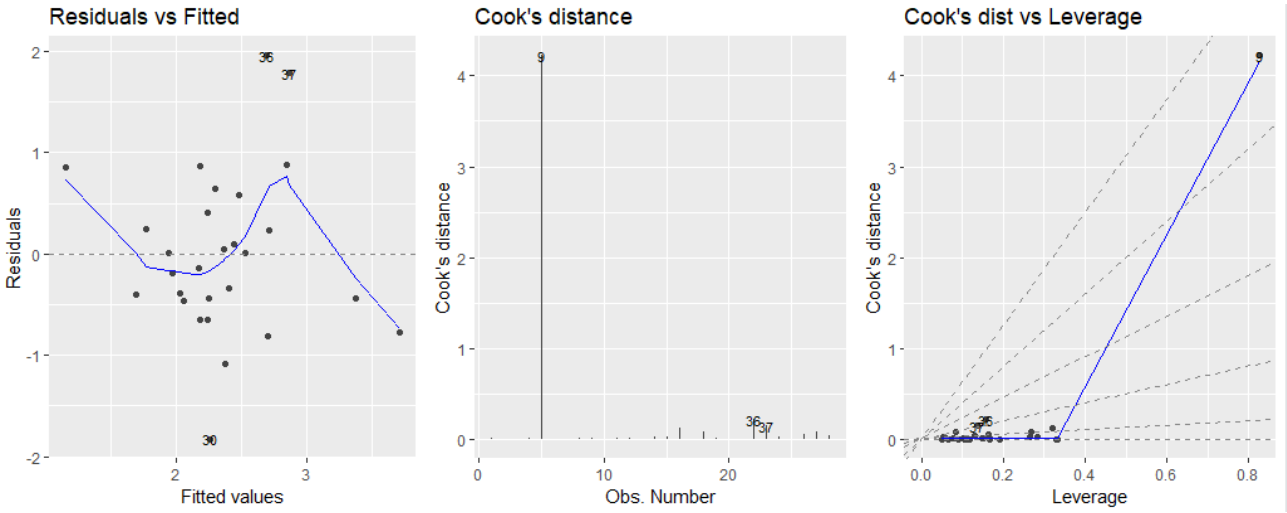

Figure 4-30: Regression Diagnostics

Visual inspection of the residual's vs fitted values shows a noticeable pattern indicating a degree of Heteroscedascity as described in section 2.3.9.3.3.

Regression Output (all Variables) without Outlier (Observation 9)

To improve the performance of the linear regression model, observation 9 was removed from the training set and the results are shown in *Figure 4-31*. There is now an improvement in the performance of the model with **DEN** now becoming statistically significant. Recall the plots in *Figure 4-28*, observation 9 was the outlier in the TOC vs Bulk Density plot. Removing the outlier, improved the p-value of this scenario and the

Adjusted R^2 value though the Heteroscedascity is still evident in the dataset from the residual's vs fitted plot Figure *4-32*.

```
Coefficients:
            Estimate Std. Error t value Pr(>|t|)
(Intercept)  2.53126    0.17132  14.775 6.66e-13 ***
GRGC        -0.30968    0.18218  -1.700   0.1033
DDLL         0.05436    0.27117   0.200   0.8430
DT           0.00480    0.16621   0.029   0.9772
DEN         -0.99824    0.39821  -2.507   0.0201 *
---
Signif. codes:  0 '***' 0.001 '**' 0.01 '*' 0.05 '.' 0.1 ' ' 1

Residual standard error: 0.8126 on 22 degrees of freedom
Multiple R-squared:  0.4021,    Adjusted R-squared:  0.2934
F-statistic: 3.699 on 4 and 22 DF,  p-value: 0.01892
```

Figure 4-31: Regression Outputs

Regression Diagnostics

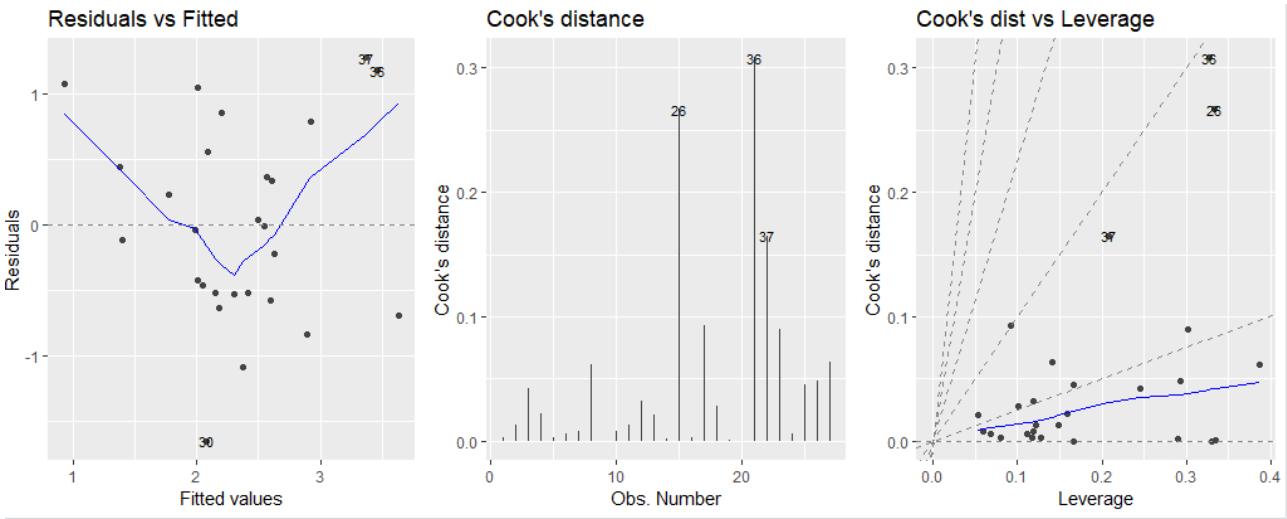

Figure 4-32: Regression Diagnostics

Regression Output without DDLL and DT

Without the deep resistivity log and sonic log, there was an improvement in the degrees of freedom and the p-value with the density and gamma ray log. The p-value was highly significant compared to the previous scenario (Figure *4-33*). Despite the positive results, the regression diagnostics suggest a data with high leverage points and Heteroscedascity (Figure 4-34) and this can create an unwanted confidence in the model as described in section 2.3.9.3.3.

```
Coefficients:
             Estimate Std. Error t value Pr(>|t|)
(Intercept)   2.5267     0.1595  15.840  3.3e-14 ***
DEN          -0.9397     0.2543  -3.695  0.00114 **
GRGC         -0.3119     0.1614  -1.932  0.06519 .
---
Signif. codes:  0 ‘***’ 0.001 ‘**’ 0.01 ‘*’ 0.05 ‘.’ 0.1 ‘ ’ 1

Residual standard error: 0.7787 on 24 degrees of freedom
Multiple R-squared:  0.401,     Adjusted R-squared:  0.3511
F-statistic: 8.034 on 2 and 24 DF,  p-value: 0.002133
```

Figure 4-33: Regression Outputs

Regression Diagnostics

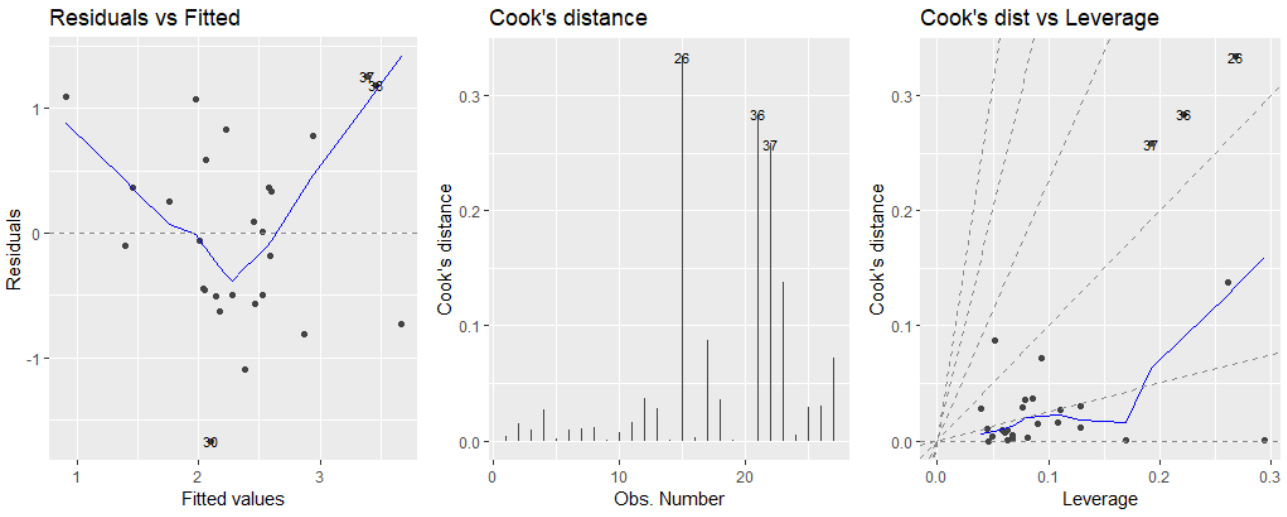

Figure 4-34

Addition of a non-linear transformation to the model

To this point, results obtained gives unwanted confidence in the dataset because of the heteroscedascity in the dataset, to improve results, a non-linear transformation was added to the model as described in section 2.3.9.3.3. Now the density and gamma ray log are more significant compared to the previous scenario along with a lower residual standard error. The regression diagnostics in Figure *4-36* also shows that Heteroscedascity has now been improved with a more stable pattern in the residuals vs fitted plot.

```
Coefficients:
             Estimate Std. Error t value Pr(>|t|)
(Intercept)   2.2367     0.1627  13.744 1.41e-12 ***
DEN          -1.1775     0.2282  -5.160 3.14e-05 ***
GRGC         -0.3320     0.1372  -2.420  0.02381 *
I(DEN^2)      0.8566     0.2668   3.211  0.00387 **
---
Signif. codes:  0 ‘***’ 0.001 ‘**’ 0.01 ‘*’ 0.05 ‘.’ 0.1 ‘ ’ 1

Residual standard error: 0.661 on 23 degrees of freedom
Multiple R-squared:  0.5864,    Adjusted R-squared:  0.5325
F-statistic: 10.87 on 3 and 23 DF,  p-value: 0.000121
```

Figure 4-35: Regression Outputs

Regression Diagnostics

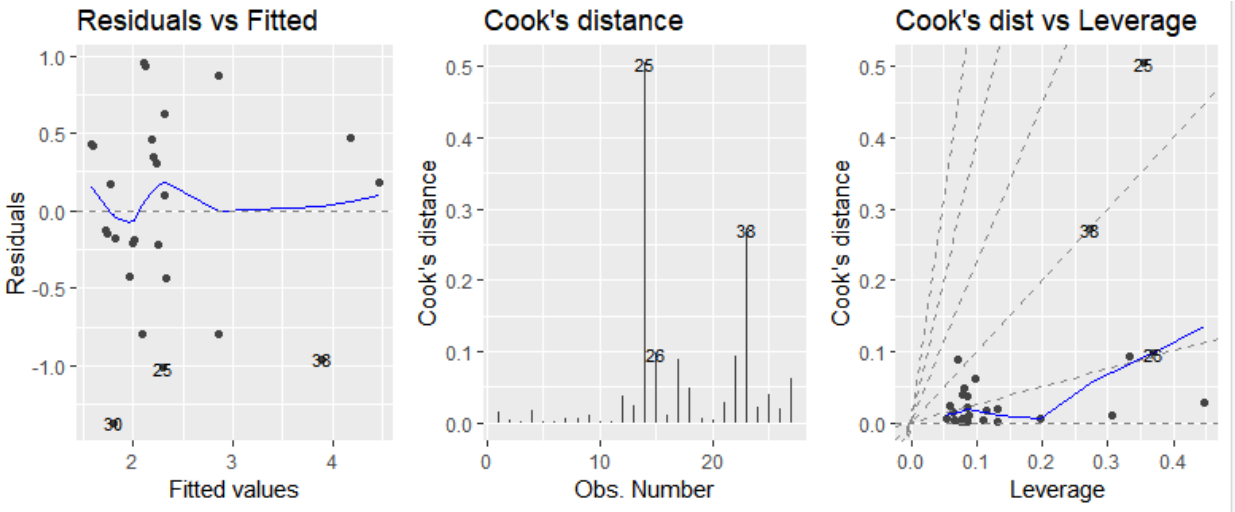

Figure 4-36

Regression Output without Observation 25

In this scenario, observation 25 was removed due to the output of the cook’s distance plot from the previous section which has drastically improved the p-value and adjusted R2 whilst making the square density term more significant. However, upon running the regression diagnostics, we observe another outlier in the dataset which was examined in Figure *4-39*.

```
Coefficients:
             Estimate Std. Error t value Pr(>|t|)
(Intercept)   2.1622     0.1569  13.783 2.66e-12 ***
DEN          -1.0702     0.2203  -4.858 7.44e-05 ***
GRGC         -0.3483     0.1288  -2.704 0.012976 *
I(DEN^2)      1.1310     0.2839   3.984 0.000628 ***
---
Signif. codes:  0 '***' 0.001 '**' 0.01 '*' 0.05 '.' 0.1 ' ' 1

Residual standard error: 0.6197 on 22 degrees of freedom
Multiple R-squared:  0.6353,    Adjusted R-squared:  0.5856
F-statistic: 12.78 on 3 and 22 DF,  p-value: 4.786e-05
```

Figure 4-37: Regression Outputs

Regression Diagnostics

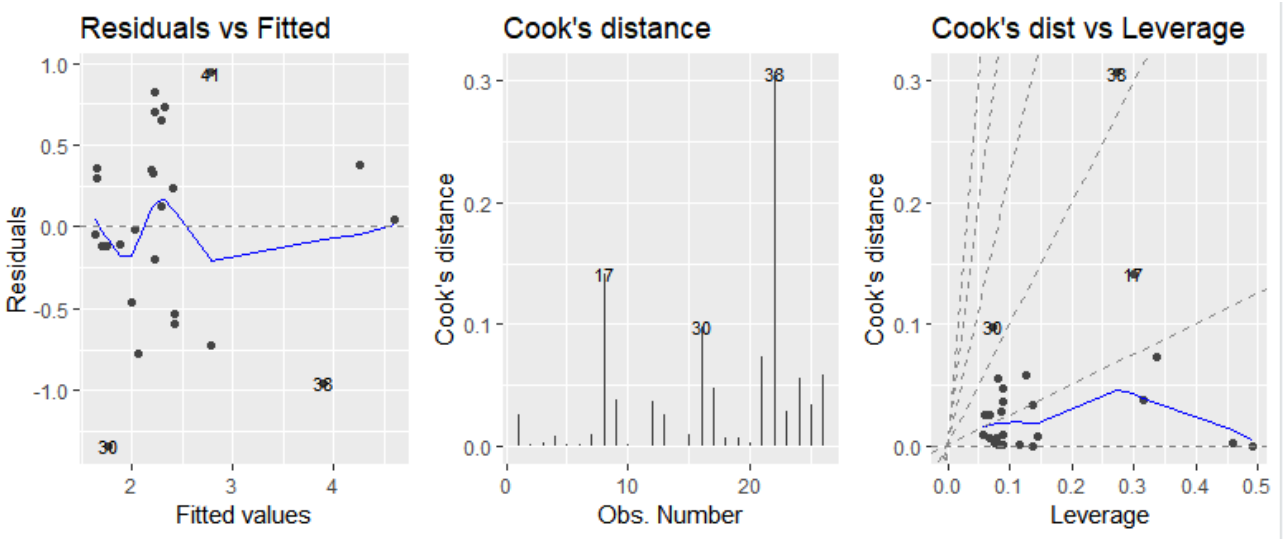

Figure 4-38

Regression Output without Observation 38 – Our Final Model

Finally, upon removing observation 38, we see an improvement in the statistical significance of the gamma ray log with better p-value and lower residual error. The diagnostics i.e. the residual vs fitted plot show randomness in the dataset.

```
Coefficients:
             Estimate Std. Error t value Pr(>|t|)
(Intercept)   2.2170     0.1509  14.692 1.60e-12 ***
DEN          -1.2215     0.2226  -5.488 1.91e-05 ***
GRGC         -0.4544     0.1337  -3.399 0.002707 **
I(DEN^2)      1.1888     0.2698   4.406 0.000246 ***
---
Signif. codes:  0 '***' 0.001 '**' 0.01 '*' 0.05 '.' 0.1 ' ' 1

Residual standard error: 0.5853 on 21 degrees of freedom
Multiple R-squared:  0.685,     Adjusted R-squared:   0.64
F-statistic: 15.22 on 3 and 21 DF,  p-value: 1.726e-05
```

Figure 4-39: Regression Outputs

Regression Diagnostics

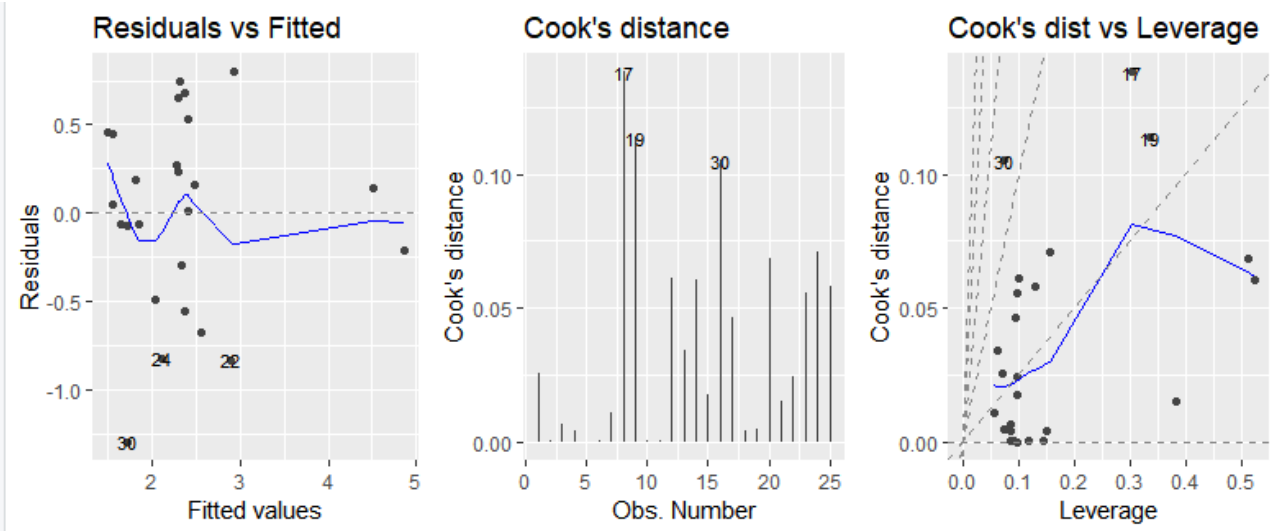

Figure 4-40

Regression Output without DDLL, DT and GRGC

Finally, we remove all variables except the density log variable and the accuracy of the model declines despite the density log been statistically significant. The shows the important of the gamma ray log in enhancing the predictive accuracy of the model as described in section 2.4.2.

```
Coefficients:
             Estimate Std. Error t value Pr(>|t|)
(Intercept)   2.5352     0.1825  13.893 1.13e-12 ***
DEN          -0.8963     0.3116  -2.876  0.00853 **
---
Signif. codes:  0 ‘***’ 0.001 ‘**’ 0.01 ‘*’ 0.05 ‘.’ 0.1 ‘ ’ 1

Residual standard error: 0.8545 on 23 degrees of freedom
Multiple R-squared:  0.2645,    Adjusted R-squared:  0.2326
F-statistic: 8.273 on 1 and 23 DF,  p-value: 0.008527
```

Figure 4-41: Regression Outputs

Summary of Training Performance

The results of the previous sections are described in the table 4.26 showing how the performance of the model varied with all the scenarios considered.

Table 4-26: Summary of Training Performance – Linear Regression

Regression Fit	R^2	Adjusted R^2
All Varaibles	26.96%	14.26%
All Varaibles without Observation 9	40.21%	29.34%
All Varaibles excluding DDLL and DT	40.10%	35.11%
All Varaibles without Observation 25	63.53%	58.56%
All Varaibles without Observation 38	68.50%	64.00%
All Varaibles excluding DDLL, DT, and GRGC	26.45%	23.26%

Final Model Equation: $TOC = 2.2170 - 1.2215 * (DEN) - 0.4544 * (GR) + 1.1888 * (DEN)^2$

Bruce Pagan Test – Heteroscedascity Check on the Final Trained Model

In addition, we carried out analytical Heteroscedascity checks on the model to compliment the visual inspections using the Bruce Pagan test. The result in Table *4-27* showed that P-value is greater than a significance level of 0.05, therefore we can fail to reject the null hypothesis that the variance of the residuals is constant and infer that heteroscedasticity is not present.

Table 4-27: Bruce-Pagan Test

Statistical Test	p-value
BP = 0.96789	0.809

Durbin-Watson Test – Autocorrelation Check

The Autocorrelation check on the model was tested with the Durbin-Watson test and the p value was also greater that 0.05 suggesting that we can fail to reject the null hypothesis that there is autocorrelation in the dataset. The concept of autocorrelation is explained in section 2.3.9.3.2.

Table 4-28: Durbin-Watson Test

Statistical Test	p-value
DW Score = 2.2568	0.6807

Variance Inflation Check – Multicollinearity Check

Collinearity reduces the accuracy of the estimates of the regression coefficients as it increases the standard error and p-value and therefore reduces the t-statistic (Casella, Fienberg and Olkin, 2017). More detail on multicollinearity and the variable inflation factor is explained in section 2.3.9.3.4. Typically, VIF = 1 (no correlation), 1<VIF<5 (moderately correlated), 5<VIF<10 (highly correlated).

Table 4-29: Variable Inflation Factor

Independent Variable	Variable Inflation Factor
Bulk Density	1.087713
Gamma Ray	1.059918
Bulk Density^2	1.043425

4.3.3.5.6. Test Set Predictions for Preese-Hall 1

Following the results of training and determining the regression expression for the model, the performance of the model was tested on Preese-Hall 1. Figure *4-42* shows a 41% confidence in predicting the actual TOC for Preese-Hall 1. The result of the training set is shown for completeness in Figure *4-43*.

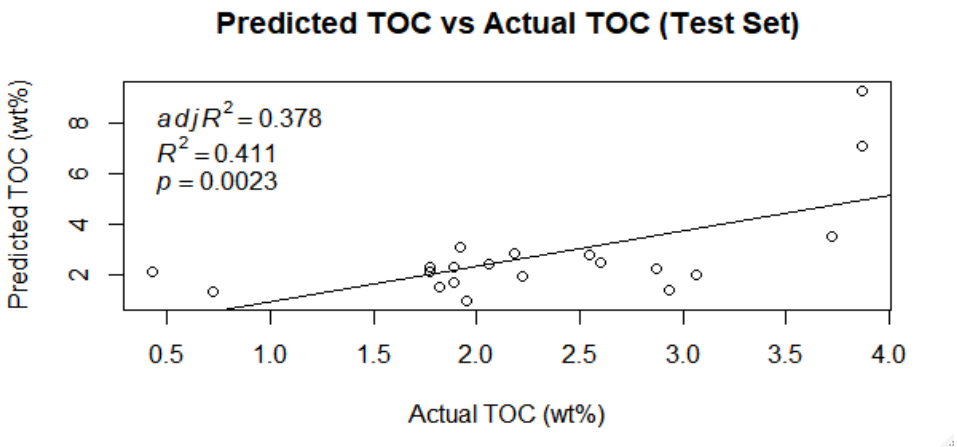

Figure 4-42

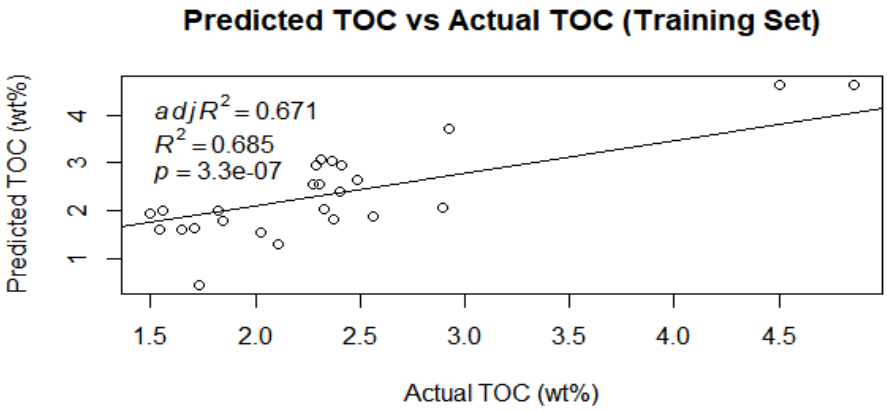

Figure 4-43

4.3.3.5.7. Trained Model Performance on Grange-Hill 1, Thistleton 1 and Hesketh 1

Contrary to Preese-Hall 1, the linear regression mode was incapable of sufficiently predicting the test set data for Grange-hill 1 and Thistleton 1 considering that the model has not been exposed to the training dataset – though there was an exception for Hesketh 1 which resulted in an R^2 of 33% and p-value of 0.05 with a comparable number of core points.

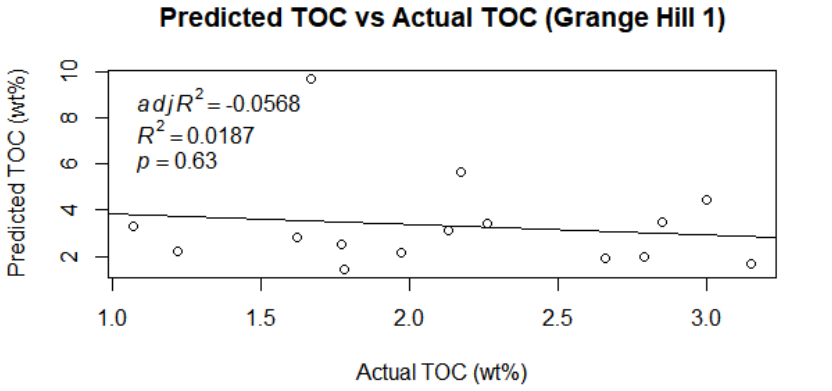

Figure 4-44

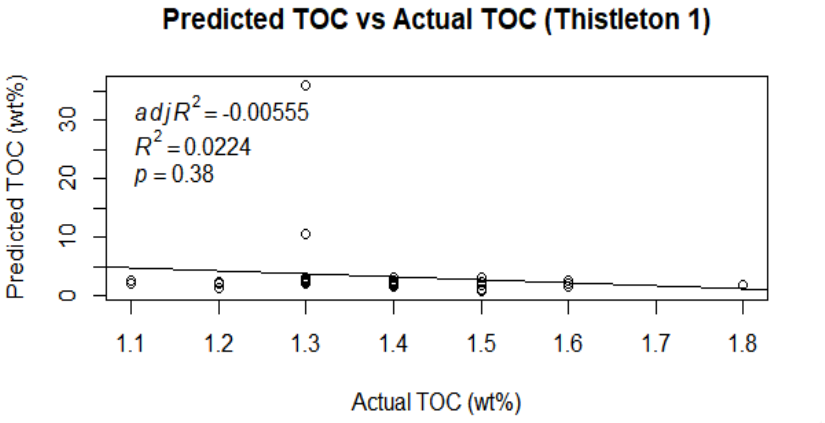

Figure 4-45

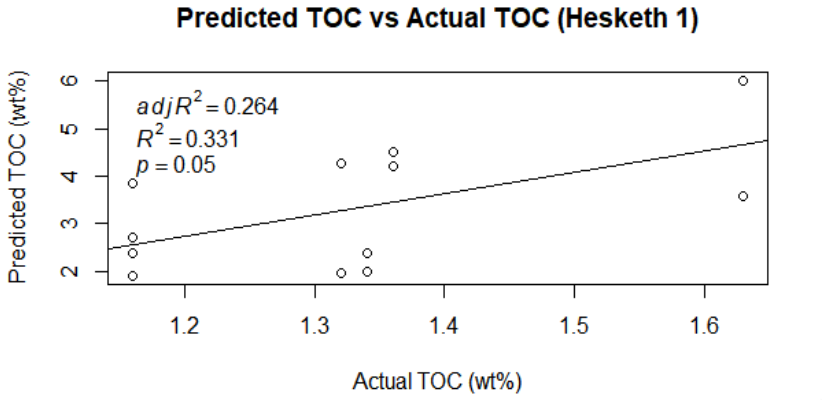

Figure 4-46

4.3.4. Conclusions

The random forest model was capable of learning the training dataset based on 900 trees, effectively more than the linear regression model however the predictive capability of the random forest regression model was not superior to the linear regression model irrespective of its superior ability to learn the training data. It is important to note that there was non-linearity present in the dataset between the independent variable (TOC) and the well log data (dependent variable) and a quadratic term was added to the linear regression model to create a better model. The linear regression model was capable of predicting the TOC on the other wells much more effectively than random forest regression, resulting in an R^2 of 33% for the Hesketh 1 well. The inclusion of the Gamma Ray log enhanced the linear model (Table 4-26). Considering a bottom-up approach in developing the Upper Bowland shale, this case study proved that it is possible to generate complete TOC for the whole reservoir area that we can include into the development of the reservoir model that will contribute to accurate future shale gas production.

Chapter 5 Reservoir Modelling and Simulation

5.1. Introduction

This chapter allows us to compile all the knowledge from previous chapters to help address the research gap articulated in this thesis i.e. the prediction of gas production from the UK Upper Bowland Shale. Various best practises from different sections, i.e. petrophysics, geochemistry, production forecasting, reservoir simulation is compiled in this chapter to produce a model that is capable of predicting gas production from the Bowland despite using the Barnett shale as an analogy for validation. Justification for using the Barnett shale have been described in section Chapter 3. It is useful to recall that the Bowland-Hodder equivalent (Mississippian) in the Bowland Basin fill contains up to 5 km of interbedded shales, calcareous mudstones, limestones, siltstones, and fine sandstones (Clarke *et al.*, 2018). Thus by using available data, including UGC maps and well tops of the intersected formations, a 3D model of the reservoir in the location of drilled key wells was generated. Figure 5-1. The model was constructed using Petrel 2016 software. Using Petrel as a Proof of Concept, the model was further developed using CMG with simulation carried out with GEM. The well tops are shown in Figure 5-2 Figure *5-3* with the zone of interest been the Upper Bowland shales.

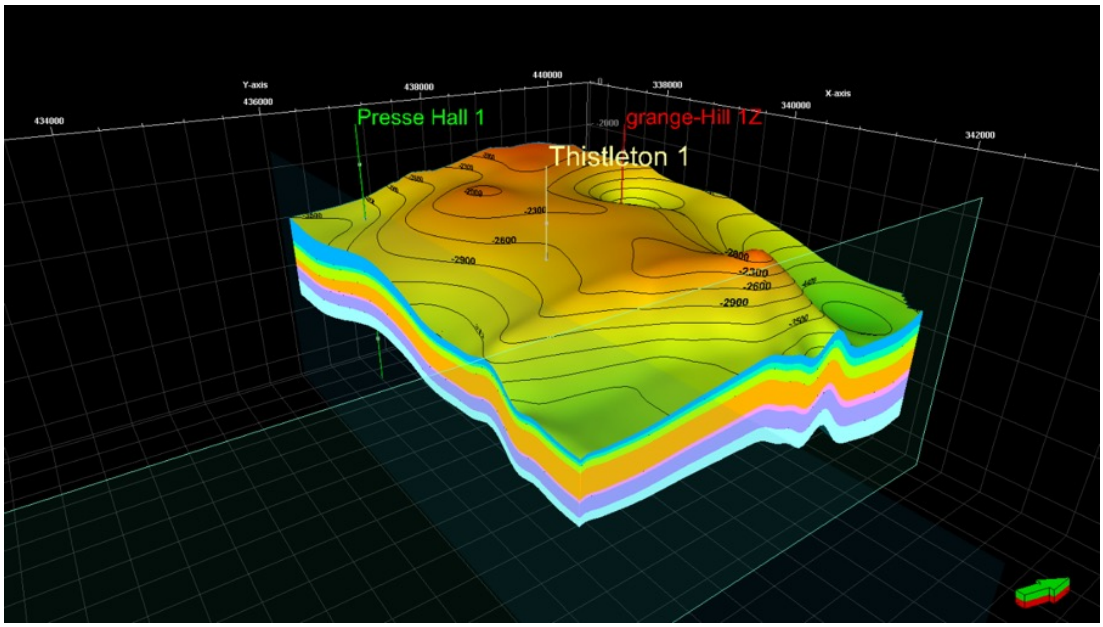

Figure 5-1: 3D modelled Bowland main reservoir, visible horizons, along with the key wells

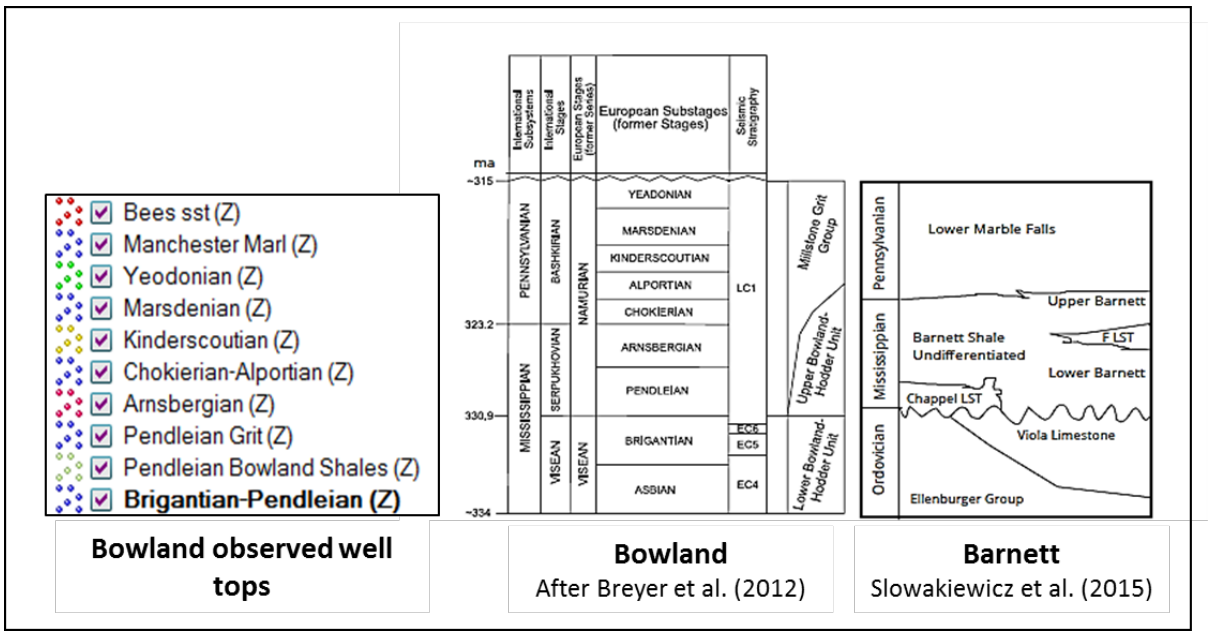

Figure 5-2: A comparison of Bowland and Barnett stratigraphy. Also observed well tops at the key wells, drilled in Bowland, are presented

System	Series	Regional substage	Lithostratigraphy	Depth (ft) MDRT
Triassic	Middle		Mercia Mudstone	Surface
	Lower		Sherwood sst	680
			Sherwood St Bees sst	1390
Permian	Upper		Manchester Marl	3380
	Lower		Collyhurst sst	3840
Pensylvanian		Langsettian	Lower Coal Measures	4090
	Bashkirian	Yeadonian	Rough Rock	4198
		Marsdenian	Upper Shales	4402
		Kinderscoutian	Kinderscout Group	4890
		Chokierian/Alportian	Sabden Shale Group	5240
Mississippian	Serphukhovian	Arnsbergian	Roeburndale Fm	5380
		Pendleian	Brennand Grit	5880
			Pendle Grit Fm	6090
			Upper Bowland Shale	6540
	Visean	Brigantian	Lower Bowland Shale	8220
			Preese Hall Lst	8225
			Weeton Lst	9004

Figure 5-3: Preese Hall 1 Formation Tops

5.2. Geological Model Development

The geological model was developed using three wells in the Bowland Basin that crossed the Upper Bowland Shale namely; Thistleton 1, Preese-Hall 1, and Grange-Hill 1 wells. The subsurface contour map from the Bowland Basin defined the shape of the simulation model and the well tops from the three wells defined the depth limits of the model Figure 5-4. The field well trajectories of each well was extracted from the well drilling report and loaded into

the model. The latitude and longitude points were obtained from the UK Onshore Geophysical Library and used along with the well trajectories.

Some base parameters in this model are in Table 5-1

Table 5-1: Table of Base Simulation Parameters

Primary Fracture Permeability in I Direction	4e-05md
Primary Fracture Permeability in J Direction	4e-05md
Primary Fracture Permeability in K Direction	8e-05md
Natural Fracture Porosity	0.08
Natural Fracture spacing, I	25ft
Natural Fracture spacing J	25ft
Natural Fracture spacing K	0ft
Rock Density	165 lb/ft3
Stimulated Fracture Permeability	100 md
Gridding	28x24x12 with a block width of 100ft in I and J directions.

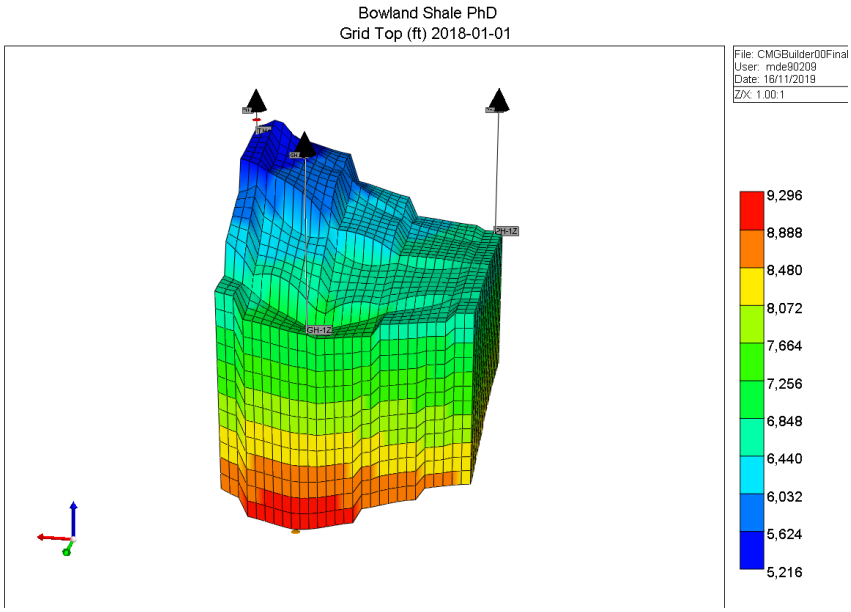

Figure 5-4: 3D Bowland Simulation Model showing the Grid Top variation in the Upper Bowland Shale within the Bowland Basin

After creating the grid blocks, petrophysical modelling was carried out with variograms using inputs from respective well logs (including well log output calculations i.e. porosity saturation, permeability etc. from chapter 4) from the three wells. The variograms resulted in output of

various realisations allowing the derived grid properties to be statistically distributed in the model using Kriging (Figure 5-5 to Figure 5-8)

Permeability

The core permeability was used here as a starting point before petrophysical modelling.

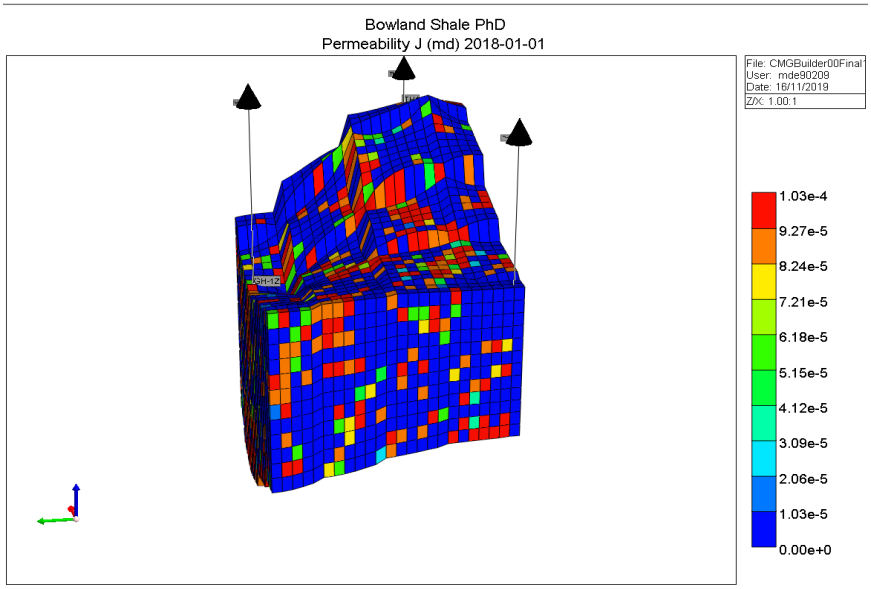

Figure 5-5

Grid Thickness

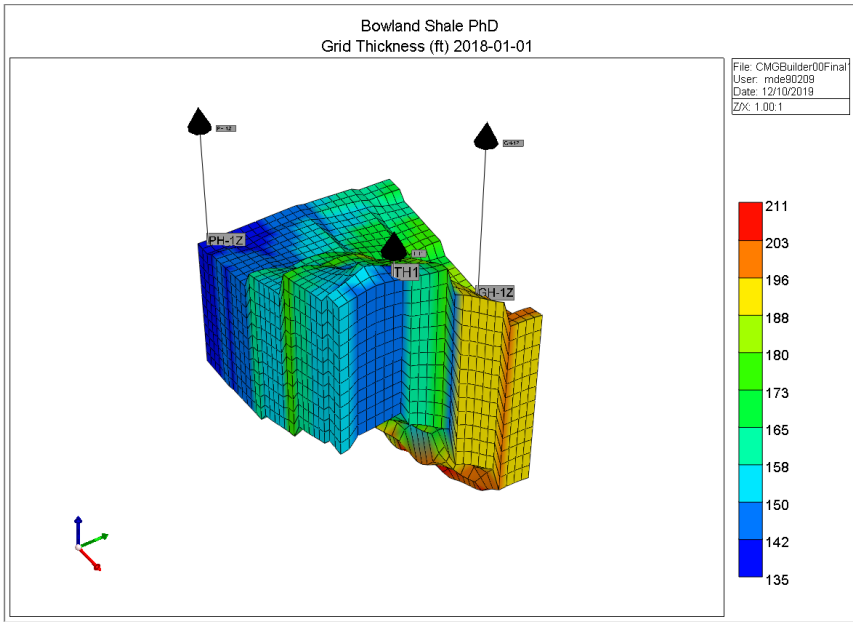

Figure 5-6

Grid Top

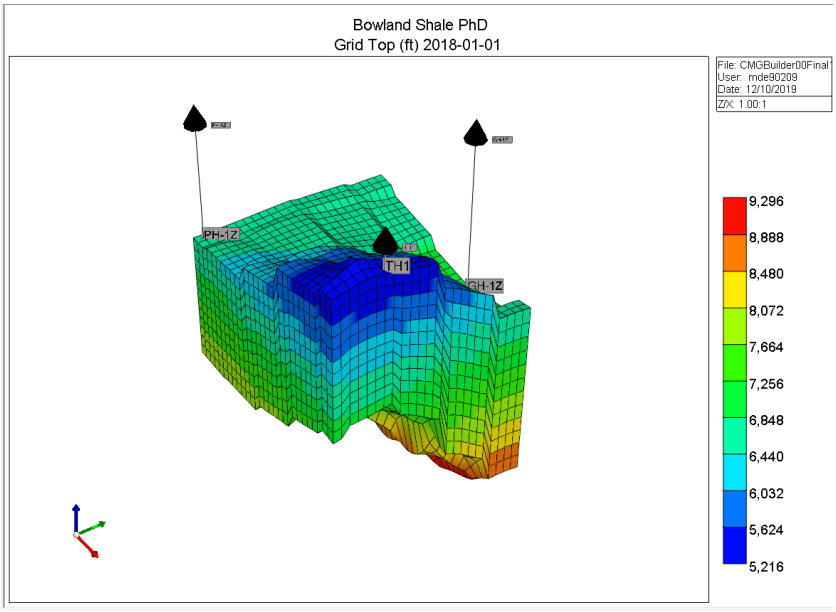

Figure 5-7

Porosity

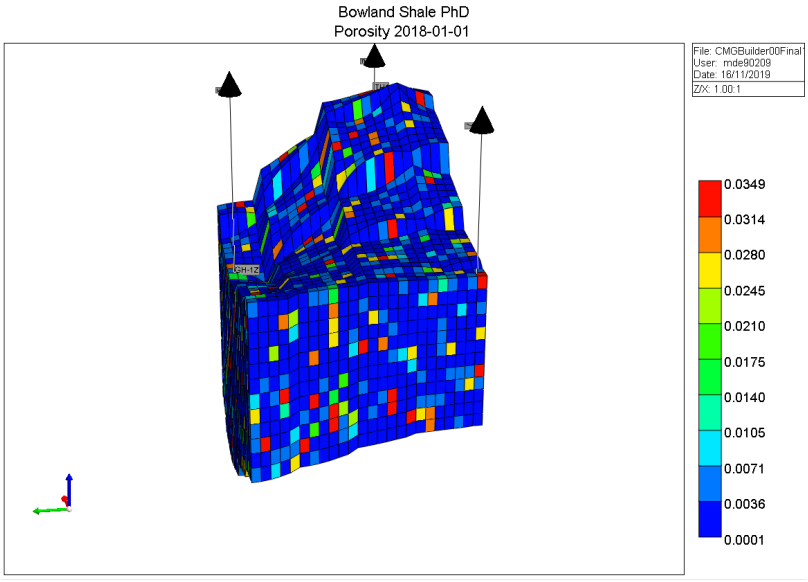

Figure 5-8

5.3. Mineralogical Modelling

Regression models were also developed to predict mineralogy effectively in the Upper Bowland shale within the Bowland Basin and the results were described in Chapter 4. The mineralogy results were also distributed through the model using mineralogy results from Preese-Hall 1 and Grange-Hill 1z. The distributions are shown in Figure 5-9 to Figure 5-13.

Quartz

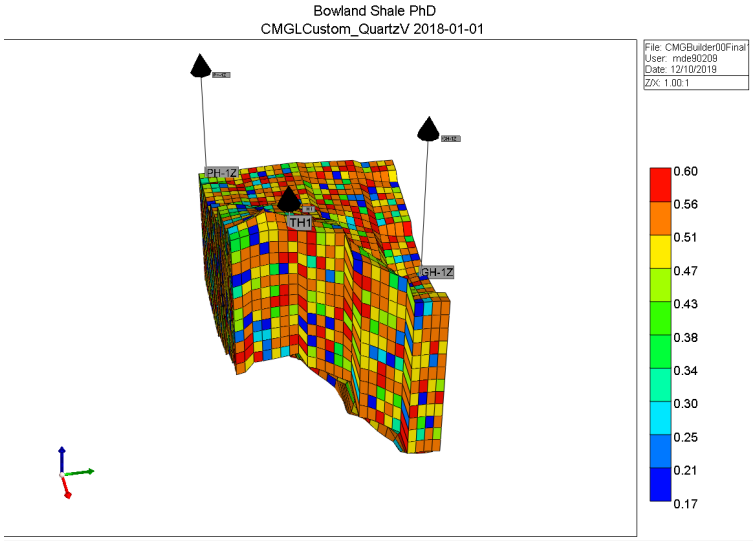

Figure 5-9

Illite

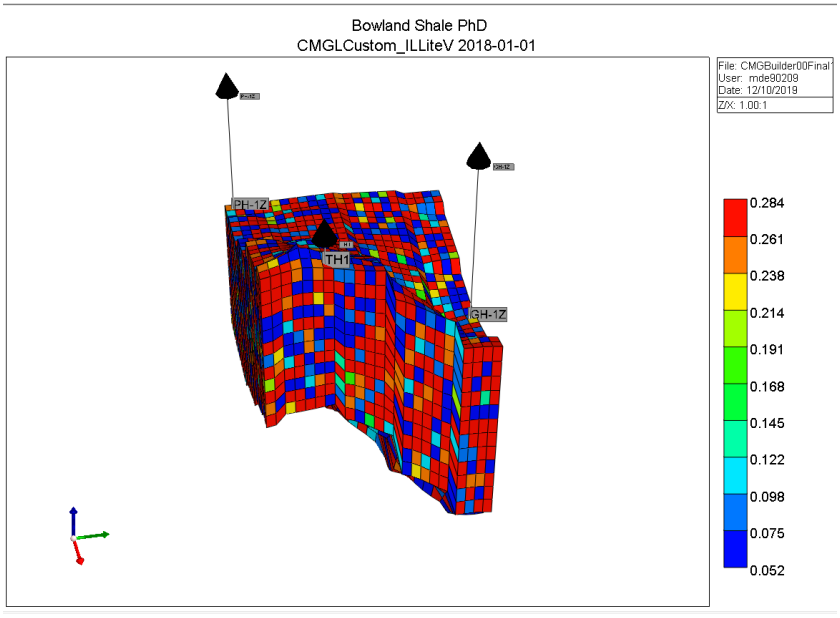

Figure 5-10

Ankerite

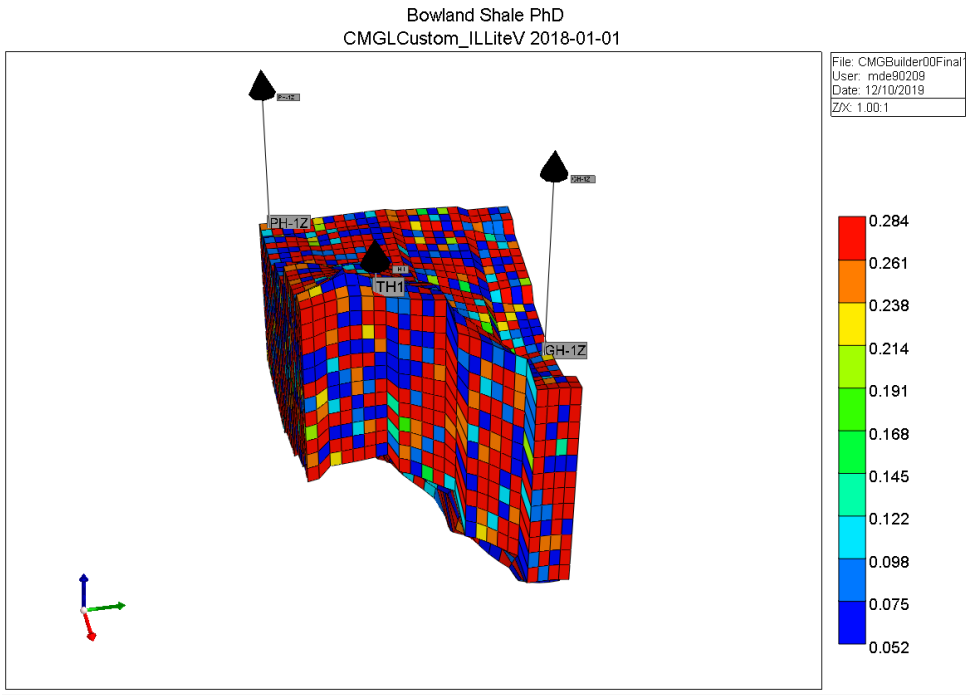

Figure 5-11

Calcite

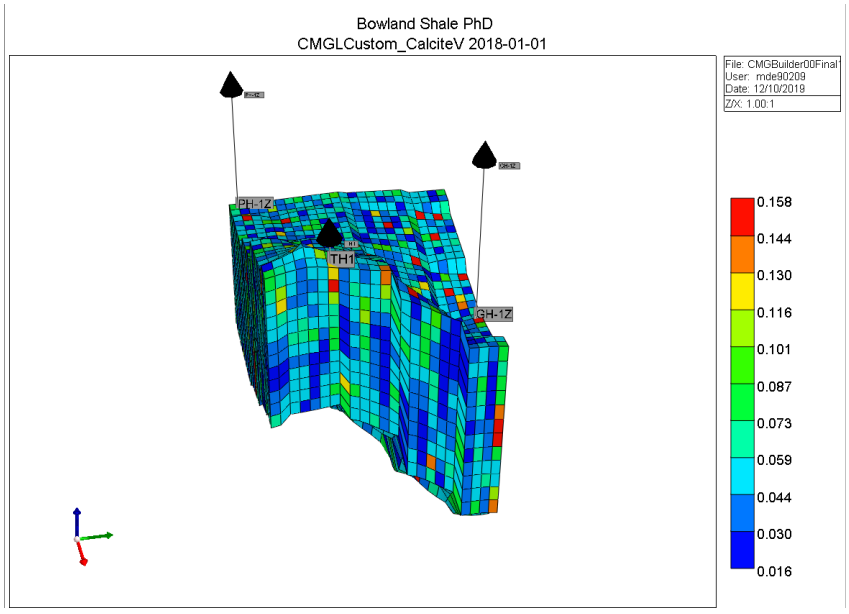

Figure 5-12

Albite

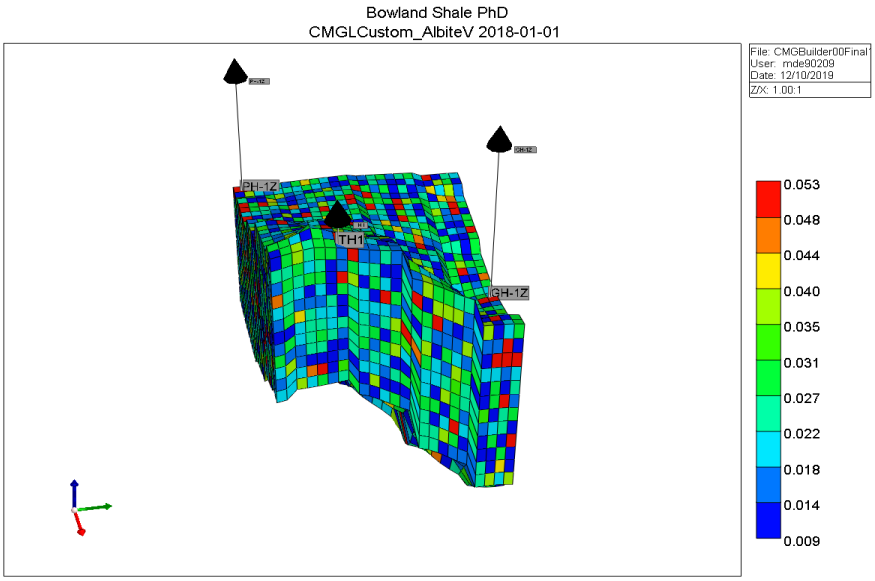

Figure 5-13

5.4. Reservoir Simulation Results

The simulation model was developed fully implementing DK-LS-LGR method (Cipolla *et al.*, 2010) to properly account for transient gas flow from the matrix to the fracture. The primary hydraulic fractures perpendicular to the wellbore were modelled explicitly with thin grid cells that retained the finite conductivity. The base case scenario for the three wells used in this model are shown in Table 5-2.

Table 5-2: Base Case Parameters

	Preese-Hall 1	Grange-Hill 1z	Becconssall 1z
Number of Fractures	12 Fractures	14 Fractures	11 Fractures
Fracture Permeability	25md	50md	25md
Fracture Width	0.002ft	0.002ft	0.002ft
Fracture Half-length	200ft	200ft	200ft
Log spaced Grid refinement	5x5x1	5x5x1	5x5x1
Reservoir Pressure	2000psi	2000psi	2000psi

Each well was set to produce at 500MScf/day with a gas content of 36scf/ton obtained from Cuadrilla's well report on the Upper Bowland Shale. The following sensitivities were carried out;

Impact of Fracture Half Length

The effect of fracture half-length was tested with a half-length of 100ft and 50ft. As expected, there was a proportional relationship between fracture half-length and gas production rate. Production from the Upper Bowland Shale showed more drastic decline in shale gas production and did not match production from the Barnett shale.

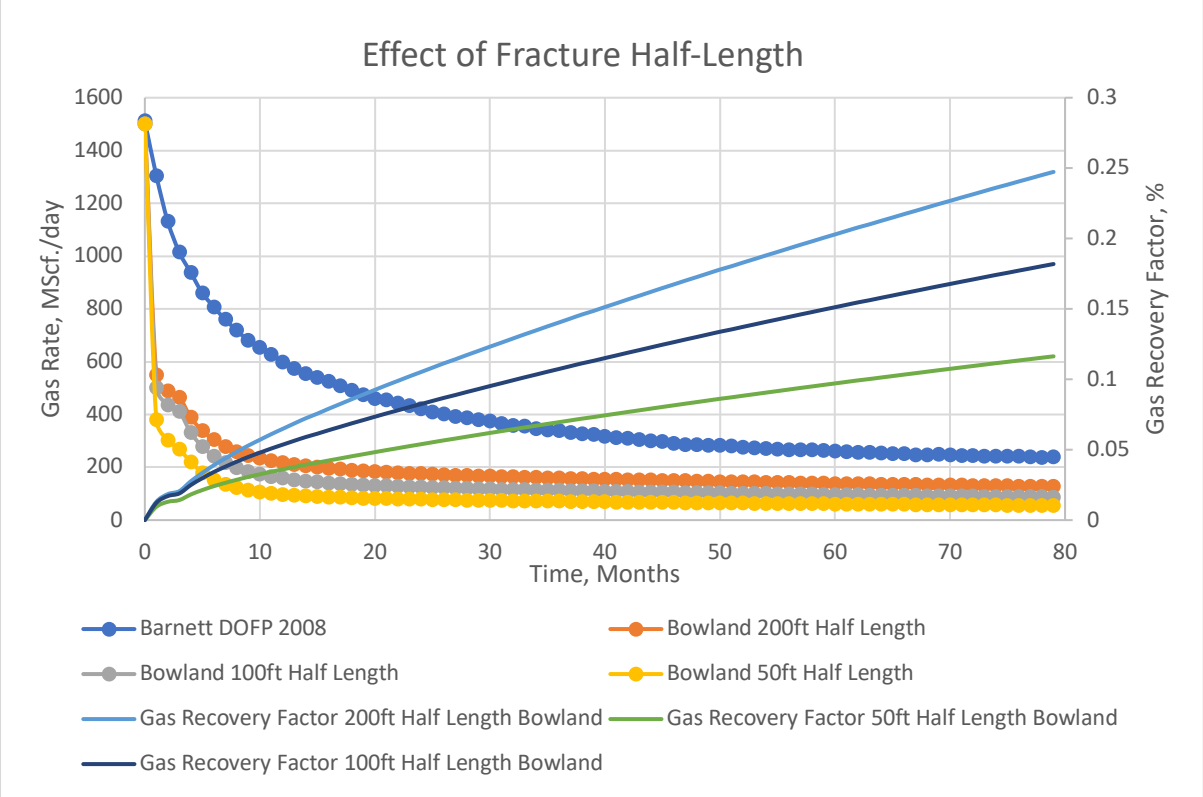

Figure 5-14: Effect of Fracture Half-length on Gas Production

Impact of Hydraulic Fracture Permeability

The effect of hydraulic fracture permeability was tested in the model. The fracture permeability for Preese-Hall 1 was increased to 50md and Grange-Hill 1z increased to 100md, and Becconssall 1z increased to 50md. Doubling the hydraulic fracture permeability resulted in a 20% increase in gas production. Production from the Upper Bowland shale at the tail-end was similar to production from the Barnett shale. At the tail end, the effect of fracture closure is

less and there is a greater contribution to gas production from adsorbed gas as reservoir pressure declines.

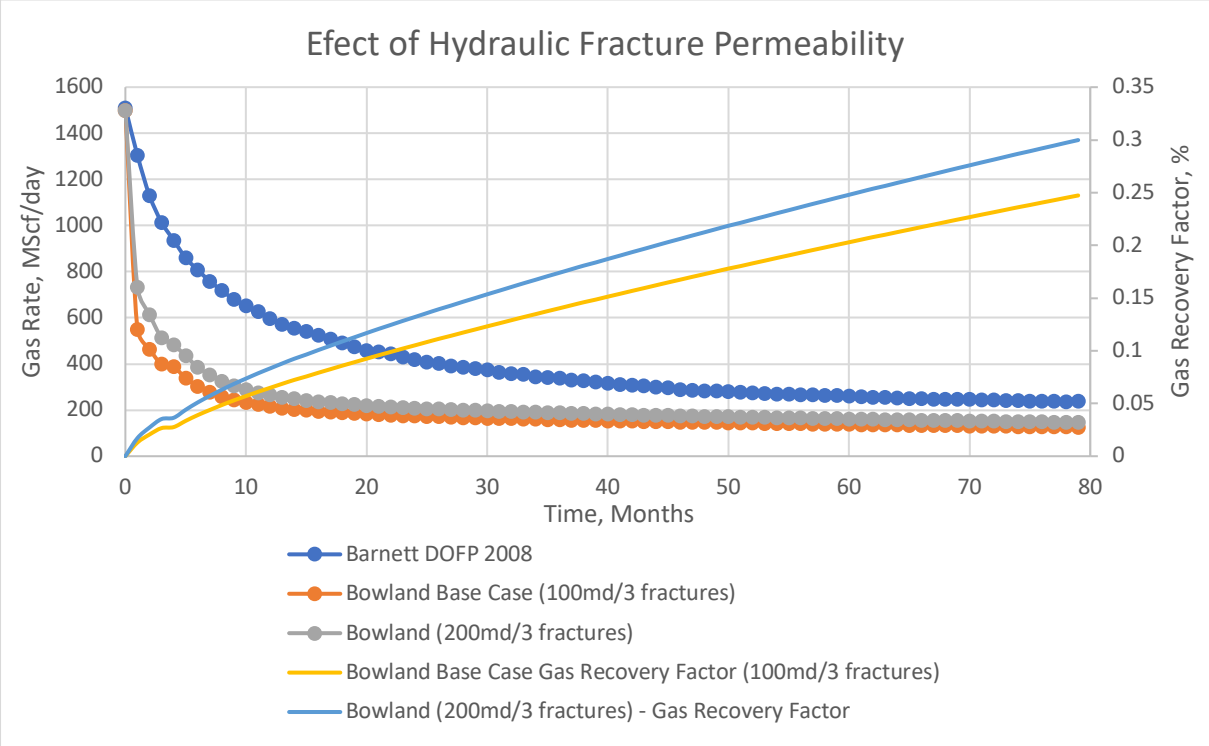

Figure 5-15: Effect of Hydraulic Fracture Permeability

Impact of Reservoir Pressure

The effect of reservoir pressure on the model was tested by observing the effect of a reservoir pressure of 3000psi and 3500psi The Upper Bowland Shale @ 3000 psi matched the tail end of the Barnett shale. Increasing the pressure from 2000psi to 3500psi resulted in a 76% increase in gas recovery.

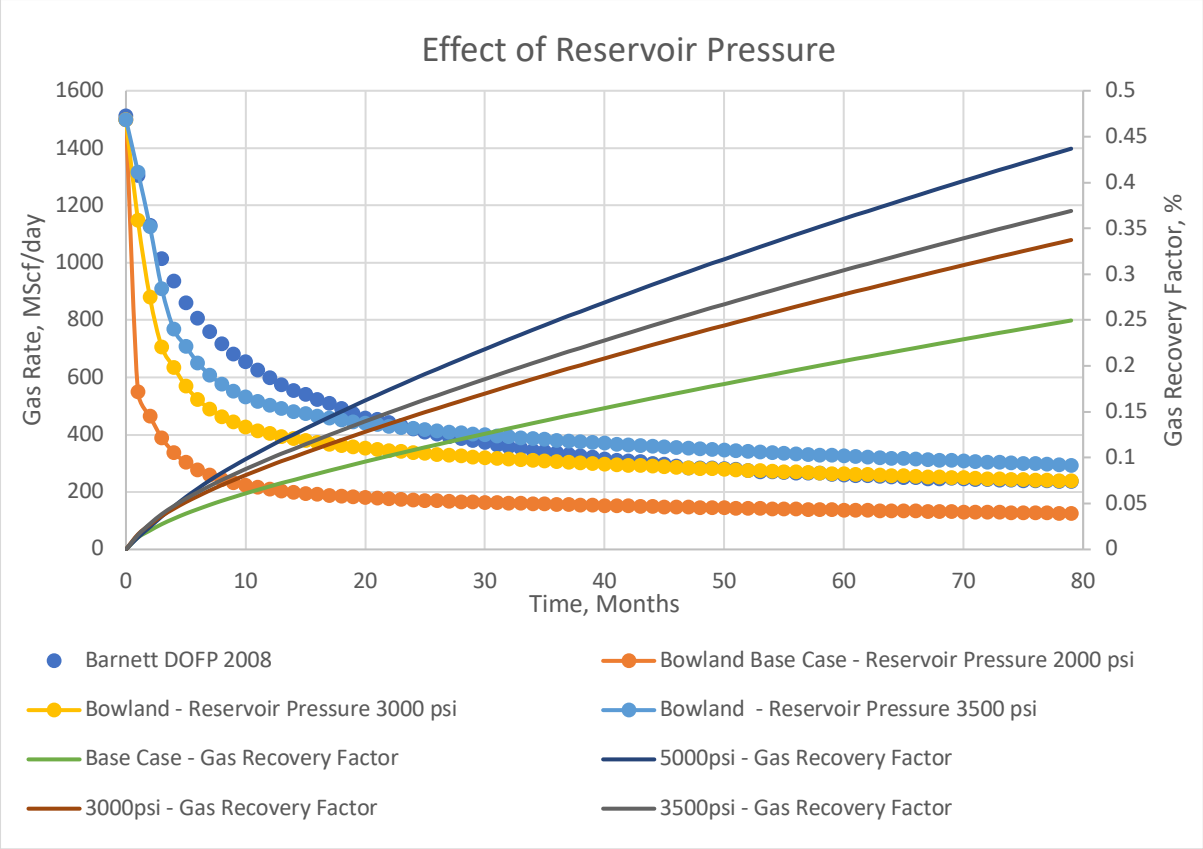

Figure 5-16: Effect of Reservoir Pressure

Impact of Local Grid Refinement

To better simulate the transient pressure distribution in the shale model, the effect of changing the logarithmically spaced local grid refinement was tested on the model but on the shale models at a reservoir pressure of 3000psi and 3500 psi (Figure 5-17). The 3x3x1 local grid refinement was poorest at modelling the transition between fracture dominated production and adsorbed gas dominated gas production i.e. between early time and late time production (Figure 5-17). The 5x5x1 and 7x7x1 better modelled this transition and larger refinement was not possible due to limitations of the number of grids blocks available as part of the software licence (Figure 5-17). All the scenarios except the scenario at 3500 psi matched the production performance of the Barnett shale at late time.

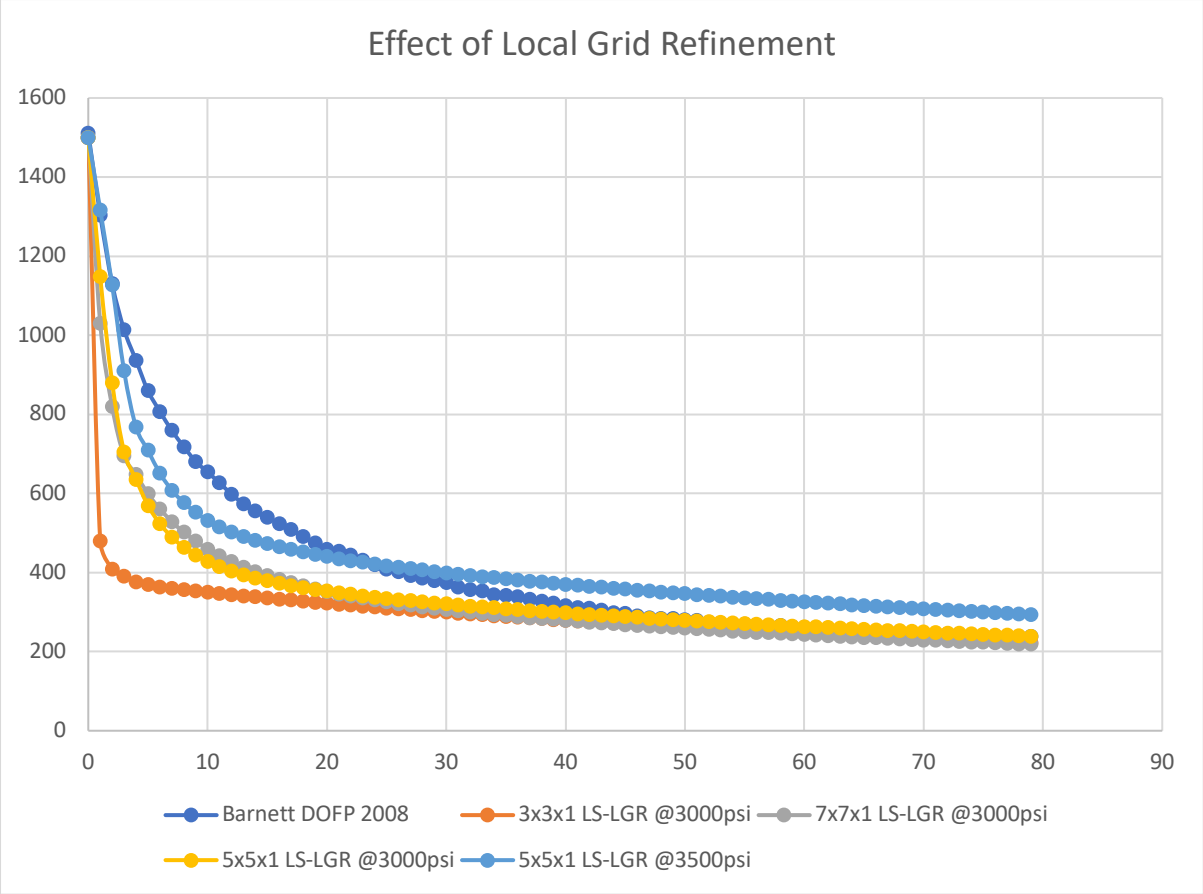

Figure 5-17: Effect of Local Grid Refinement

In all the results presented, the model was capable of matching the tail-end of the Barnett shale but not capable of accurately modelling the early/transition stage of gas production.

5.5. Conclusions

Accurate simulation of the transient flow behaviour in shale is important through the use of log spaced local grid refinement to accurately model the transition between fracture dominated and reservoir pressure dominated flow regimes. The 3x3x1 local grid refinement was least able to capture this transient behaviour. In all the cases examined, the Bowland shale and Barnett shale mostly showed comparable gas production rate at the tail end of the simulation, typically around the period from 30 to 80 months. The Bowland shale model was incapable of fully capturing for the early sharp decline/and or sometimes slower decline in gas production rate in all cases examined reflecting the need to develop a more robust geomechanically responsive model for future cases. Owing to the comparable thicker Bowland shale and lower gas content compared to the Barnett shale, the use of three vertical wells proved more effective compared to horizontal wells in predicting the performance of the Bowland shale.

This thesis showed the importance of a bottom-up approach in managing undeveloped shale gas reservoirs and using an analogue from the Barnett shale to validate the model. We produced a model that is capable of forecasting shale gas production in the UK.

Chapter 6 Conclusions and Further Work

Following the review of literature, four main research questions for this thesis were identified as follows;

1. Can a numerical or analytical simulation model be developed to reflect the Bowland shale?
2. What are the main factors that affects shale gas reservoir performance in relation to the aforementioned simulation model?
3. Can these models be validated with appropriate production data from the Barnett shale?
4. Can future shale gas production in the UK be predicted using the numerical simulation models?

We now refer back to these objectives and the main points of conclusion that can be drawn from the research.

Research Question 1: Can a numerical or analytical simulation model be developed to reflect the Bowland shale capable of predicting future shale gas production.

A numerical simulation model was developed using the provided contour map data from Oil and Gas Authority for the Bowland Basin which was inputted as a map file into CMG. Well tops from Thistleton 1, Preese-Hall, and Grange-Hill 1z was used to develop a grid representative of the shale within the Bowland Basin. Petrophysical modelling was then carried out in CMG to distribute properties e.g. (porosity, permeability, saturation, Poisson's ratio, mineralogy distributions) that have been obtained from analysing these wells within the model. Other parameters like gas content, total organic carbon distribution and rock compressibility were also included in this simulation model. The model was reflective of the topography of the Bowland basin covering both the upper Bowland shale and lower Bowland shale and this thesis was focussed on the former.

Research Question 2: What are the main factors that affects shale gas reservoir performance in relation to the aforementioned simulation model?

Four main sensitivities were carried out i.e. pressure, local grid refinement, fracture half-length and hydraulic fracture permeability in the context of the simulation model studied. From the result observations, the effect of local grid refinement was most important as it highly defined the shape of the production profile compared to the other scenarios and is indicative of the importance of capturing the long transient flow behaviour commonly observed in shale systems. The other parameters strongly affected the magnitude of gas production observed.

Research Question 3: Can these models be validated with appropriate production data from the Barnett shale?

The Barnett shale was described by (Andrews, 2013) as been a possible analogy to the Bowland shale as well as been of similar Mississippian age to the Barnett shale. Analysis of the production data in this thesis showed that the Barnett shale experiences a more gradual decline in gas production and lower reservoir pressures compared to other US shale gas plays like Marcellus or Haynesville. The clay content and reservoir pressures are also comparably lower than the Bowland shale as well as notable shale plays like the Marcellus or Haynesville. The level of faulting and geological complexity in the Bowland shale is also comparably more as compared to the Barnett shale. Nevertheless, the Bowland shale model was able to predict the tail end of gas production in most scenarios except under the hydraulic fracture and half-length scenarios mainly due to a lower reservoir pressure of 2000 psi been used – raising the reservoir pressure to 3000psi, a typical average for the Barnett shale resolved this challenge.

Research Question 4: Can future shale gas production in the UK Bowland Shale be predicted using the numerical simulation models?

The model is reflective of the Bowland shale and capable of predicting gas production performance at the tail end of gas production circa after 30 months under the scenarios investigated considering the use of the Barnett shale to validate production performance. The reservoir pressures in the Bowland Shale are higher (~ 6000 psi) compared to the Barnett shale (~3000 – 3500 psi) and as a result the model would need to be adjusted to reflect this and consequently validated with production data from the Upper Bowland shale which is limited and is not available for public or academic use at the present. This model is however not capable of accurately predicting the early stage of gas production which tends to be fracture dominated and cannot be relied upon considering the paucity of production data and available to validate these conclusions.

The following points are limitations and recommendations for future improvement of this work;

There is a lack of production data available from the Bowland shale and the Bowland shale is an active use-case and currently the point of discourse technically and politically. As such data

is highly confidential and is unlikely to be available to help validate the simulation model. Seismic data from the Bowland shale is confidential and yet to be available to the public. This will help capture the complex tectonics, natural fractures present in the Bowland shale that will further validate the numerical model and improve forecasting. There is also a lack of micro seismic hydraulic fracture data considering the initial fracturing of the Preese-hall 1 well was stopped due to safety fears and public disagreement. The second round of fracturing in 2019 was also stopped on the 4th of November 2019 where the UK Government withdrew support for hydraulic fracturing. Any data collected is unlikely to be available for the foreseeable future. Micro-seismic data and geomechanical data can be used to develop a discrete fracture network which can properly reflect fracture interactions in the Bowland shales and along with the mineralogical modelling carried out in this work, the model can accurately capture early time behaviour that tends to be fracture dominated. Relative permeability data was also limited, and hence empirical data was used to run the simulation models. A comprehensive review of the total organic carbon was also carried out in this thesis and the results were distributed across the simulation model using data from the three wells i.e. Thistleton 1, Preese-Hall 1 and Grange-Hill 1z. Future work can evaluate different realisations of total organic content and convert to adsorbed gas content using the volume of kerogen to better understand the adsorbed gas content variations and how it affects late time gas production.

The model developed in this work proved that a numerical simulation model can be developed for the Bowland shale albeit the accuracy of the outputs would be based on resolving the aforementioned concerns. The keynote from this thesis is that the Barnett shale cannot be blankly regarded as similar to the Bowland shale, but this work can give reservoir engineers a simulated performance of the Bowland shale and how it compares to the Barnett shale and the simulation results showed that the Bowland shale is capable of producing at similar rate to an average horizontal Barnett shale well (~ 2200 wells) with the use of 3 vertical wells. This also highlights the considerable thickness of the Bowland shale compared to the Barnett shale such that a combination of vertical wells or side-tracks can be used effectively in the Bowland shale.

References

Ambrose, R. J. *et al.* (2010) 'New Pore-scale Considerations for Shale Gas in Place Calculations', *SPE Unconventional Gas Conference*. Society of Petroleum Engineers. doi: 10.2118/131772-MS.

Anandarajah, G. and Nwaobi, U. (2015) *A Critical Review of Shale Gas Production Analysis and Forecast Methods Ukadike*. London. Available at: http://repositorio.unan.edu.ni/2986/1/5624.pdf.

Andrews, I. J. (2013) 'The Carboniferous Bowland Shale gas study: geology and resource estimation', *British Geological Survey for Department of Energy and Climate Change, London, UK*, p. 64pp. doi: 10.1080/10962247.2014.897270.

Archie, G. E. (1942) 'The Electrical Resistivity Log as an Aid in Determining Some Reservoir Characteristics', *Transactions of the AIME*. Society of Petroleum Engineers, 146(01), pp. 54–62. doi: 10.2118/942054-G.

Baihly, J. *et al.* (2010) 'SPE 135555 Shale Gas Production Decline Trend Comparison Over Time and Basins', *Production*, (September), pp. 19–22. doi: 10.2118/135555-MS.

Baihly, J. *et al.* (2011) 'Study Assesses Shale Decline Rates', *The American Oil & Gas Reporter*, (May), p. 5. Available at: https://www.slb.com/~/media/Files/dcs/industry_articles/201105_aogr_shale_baihly.ashx.

Bello, R. O., Wattenbarger, R. A. and Texas, A. (2008) 'Rate Transient Analysis in Naturally Fractured Shale Gas Reservoirs', *Society*, (June), pp. 16–19. doi: 10.2118/114591-MS.

Bowker, K. A. (2003) 'Recent Development of the Barnett Shale Play, Forth Worth Basin', *West Texas Geol Soc Bull*, 2(January 2000), p. 6.

Bowker, K. A. (2007) 'Barnett Shale gas production, Fort Worth Basin: Issues and discussion', *AAPG Bulletin*, 91(4), pp. 523–533. Available at: http://dx.doi.org/10.1306/06190606018.

Brinberg, M. (2019) *Cross-Validation Tutorial*, *PennState Social Science Research Instituite*. Available at: https://quantdev.ssri.psu.edu/tutorials/cross-validation-tutorial (Accessed: 29 April 2019).

Britt, L. K. and Schoeffler, J. (2009) 'The Geomechanics Of A Shale Play: What Makes A

Shale Prospective!', *SPE Eastern Regional Meeting*, (September), pp. 23–25. doi: 10.2118/125525-MS.

Brownlee, J. (2016) *Bagging and Random Forest Ensemble Algorithms for Machine Learning*, *Machine Learning Mastery*.

Bruner, K. R. and Smosna, R. (2011) 'A comparative study of the Mississippian Barnett Shale, Fort Worth Basin, and Devonian Marcellus Shale, Appalachian Basin', *US DoE Report*, p. 118. doi: DOE/NETL-2011/1478.

Bust, V. K. *et al.* (2013) 'The petrophysics of shale gas reservoirs: Technical challenges and pragmatic solutions', *Petroleum Geoscience*, 19(2), pp. 91–103. doi: 10.1144/petgeo2012-031.

Casella, G., Fienberg, S. and Olkin, I. (2017) *An Introduction to Stastical Learning*. Springer Texts in Statistics.

Cauter, F. Van (2013) *Predicting Decline in Unconventional Reservoirs Using Analytical and Empirical Methods*. Available at: https://spiral.imperial.ac.uk/handle/10044/1/24264.

Charpentier, R. R. and Cook, T. A. (2013) 'Variability of oil and gas well productivities for continuous (unconventional) petroleum accumulations: U.S. Geological Survey Open-File Report 2013–1001, 3 sheets.', *U.S. Geological Survey Open-File Report 2013–1001*, 80281, p. 3 sheets,.

Chemali, R., Gianzero, S. and Su, S. M. (1987) 'The Effect Of Shale Anisotropy On Focused Resistivity Devices'. Society of Petrophysicists and Well-Log Analysts.

Chopra, S. *et al.* (2013) 'Shale gas reservoir characterization workflows', *Abstracts: Annual Meeting - American Association of Petroleum Geologists*, 2013. Available at: http://login.ezproxy.library.ualberta.ca/login?url=http://search.ebscohost.com/login.aspx?direct=true&db=geh&AN=2014-063707&site=ehost-live&scope=site%5Cnhttp://www.searchanddiscovery.com/abstracts/html/2013/90163ace/abstracts/chop.htm.

Cipolla, C. *et al.* (2010) 'Reservoir Modeling in Shale-Gas Reservoirs', *SPE Reservoir Evaluation & Engineering*, 13(4), pp. 23–25. doi: 10.2118/125530-PA.

Cipolla, C. L. *et al.* (2009) 'Fracture Design Considerations in Horizontal Wells Drilled in

Unconventional Gas Reservoirs'. Society of Petroleum Engineers. doi: 10.2118/119366-MS.

Clarke, H. *et al.* (2018) 'Shale gas resources of the Bowland Basin, NW England: a holistic study', *Petroleum Geoscience*. Available at: http://pg.lyellcollection.org/content/early/2018/05/04/petgeo2017-066.abstract.

Clarke, H., Bustin, M. and Turner, P. (2014) 'Unlocking the resource potential of the Bowland Basin, NW England', *SPE/EAGE European Unconventional Resources Conference and Exhibition, 25-27 February, Vienna, Austria*, (February), p. SPE 167776, 11 pp. doi: 10.2118/167776-MS.

CMG (2015) 'Modelling of Shale , Tight Oil and Gas Reservoirs'.

Crafton, J. W. (2008) 'Modeling Flowback Behavior or Flowback Equals "Slowback"', *SPE Shale Gas Production Conference*. Fort Worth, Texas, USA: Society of Petroleum Engineers, p. 10. doi: 10.2118/119894-MS.

CUI, X., BUSTIN, A. M. M. and BUSTIN, R. M. (2009) 'Measurements of gas permeability and diffusivity of tight reservoir rocks: different approaches and their applications', *Geofluids*. John Wiley & Sons, Ltd, 9(3), pp. 208–223. doi: 10.1111/j.1468-8123.2009.00244.x.

Dean, M. T. *et al.* (2011) *A lithostratigraphical framework for the Carboniferous successions of northern Great Britain (onshore)*, *British Geological Survey Research Report RR/09/01*. Available at: https://books.google.co.uk/books?id=qPjUXwAACAAJ.

Duong, A. (2011) 'Rate-Decline Analysis for Fracture-Dominated Shale Reservoirs', *SPE Reservoir Evaluation & Engineering*, 14(3), pp. 19–21. doi: 10.2118/137748-PA.

EIA (2013) 'EIA/ARI World Shale Gas and Shale Oil Resource Assessment', (June), p. 707. Available at: http://www.adv-res.com/pdf/A_EIA_ARI_2013 World Shale Gas and Shale Oil Resource Assessment.pdf.

Elgmati, M. *et al.* (2011) 'SPE 144050: Submicron-Pore Characterization of Shale Gas Plays', *SPE North American Unconventional Conference and Exhibition*. Society of Petroleum Engineers, pp. 1–19. doi: 10.2118/144050-ms.

Eremenko, K. (2019) 'Machine Learning A-Z: Hands-On Python & R In Data Science'. udemy.

Ernst and Young (2014) ‘Getting ready for UK shale gas’, *United Kingdom Onshore Operators Group*, (April), pp. 1–44. Available at: http://www.ey.com/Publication/vwLUAssets/Getting_ready_for_UK_shale_gas/%24FILE/EY-Getting-ready-for-UK-shale-gas-April-2014.pdf.

Fan, L. *et al.* (2011) ‘The Bottom-Line of Horizontal Well Production Decline in the Barnett Shale’, *SPE Production and Operations Symposium*. Oklahoma City, Oklahoma, USA: Society of Petroleum Engineers, p. 10. doi: 10.2118/141263-MS.

Fertl, W. H. and Chilingar, G. V (1988) ‘Total Organic Carbon Content Determined From Well Logs’, *SPE Formation Evaluation*. Society of Petroleum Engineers, 3(02), pp. 407–419. doi: 10.2118/15612-PA.

Fertl, W. H. and Rieke III, H. H. (1980) ‘Gamma Ray Spectral Evaluation Techniques Identify Fractured Shale Reservoirs and Source-Rock Characteristics’. Society of Petroleum Engineers. doi: 10.2118/8454-PA.

Genuer, Robin; Poggi, Jean-Michel; Tuleau, C. (2008) *Random Forests: some methodological insights*.

Glorioso, J. C. and Rattia, A. (2012) ‘Unconventional Reservoirs : Basic Petrophysical Concepts for Shale Gas’, *Spe 153004*. Society of Petroleum Engineers, pp. 1–38. doi: 10.2118/153004-MS.

Gross, D. *et al.* (2015) ‘Organic geochemistry of Mississippian shales (Bowland Shale Formation) in central Britain: Implications for depositional environment, source rock and gas shale potential’, *Marine and Petroleum Geology*, 59, pp. 1–21. doi: https://doi.org/10.1016/j.marpetgeo.2014.07.022.

Guidry, F. K. and Walsh, J. W. (1993) ‘Well Log Interpretation of a Devonian Gas Shale: An Example Analysis’, *SPE Eastern Regional Meeting*, pp. 393–394. doi: 10.2118/26932-MS.

Hill, R. J. *et al.* (2007) ‘Modeling of gas generation from the Barnett Shale, Fort Worth Basin, Texas’, *American Association of Petroleum Geologists Bulletin*, 91(4), pp. 501–521. doi: 10.1306/12060606063.

Ilk, D. *et al.* (2008) ‘Exponential vs. Hyperbolic Decline in Tight Gas Sands — Understanding the Origin and Implications for Reserve Estimates Using Arps’ Decline

Curves', *Spe-116731*. Society of Petroleum Engineers. doi: 10.2118/116731-MS.

Jacobi, D. *et al.* (2008) 'Integrated Petrophysical Evaluation of Shale Gas Reservoirs', *CIPC/SPE Gas Technology Simposium 2008 Joint Conference*. Society of Petroleum Engineers, pp. 1–23. doi: 10.2118/114925-MS.

Jacobi, D. *et al.* (2009) 'Effective Geochemical and Geomechanical Characterization of Shale Gas Reservoirs from the Wellbore Environment: Caney and the Woodford Shale', *SPE Annual Technical Conference and Exhibition*. Society of Petroleum Engineers, pp. 1–20. doi: 10.2118/124231-MS.

Jarvie, D. *et al.* (2004) 'Evaluation of Hydrocarbon Generation and Storage in the Barnett Shale, Ft. Worth Basin, Texas', pp. 22–23. Available at: http://teamfrack.pbworks.com/w/file/fetch/48478518/Evaluation of Hydrocarbon Genration and Storage in the Barnett Shale.pdf.

Jarvie, D. M. *et al.* (2001) 'Oil and shale gas from the Barnett Shale, Ft. Worth Basin Texas', *AAPG National Convention*, (November), p. 28.

Jarvie, D. M. *et al.* (2007) 'Unconventional shale-gas systems: The Mississippian Barnett Shale of north-central Texas as one model for thermogenic shale-gas assessment', *American Association of Petroleum Geologists Bulletin*, 91(4), pp. 475–499. doi: 10.1306/12190606068.

Jarvie, D. M. (2012a) 'Extended Abstract—Shale Resource Systems for Oil and Gas', pp. 1–3. doi: 10.1306/13321445M973489.

Jarvie, D. M. (2012b) 'Shale Resource Systems for Oil and Gas: Part 1—Shale-gas Resource Systems', *Shale reservoirs—Giant resources for the 21st century: AAPG Memoir 97*, pp. 69–87. doi: 10.1306/13321446M973489.

Joshi, K. (2012) *Comparison of Various Deterministic Forecasting Techniques in Shale Gas Reservoirs with Emphasis on the Doung Method*. Available at: http://oaktrust.library.tamu.edu/bitstream/handle/1969.1/ETD-TAMU-2012-08-11882/JOSHI-THESIS.pdf?sequence=2.

Joshi, K. and Lee, J. (2013) 'Comparison of Various Deterministic Forecasting Techniques in Shale Gas Reservoirs', *SPE Conference*, p. 12. doi: 10.2118/163870-MS.

Kale, S. V., Rai, C. S. and Sondergeld, C. H. (2010) 'Petrophysical Characterization of Barnett Shale', *SPE Unconventional Gas Conference*. Society of Petroleum Engineers, pp. 1–17. doi: 10.2118/131770-MS.

Kanfar, M. and Wattenbarger, R. (2012a) 'Comparison of Empirical Decline Curve Methods for Shale Wells', in *Proceedings of SPE Canadian Unconventional Resources Conference*. Calgary: SPE162648, pp. 1–12. doi: 10.2118/162648-MS.

Kanfar, M. and Wattenbarger, R. (2012b) 'Comparison of Empirical Decline Curve Methods for Shale Wells', *Proceedings of SPE Canadian Unconventional Resources Conference*, (November), pp. 1–12. doi: 10.2118/162648-MS.

King, G. E. *et al.* (2008) 'Increasing Fracture Path Complexity and Controlling Downward Fracture Growth in the Barnett Shale', *SPE Shale Gas Production Conference*. Fort Worth, Texas, USA: Society of Petroleum Engineers, p. 8. doi: 10.2118/119896-MS.

King, G E (2010) 'Thirty years of gas-shale fracturing: What have we learned?', *JPT Journal of Petroleum Technology*, 62(September), pp. 88–90. doi: 10.2118/133456-MS.

King, George E (2010) 'Thirty Years of Gas Shale Fracturing : What Have We Learned ?', *Technology*, SPE 133456(November), pp. 19–22. doi: 10.2118/133456-MS.

King, G. E. and Corporation, A. (2010) 'SPE 133456 Thirty Years of Gas Shale Fracturing : What Have We Learned ?', (September), pp. 19–22.

Kochenov, A. V and Baturin, G. N. (2002) 'The Paragenesis of Organic Matter, Phosphorus, and Uranium in Marine Sediments', *Lithology and Mineral Resources*, 37(2), pp. 107–120. doi: 10.1023/A:1014816315203.

Kumar, A. (2014) *Data Science - How to Scale or Normalize Numerica Data using R*, *Reskilling IT*.

Kupchenko, C. L., Gault, B. W. and Mattar, L. (2008) 'SPE 114991 Tight Gas Production Performance Using Decline Curves', *Production*, (June), pp. 16–19. doi: 10.2118/114991-MS.

Labani, M. M. and Rezaee, R. (2012) 'Thermal maturity estimation of gas shale layers from conventional well log data: A case study from Kockatea Shale and Carynginia Formation of Perth Basin, Australia'. Society of Petroleum Engineers. doi: 10.2118/158864-MS.

LaFollette, R. F. and Carman, P. S. (2010) ‘Proppant Diagenesis: Results So Far’, *SPE Unconventional Gas Conference*. Pittsburgh, Pennsylvania, USA: Society of Petroleum Engineers, p. 14. doi: 10.2118/131782-MS.

Lee, W. J. and Sidle, R. (2010) ‘Gas-Reserves Estimation in Resource Plays’, *SPE Economics & Management*. Society of Petroleum Engineers, 2(2), pp. 23–25. doi: 10.2118/130102-PA.

Leeder, M. R. (1982) ‘Upper Palaeozoic basins of the British Isles—Caledonide inheritance versus Hercynian plate margin processes’, *Journal of the Geological Society*, 139(4), pp. 479–491. Available at: http://dx.doi.org/10.1144/gsjgs.139.4.0479.

Loucks, R. G. *et al.* (2009) ‘Morphology, Genesis, and Distribution of Nanometer-Scale Pores in Siliceous Mudstones of the Mississippian Barnett Shale’, *Journal of Sedimentary Research*, 79(12), pp. 848–861. doi: 10.2110/jsr.2009.092.

Luffel, D., Guidry, F. and Curtis, J. (1992) ‘Evaluation of Devonian shale with new core and log analysis methods’, *Journal of Petroleum Technology*. Society of Petroleum Engineers, 40646(November), pp. 1192–1197. doi: 10.2118/21297-PA.

Ma, Zee Y; Holditch, S. A. (2016) *Unconventional Oil and Gas Resources Handbook*. Gulf Professional Publishing.

Machine Learning Plus (2019) *Complete Introduction to Linear Regression in R*, *Machine Learning Plus*.

Mahmoud, A. A. *et al.* (2017) *Determination of the total organic carbon (TOC) based on conventional well logs using artificial neural network*, *International Journal of Coal Geology*. doi: 10.1016/j.coal.2017.05.012.

Mayerhofer, M. J. *et al.* (2010) ‘What Is Stimulated Reservoir Volume?’, *SPE Production & Operations*, 25(1), pp. 16–18. doi: 10.2118/119890-PA.

McGlade, C., Speirs, J. and Sorrell, S. (2013) ‘Methods of estimating shale gas resources - Comparison, evaluation and implications’, *Energy*. Elsevier Ltd, 59, pp. 116–125. doi: 10.1016/j.energy.2013.05.031.

Medeiros, F. *et al.* (2010) ‘Analysis of Production Data From Hydraulically Fractured Horizontal Wells in Shale Reservoirs’, *SPE Reservoir Evaluation & Engineering*, 13(3), pp.

559–568. doi: 10.2118/110848-PA.

Montgomery, S. L. *et al.* (2005) 'Mississippian Barnett Shale, Fort Worth basin, north-central Texas: Gas-shale play with multi-trillion cubic foot potential', *AAPG Bulletin*, 89(2), pp. 155–175. doi: 10.1306/09170404042.

Mullen, J. (2010) 'Petrophysical Characterization of the Eagle Ford Shale in South Texas', *Canadian Unconventional Resources & International Petroleum Conference held in Calgary*. Society of Petroleum Engineers, pp. 19–21. doi: 10.2118/138145-MS.

Myers, R. R. (2008) 'Stimulation and Production Analysis of Underpressured (Marcellus) Shale Gas', *SPE Shale Gas Production Conference*. Fort Worth, Texas, USA: Society of Petroleum Engineers, p. 8. doi: 10.2118/119901-MS.

Olsen, T. N., Bratton, T. R. and Thiercelin, M. J. (2009) 'Quantifying Proppant Transport for Complex Fractures in Unconventional Formations', *SPE Hydraulic Fracturing Technology Conference*. The Woodlands, Texas: Society of Petroleum Engineers, p. 12. doi: 10.2118/119300-MS.

Palmer, I. D., Moschovidis, Z. A. and Cameron, J. R. (2007) 'Modeling Shear Failure and Stimulation of the Barnett Shale After Hydraulic Fracturing', *SPE Hydraulic Fracturing Technology Conference*. College Station, Texas, U.S.A.: Society of Petroleum Engineers, p. 9. doi: 10.2118/106113-MS.

Passey *et al.* (1990) 'A practical model for organic richness from porosity and resistivity logs', *American Association of Petroleum Geologists Bulletin*. United States, 74(12), pp. 1777–1794. doi: 10.1306/0c9b25c9-1710-11d7-8645000102c1865d.

Passey, Q. R. *et al.* (2010) 'From Oil-Prone Source Rock to Gas-Producing Shale Reservoir - Geologic and Petrophysical Characterization of Unconventional Shale Gas Reservoirs'. Society of Petroleum Engineers. doi: 10.2118/131350-MS.

Pemper, R. *et al.* (2009) 'The Direct Measurement of Carbon in Wells Containing Oil and Natural Gas using a Pulsed Neutron Mineralogy Tool', *SPE Annual Technical Conference and Exhibition*, (124234), p. 14. doi: SPE124234.

Pemper, R. R. *et al.* (2006) 'A New Pulsed Neutron Sonde for Derivation of Formation Lithology and Mineralogy', *SPE Annual Technical Conference and Exhibition*. Society of

Petroleum Engineers. doi: 10.2118/102770-MS.

Penny, G. S., Dobkins, T. A. and Pursley, J. T. (2006) 'Field Study of Completion Fluids To Enhance Gas Production in the Barnett Shale', *SPE Gas Technology Symposium*. Calgary, Alberta, Canada: Society of Petroleum Engineers, p. 10. doi: 10.2118/100434-MS.

Pollastro, R. M. *et al.* (2007) 'Geologic framework of the Mississippian Barnett Shale, Barnett-Paleozoic total petroleum system, Bend arch-Fort Worth Basin, Texas', *American Association of Petroleum Geologists Bulletin*, 91(4), pp. 405–436. doi: 10.1306/10300606008.

Qu, W., Yoon, S. M. and Mudawar, I. (2004) 'Two-phase flow and heat transfer in rectangular micro-channels', *Journal of Electronic Packaging, Transactions of the ASME*, 126(3), pp. 288–300. doi: 10.1115/1.1756589.

Railroad Commisson of Texas (2017) *Barnett Shale Information*. Available at: http://www.rrc.state.tx.us/oil-gas/major-oil-gas-formations/barnett-shale-information/ (Accessed: 8 April 2017).

Ramirez, T. *et al.* (2011) 'Comparative Study of Formation Evaluation Methods for Unconventional Shale Gas Reservoirs: Application to the Haynesville Shale (Texas)', *North American Unconventional Gas Conference and Exhibition*. Society of Petroleum Engineers, p. 31. doi: 10.2118/144062-MS.

Rezaee, R. (2015) *Fundamental of Gas Shale Reservoirs*. Wiley. doi: 10.1002/9781119039228.

Rickman, R. *et al.* (2008) 'A practical use of shale petrophysics for stimulation design optimization: All shale plays are not clones of the Barnett Shale', *SPE Annual Technical Conference and Exhibition. Society of Petroleum Engineers*, (Wang), pp. 1–11. doi: 10.2118/115258-MS.

Rider, M. H. (1986) *The geological interpretation of well logs*. Blackie. Available at: https://inis.iaea.org/search/search.aspx?orig_q=RN:18074208 (Accessed: 16 January 2018).

Ruble, T. E., Drozd, R. J. and Heck, W. A. (2012) 'Practical geochemical methods to assess unconventional reservoirs a case study from the Permian Basin, Texas', *WTGS Fall Symposium 2012*, p. 47pp. Available at:

http://www.wtgs.org/media/files/None/2012_Ruble_WFTL_WTGS_Presentation.pdf.

Schmoker, J. W. (1981) 'Determination of organic-matter content of Appalachian Devonian shales from gamma-ray logs.', *American Association of Petroleum Geologists Bulletin*, 65(7), pp. 1285–1298.

Schmoker, J. W. (2002) 'Resource-assessment perspectives for unconventional gas systems', *American Association of Petroleum Geologists Bulletin*, 86(11), pp. 1993–1999. Available at: http://pubs.er.usgs.gov/publication/70024198.

Schmoker, J. W. and Hester, T. C. (1983) 'Organic carbon in Bakken Formation, United States portion of Williston Basin'. United States.

Sondergeld, C. H., Ambrose, R. J., *et al.* (2010) 'Micro-Structural Studies of Gas Shales', *SPE Unconventional Gas Conference*. Society of Petroleum Engineers. doi: 10.2118/131771-MS.

Sondergeld, C. H., Newsham, K. E., *et al.* (2010) 'Petrophysical Considerations in Evaluating and Producing Shale Gas Resources', *SPE Unconventional Gas Conference*. Society of Petroleum Engineers. doi: 10.2118/131768-MS.

Spears, R. and Jackson, S. L. (2009) 'Development of a Predictive Tool For Estimating Well Performance In Horizontal Shale Gas Wells In the Barnett Shale, North Texas, USA'. Society of Petrophysicists and Well-Log Analysts.

Srinidihi, S. (2019) *Different types of Validations in Machine Learning (Cross Validation)*, *The Tech Check*. Available at: https://blog.contactsunny.com/data-science/different-types-of-validations-in-machine-learning-cross-validation.

Taylor, C., Lewis, D. and Byles, D. (2013) 'Getting shale gas working', *IGas* , 6, p. 110.

Valko, P. (2009) 'Assigning Value to Stimulation in the Barnett Shale: A Simultaneous Analysis of 7000 Plus Production Histories and Well Completion Records', *Proceedings of SPE Hydraulic Fracturing Technology Conference*. Society of Petroleum Engineers, pp. 1–19. doi: 10.2118/119369-MS.

Vernik, L. and Milovac, J. (2011) 'Rock physics of organic shales', *The Leading Edge*. Society of Exploration Geophysicists, 30(3), pp. 318–323. doi: 10.1190/1.3567263.

Waldo, D. A. (2015) ‘Geologic factors associated with successful shale gas plays’, *SPE Queensland Section, lunchtime presentation*, pp. 1–29. Available at: https://www.spe-qld.org/useruploads/files/spedlpresowaldodavidrevised_february2015.pdf.

Wang, F. P. and Reed, R. M. (2009) ‘Pore Networks and Fluid Flow in Gas Shales’, *SPE Annual Technical Conference and Exhibition*. Society of Petroleum Engineers. doi: 10.2118/124253-MS.

Warpinski, N. R. *et al.* (2009) ‘Stimulating unconventional reservoirs: Maximizing network growth while optimizing fracture conductivity’, *Journal of Canadian Petroleum Technology*, 48(10), pp. 39–51. doi: 10.2118/114173-PA.

Weijermars, R. (2013) ‘Economic appraisal of shale gas plays in Continental Europe’, *Applied Energy*, 106, pp. 100–115. doi: https://doi.org/10.1016/j.apenergy.2013.01.025.

Wright, L. (2016) *The Potential of Shale Gas In The Bowland-Hodder, Is It The Next Barnett?* University of Oxford. doi: 10.13140/RG.2.2.13223.55203.

Yu, G. and Aguilera, R. (2011) ‘Use of Pickett Plots for evaluation of shale gas formations’, *SPE Annual Technical Conference, Denver*. Society of Petroleum Engineers, p. 16pp. doi: 10.2118/146948-MS.

Zhao, H., Givens, N. B. and Curtis, B. (2007) ‘Thermal maturity of the Barnett Shale determined from well-log analysis’, *AAPG Bulletin*, 91(4), pp. 535–549.

Zhao, J. *et al.* (2015) ‘Petroleum accumulation: From continuous to discontinuous’, *Acta Geologica Sinica - English Edition*, 89(s1), pp. 303–306. doi: 10.1111/1755-6724.12305_2.

Zou, C. (2013) *Unconventional Petroleum Geology*. Elsevier. doi: doi: 10.1016/B978-0-12-397162-3.00005-0.

APPENDIX A

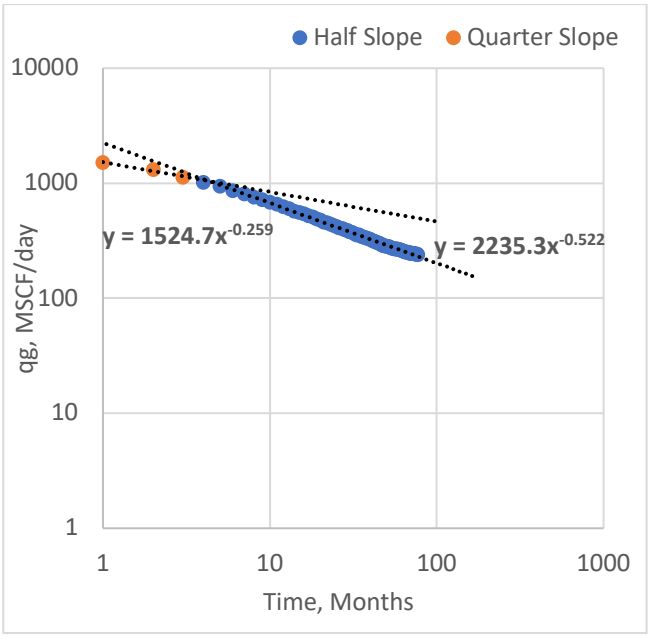

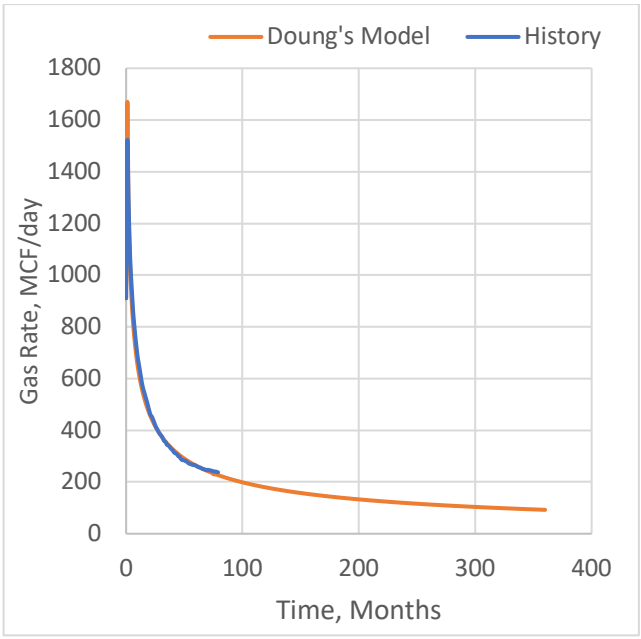

DOFP 2008 – 78 month production history

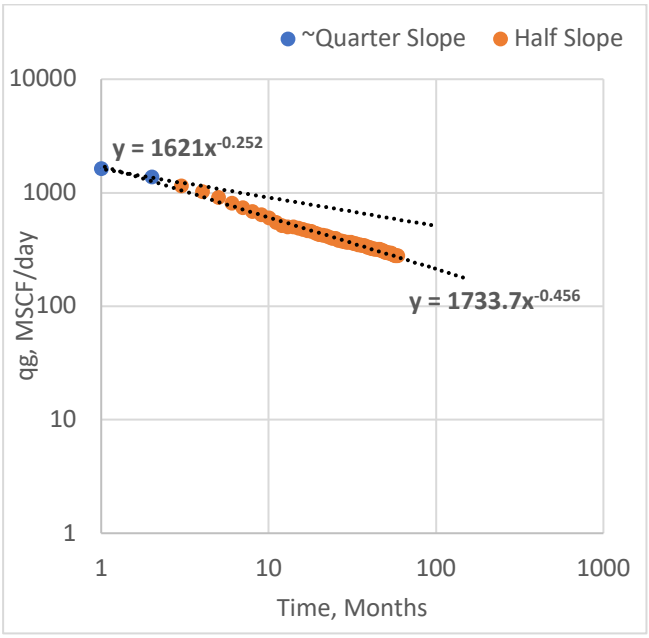

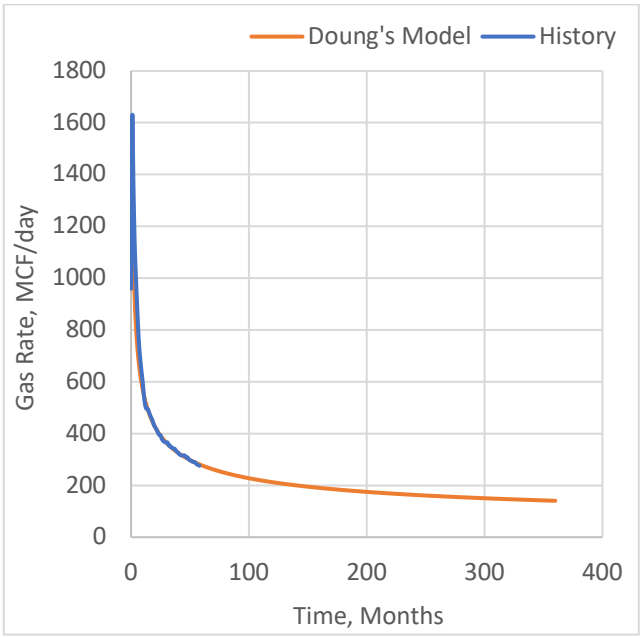

DOFP 2009 – 58 month production history

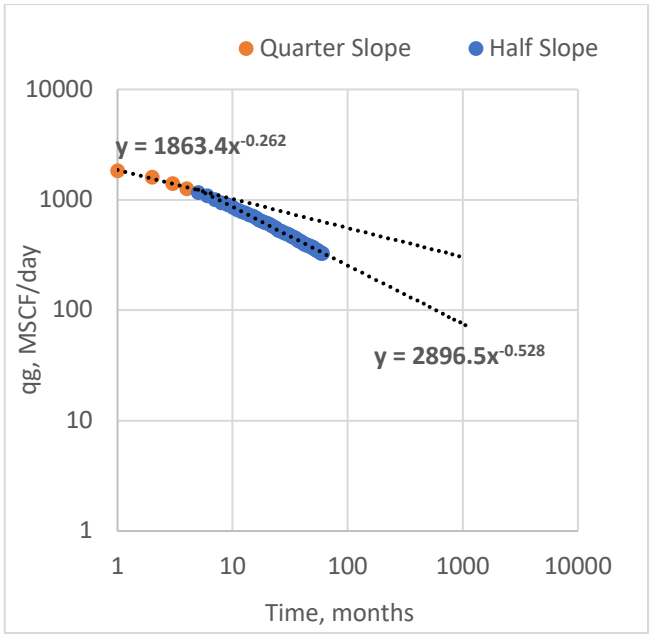

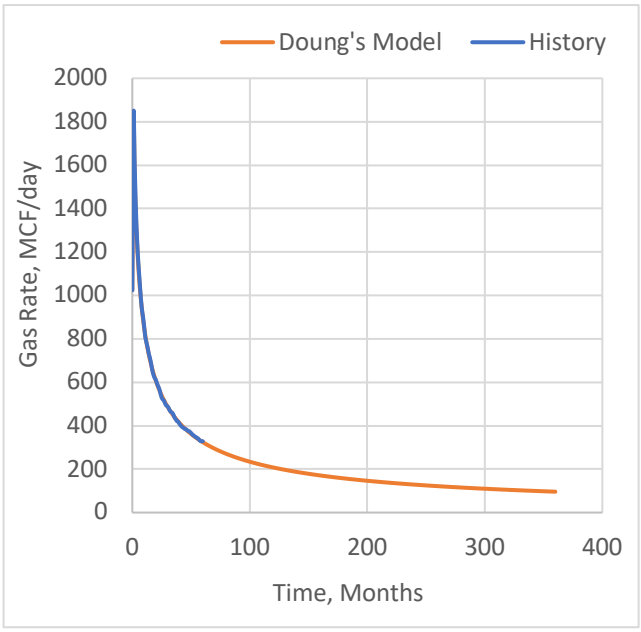

DOFP 2010 – 60 month production history

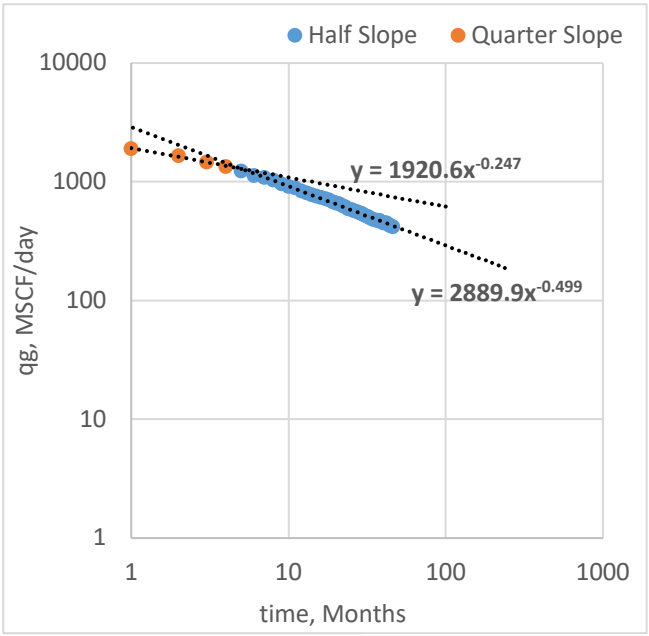

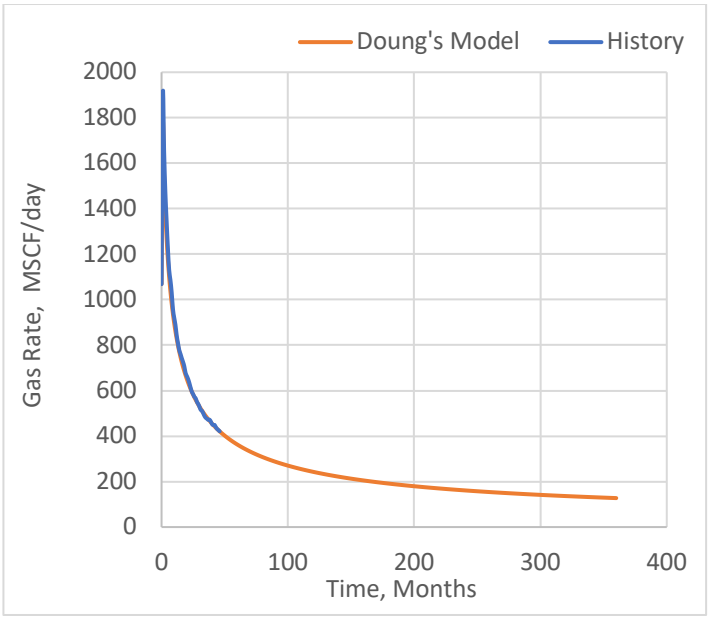

DOFP 2011 - 46 month production history

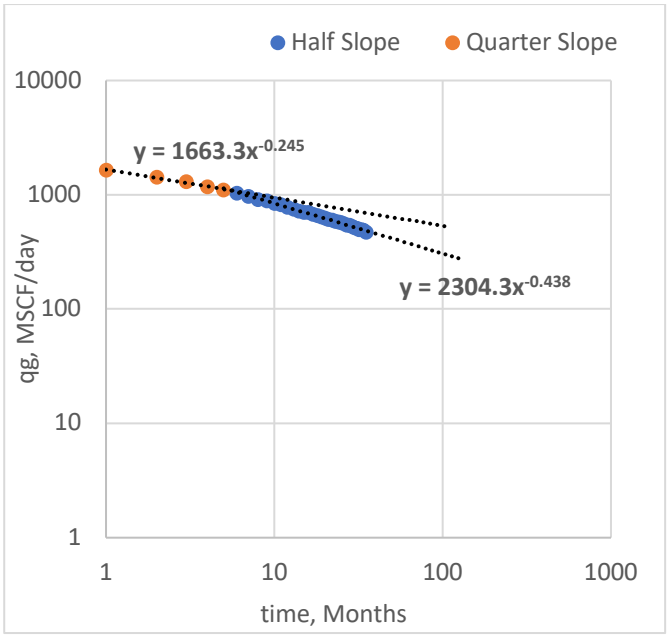

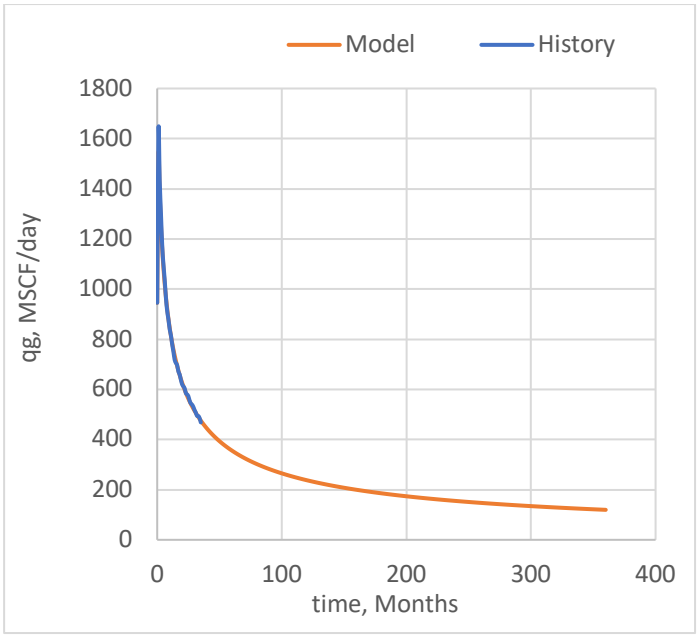

DOFP 2012 – 35-month production history

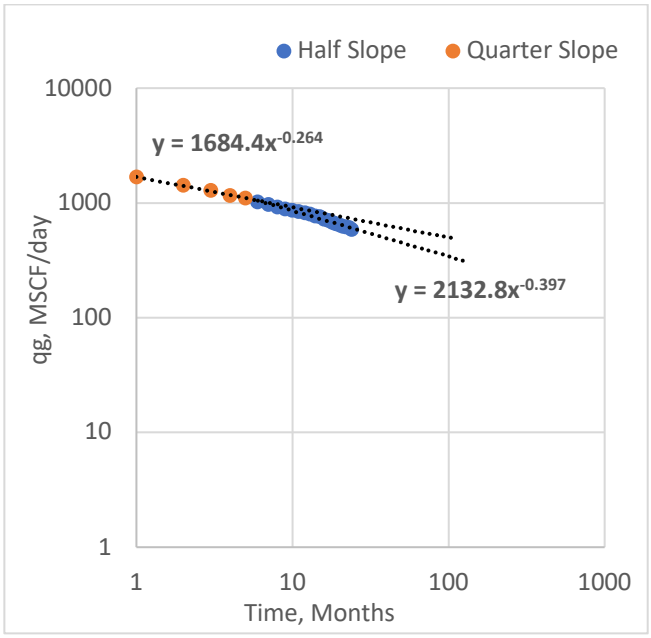

DOFP 2013 – 24-month production history

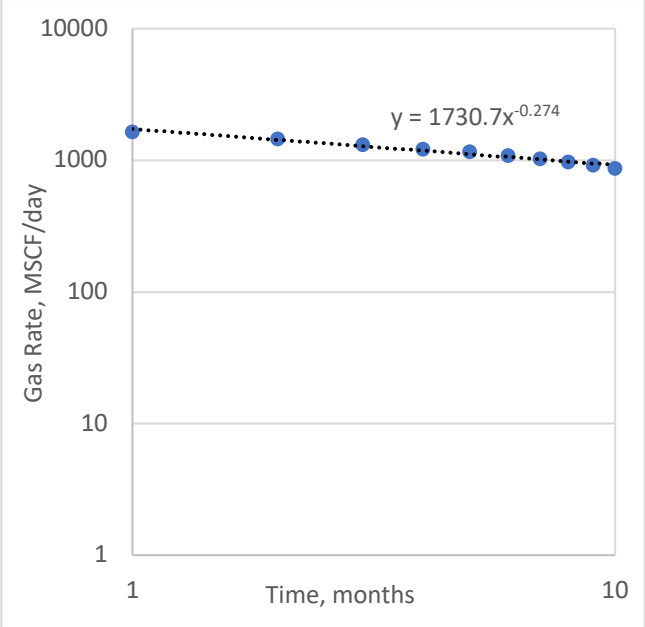

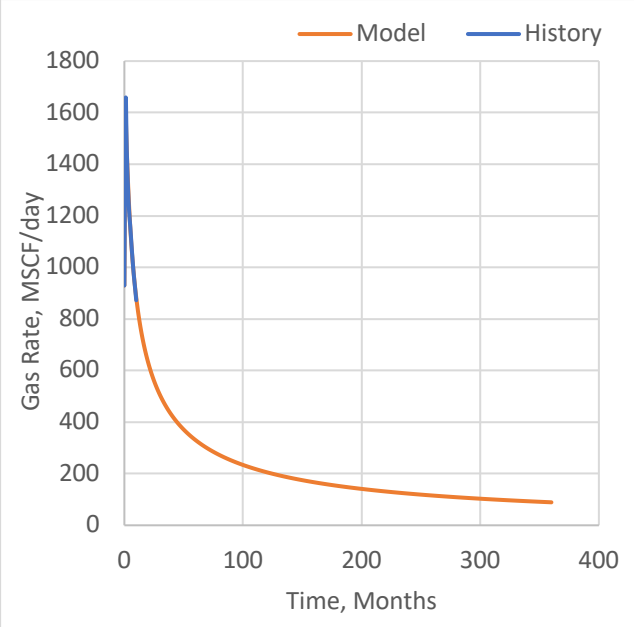

Figure 0-1: DOFP 2014 - 11-month production history

APPENDIX B

Strawn Basin

F&DC and gas prices for P90 wells that satisfy the investment hurdle (EUR: 1.99BCF)

F&DC	$1,000,000.00	$2,000,000.00	$4,000,000.00
Gas Price			
$2.00	No	No	No
$4.00	Yes	No	No
$6.00	Yes	Yes	No
$8.00	**Yes**	**Yes**	**Yes**
$10.00	**Yes**	**Yes**	**Yes**
$12.00	**Yes**	**Yes**	**Yes**
$13.00	**Yes**	**Yes**	**Yes**

F&DC and gas prices for P50 wells that satisfy the investment hurdle (EUR: 0.91BCF)

F&DC	$1,000,000.00	$2,000,000.00	$4,000,000.00
Gas Price			
$2.00	No	No	No
$4.00	No	No	No
$6.00	**Yes**	No	No
$8.00	**Yes**	**Yes**	No
$10.00	**Yes**	**Yes**	No
$12.00	**Yes**	**Yes**	No
$13.00	**Yes**	**Yes**	No

F&DC and gas prices for P10 wells that satisfy the investment hurdle (EUR: 0.28BCF)

F&DC	$1,000,000.00	$2,000,000.00	$4,000,000.00
Gas Price			
$2.00	No	No	No
$4.00	No	No	No
$6.00	No	No	No
$8.00	No	No	No
$10.00	No	No	No
$12.00	No	No	No
$13.00	**Yes**	No	No

Bend-Arch Basin

F&DC and gas prices for P90 wells that satisfy the investment hurdle (EUR: 0.96BCF)

F&DC	$1,000,000.00	$2,000,000.00	$4,000,000.00
Gas Price			
$2.00	No	No	No
$4.00	No	No	No
$6.00	**Yes**	No	No
$8.00	**Yes**	**Yes**	No
$10.00	**Yes**	**Yes**	No
$12.00	**Yes**	**Yes**	No
$13.00	**Yes**	**Yes**	No

F&DC and gas prices for P50 wells that satisfy the investment hurdle (EUR: 0.22BCF)

F&DC	$1,000,000.00	$2,000,000.00	$4,000,000.00
Gas Price			
$2.00	No	No	No
$4.00	No	No	No
$6.00	No	No	No
$8.00	No	No	No
$10.00	No	No	No
$12.00	No	No	No
$13.00	No	No	No

F&DC and gas prices for P10 wells that satisfy the investment hurdle (EUR: 0.04BCF)

F&DC	$1,000,000.00	$2,000,000.00	$4,000,000.00
Gas Price			
$2.00	No	No	No
$4.00	No	No	No
$6.00	No	No	No
$8.00	No	No	No
$10.00	No	No	No
$12.00	No	No	No
$13.00	No	No	No

Ouachita Folded Belt

F&DC and gas prices for P90 wells that satisfy the investment hurdle (EUR: 1.32BCF)

F&DC	$1,000,000.00	$2,000,000.00	$4,000,000.00
Gas Price			
$2.00	No	No	No
$4.00	**Yes**	No	No
$6.00	**Yes**	**Yes**	No
$8.00	**Yes**	**Yes**	No
$10.00	**Yes**	**Yes**	No
$12.00	**Yes**	**Yes**	**Yes**
$13.00	**Yes**	**Yes**	**Yes**

F&DC and gas prices for P50 wells that satisfy the investment hurdle (EUR: 0.66BCF)

F&DC	$1,000,000.00	$2,000,000.00	$4,000,000.00
Gas Price			
$2.00	No	No	No
$4.00	No	No	No
$6.00	**Yes**	No	No
$8.00	**Yes**	No	No
$10.00	**Yes**	No	No
$12.00	**Yes**	**Yes**	No
$13.00	**Yes**	**Yes**	No

F&DC and gas prices for P10 wells that satisfy the investment hurdle (EUR: 0.22BCF)

F&DC	$1,000,000.00	$2,000,000.00	$4,000,000.00
Gas Price			
$2.00	No	No	No
$4.00	No	No	No
$6.00	No	No	No
$8.00	No	No	No
$10.00	No	No	No
$12.00	No	No	No
$13.00	No	No	No

Forth-Worth Syncline

F&DC and gas prices for P90 wells that satisfy the investment hurdle (EUR: 1.76BCF)

F&DC	$1,000,000.00	$2,000,000.00	$4,000,000.00
Gas Price			
$2.00	No	No	No
$4.00	Yes	No	No
$6.00	Yes	Yes	No
$8.00	Yes	Yes	No
$10.00	Yes	Yes	Yes
$12.00	Yes	Yes	Yes
$13.00	Yes	Yes	Yes

F&DC and gas prices for P50 wells that satisfy the investment hurdle (EUR: 0.80BCF)

F&DC	$1,000,000.00	$2,000,000.00	$4,000,000.00
Gas Price			
$2.00	No	No	No
$4.00	No	No	No
$6.00	**Yes**	No	No
$8.00	**Yes**	No	No
$10.00	**Yes**	Yes	No
$12.00	**Yes**	Yes	No
$13.00	**Yes**	Yes	No

Appendix C

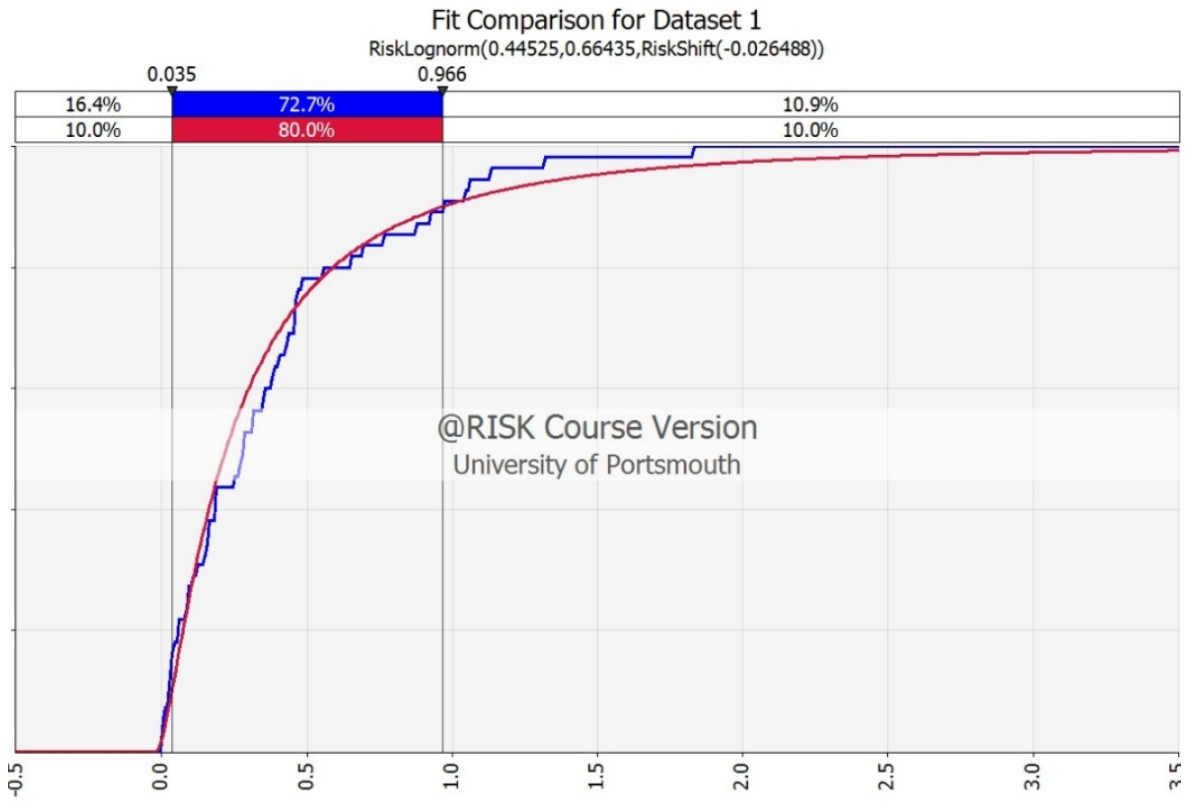

Figure 0-1: Montecarlo Results for Bend-Arch Basin showing P10 and P90

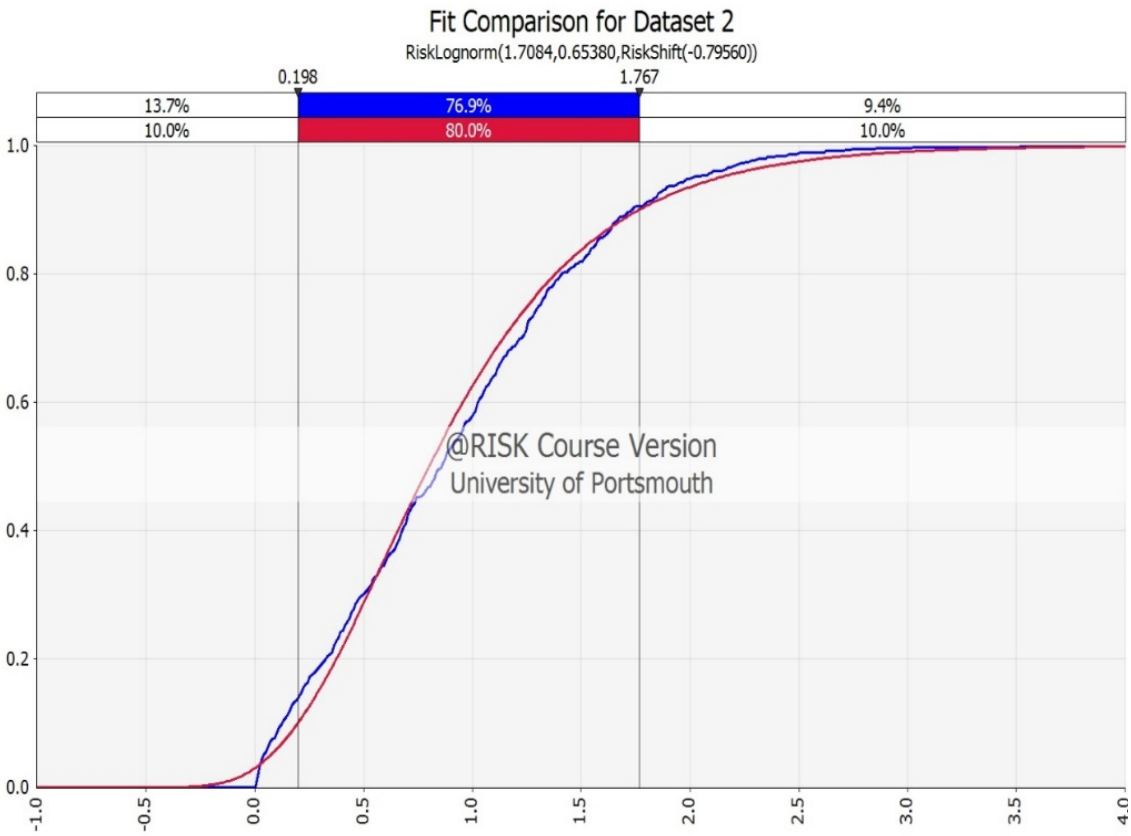

Figure 0-2: Monte-carlo Results for Forth-Worth Syncline showing P10 and P90

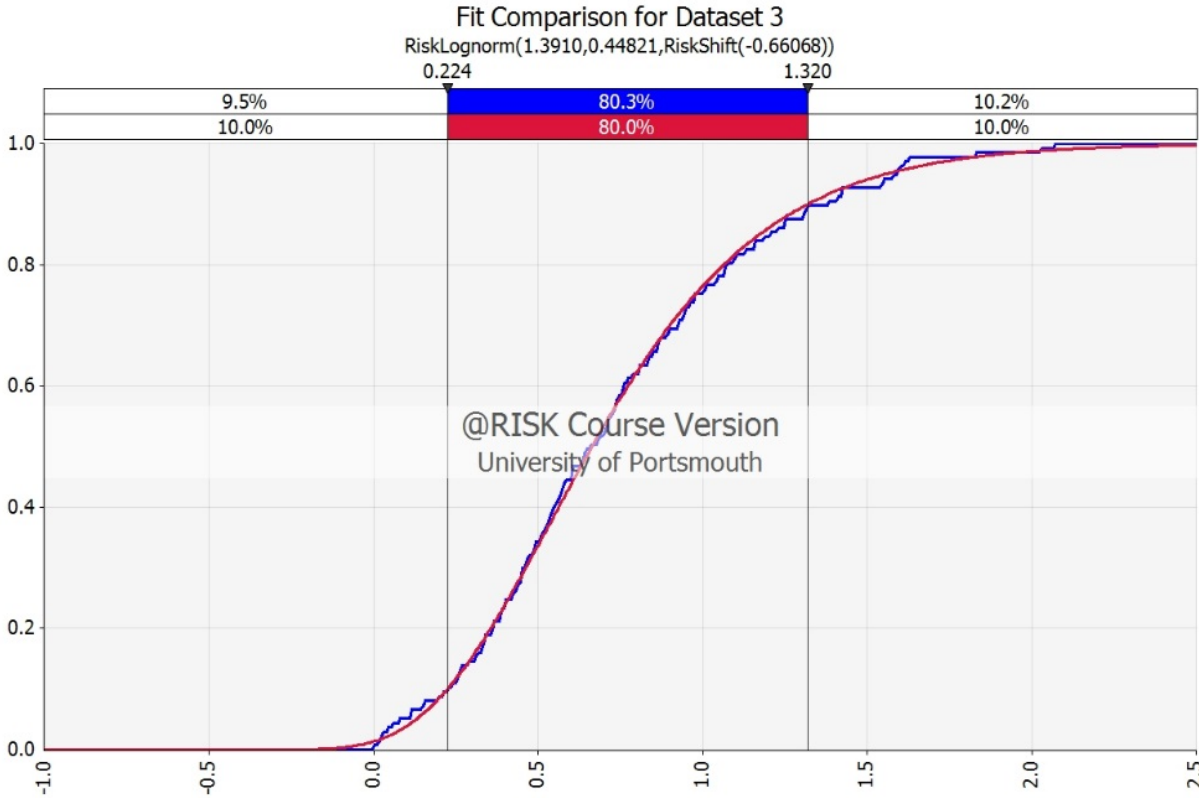

Figure 0-3: Monte Carlo Results for Ouachita Fold Belt showing P10 and P90

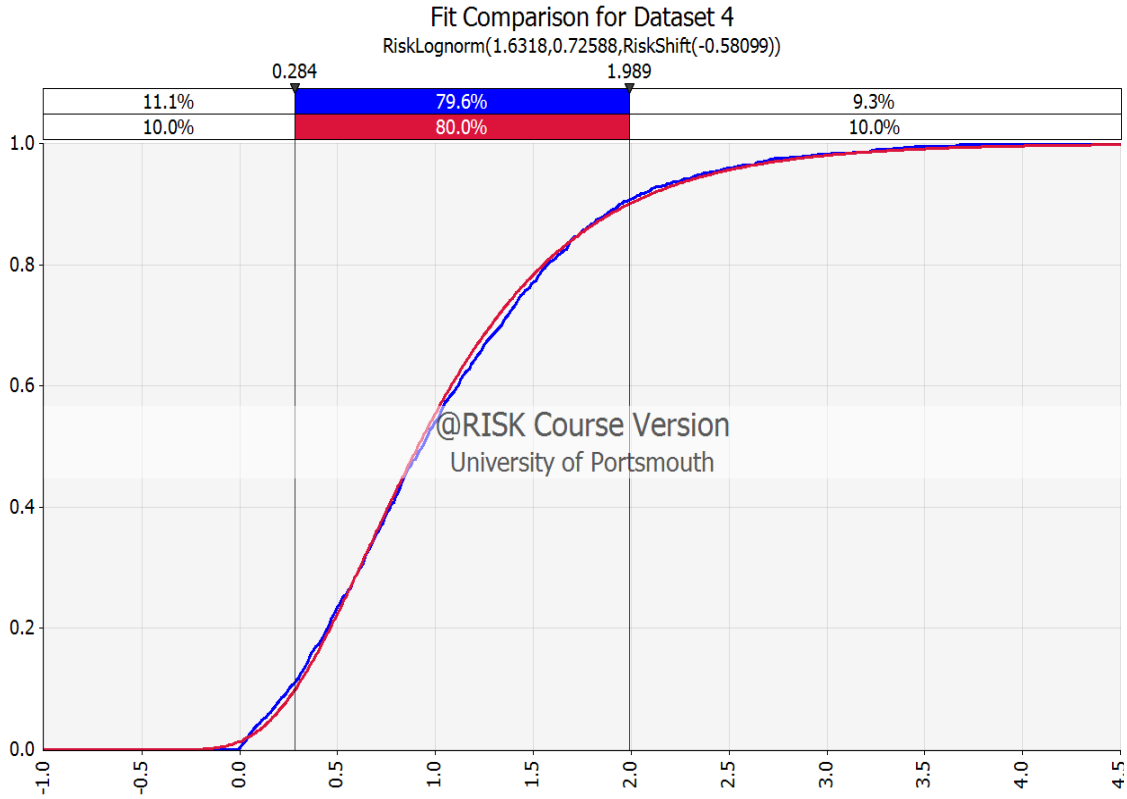

Figure 0-4: Monte Carlo Results for Strawn Basin showing P10 and P90

APPENDIX D – UPR16

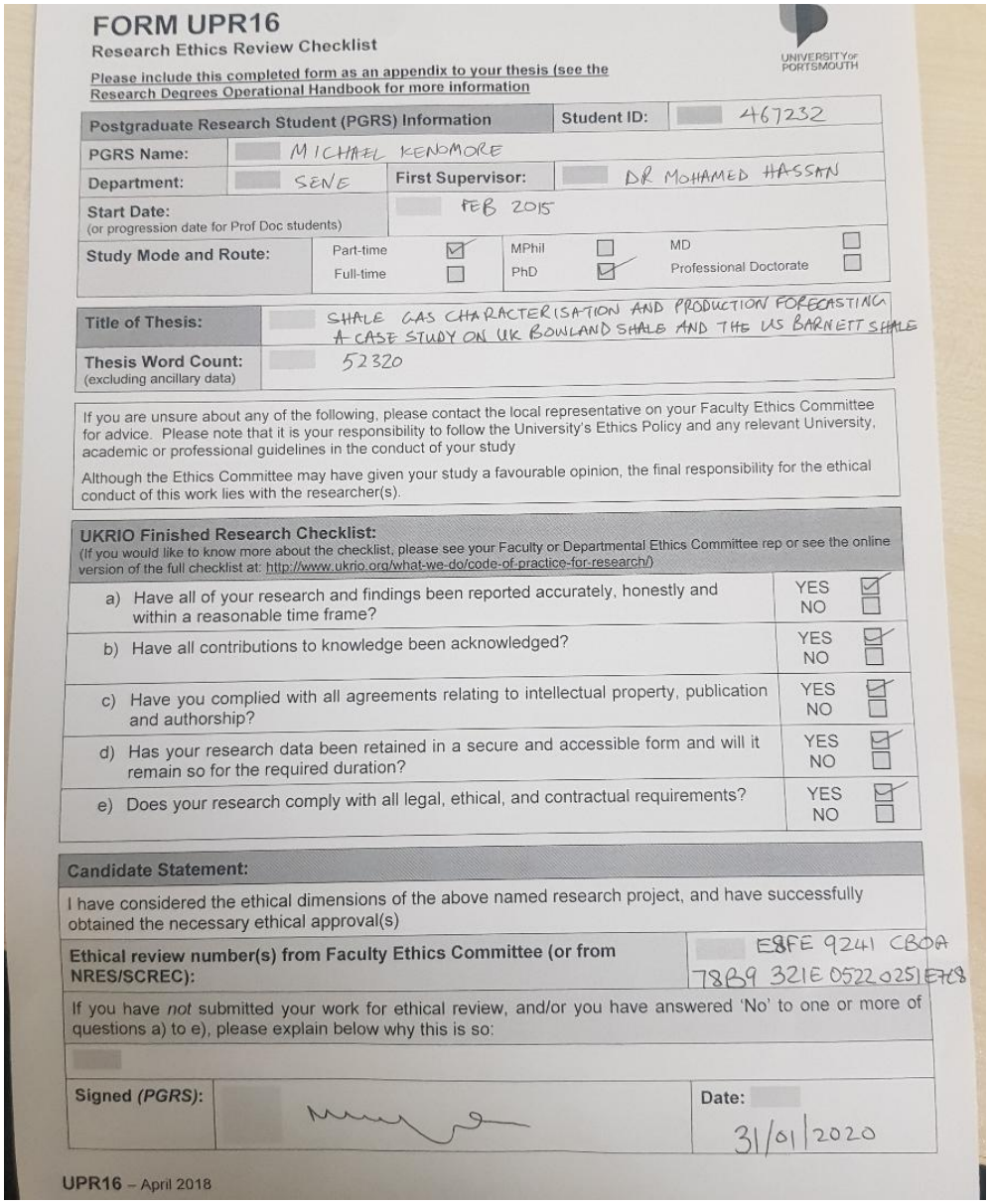

FORM UPR16

Research Ethics Review Checklist

UNIVERSITY OF PORTSMOUTH

Please include this completed form as an appendix to your thesis (see the Research Degrees Operational Handbook for more information

Postgraduate Research Student (PGRS) Information		Student ID:	467232
PGRS Name:	MICHAEL KENDMORE		
Department:	SENE	First Supervisor:	DR MOHAMED HASSAN
Start Date: (or progression date for Prof Doc students)	FEB 2015		
Study Mode and Route:	Part-time ☑ / Full-time ☐	MPhil ☐ / PhD ☑	MD ☐ / Professional Doctorate ☐
Title of Thesis:	SHALE GAS CHARACTERISATION AND PRODUCTION FORECASTING A CASE STUDY ON UK BOWLAND SHALE AND THE US BARNETT SHALE		
Thesis Word Count: (excluding ancillary data)	52320		

If you are unsure about any of the following, please contact the local representative on your Faculty Ethics Committee for advice. Please note that it is your responsibility to follow the University's Ethics Policy and any relevant University, academic or professional guidelines in the conduct of your study

Although the Ethics Committee may have given your study a favourable opinion, the final responsibility for the ethical conduct of this work lies with the researcher(s).

UKRIO Finished Research Checklist:
(If you would like to know more about the checklist, please see your Faculty or Departmental Ethics Committee rep or see the online version of the full checklist at: http://www.ukrio.org/what-we-do/code-of-practice-for-research/)

a)	Have all of your research and findings been reported accurately, honestly and within a reasonable time frame?	YES ☑ NO ☐
b)	Have all contributions to knowledge been acknowledged?	YES ☑ NO ☐
c)	Have you complied with all agreements relating to intellectual property, publication and authorship?	YES ☑ NO ☐
d)	Has your research data been retained in a secure and accessible form and will it remain so for the required duration?	YES ☑ NO ☐
e)	Does your research comply with all legal, ethical, and contractual requirements?	YES ☑ NO ☐

Candidate Statement:

I have considered the ethical dimensions of the above named research project, and have successfully obtained the necessary ethical approval(s)

Ethical review number(s) from Faculty Ethics Committee (or from NRES/SCREC): E8FE 9241 CB0A 78B9 321E 0522 0251 E7C8

If you have *not* submitted your work for ethical review, and/or you have answered 'No' to one or more of questions a) to e), please explain below why this is so:

Signed *(PGRS)*: [signature] **Date:** 31/01/2020

UPR16 – April 2018